

See discussions, stats, and author profiles for this publication at: <https://www.researchgate.net/publication/230636789>

Update 1 of: Strong Ionic Hydrogen Bonds

ARTICLE *in* CHEMICAL REVIEWS · AUGUST 2012

Impact Factor: 46.57 · DOI: 10.1021/cr200430n · Source: PubMed

CITATIONS

46

READS

60

1 AUTHOR:



Michael Noah Mautner

Virginia Commonwealth University

198 PUBLICATIONS 5,112 CITATIONS

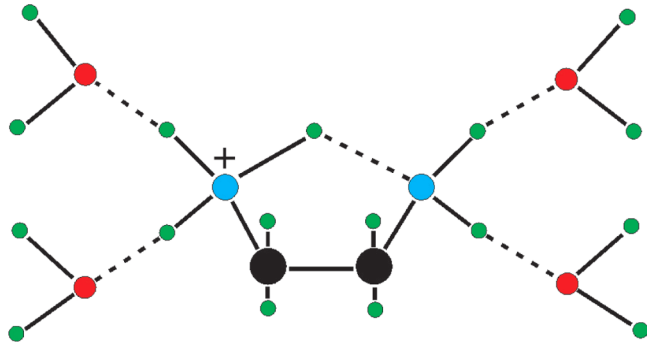
SEE PROFILE

Update 1 of: Strong Ionic Hydrogen Bonds

Michael Meot-Ner (Mautner)*

Department of Chemistry, Virginia Commonwealth University, Richmond, Virginia 23284, United States

This is a *Chemical Reviews* Perennial Review. The root paper of this title was published in *Chem. Rev.* 2005, 105, 213–284, DOI: 10.1021/cr941178s; Published (Web) January 12, 2005. Updates to the text appear in red type.



CONTENTS

1. Introduction and Overview			
1.1. Historical Background	PR23		
1.2. An Overview of IHB Structures and Energetics	PR23		
1.2.1. Dimers	PR25		
1.2.2. Higher Clusters	PR25		
1.2.3. Polyfunctional Molecules, Biomolecules, and Cluster Models of Bioenergetics	PR26		
1.2.4. Relationship between Gas-Phase and Bulk Solvation	PR26		
2. Hydrogen-Bonded Dimers			
2.1. Thermochemistry and Structures of Hydrogen-Bonded Dimers	PR26		
2.1.1. Structural Effects of Ionic Hydrogen-Bond Formation	PR26		
2.2. Hydrogen-Bond Strengths and Correlations with Proton Affinities	PR29		
2.2.1. Cationic Dimers and Correlations with Proton Affinities	PR29		
2.2.2. Dimer Anions: Bond Strengths and Correlations with Acidities	PR32		
2.3. Structural Effects: Isotropy, Resonance, and Steric Hindrance	PR35		
2.3.1. Does Isotropy Affect the Bond Strengths?	PR35		
2.3.2. Resonance	PR35		
2.3.3. Steric Hindrance	PR36		
2.4. Carbon-Based Bonds	PR36		
2.4.1. Cationic Complexes with CH Donors	PR36		
2.4.2. Anionic Complexes with Carbon-Based Bonds	PR40		
2.4.3. Complexes of Carbon Lone-Pair Acceptors	PR41		
2.4.4. Complexes of π -Acceptors	PR41		
2.4.5. Hydrogen-Bonded Isomers of Covalent Ions	PR41		
2.5. Radical Ions and Distonic Dimers	PR43		
2.5.1. Reaction Intermediates and Distonic Dimers	PR43		
2.5.2. Complexes of Ionized Aromatics: Solvation of the Benzene and Pyridine Cations	PR43		
3. Larger Clusters and Hydrogen-Bond Networks	PR44		
3.1. Neat Aggregates and Solvation Sequences	PR44		
3.1.1. Thermochemical Studies of Stepwise Solvation	PR44		
3.1.2. Effects of Stepwise Solvation on Charge Distributions and Hydrogen-Bond Lengths	PR45		
3.1.3. Consecutive Bonding Energies and Some Predictive Relations	PR47		
3.1.5. The Evolution of Hydrogen-Bond Networks and Thermochemical Effects of Isomeric Clusters	PR52		
3.1.6. Location of the Ion: Interior-Ion and Exterior-Ion Structures	PR53		
3.1.7. Approach to Condensation	PR54		
3.2. Mixed Clusters	PR54		
3.2.1. Unlimited and Blocked IHB Networks	PR54		
3.2.2. The Location of the Proton	PR54		
3.2.3. Relations between Cluster Composition and Binding Energies	PR55		
3.3. Effects of Partial Solvation on Acidities, Basicities, and on Ionic Aggregation	PR57		
3.3.1. Effects of Partial Solvation on Basicities	PR57		
3.3.2. Effects of Partial Solvation on Ionic Aggregation	PR59		
4. Complex Molecules: Intramolecular and Multiple Bonds	PR60		
4.1. Intramolecular Hydrogen Bonds	PR60		
4.1.1. Thermochemistry of Internal Hydrogen Bonds	PR60		
4.1.2. Thermal Stabilities of Internal Hydrogen Bonds	PR61		
4.1.3. Ring-Size and Strain Effects	PR63		
4.1.4. Mutual Effects of Intramolecular and External Solvation	PR63		
4.2. Polydentate Bonding	PR64		
4.2.1. Thermochemistry and Structures of Polydentate Complexes	PR64		
4.2.2. Solvent Bridges in Polydentate Complexes	PR66		

Received: November 14, 2011

Published: October 10, 2012



5. Spectroscopy of Hydrogen-Bonded Clusters	PR66	8.2. Biological Systems	PR86
5.1. Spectroscopy of Dimers and Correlations Between Bond Energies and Proton Affinities	PR66	8.3. Ionic Hydrogen Bonds in Solids	PR86
5.2. Spectroscopic Effects of Shell Filling and Isomers, and the Location of the Proton	PR67	9. Relations between Clusters and Bulk Solvation: A Cluster-Based Analysis of Ion Solvation Energies and Factors	PR87
5.2.1. Clusters of Water, Alcohols, and Amines with Unlimited IHB Networks	PR67	9.1. Relations between Clusters and Bulk Solvation	PR87
5.2.2. Spectroscopy of Mixed Clusters of Non-blocked and Blocked Components	PR69	9.1.1. Overview of the Thermochemical Results	PR87
5.3. Spectroscopy of Carbon-Based Hydrogen Bonds	PR71	9.1.2. Experimental Observations and Implications	PR87
5.4. Spectroscopy of Carbon-Based Bonds in Ionized Aromatics	PR71	9.1.3. Historical Background of Partial Solvation in Clusters	PR90
5.5. Spectroscopic Consequences of Intramolecular and External Solvation	PR72	9.1.4. Relative Ion Solvation Energies in Small Clusters and in Solution	PR90
5.6. Spectroscopy of IHB Networks about Anions	PR72	9.1.5. Extrapolating from Clusters to Bulk Solvation and the Binding Energies of Large Clusters	PR90
5.7. Summary of Spectroscopic Studies	PR72	9.1.6. Cluster-Based Single-Ion Solvation Energies	PR91
6. Kinetics of Hydrogen-Bond Formation and Dissociation	PR73	9.1.7. Alternative Thermochemical Cycle for Ion Solvation	PR91
6.1. Formation and Dissociation of Hydrogen Bonds	PR73	9.1.8. Relations among Proton Affinities and Bulk Solvation Energies	PR91
6.1.1. Formation of Hydrogen-Bonded Clusters	PR73	9.1.9. Compression of Basicity Scales by Ion Solvation	PR91
6.1.2. Reactions Driven by Hydrogen-Bond Formation: Associative Proton-Transfer Reactions	PR73	9.2. Cluster-Based Analysis of Solvation Factors	PR92
6.1.3. Reactions Driven by Hydrogen-Bond Formation or Dissociation and Entropy-Driven Reactions	PR73	9.2.1. Cluster-Based Procedure to Calculate Solvation Factors	PR93
6.2. Hydrogen-Bonded Complexes as Reaction Intermediates	PR74	9.2.2. Solvation Factors of the $(BH^+ \cdot 4H_2O)$ Clusters	PR93
7. Ionic Hydrogen Bonds in Biomolecules	PR74	9.2.3. Solvation Factors of Onium Ions	PR93
7.1. Intramolecular Solvation and Conformation	PR75	10. Conclusions and Outlook	PR94
7.1.1. Amino Acids and Derivatives	PR75	10.1. Correlations between Bond Strengths and the Relative Acidities and Basicities of the Components	PR94
7.1.2. Peptides	PR75	10.2. Unconventional, Internal, and Polydentate Bonds	PR94
7.1.3. Proteins	PR77	10.3. Hydrogen-Bond Networks	PR94
7.2. Stepwise Solvation of Biological Ions and Mutual Effects of Intramolecular and External Solvation	PR78	10.4. Effects on Acidities and Basicities	PR94
7.2.1. Stepwise Solvation of Amino Acids and Peptides and the Effects of Internal Solvation	PR78	10.5. Biomolecules and the Condensed Phase	PR94
7.2.2. Stepwise Solvation of Amino Acids and Peptides, and the Formation of Zwitterions and Salt Bridges	PR78	10.6. Partial and Bulk Solvation	PR94
7.2.3. Stepwise Hydration of Peptides	PR79	10.7. Large Clusters and Single-Ion Solvation Energies	PR95
7.2.4. Thermochemical and Structural Effects of Stepwise Hydration	PR80	10.8. Compression of Basicity Scales by Ion Solvation	PR95
7.3. Intermolecular Association and Polydentate Bonding in Biological Ions	PR80	10.9. Cluster-Based Analysis of Solvation Factors	PR95
7.4. Ionic Hydrogen Bonds in Nucleic Bases, Nucleosides, and Nucleotides	PR81	10.10. Outlook	PR95
7.5. Cluster Models of Bioenergetics	PR81	Author Information	PR95
7.5.1. Enzymatic Hydration of CO_2	PR81	Corresponding Author	PR95
7.5.2. Enzyme Energetics: Ionic Hydrogen Bonds to Backbone Peptide Links	PR81	Notes	PR95
7.5.3. Formation of Biological Membranes	PR83	Biography	PR95
7.5.4. Proton Transport in Membranes	PR83	Acknowledgments	PR95
7.5.5. Acetylcholine Neuroreceptors	PR83	References	PR95
8. Ionic Hydrogen Bonds in the Condensed Phase	PR83	1. INTRODUCTION AND OVERVIEW	
8.1. Dimers, Intramolecular Bonds, and IHB Chains	PR83	1.1. Historical Background	
8.1.1. Homodimers and Heterodimers	PR84	Hydrogen bonds ^{1,2} are one of the principal intermolecular forces. A special class are strong ionic hydrogen bonds (IHBs) that form between ions and molecules with bond strengths of 5–35 kcal/mol, up to a third of the strength of covalent bonds. Because of these properties, these bonds are also known as strong hydrogen bonds. These strong hydrogen bonds are	
8.1.2. Intramolecular and Polydentate Bonds	PR85		
8.1.3. Hydrogen-Bond Chains	PR85		
	PR85		
	PR86		

critical, for example, in ionic clusters and nucleation; in electrolytes, ion solvation, and acid–base chemistry; in the structures of ionic crystals, surfaces, silicates, and clays; in surface adsorption; and in self-assembly in supramolecular chemistry and molecular crystals.³ IHBs are also important in bioenergetics including protein folding, enzyme-active centers, formation of membranes and proton transport, and biomolecular recognition. With such wide-ranging roles, the fundamental properties of strong ionic hydrogen bond interactions need to be understood.

The energetics of IHB interactions cannot be isolated and quantified in the condensed phase. However, these interactions can be isolated and studied quantitatively in the gas phase. These studies lead to a fundamental understanding of relations between strong ionic hydrogen bond strengths and molecular structure, the solvation of ions, especially in the critical inner shells, and acid–base phenomena and bioenergetics.

This review will present the basic insights that have been obtained in the past four decades. It will present a comprehensive review of the thermochemistry and its structural implications obtained from ab initio calculations. Relevant recent results from spectroscopy also will be illustrated.

The advent of variable-temperature high-pressure mass spectrometry (HPMS) introduced by Field and co-workers in the 1960s⁴ and pulsed high-pressure mass spectrometry (PHPMS) introduced by Kebarle in the late 1960s⁵ have been particularly significant. These workers realized that, at pressures of several torrs and gas densities of 10^{16} – 10^{17} cm⁻³ in ion sources, ions can undergo 10^3 – 10^6 collisions with neutral molecules during typical residence times of 0.1–10 ms and establish thermal ion populations and equilibria. This method can measure equilibrium constants for ion-neutral association reactions usually involving 1–8, sometimes up to 20, ligand molecules.

Many of these studies addressed hydrogen-bonded adducts formed in reaction 1 where the hydrogen donor ion, BH⁺, is usually a protonated base and the hydrogen receptor, B', is a base with an electron donor heteroatom (“unconventional” carbon-based IHBs will be also reviewed).



The anionic counterpart is reaction 2, where A⁻ is usually a deprotonated Bronsted acid and AH is a hydrogen donor, usually a Bronsted base.



In pulsed, time-resolved experiments, equilibrium can be verified when the product/reactant ion ratio, [BH⁺·B']/[BH⁺], reaches a constant value as a function of reaction time. The equilibrium constant K is then calculated from eq 3, where P(B') is the partial pressure of B' in the ion source.

$$K = \frac{[\text{BH}^+\cdot\text{B}']}{\text{P}(\text{B}')[\text{BH}^+\cdot\text{B}']} \quad (3)$$

Temperature studies yield the IHB bond dissociation enthalpies, $\Delta H^\circ_{\text{D}}$, and entropies, $\Delta S^\circ_{\text{D}}$. The uncertainty of $\Delta H^\circ_{\text{D}}$ values measured by pulsed high-pressure mass spectrometry is usually ± 1 kcal/mol, and that of $\Delta S^\circ_{\text{D}}$ is ± 1.5 cal/(mol K).

Information on IHB bond strengths can also be obtained from ligand exchange equilibria, which were used in low-pressure ion-cyclotron resonance (ICR)^{6–10} and selected injection ion flow (SIFT) measurements.¹¹ More recently, equilibria are being measured by variable-temperature drift cell ion mobility

apparatus that provides both thermochemical and structural information. Applications of these methods to ion solvation and biomolecules were introduced by Bowers, Kemper, Wyttenbach, and co-workers.^{12a–c,13} Thermochemical data are also being obtained by threshold dissociation measurements on cluster ions,¹⁴ and recently, by zero-pressure blackbody infrared thermal dissociation (BIRD) measurements.^{15–18} The latter can be applied to systems not amenable to equilibrium measurements, for example, clusters with involatile ligands and clusters generated by electrospray, allowing studies on bioions and multiply charged ions.

Cluster hydrogen bond energies correlate with proton affinities (PAs) and gas-phase acidities and basicities. Extensive PA scales were constructed by Yamdagni and Kebrale,¹⁹ Taft,²⁰ Meot-Ner and Sieck,²¹ Szuleko and McMahon,²² and Radom and co-workers^{23,24} and tabulated by Hunter and Lias.²⁵ Our recent review found that these scales can be reconciled within ± 0.8 kcal/mol for 38 key reference compounds spanning a PA range of 120 kcal/mol.²⁶ PA values in the NIST database²⁷ that are used here are accurate to this level.

Experimental thermochemical data on cluster ions, including hydrogen-bonded clusters, were compiled by Keesee and Castleman.²⁸ A recent updated computer-based compilation contains over 2000 items of thermochemical data,²⁹ and anion cluster data also appear in a tabulation of anion thermochemistry.³⁰ Theoretical work on IHB interactions was reviewed recently,^{31,32a} and the relation between the symmetry, length, and strengths of hydrogen bonds was also reviewed recently.^{32b,c}

From the 1960s through the 1980s, the thermochemistry of strong ionic hydrogen bonds was studied in cluster ions, with structures inferred from thermochemistry and ab initio calculations. These studies revealed some general features:

- Correlations between the proton affinities, hydrogen-bond strengths, and partial donor–acceptor proton transfer (in donor N and O bases).
- Filling of solvent shells and formation of ring and cage structures in higher solvation steps.
- Competition between solvation and aggregation in multicomponent clusters (acetic acid/water clusters).
- Protonated solvent cores surrounded by blocked ligands (water/acetonitrile, ether, and ketone clusters).
- Unconventional carbon-based and π -complex IHBs.
- Intramolecular and strained IHBs in polyfunctional ions (in diamines, dialcohols, diketones, polyethers, and amino acid derivatives).
- Mutual weakening of internal and external solvation (in diamines, polyethers, and amino acid derivatives).
- Formation of solvent bridges, zwitterions, and salt bridges (in diethers and carboxylic acid/water clusters).
- Polydentate bonds between ions and polyfunctional ligands (polyethers).
- Relative solvation energies by 4–6 H₂O molecules that reproduce the relative bulk solvation energies of diverse onium ions; consequently, the enthalpies of further bulk solvation are similar for these ions, although it introduces very different solvation terms for these ions.
- Increasing basicity reflects increasing charge delocalization in BH⁺ ions, leading to weaker hydrogen bonds to solvent molecules and less efficient ion solvation.
- As a result, basicity scales are much compressed and sometimes reversed in solution versus the gas phase.

Table 1. Representative Thermochemistry of Homodimers $\text{BH}^+\cdot\text{B}$ and Hydrated Complexes $\text{BH}^+\cdot\text{H}_2\text{O}$ and $\text{BH}^+\cdot 4\text{H}_2\text{O}^\alpha$

BH^+	PA(B) ^b	$\Delta H^\circ_{\text{internal}}$ ($\Delta H^\circ_{\text{strain}}$) ^c	$\Delta H^\circ_{\text{D}}$ ($\text{BH}^+\cdot\text{B}$) ^d	$\Delta H^\circ_{\text{D}}$ ($\text{BH}^+\cdot\text{H}_2\text{O}$) ^d	$\Delta H^\circ_{\text{D}}$ ($\text{BH}^+\cdot 4\text{H}_2\text{O}$) ^d	$-\Delta H^\circ_{\text{g}\rightarrow\text{aq}}$ (BH^+) ^e	$-\Delta H^\circ_{\text{g}\rightarrow\text{aq}}$ (IHB) ^e	$-\Delta H^\circ_{\text{g}\rightarrow\text{aq}}$ (hydrophobic) ^e	$-\Delta H^\circ_{\text{g}\rightarrow\text{aq}}$ ($\text{BH}^+\cdot 4\text{H}_2\text{O}$) ^e	$\Delta S^\circ_{\text{D}}$ ($\text{BH}^+\cdot\text{B}$) ^d
H_3O^+	165.0		32.1	32.1	81.9	117.0	44.5		75.3	26.4
MeOH_2^+	180.3		32.5	26.4	72.8	101.3	38.0	13.2	70.5	28.8
$(\text{Me})_2\text{OH}^+$	189.0		31.4	23.4	62.3	92.6	26.8	24.9	72.8	30.8
$(\text{MeOCH}_2\text{CH}_2\text{OMe})\text{H}^+$	205.1	10 (21)	27.4	16.4	54.2					30.9
$(\text{Me}(\text{OCH}_2\text{CH}_2)_2\text{OMe})\text{H}^+$	219.6	25	21.3	17.6	51.1					38.0
NH_4^+	204.0		25.2	20.2	59.0	88.6	28.5	(0)	68.1	26.3
MeNH_3^+	214.9		23.6	17.8	55.1	81.0	25.6	8.1	69.0	25.5
Me_2NH_2^+	222.2		22.5	15.0	50.3	74.6	20.2	15.3	67.2	26.9
Me_3NH^+	226.8		22.2	14.5	45.2	66.8	12.6	21.2	64.5	28.8
Et_3NH^+	234.7		23.8	13.2		63.9	9.8	34.0	68.6	41.0
pyridine H^+	222.2		25.0	15.6	41.1	66.3	10.3	25.3	67.2	29.5
$\text{H}_2\text{NCH}_2\text{CH}_2\text{CH}_2\text{NH}_3^+$	235.9	16 (8)		11.4						
H_3S^+	168.0		15.1	21.2						20.3

^aInternal hydrogen-bond strengths, cluster bonding energies, solvation enthalpies, and solvation factors were derived using cluster thermochemistry. All ΔH° values are in kcal/mol, and ΔS° are in cal/(mol K). ^bProton affinities from ref 27. ^cBond strength and strain (in parentheses) of internal IHBs.³³ ^dAverage or recommended values from ref 34. ^eCalculated as in ref 35 but using updated thermochemistry (see Tables 11 and 12). Ionic hydrogen bonding and hydrophobic solvation factors in ion solvation are based on solvation factor analysis.³⁵

- Cluster-based analysis that quantifies IHB and hydrophobic solvation in simple terms; it shows that each $\text{NH}^+\cdots\text{OH}_2$, $\text{OH}^+\cdots\text{OH}_2$, $\text{CH}^{\delta+}\cdots\text{OH}_2$ bond contributes a constant term to the solvation energies of diverse onium ions.

These effects were identified in model compounds that were sufficiently volatile for gas-phase studies. Important advances since the 1990s, many since the 2005 version of this review, were made by spectroscopy that confirmed several of the listed effects. Further, new methods, especially electrospray, allowed the studies of IHBs in involatile compounds. Several of the listed effects have been confirmed in ionized peptides, proteins, nucleotides, and organometallics. This update article reviews in some detail these new results and their relation to the earlier findings in volatile compounds.

1.2. An Overview of IHB Structures and Energetics

The main structure–energy relations in IHB systems are illustrated by the examples in Table 1 and then summarized in a general overview. The following are the major trends observed in ionic hydrogen-bond systems.

1.2.1. Dimers.

1. Ionic hydrogen bonds (IHBs) are strong intermolecular forces with bond strengths usually of 5–35 kcal/mol. IHBs form both in cationic and in anionic systems.
2. The formation of the $\text{B}-\text{H}^+\cdot\text{B}'$ bond involves partial proton transfer from the donor to the acceptor. The bond strengths correlate with the efficiency of proton transfer. The bonding proton becomes more positive, the acceptor and donor heteroatoms become more negative, the $\text{B}-\text{H}^+$ bond of the donor lengthens upon the formation of the complex, and part of the charge is transferred to the acceptor. In anions, similar changes occur in forming $\text{A}-\text{H}\cdot\text{A}^-$ bonds.
3. In homodimers $\text{BH}^+\cdot\text{B}$, for example, $(\text{H}_2\text{O})_2\text{H}^+$, $(\text{MeOH})_2\text{H}^+$, and $(\text{Me}_2\text{O})_2\text{H}^+$, and in anionic homodimers, $\text{A}-\text{H}\cdot\text{A}^-$, both components have equal proton affinities (PAs) or acidities and share the proton efficiently. The bond strengths in the homodimers $\text{R}_2\text{OH}^+\cdot\text{OR}_2$ and $\text{R}_3\text{NH}^+\cdot\text{NR}_3^-$ are affected little by the absolute proton affinities of the monomers (see Table 1, column 4).
4. In heterodimers $\text{BH}^+\cdot\text{B}'$, the bond strengths decrease with increasing PA difference (ΔPA) between the

components, as a donor with a higher PA transfers proton less efficiently to an acceptor with a lower PA (for example, see the $\text{BH}^+\cdot\text{H}_2\text{O}$ complexes in Table 1, column 5). Quantitatively, inverse linear correlations are observed between the bond dissociation energies, $\Delta H^\circ_{\text{D}}$, and ΔPA over wide ranges of ΔPA (up to 60 kcal/mol). In anions, similar correlations are observed between $\text{AH}\cdot\text{A}^-$ bond strengths and the relative acid dissociation energies. These relationship between ΔPA , bond energies, and partial proton transfer were confirmed recently by spectroscopy.

5. The formation of dimers involves significant negative entropy changes, that is, the dimers have large positive entropies of dissociation, $\Delta S^\circ_{\text{D}}$, usually 20–30 cal/(mol K). These entropy changes are smaller than those associated with covalent bond formation, due to internal rotation and low-frequency vibrations that are retained about the hydrogen bond in the dimers. However, steric hindrance (e.g., $(\text{Et}_3\text{N})_2\text{H}^+$ in Table 1) or polydentate bonding can lead to $\Delta S^\circ_{\text{D}}$ values up to 60 cal/(mol K).
6. Unconventional carbon-based IHBs form where the donors are hydrocarbon CH groups and/or the acceptors are carbon lone pairs, olefin double bonds, or aromatic π -systems.

1.2.2. Higher Clusters.

7. Several ligand molecules can add stepwise to ions to form clusters $\text{BH}^+\cdot n\text{L}$. In many clustering sequences, the consecutive binding energies, $\Delta H^\circ_{n-1,n}$, decrease by a factor of 0.7 ± 0.1 with each consecutive step.
8. The bonding energies of consecutive solvent molecules to ions approach the condensation enthalpy of the bulk solvent within ± 1 kcal/mol, usually after as few as 4–6 solvent molecules.
9. Large clusters often have many isomeric structures with similar energies, which may coexist in equilibrium under thermal conditions.
10. Clusters of nonblocked components can form indefinite hydrogen-bond networks. Filled solvent shells and cyclic solution-like IHB networks may start to develop already after 2–4 solvent molecules bind. In mixed nonblocked clusters of a given size, the stability of the IHB network

- increases with increasing mole fraction of the stronger base.
11. The filling of solvent shells can cause drops of 1–4 kcal/mol in the consecutive binding energies. Larger drops are observed when blocked components (e.g., Me₂O and Me₃N) fill a shell and prevent the formation of further strong IHBs.
 12. In mixed clusters of unblocked and blocked components, the protons can be transferred to the former, often water, to form a (H₂O)_nH⁺ core where the proton is stabilized by a network of strong hydrogen bonds. The proton can remain in a water core even when it is surrounded by alkyl-blocked molecules that have higher proton affinities. This has significant biological consequences, as in membrane transport.
 13. Solvation compresses, and sometimes reverses, the intrinsic gas-phase acidities and basicities of molecules. The solvent effects on acidities and basicities can be as significant as the effects of the intrinsic molecular parameters themselves. Energies of ionic aggregation to form B_nH⁺ aggregates are also compressed by stepwise solvation.
 14. Cluster studies show the stepwise development of solvation effects. A large fraction of these effects, often 80% or more, results from the first 4–6 solvent molecules.
 15. All of these observations are paralleled in anionic clusters, where the role of proton affinity (PA(B)) is replaced by PA(A⁻) (i.e., the acid dissociation enthalpy, ΔH°_{acid} (AH)).

1.2.3. Polyfunctional Molecules, Biomolecules, and Cluster Models of Bioenergetics.

16. Polyfunctional molecules show increased proton affinities and significant negative entropies of protonation compared with monofunctional analogues. These effects indicate the formation of internal hydrogen bonds (iIHBs) of 4–30 kcal/mol (see polyethers and diamine in Table 1).
17. Internal IHBs can create strained cyclic structures. The strain decreases and the bond becomes stronger with increasing ring size.
18. External solvation decreases the strength of internal hydrogen bonds. Conversely, internal hydrogen bonds weaken bonds to external solvent molecules. In these respects the internal hydrogen bond serves as the first solvent molecule.
19. Solvent molecules can insert into the internal hydrogen bond to form solvent bridges between the functional groups.
20. The bonding of ions to polydentate ligands shows increased bond strengths and negative entropies of complexation compared with monodentate ligands, due to multiple IHBs and electrostatic stabilization of the charge by several polar groups.
21. In protonated polyfunctional ions, hydrogen-bonded solvent bridges can form between functional groups.
22. Ligands bond strongly to multiply protonated ions. The bonding becomes stronger with decreasing separation and increasing Coulomb repulsion between the charges.
23. Internal and polydentate IHBs are common in protonated polyfunctional biomolecules. Interactions between internal IHB and external solvation can affect the conformation of biomolecules.
24. Cluster models suggest that IHBs to protein backbone amide NH or CO groups can stabilize ionic intermediates

by 35 kcal/mol. In proton transport, cluster models suggest that the proton can remain in the water chain even when surrounded by strongly basic protein groups.

25. Several ionic hydrogen-bond effects were inferred from thermochemistry and computation: relations between ΔPA, IHB bond energies, and partial proton transfer; protonated solvent cores surrounded by blocked ligands; the formation of solvent bridges between functional groups; and the formation of zwitterions and salt bridges. These effects have been confirmed recently by spectroscopy and extended biomolecules.

1.2.4. Relationship between Gas-Phase and Bulk Solvation.

26. The relative solvation energies by 4 H₂O molecules reproduce the relative bulk hydration enthalpies of diverse ions. This applies although continuum solvent terms and hydrophobic hydration are present only in solution but not in the clusters.
27. This relation shows that the energies of solvent cavity formation, dielectric charging, and hydrophobic solvation vary in an almost exactly canceling manner in the hydration of ions of diverse sizes and structures, although these terms are physically independent.
28. Quantitatively, the cluster solvation enthalpies, ΔH°_{g-aq} (BH⁺·4H₂O), are 70 ± 3 kcal/mol for diverse ions (Table 1, column 10). This result quantifies the cumulative excess cluster ion binding energies from $n = 5$ to ∞ of diverse ions as a constant 70 ± 3 kcal/mol.
29. Alternatively, result 26 yields cluster-based, purely single-ion solvation energies smaller by 70 ± 3 kcal/mol than the conventional solvation energies that are derived from solutions with ion pairs.
30. The binding energies of solvent molecules approach within ±1 kcal/mol the macroscopic condensation enthalpy of water, -10.5 kcal/mol, already after 4–6 solvent molecules. If this value remains constant in higher clusters, the cluster-based ion solvation energies in point 29 apply. The correct interpretations of cluster data, point 28 or 29, may be identified by accurate data on large clusters.
31. A cluster-based analysis decomposes ion solvation into a few simple factors. It shows that each protic hydrogen contributes a constant term and each CH hydrogen contributes a smaller constant term to the enthalpies of hydration (e.g., -10 kcal/mol by R₂NH⁺···OH₂ bond, 2.5 kcal/mol by CH^{δ+}···OH₂ bond of alkylammonium ions).
32. In extension of the gas-phase bond energy/ΔPA correlations, the bulk hydration energies of diverse onium ions, ΔH°_{g-aq} (BH⁺), can be predicted from one parameter, the gas-phase proton affinities of the bases B alone.

2. HYDROGEN-BONDED DIMERS

2.1. Thermochemistry and Structures of Hydrogen-Bonded Dimers

- 2.1.1. Structural Effects of Ionic Hydrogen-Bond Formation. The formation of IHBs causes a redistribution of atomic charges and changes in bond lengths and angles. The changes affect primarily the bonding proton, the donor and acceptor heteroatoms, and the B-H⁺···B' or A-H···A⁻ bond

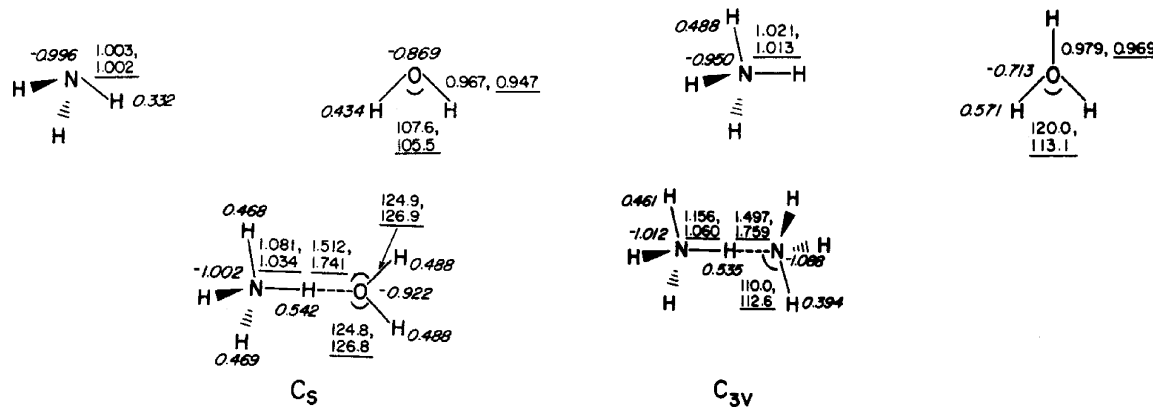


Figure 1. Geometries and atomic charge densities of H_2O , NH_3 , NH_4^+ , $\text{NH}_4^+\cdot\text{H}_2\text{O}$, and $\text{NH}_4^+\cdot\text{NH}_3$. Structures were calculated from 3-21G and 6-31G* (underlined) optimizations. Only the values of the bond lengths (in Å) and bond angles (in degrees) that were varied in the computations are shown. Atomic charges from population analysis (6-31G* basis set) are given in italics. Reproduced with permission from ref 36. Copyright 1986 American Chemical Society.

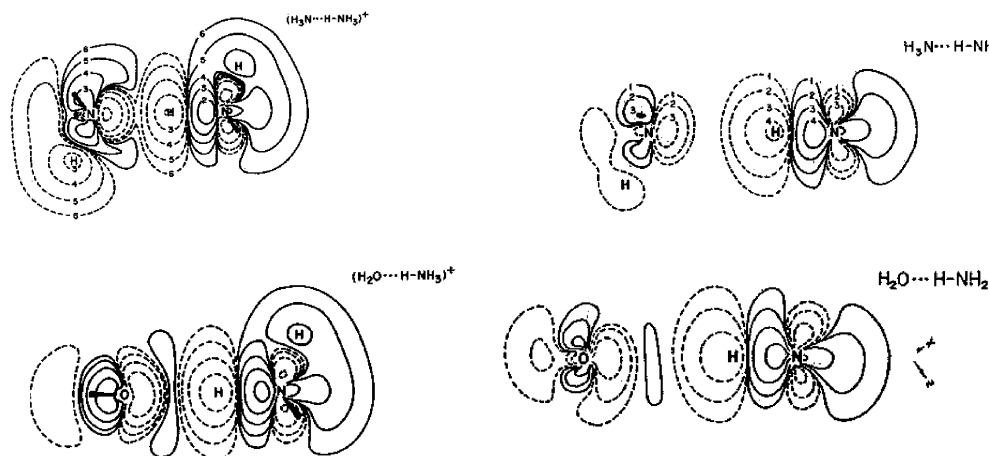


Figure 2. Charge density changes upon the formation of hydrogen-bonded ionic and analogous neutral complexes. Solid lines correspond to electron density gain and dotted lines to loss, as obtained from 4-31G calculations. The scale (in $e/\text{\AA}^3$) is as follows: 1 = 0.676; 2 = 0.214; 3 = 0.0676; 4 = 0.0214; 5 = 0.00676; 6 = 0.00214. Reproduced with permission from ref 37. Copyright 1980 American Physical Society.

lengths. The IHB bond strengths are correlated with these changes.

Examples of the strengths of IHBs in dimers are given in Table 1, and the bond strengths are illustrated in the 0,1 equilibria in Tables 4–6. The thermochemistry and structures were subject to extensive theoretical studies that were reviewed recently.^{31,32a}

Some of the basic effects of IHB formation are illustrated in Figure 1 by the prototype homodimer $\text{NH}_4^+\cdot\text{NH}_3$ and heterodimer $\text{NH}_4^+\cdot\text{H}_2\text{O}$.³⁶ The changes in charge densities upon complex formation are illustrated in Figure 2. The bonding hydrogen always loses electron density and becomes more positive (dotted lines), whereas the acceptor and donor heteroatoms always gain electron density and become more negative (solid lines). The same areas experience gain or lose charge in the ionic and in the analogous neutral complexes, but the changes are larger in the more strongly bonded dimer ions. Also, the changes are larger in the more strongly bonded $\text{NH}_4^+\cdot\text{NH}_3$ homodimer than in the $\text{NH}_4^+\cdot\text{H}_2\text{O}$ heterodimer. In the heterodimer, an area of electron density gain develops between the proton and the acceptor O atom. This gain becomes more pronounced with acceptor atoms of greater electronegativity, such as in complexes of NH_4^+ with HF, PH₃, H₂S, and HCl. Charge loss about the proton decreases in the

same order. A strong correlation exists between the bond strength and the electron gain in the donor bond. This shows the significance of the proton donor in determining the properties of the strong ionic hydrogen bond.³⁷

The examples in Figures 1 and 2 show that, compared with the uncomplexed species, the formation of the hydrogen bond increases the positive charge on the bonding proton, increases the negative charges on the hydrogen donor and acceptor atoms, delocalizes some of the net positive charge from the donor molecule onto the acceptor molecule, and increases the B–H⁺ bond length of the hydrogen donor.

These changes are largest when the two components are identical and the proton is shared efficiently. In heterodimers, the effects of forming the bond, along with the bond strengths, decrease with increasing proton affinity difference (ΔPA) between the components.^{38,39} All of the above features are observed in the model dimers $\text{NH}_4^+\cdot\text{NH}_3$ and $\text{NH}_4^+\cdot\text{H}_2\text{O}$ in Figure 1, which compares the homodimer $\text{NH}_4^+\cdot\text{NH}_3$ where $\Delta PA = 0$ and $\Delta H^\circ_D = 25.7 \text{ kcal/mol}$ with the more weakly bonded heterodimer $\text{NH}_4^+\cdot\text{H}_2\text{O}$ where $\Delta PA = 39.5 \text{ kcal/mol}$ and $\Delta H^\circ_D = 20.2 \text{ kcal/mol}$. Comparing $\text{NH}_4^+\cdot\text{NH}_3$ with $\text{NH}_4^+\cdot\text{H}_2\text{O}$, the amount of charge transferred from the ion to the neutral decreases from 0.094 to 0.054 unit charge and the N–H⁺ bond becomes less stretched, from 1.060 to 1.034 Å, in

the more weakly bonded heterodimer. Also, the length of the hydrogen bond increases with decreasing bond strength. Similar trends were found by Desmeules and Allen in an ab initio 4-31G study of complexes of NH_3 , H_2O , FH , PH_3 , SH_2 , and HCl .³⁷ These workers, as well as Kebarle and co-workers, analyzed IHB bond strengths as a function of proton transfer in the bond. Figure 3 shows that the bond strengths correlate with the degree of proton transfer in the bonds as measured by the

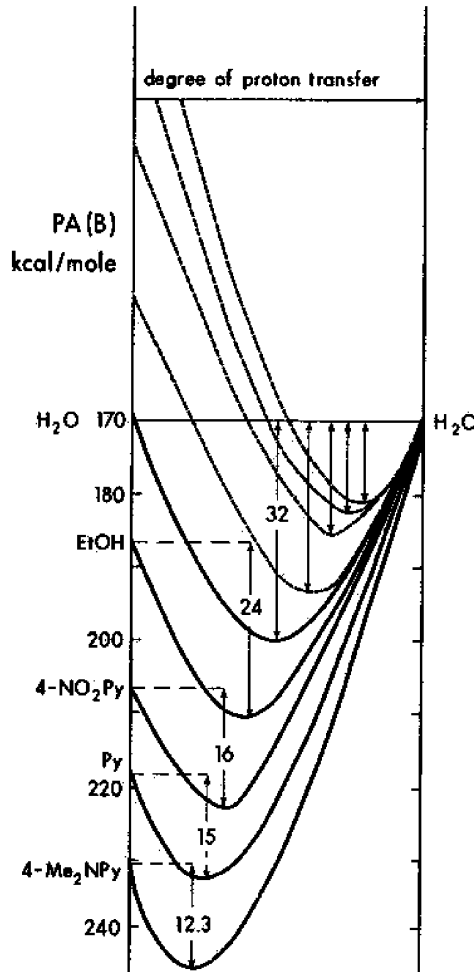


Figure 3. Plot of stabilization energies, E_s , due to hydrogen bonding in $\text{BH}^+\cdot\text{H}_2\text{O}$ complexes, corresponding to dissociation to $\text{BH}^+ + \text{H}_2\text{O}$ (solid curves) or to $\text{H}_3\text{O}^+ + \text{B}$ (dashed curves), where B are substituted pyridines with proton affinities shown on the y coordinates. The minima show the hydrogen-bond energies from experimental data. The degree of proton transfer from BH^+ to H_2O (horizontal coordinate) is arbitrarily chosen. The diagram illustrates how the energy minima may be reached at further distances from the donor on the left and may be deeper as $\text{PA}(\text{B})$ decreases and approaches $\text{PA}(\text{H}_2\text{O})$ and the proton can be transferred more efficiently to H_2O , proceeding up from lower to higher curves. The hypothetical dashed curves suggest that the binding energy would decrease further and the proton would be bound to H_2O with proton donors when the PAs of the proton are lower than those of water. Reproduced with permission from ref 40a. Copyright 1979 American Chemical Society.

$\text{B}-\text{H}^+$ bond length.^{40a} The thermochemical relationships among the relative PAs, the IHB bond strengths, and proton sharing were confirmed spectroscopically,^{40b-g} as discussed later.

As suggested in Figure 3, Desmeules and Allen showed that in hydride dimers the stretching of the $\text{B}-\text{H}^+$ bond is related inversely to the ΔPA (Figure 4). In turn, there is an inverse

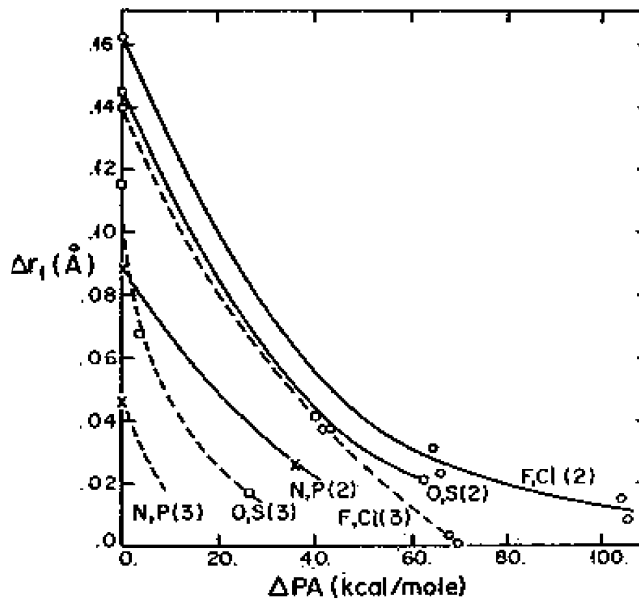


Figure 4. Correlation of the calculated proton movement, that is, increase of $\text{B}-\text{H}^+$ bond length upon bond formation, with ΔPA for the hydrides of the electron donors as indicated with second row proton donors (solid lines) and third row proton donors (dashed lines). The inverse correlation shows that with increasing ΔPA the proton is shared less efficiently, which in turn decreases the bond strength (see Figure 5). Reproduced from ref 37 with permission. Copyright 1980 American Physical Society.

linear correlation between the lengths of the $\text{B}-\text{H}^+$ bonds and the bond strength (Figure 5). Together, these theoretical results imply an inverse relation between the ΔPA and the hydrogen bond strength.³⁷ These results are consistent with experimental observations.

In a set of dimers, the IHB bond strengths also correlate with charges on the acceptor and donor atoms before and after bond formation. In a set of dimers between various hydrogen-donor ions and a given ligand, the main parameter that affects the bond strength is the charge on the bonding hydrogen atom (q_h). Examples were found by the Kebarle group for (pyridinium) $\text{H}^+\cdot\text{H}_2\text{O}$ complexes^{40a} (Figure 6) and for bonds of ROH with halide anions.⁴¹

The relation between charge densities on the donor (q_h), the electron density on the receptor, the amount of charge transfer in the complex (Δq_{CT}), and the bonding energies apply both in conventional and in unconventional carbon-based IHBs. For example, both in $\text{RNH}_3^+\cdot\text{RCN}$ (with nitrogen acceptors) and in $\text{BH}^+\cdot\text{RNC}$ complexes (with C lone-pair acceptors), ΔE_D correlates with the parameter $q_{\text{H}}q_B/r_2$ (q_B is the charge on the hydrogen-receptor atom prior to hydrogen-bond formation and r_2 is the distance between the hydrogen-bonded proton and the receptor atom) and also with the amount of charge transferred, Δq_{CT} .⁴² Interestingly, the bonding energies of complexes of cyanide and isocyanide ligands are comparable, but the charge transfer, Δq_{CT} , and the stretching of the donor bond are larger with the isocyanide acceptors, consistent with the greater σ -donating ability and lower ionization potential of the isocyanide bases. These data suggest that the relative importance of the

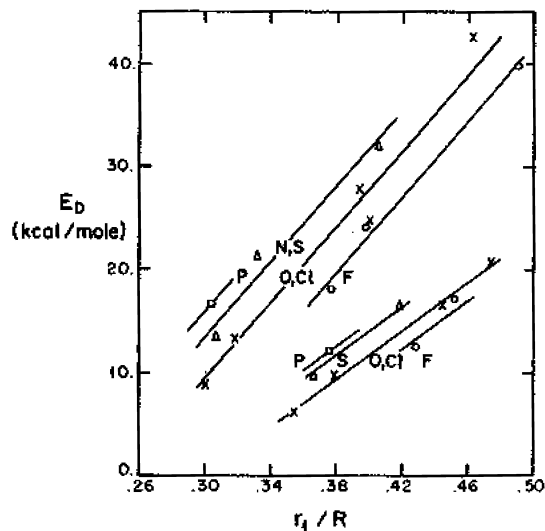


Figure 5. Correlation of calculated bond dissociation energies, E_D , with the $B-\text{H}^+$ bond length expressed as r_1/R ($r_1 = \text{B}-\text{H}^+$ bond length, $R = \text{B}$ to B' bond length in $\text{B}-\text{H}^+\cdot\text{B}'$) for various hydrides as electron donors. Upper set of four lines are for complexes with second row proton donors and the lower set of four for those with third row proton donors. Increasing r_1/R corresponds to shifting the proton from the donor to the acceptor, that is, better proton sharing. The plot shows that this correlates with increasing bond strength. Reproduced with permission from ref 37. Copyright 1980 American Physical Society.

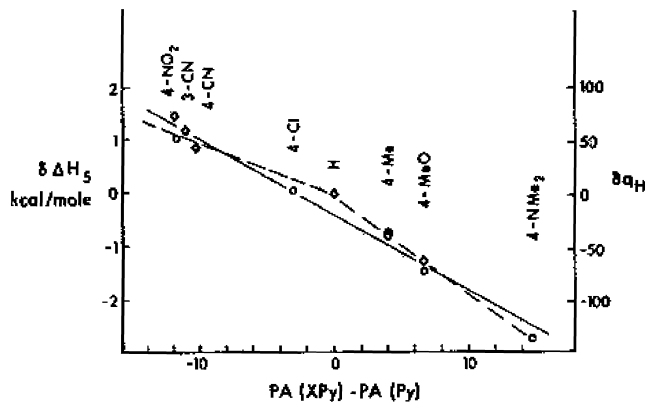


Figure 6. Correlation between the proton affinity differences and the relative positive charge on the bonding hydrogen atom (q_H) and bond strength in (pyridinium ion) $\text{H}^+\cdot\text{H}_2\text{O}$ complexes. Reproduced with permission from ref 40a. Copyright 1979 American Chemical Society.

electrostatic and delocalization components differ in the cyano and isocyanide complexes.⁴² The effect of q_H on the bond strength depends on the donor–ligand geometry and distance. For example, the interaction energy of NH_4^+ with a model dipole depends strongly on the charge distribution in NH_4^+ , on its orientation, and especially on the ion–dipole distance. At short distances, the charge on the bonding hydrogen would be significant, but at realistic bond distances, the ion acts as if it were a point charge concentrated at its center (see Figure 17).^{43a}

2.2. Hydrogen-Bond Strengths and Correlations with Proton Affinities

2.2.1. Cationic Dimers and Correlations with Proton Affinities. In the preceding sections, we noted relationships between hydrogen-bond strengths and relative proton affinities

of the components. Such relations apply from dimers of small molecules to those of complex organics.

In small molecules, such relations were observed spectroscopically; in the infrared, vibrational predissociation spectra of $\text{OCH}^+\cdot\text{H}_2$ and $\text{N}_2\text{H}^+\cdot\text{H}_2$ indicated T-shaped complexes.^{44,45} The proton assumes a position between B and H_2 in these complexes that depends on the relative PAs. With increasing $\text{PA}(\text{B})$, the system is transformed from an $\text{H}_3^+\cdot\text{B}$ to a $\text{BH}^+\cdot\text{H}_2$ structure. When the bond $\text{BH}^+\cdot\text{H}_2$ is formed, electron density shifts from the H_2 ligand σ -bond to the protonated ion to establish the intermolecular bond. The H–H stretching motion becomes coupled to the intermolecular motion, weakening the H_2 bond and resulting in a red shift of the H–H vibration. These effects are inversely related to the PA difference. For example, the BH^+-H_2 shift is largest, 251 cm^{-1} in $\text{H}_3^+\cdot\text{H}_2$, 199 cm^{-1} in $\text{N}_2\text{H}^+\cdot\text{H}_2$, 100 cm^{-1} in $\text{OCH}^+\cdot\text{H}_2$, and 115 cm^{-1} in $\text{OH}_3^+\cdot\text{H}_2$. Similar trends were observed in the complexes of HeH^+ , NeH^+ , ArH^+ , KrH^+ , N_2H^+ , and HCO^+ with H_2 .⁴⁶ In a complex where the PAs are reasonably close, such as in $\text{N}_2\text{H}^+\cdot\text{H}_2$ where $\Delta\text{PA} = 18\text{ kcal/mol}$, a significant shift of -170 cm^{-1} also occurs in the H_2 stretch and of $>700\text{ cm}^{-1}$ in the $\text{N}-\text{H}^+$ stretch, and rapid vibrational predissociation was observed in the H–H and N–H⁺ stretches. The magnitudes of all of these changes correlate with the PA differences of the components.^{44,45}

In all the above dimer ions, the components are free to assume geometries where the hydrogen bond can optimize. In a constrained system, the bond may be stretched or bent, causing significant weakening.⁴⁷

In more complex molecules, the bonding energies of several hundred dimers with strong ionic hydrogen bonds have been measured. Some of the major studies concern $\text{NH}^+\cdot\text{N}$ amine dimers,³⁹ $\text{BH}^+\cdot\text{H}_2\text{O}$ complexes,^{40a,48–50,51a,b} $\text{OH}^+\cdot\text{O}$ dimers,⁵⁰ complexes $\text{CH}_3\text{NH}_3^+\cdot\text{B}$ and $\text{NH}^+\cdot\text{O}$ dimers,⁴⁸ and $\text{BH}^+\cdot\text{CH}_3\text{CN}$ complexes.^{51c} The large amount of data yields some general structure–energy relations.

Correlations between the bond dissociation energies, ΔH°_D , and the proton affinity difference between the components, ΔPA , were first observed by the Kellar group.^{38,39,52} For anions, similar relations apply between ΔH°_D and the acid dissociation energy difference, $\Delta\Delta H^\circ_{\text{acid}}$, between the components. Note that this is equivalent to proton affinity differences as $\Delta H^\circ_{\text{acid}} (\text{A}^--\text{H}^+) = \text{PA}(\text{A}^-)$. Kellar and co-workers interpreted these relations in terms of the efficiency of partial proton transfer in $\text{R}_3\text{NH}^+\cdot\text{NR}_3$ and $\text{Cl}^-\cdot\text{HR}$ complexes and showed an extended correlation between ΔPA (from 0 to 64 kcal/mol) and ΔH°_D (from 32 to 12 kcal/mol) for the association of H_2O with OH^+ and NH^+ groups in protonated O and N bases, especially in substituted pyridines.^{40a}

For a set of $\text{OH}^+\cdot\text{O}$ dimers, Larson and McMahon⁵⁰ found linear relations involving the ΔH°_D and ΔPA in homodimers $\text{BH}^+\cdot\text{B}$ and heterodimers $\text{BH}^+\cdot\text{B}'$ for dissociations to BH^+ or BH^+ (Figure 7), leading to eqs 4 and 5.

$$\begin{aligned}\Delta H^\circ_D(\text{BH}^+\cdot\text{B}') - \Delta H^\circ_D(\text{BH}^+\cdot\text{B}) \\ = 0.46(\text{PA}(\text{B}') - \text{PA}(\text{B}))\end{aligned}\quad (4)$$

$$\begin{aligned}\Delta H^\circ_D(\text{B}'\text{H}^+\cdot\text{B}) - \Delta H^\circ_D(\text{BH}^+\cdot\text{B}) \\ = -0.54(\text{PA}(\text{B}') - \text{PA}(\text{B}))\end{aligned}\quad (5)$$

In the same period, many dimers $\text{BH}^+\cdot\text{B}'$ with various *n*-donor heteroatom combinations were investigated by Meot-Ner and

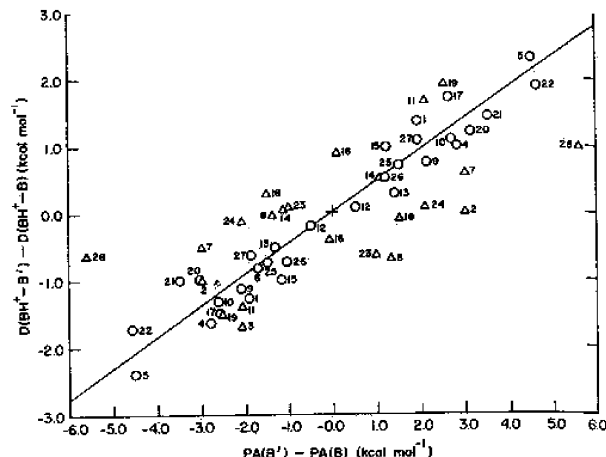


Figure 7. Correlations of $\Delta\Delta H^\circ_D$ and $\Delta PA = PA(B') - PA(B)$ for homodimers and heterodimers of protonated oxygen compounds. Here $\Delta\Delta H^\circ_D = \Delta H^\circ_D(BH^+\cdots B') - \Delta H^\circ_D(BH^+\cdots B)$ is the difference between the bond strength of a heterodimer and that of an optimized homodimer. Reproduced with permission from ref 50. Copyright 1982 American Chemical Society.

co-workers.^{33,42,48} Linear correlations were found between ΔPAs and bond dissociation energies, ΔH°_D , over ΔPA (for anions, $\Delta\Delta H^\circ_{acid}$) ranges up to 60 kcal/mol in $NH^+\cdots O$ and $NH^+\cdots S$ bonds (Figure 8). Table 2 shows correlation parameters for various bond types.

$$\Delta H^\circ_D(BH^+\cdots B') = a - b\Delta PA \quad (6)$$

$$\Delta H^\circ_D(AH\cdots A') = a - b\Delta\Delta H^\circ_{acid} \quad (7)$$

The intercepts (a) in Table 2 give the bond strengths for $\Delta PA = 0$, that is, the maximum bond strengths for a given type of reactant pair when the proton sharing is optimal. This can be seen as the intrinsic bond strength for a given type of hydrogen bond. For $OH^+\cdots O$, $OH^+\cdots N$, $NH^+\cdots O$, and $O^-\cdots HO$ bonds, the intrinsic strengths are about 30 kcal/mol, while $NH^+\cdots N$ and $SH^+\cdots S$ bonds are intrinsically weaker. Cyanide ligands give stronger bonds than other nitrogen bases, possibly due to the larger dipole moment, the highly directional sp hybridization of

Table 2. Parameters for Linear Correlations $\Delta H^\circ_D = a - b\Delta PA$ and $\Delta H^\circ_D = a - b\Delta\Delta H^\circ_{acid}$ between Bond Dissociation Energies and Proton Affinity Differences or Acid Dissociation Energy Differences between the Components (kcal/mol) for Reactions $BH^+\cdots B' \rightarrow BH^+ + B'$, Where $PA(B) \geq PA(B')$, and Analogous Relations for Anions^a

bond type	<i>a</i>	<i>b</i>	<i>n</i>	coeff	refs
$OH^+\cdots O$	30.4	0.40		0.999	53
$OH^+\cdots OH_2$	30.4(0.4)	0.30(0.01)	20	0.979	48
$OH^+\cdots NCR$	30.9	0.43			33
$NH^+\cdots O$	28.3(0.3)	0.23(0.01)	48	0.979	48
$NH^+\cdots OH_2$	30.0(1.5)	0.26(0.03)	19	0.923	48
$NH^+\cdots N$	23.2(0.7)	0.25(0.05)	8	0.897	48
$NH^+\cdots NCR$	35.3(0.5)	0.34(0.01)	4	0.984	42
$NH^+\cdots CNR$	25.7((1.0)	0.22(0.01)	5	0.914	42
$NH^+\cdots S$	22.3(0.9)	0.26(0.03)	5	0.970	48
$RCNH^+\cdots N$	33.2	0.31		0.812	53
$RCNH^+\cdots NCR$	28.1	0.37			33
$RCNH^+\cdots O$	28.3(0.7)	0.31(0.01)	5	0.977	42
$RCNH^+\cdots O$	31.9	0.38		0.991	53
$RNCH^+\cdots O$	23.9(0.2)	0.25(0.01)	3	0.998	42
$SH^+\cdots OH_2$	22.7(0.3)	0.26(0.01)	4	0.998	48
$SH^+\cdots OH_2$	18.6(0.3)	0.16(0.01)	8		54
$OH^-\cdots O^-$	28.1(0.4)	0.29(0.01)	13	0.981	55
$ROH\cdots S^-R$	19.9(0.3)	0.15(0.01)	5	0.989	56
$ROH\cdots S^-C_6H_5$	22.1(0.2)	0.20(0.01)	6	0.997	56
$ROH\cdots F^-$	34.2	0.59			57
$ROH\cdots Cl^-$	27.2	0.22			7
$c-C_5H_5^-\cdots HOR$	24.4	0.41			58

^aHere *n* is the number of data points and coeff is the correlation coefficient in each experimental correlation.

the nitrogen lone pair, or both. In relation to hybridization effects, the correlations do not apply to dimers of small molecules with hybridization of the acceptor lone pair other than sp^3 such as in $O_2H^+\cdots O_2$ ($\Delta H^\circ_D = 20.6$ kcal/mol), $CO_2H^+\cdots CO_2$ (16.2 kcal/mol), $N_2H^+\cdots N_2$ (16.0 kcal/mol), and $CS_2H^+\cdots CS_2$ (11.1 kcal/mol).⁵⁹ These homodimers have much smaller bond energies than organic or hydride $OH^+\cdots O$, $NH^+\cdots N$, or $SH^+\cdots S$ homodimers.^{60,61}

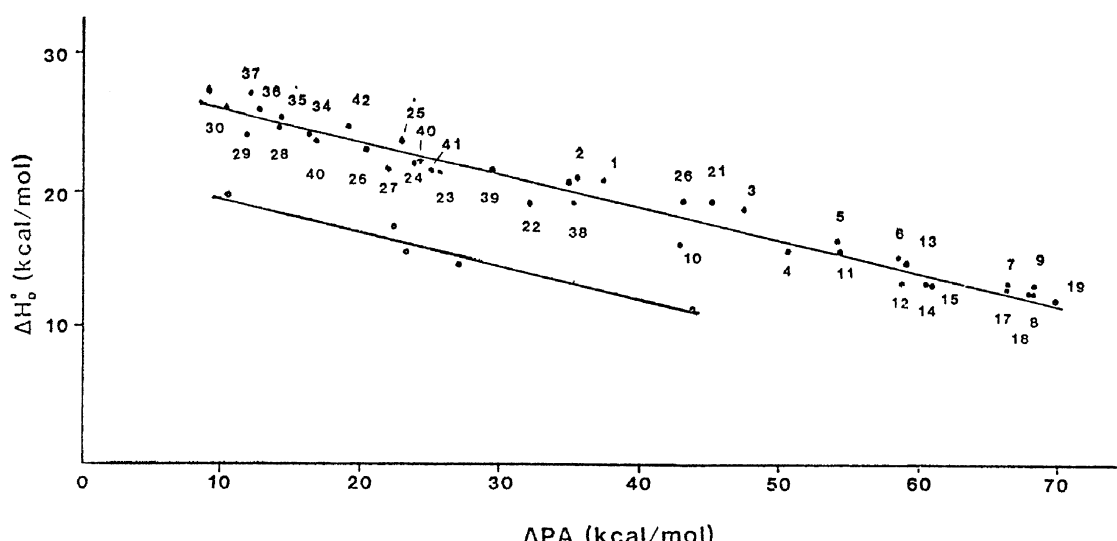


Figure 8. Correlation between the bond strength, ΔH°_D , and the difference between the proton affinities of the components ΔPA for $NH^+\cdots O$ bonds (top line) and $NH^+\cdots S$ bonds (bottom line). Reproduced with permission from ref 48. Copyright 1984 American Chemical Society.

A relationship is noted between the intercepts of the correlation lines and their slopes. The energies of intrinsically stronger bonds tend to decrease faster with increasing proton affinity difference. This can be explained in simple electrostatic terms because both the bond energy, ΔH°_{HB} , and its partial derivative with respect to PA, that is, $\partial \Delta H^{\circ}_{HB} / \partial PA$, depend on the polarizability and dipole moment of the ligand.⁵⁴

The correlations suggest that the bond strengths should be constant for homodimers of a given type because $\Delta PA = 0$ for all homodimers. On the other hand, it could be expected that, in a series of homodimers $BH^+\cdot B$ where the proton affinity of B increases, the charge in BH^+ becomes more delocalized in the donor ion and removed away from the bonding hydrogen, decreasing the electrostatic interactions with the ligand and weakening the bond. Such trends are observed but the effect is small because, when BH^+ becomes a less efficient hydrogen donor, the neutral B becomes a more efficient hydrogen acceptor. For example, in a series of $OH^+\cdot O$ homodimers, the bond strength of 32 kcal/mol in $H_3O^+\cdot H_2O$ decreases by only 2 kcal/mol in going to $(C_2H_5)_2OH^+\cdot(C_2H_5)_2O$, while PAs of the monomer components increased by 35 kcal/mol. Similarly small changes in bond strengths are observed in $NH^+\cdot N$ homodimers of alkylamines and pyridines.⁶² The IHB bond energies of proton-bound dimers of primary amides are constant at 27 ± 2 kcal/mol despite a variation of the gas-phase basicities (GBs) by 16 kcal/mol, but the IHBs were weaker in the secondary N,N -dimethylamides whose GBs are still higher. In this set, the protonated dimer of formamide with the lowest GB had the highest bond energy, and that of N,N -dimethylpivalamide with the highest GB had the weakest IHB.⁶³ Similarly, homodimers of the amino acids alanine, glycine, and lysine all have bonding energies of 26.5 ± 1.5 kcal/mol, similar to amine dimers, despite their various PAs and structures.¹⁸

However, $SH^+\cdot S$ bonds behave differently. Bond energies of 12.8 or 15.4 kcal/mol were reported for $H_2SH^+\cdot H_2S$,^{61,64a} but much larger values of 26.4 kcal/mol for $(CH_3)_2SH^+\cdot(CH_3)_2S$ and 26.4 kcal/mol for $(CH_3)(C_2H_5)SH^+\cdot(CH_3)(C_2H_5)S$ were measured.⁵⁴

A recent theoretical study addressed the relation between $PA(B)$ and IHB bond strength in $(B\cdots H^+\cdots B)$ homodimers of

N , O , and F bases substituted by F , Me , and t - Bu groups. The results showed that in each series the binding energies first increase then decrease quadratically as $PA(B)$ increases. At first the more efficient partial protonation of the neutral base B with increasing $PA(B)$ dominates, but then the increasing energy of deprotonation of BH^+ becomes dominant.^{64b} For example, the calculated binding energies increase from 12.8 kcal/mol for the $(NF_3)_2H^+$ dimer to 25.8 kcal/mol for the $(NH_3)_2H^+$ dimer but decrease again slightly to 23.4 kcal/mol for the $(CH_3N(t-C_4H_9))_2H^+$ dimer, as the calculated $PA(B)$ increases from 136 to 204 and 234 kcal/mol.^{64b} This latter small decrease in the binding energy by 2.4 kcal/mol as $PA(B)$ increases by 30 kcal/mol is consistent with observations in amine and pyridine dimers.⁶² Computational results also showed that protonated homodimers are symmetric for fluorine, oxygen, and sp-hybridized nitrogen bases B with a wide range of PAs but asymmetric if the heavy atom of the base B is less electronegative such as in sp^2 - and sp^3 -hybridized protonated amine dimers.^{64c}

Other than S, there are only a few studies on IHB interactions with acceptors or donors of third or higher row elements. An early study found a relatively weak binding energy of $PH_4^+\cdot PH_3$ of 11.5 kcal/mol, decreasing to 9.2, 7.3, 6.2, and 5.5 kcal/mol for the bonding of further PH_3 molecules. The bonding energies of $P_2H_5^+$ and $P_3H_6^+$ to PH_3 were 9 and 10.8 kcal/mol, respectively. The small bonding energy in $PH_4^+\cdot PH_3$ was attributed to the small dipole moment and the large radius and large ion-neutral separation.⁶⁵

The bonding energy of protonated ferrocene Cp_2FeH^+ to CH_3CN was found to be <8 kcal/mol. H/D exchange reactions indicated that Cp_2FeH^+ is protonated on Fe, and this suggested that $-FeH^+$ is a poor IHB donor.⁶⁶ However, the poor bonding of Cp_2FeH^+ may be a special case resulting from a shielded or agostically bonded proton, because subsequently $(CO)_3FeH^+$ was found to bond to CH_3CN by 17 kcal/mol, and proton affinity correlation considerations suggested that the donor efficiency of the $-FeH^+$ is similar to $-SH^+$ donors.⁶⁷

Although the above linear correlations reproduce measured strong hydrogen-bond energies for practical purposes, there is no basic reason that these correlations should be linear.

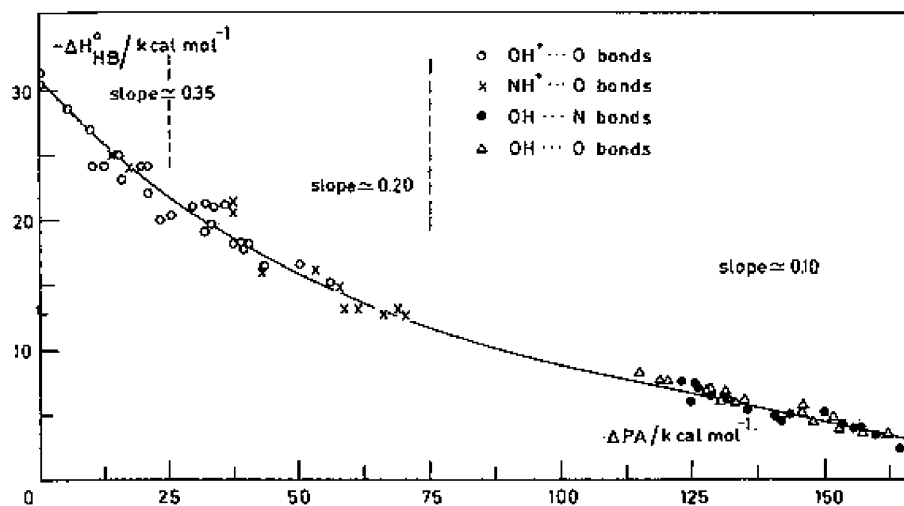


Figure 9. Correlations between hydrogen-bond energies and proton affinity differences for ionic and neutral O and N bases. The neutral bonds are considered $RO^-H^+\cdots N$ or $RO^-H^+\cdots O$ bonds, and ΔPA represents the difference between the PAs of RO^- and of the proton acceptor N or O base. Reproduced with permission from ref 68. Copyright 1986 Elsevier.

Zeegers-Huyskens pointed this out and proposed an exponential form of the correlation, where $\Delta H^\circ_D = x \exp(-x\Delta PA)$. This was found to agree better with experiment than the Marcus equation. The derivative of the exponential equation was found to be related to the potential curve and barrier for proton motion between the components. Interestingly, Zeegers-Huyskens and co-workers also showed that the correlations between proton affinity or acidity differences and hydrogen-bond energies include even neutral OH···O and NH···N hydrogen bonds from dimers of simple molecules to complexes of nucleic bases with water.^{68–73} Such dimers may be considered as A⁻–H⁺···B dimers, and the hydrogen-bond energy is correlated with the proton affinity difference between A⁻ and B. The relationship in Figure 9 shows a continuous nonlinear relation over hydrogen bonds from 3 to 30 kcal/mol and over a very wide ΔPA range from 0 to 170 kcal/mol. It can be seen to be composed of three linear ranges, and the slopes are correlated with the absolute strengths of the bonds in each range. The neutral hydrogen bonds involve substituted phenol donors and various organic O and N bases as acceptors. The value of ΔPA was found to be an important determinant of hydrogen-bond energy, but since not all homodimers (ΔPA = 0) have equal bond energies, it was concluded that other factors are also significant.⁶⁸

2.2.2. Dimer Anions: Bond Strengths and Correlations with Acidities. Correlations similar to the cationic IHBs also apply in anionic A⁻···HA' hydrogen bonds. The first linear correlation between ΔH°_D and the difference between the gas-phase acid dissociation energies of the components, $\Delta\Delta H^\circ_{\text{acid}}$, was observed by the Kebarle group in 1971 in the hydration of the halide and NO₂⁻, NO₃⁻, and OH⁻ anions.^{38,74} Larson and McMahon presented several major data sets for anionic IHBs in OH·F⁻, SH·F⁻, and CH·F⁻ type bonds and discussed the factors that contribute to bonding.⁵⁷ The thermochemistry of other bond types investigated by several groups include OH·Cl⁻ and CH·Cl⁻,^{7,41} bihalide ion XHX⁻ and XHY⁻ complexes,⁷⁵ halide ion complexes with ROH and RCOOH⁷⁶ and with NH₃,⁷⁷ complexes of CN⁻ with OH, SH, and CH donors,^{8,78} the bonding of CH₃COO⁻, HS⁻, CN⁻, and Cl⁻ with ROH, RCOOH, and CH hydrogen donors,⁷⁹ further studies of OH·O⁻ bonds,³³ and bonds of carbanions with OH and CH donors.⁵⁸ Table 2 lists empirical linear correlation parameters between ΔH°_D and $\Delta\Delta H^\circ_{\text{acid}}$ from some of these studies.

a. Oxygen Acids. Anionic IHBs of the OH·O⁻ type involving neutral and ionic H₂O, RCOOH, and ROH groups are of general interest because they occur in solution as well as in biology. As in the formation of cation dimers, in these bonds the positive charge also increases on the bonding hydrogen, the bonding O atoms become more negatively charged, and the H–O⁻ bond stretches upon the formation of the strong hydrogen bond.

Correlations between ΔH°_D and $\Delta\Delta H^\circ_{\text{acid}}$ for OH·O⁻ bonds were expressed by a two-parameter linear equation for ROH·O⁻R' complexes.⁶

$$\Delta H^\circ_D = -0.31\Delta H^\circ_{\text{acid}}(\text{ROH}) + 0.40\Delta H^\circ_{\text{acid}}(\text{R}'\text{OH}) - 15.0 \text{ kcal/mol} \quad (8)$$

Subsequently, a single-parameter correlation covered RO⁻···HO and RCOO⁻···HO bonds adequately, as shown in Figure 10, leading to the parameters in Table 2.

The parameters in Table 2 show the similarity between the OH⁺·O and OH·O⁻ bond strength for an equal ΔPA or

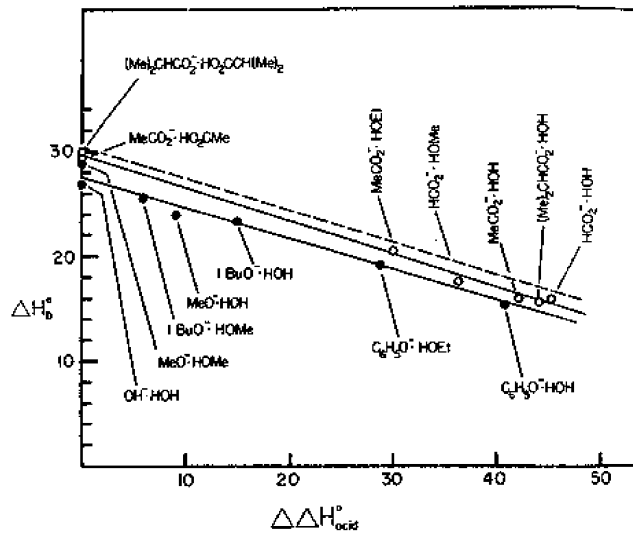


Figure 10. Correlation between ΔH°_D and $\Delta\Delta H^\circ_{\text{acid}}$ for RCOO⁻·HO bonds (○) and RO⁻·HO bonds (●) and for protonated cationic OH⁺·O bonds (dashed line). Reproduced with permission from ref 55. Copyright 1986 American Chemical Society.

$\Delta\Delta H^\circ_{\text{acid}}$ difference (as noted above, the ΔPA or $\Delta\Delta H^\circ_{\text{acid}}$ parameters are equivalent as $\Delta H^\circ_{\text{acid}}(A^-·H^+) = PA(A^-)$). In terms of the absolute PAs of the components, we note that OH⁺·O and OH·O⁻ complexes for components with a given ΔPA or $\Delta\Delta H^\circ_{\text{acid}}$ have similar bond energies, although the absolute proton affinities of the components of cationic dimers (PA(B)) are usually 160–240 kcal/mol while those for the anionic dimers (PA(A⁻)) are much higher, usually 360–420 kcal/mol.

Linear correlations were also found to apply to further dimers of CH₃COO⁻, CN⁻, Cl⁻, and SH⁻ with ROH, RCOOH, and C₄H₄NH (pyrrole), while the carbon acids CH₃CHO, (CH₃)₂CO, and CH₃CN gave bonds weaker by about 4 kcal/mol.^{56,58,79}

A special case of OH·O⁻ and OH·N⁻ bonds involves the carbanions CH₂CN⁻, CH₂CO⁻, CH₃COCH₂⁻, and CF₃COCH₂⁻, which bond to H₂O by 13–15 kcal/mol. The thermochemistry and theoretical calculations suggested that the oxygen atoms are the favored acceptor sites to bind the hydrogen of the donor H₂O molecules.⁸⁰

The pyrrolide anion, c-C₄H₄N⁻, also bonds fairly strongly to H₂O (15.7 kcal/mol) and to CH₃OH (18.6 kcal/mol), more strongly than the bonding of the delocalized c-C₅H₅⁻ anion to these ligands. This suggests localized OH·N⁻ interactions in the complexes of the pyrrolidine anion.⁵⁸

b. Complexes of Halide Ions. Early studies showed correlations between ΔH°_D and the acid dissociation energy, $\Delta\Delta H^\circ_{\text{acid}}$, of the hydrogen donor ligands in complexes of Cl⁻ with substituted phenols⁸¹ and with substituted acids.⁴¹ A two-parameter correlation for various AH·A⁻ bonds was given by Yamdagni and Kebarle.³⁹

$$\Delta H^\circ_D = -0.134\Delta H^\circ_{\text{acid}}(\text{AH}) + 0.20\Delta H^\circ_{\text{acid}}(\text{R}'\text{OH}) \quad (9)$$

Similar relations were observed in complexes of F⁻ with alcohols, and parallel correlation lines were established for complexes of F⁻ with various carboxylic and CH, SH, and NH acids over a ΔH°_D range of 22–48 kcal/mol and a $\Delta\Delta H^\circ_{\text{acid}}$ range of 40 kcal/mol (Figure 11). The weaker bonding energies

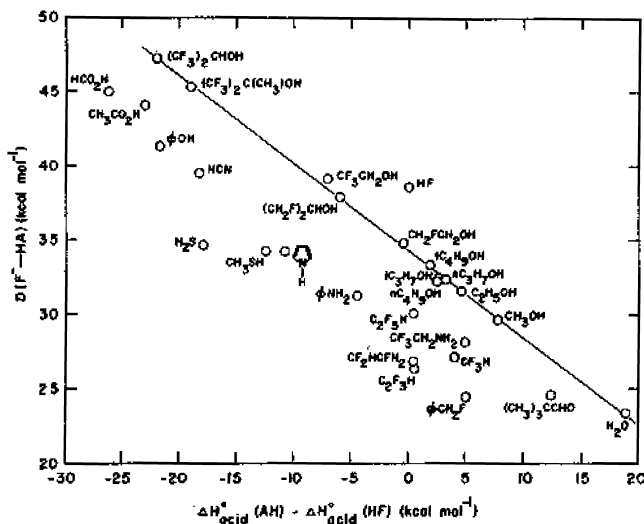


Figure 11. Correlation of fluoride bonding energies with the difference between the acid dissociation enthalpies of the hydrogen-donor Bronsted acids and that of HF. Reproduced with permission from ref 57. Copyright 1983 American Chemical Society.

for the complexes of ROOH and C_6H_5OH versus ROH donors suggest that IHB formation decreases the resonance stabilization of the neutral donors.^{57,82a}

In addition, F^- bonds strongly with strongly acidic fluorinated ammonia, with computed bond strengths of $F^- \cdots NH_3$, $F^- \cdots NFH_2$, and $F^- \cdots NF_2H$ of 15.2, 28.7, and 43.3 kcal/mol, respectively. The $F^- \cdots NF_2H$ complex in turn bonds efficiently, by 16.3 kcal/mol, with an additional CH_3OH solvent molecule.

The fact that the relation is continuous for donors with ΔH°_{acid} both below and above HF suggested that the nature of the bonding does not change whether the proton is near F or O in the $FH \cdots O^-$ bonds, indicating a single-well or a low-barrier double-well bonding surface. Figure 12 shows that this was confirmed theoretically.

Inverse correlations along continuous nonlinear lines between ΔH°_D and $\Delta\Delta H^\circ_{acid}$ were also found in the association of

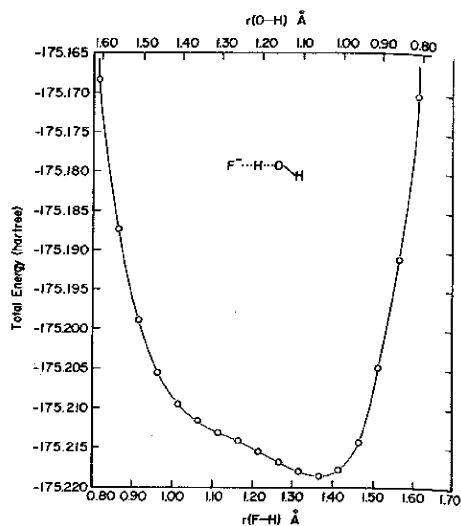


Figure 12. Proton potential for the hydrogen-bonded adduct of F^- and H_2O obtained at a total separation of 2.52 Å, using 4-31G basis set calculation. Reproduced with permission from ref 57. Copyright 1983 American Chemical Society.

alcohols and acids with Cl^- , NO_2^- , and $C_6H_5NO_2^-$, the first two ions giving bonding energies higher by about 2.1 kcal/mol than the latter ion.^{83a} Larson and McMahon suggested an empirical correlation based on the gas-phase acidities and electronegativities, χ , of the components.

$$\begin{aligned} \Delta H^\circ_D(X^- \cdot HY) = & (443 - \Delta H^\circ_{acid}(Y^- \cdot H))[(\chi(X) \\ & + \chi(Y))/12 + (\Delta H^\circ_D(X^- \cdot H^+))/300 - 1.4] \end{aligned} \quad (10)$$

The authors applied the equation successfully with a standard deviation of 2.0 kcal/mol to 56 dimers of a wide range of complexes involving halide, alkoxide, acetate, and $C_6H_5C_2^-$ anion acceptors and alcohols, acids, hydrogen halides, H_2S , and several carbon acids, such as C_6H_6 , CH_3COCH_3 , CF_3H , and $C_6H_5CH_2F$, as donors.⁸

Interestingly, the bond strengths of CH_3COO^- , CN^- , Cl^- , and HS^- with a given neutral ligand are usually similar.⁷⁹ This occurs although different factors affect the bond strengths in these complexes. Bonding to the first two ions is weakened by delocalization, while that to the last two is weakened by polarization and ionic radius effects.⁸⁰ The complex forces seem to balance to give a fortuitously simple uniform behavior.

Hydrogen bonding of the Cl^- ion was investigated extensively. The Kellar group determined the binding free energies of Cl^- with 40 OH and CH donors. The OH donors included H_2O , CH_3OH , $t-C_4H_9OH$, $HCOOH$, CH_3COOH , and C_6H_5OH , and the CH donors included various ketones and toluenes. For the OH donors continuous inverse correlations were found between $\Delta\Delta H^\circ_{acid}$ and ΔH°_D over an acidity range of 60 kcal/mol.

Similar relations applied for the CH acids, but for a given $\Delta\Delta H^\circ_{acid}$, the bonding energies were lower by about 8–10 kcal/mol. Molecular orbital STO-3G calculations showed good correlations between the bond dissociation energies and the charge on the donor protons (Figure 13) and also a correlation

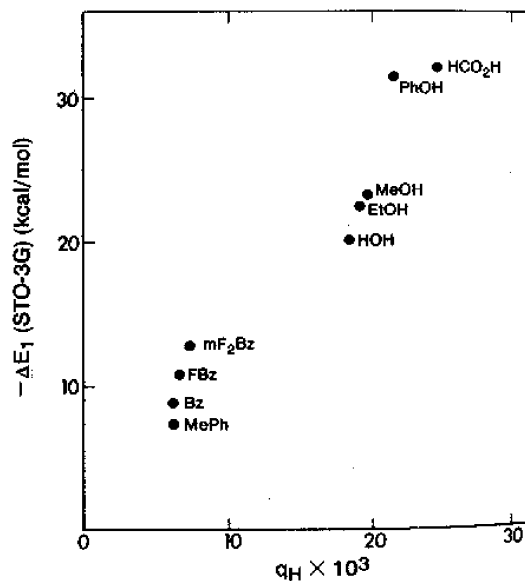


Figure 13. Correlation between the bonding energy, ΔH°_D , of Cl^- complexes and the charge on the bonding hydrogen atoms of the donor molecule, q_H , before bond formation. The plot illustrates the significance of the electrostatic interactions between the bonding hydrogen and the chloride anion. Reproduced with permission from ref 41. Copyright 1982 NRC Research Press.

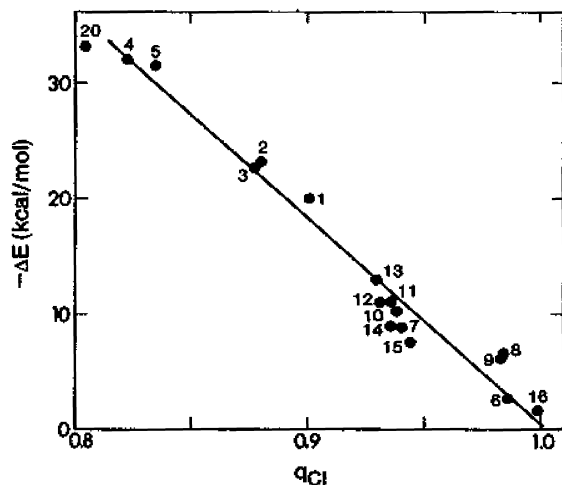


Figure 14. Correlation between ΔH°_D of Cl^- complexes and the negative charge on Cl^- in $\text{RH}\cdot\text{Cl}^-$ complexes after bond formation. The plot shows good correlation between the bonding in the complex and the negative charge transferred from Cl^- to RH on formation of the complex. Reproduced with permission from ref 41. Copyright 1982 NRC Research Press.

with the charge transferred from Cl^- to the proton donors (Figure 14).⁴¹

The bonding energies of Cl^- with ethers and halogenated ethers ranged from 7.5 kcal/mol for $(\text{CH}_3)_2\text{O}$ to 28.2 kcal/mol for $\text{CF}_2\text{HOCl}_2\text{H}$, the latter possibly stabilized by two $\text{CH}\cdots\text{Cl}^-$ hydrogen bonds.^{83b} Complexes of Cl^- with acetone and fluorinated acetone showed bond strengths from 14.1 kcal/mol for $(\text{CH}_3)_2\text{CO}$ to 26.1 kcal/mol for $\text{CF}_3\text{COCl}_2\text{H}$ and 28.8 kcal/mol for $\text{CF}_3\text{COClF}_3$. In the latter complexes Cl^- interacts with the carbonyl carbon, although a strong IHB would be expected with the acidic $\text{CF}_3\text{COCl}_2\text{H}$ ligand.^{83c}

A further study of the bonding of ROH and RCOOH ($\text{R} = \text{H, Me, Et, }i\text{-Pr, or }t\text{-Bu}$) ligands to F^- , Cl^- , and I^- showed bonding energies from 23 to 34 kcal/mol for $\text{ROH}\cdot\text{F}^-$ and as large as 41.7 and 45.3 kcal/mol in $\text{MeCOOH}\cdot\text{F}^-$ and $\text{HCOOH}\cdot\text{F}^-$, respectively. Bonding energies to Cl^- and I^- were smaller, as may be expected on the basis of the ionic radii. An interesting feature illustrated in Figure 15 is the bifurcated

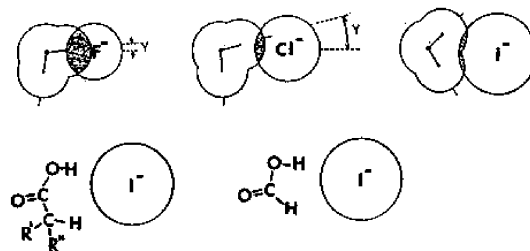


Figure 15. Geometries of complexes of halide anions. The geometries of the $\text{HOH}\cdot\text{F}^-$ and $\text{HOH}\cdot\text{Cl}^-$ complexes were obtained from ab initio calculations. The geometries of $\text{HOH}\cdot\text{I}^-$ and the proposed polydentate structures for complexes of carboxylic acids with I^- were obtained from electrostatic calculations. These geometries maximize the interactions of OH, CO, and CH dipoles with the ions. Reproduced with permission from ref 76. Copyright 1984 American Chemical Society.

structure in $\text{H}_2\text{O}\cdot\text{I}^-$ and both an OH and a CH bond to the ion in $\text{RCOOH}\cdot\text{I}^-$ complexes.⁷⁶

Complexes of halide ions with NH_3 were found by Castleman and co-workers to have relatively small bonding energies of 8.2 kcal/mol ($\text{NH}_3\cdot\text{Cl}^-$), 7.7 kcal/mol ($\text{NH}_3\cdot\text{Br}^-$), and 7.4 kcal/mol ($\text{NH}_3\cdot\text{I}^-$), corresponding to the low acidity of NH_3 .⁷⁷ These workers analyzed the electrostatic factors that contribute to the bonding and found various orientations of the NH_3 molecule with respect to the various halide ions with significant effects of the quadrupole moments.

Most of the thermochemistry of dimers was obtained by equilibrium measurements, but some were verified by different techniques. One such verification concerned $\text{Cl}^-(\text{H}_2\text{O})_n$ bonding energies, which were measured by thermal radiation-induced dissociation as 11.6 and 9.5 kcal/mol for $n = 2$ and 3, respectively, in good agreement with equilibrium studies.¹⁵ The calculated density functional theory (DFT) minimum-energy structures in Figure 16 show that, even in these small clusters, a

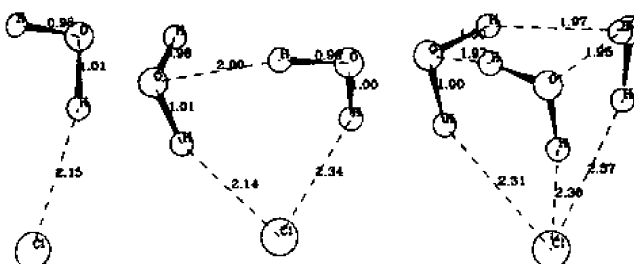


Figure 16. Hydrogen-bond networks in $\text{Cl}^-(\text{H}_2\text{O})_n$ complexes calculated using density functional theory (DFT) with a DZVP basis set. Reproduced with permission from ref 15. Copyright 1995 American Chemical Society.

network of water–water IHBs was formed. Also, the bonding energies of water clusters $(\text{H}_2\text{O})_n\text{H}^+$ were verified by collisional dissociation measurements.¹⁴

c. *Theory and Spectroscopy of Anionic Complexes.* Theoretical calculations support the experimental bonding energies of dimer ions. For example, Pudzianowski studied 10–15 key anionic $\text{O}^-\cdot\text{HO}$ as well as cationic $\text{OH}^+\cdot\text{O}$, $\text{NH}^+\cdot\text{N}$, and $\text{NH}^+\cdot\text{O}$ type dimers both at high-level ab initio and density functional theory methods. In most dimers, the calculations agreed with experiment within the experimental uncertainty of ± 2 kcal/mol of the binding energies.^{84,85} Numerous other theoretical studies agreed with experiment for various dimers and larger clusters.

The development of IHB networks about halide ions was investigated by IR spectroscopy. A recent review summarized the applications of vibrational dissociation spectroscopy to the morphology of small water networks attached to anions. Charge transfer to the solvent affects the structures of IHB networks about the ions. The negatively charged water clusters $(\text{H}_2\text{O})_n^-$ provide information on how diffuse excess electrons interact with the water networks.⁸⁶ Important factors contributing to the ion-bound OH stretch frequencies were found to be the radius and excess charge associated with the halide, which determine the electric field at the surface of the ion.⁸⁷

As to the location of the ion, the solvation of F^- by up to five H_2O molecules indicated the ion to be inside the solvent shell. In contrast, Cl^- , Br^- , and I^- remain on the surface of solvating water clusters. Similarly, Cl^- and I^- remain on the surface of solvating methanol clusters, in which methanol–methanol hydrogen bonds appear after four or more methanol molecules.^{88a}

d. Bihalide Complexes. A strong IHB of 38.6 kcal/mol was observed in $\text{F}^- \cdot \text{HF}$ by Larson and McMahon, who also investigated many complexes of F^- , Cl^- , and CN^- with OH hydrogen donors (alcohols and acids), as well as CH hydrogen donors. These studies showed a stronger dependence of the F^- binding energies on the gas-phase acidity of the donors, with a correlation slope of 0.5, than in the Cl^- bonding energies, with a correlation slope of 0.2. The F^- bonding also shows more preference to OH versus CH donors than Cl^- bonding. Both trends are consistent with a stronger covalent component in the F^- complexes, while the Cl^- complexes are mostly electrostatic.⁷

Bond strengths in bihalide ions, as well as the bonding energies to SO_2 , were measured by Caldwell and Kebarle. In the homodimers $\text{XH}\cdot\text{X}^-$, the ΔH°_D values decrease from 38.6 to 23.5, 20.9, and 17.0 kcal/mol for $\text{X} = \text{F}$, Cl , Br , and I , respectively, as may be expected based on the ionic radii. In mixed dimers $\text{YH}\cdot\text{X}^-$, the ΔH°_D values increase with increasing acidity of YH , similar to other correlations of ΔH°_D and $\Delta\Delta H^\circ_{\text{acid}}$.⁷⁵

The bonding energies of $\text{FHF}^- \cdots \text{H}_2\text{O}$, $\text{FHF}^- \cdots \text{CH}_3\text{OH}$, and $\text{FHF}^- \cdots \text{C}_2\text{H}_5\text{OH}$ were measured recently as 18.8, 19.4, and 20.7 kcal/mol, respectively. Forming these complexes increases the negative charge on the fluorine atom. In the complex with $\text{C}_2\text{H}_5\text{OH}$, the interactions of the alkyl group with fluorine contribute to the binding energy.^{88b}

2.3. Structural Effects: Isotropy, Resonance, and Steric Hindrance

2.3.1. Does Isotropy Affect the Bond Strengths? The bond strengths of complexes of CH_3COO^- , CN^- , and HS^- with a variety of ligands are comparable to the complexes of Cl^- , although the former are anisotropic while the latter is a spherical monatomic ion. Similarly, bond strengths in complexes of CN^- versus Cl^- with HCN and of NH_4^+ versus K^+ with various neutrals were comparable, as is also the thermochemistry of CN^- versus Cl^- , of H_3O^+ versus Na^+ , and of NH_4^+ versus K^+ in the condensed phase.^{8,43a,b,89,90} For example, the bonds of CN^- and Cl^- to an HCN or H_2O molecule have similar energies. Theory shows that with CN^- the bonding of a ligand molecule to the C or N end are similar. With 2 H_2O molecules, CN^- forms a linear structure whereas Cl^- allows for water–water interactions. However, in clusters with 3 and 4 ligand molecules, both ions are on the surface, and in the CN^- clusters the ion rotates nearly freely. In these respects CN^- is comparable to the spherical Cl^- ion and shows a nearly isotropic behavior.^{8,43a,b}

Whether the ion appears isotropic or anisotropic to a ligand depends on the distance. For example, the interaction energy of NH_4^+ with a model dipole depends strongly on the charge distribution and orientation of the ion when the distance from the central N atom to the center of the dipole is $< 2.5 \text{ \AA}$ since at such short hypothetical distances the effects of the atoms closest to the ligand would dominate. However, these factors have little effect at realistic separations of $> 3 \text{ \AA}$, as illustrated in Figure 17. At these distances the contributions of the various atoms of the ion balance so that NH_4^+ appears to the ligand as an isotropic spherical ion with unit charge at the central N atom.⁸⁹ However, larger ions where some partially charged groups are much more distant from the ligand may not act as point charges, and the charge density at the bonding proton may be dominant.

2.3.2. Resonance. The hydrogen-bond strength can be affected by special structural factors. For example, when an ion is stabilized by charge resonance such as $(\text{CH}_3\text{COOH})\text{H}^+ = \text{CH}_3\text{C}(\text{OH})_2^+$, then formation of the IHB can perturb the

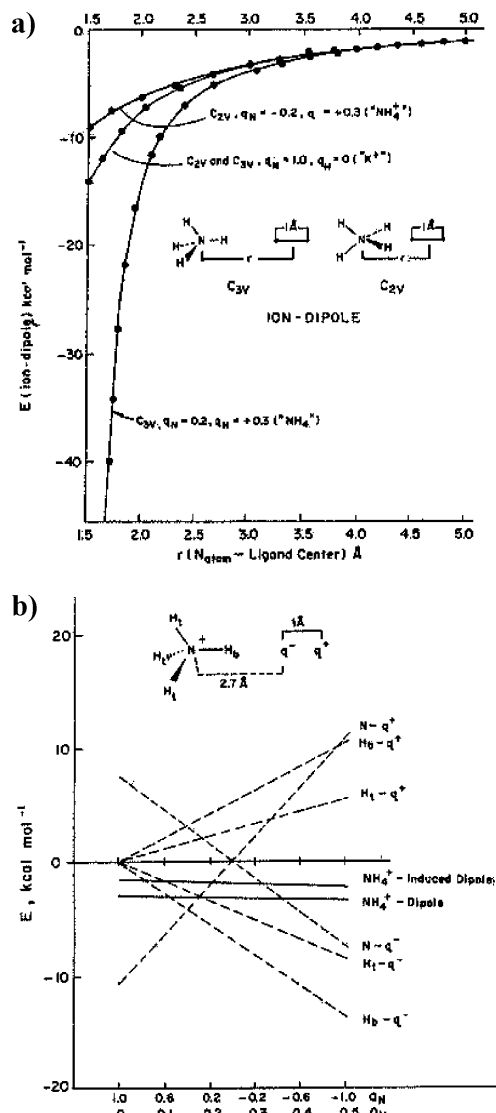


Figure 17. Calculated electrostatic bonding energies between NH_4^+ and its atoms and a model polar molecule with polarizability of 1 \AA^3 and dipole moment of 1 D. Panel a illustrates effects of orientation. The panel shows the variation of the ion–dipole energy with the N atom to ligand center distance r for complexes in which the NH_4^+ ion has two different orientations and two different charge distributions. In the C_{2v} geometry NH_4^+ is shown with charge distribution $q_N = 1.0$ and $q_H = 0$ unit charge, equivalent to the spherical K^+ cation, and with $q_N = -0.2$ and $q_H = +0.3$, which represents the NH_4^+ cation. The C_{2v} and C_{3v} curves for the K^+ like spherical charge distribution are identical. The graph shows that the overall binding energy of the complex in either geometry or ionic charge distribution become nearly equal when $r(\text{N}_{\text{atom}}-\text{ligand center}) > 3 \text{ \AA}$, at realistic ion–ligand distances. The ion-induced dipole forces were found to behave similarly. Panel b illustrates effects of charge distribution. Interaction energies of individual atomic charges on NH_4^+ in a C_{3v} complex with the polar molecule at a N to negative dipole end distance of 2.7 \AA are shown as the charge distributions on NH_4^+ vary from $q_N = 1.0$ and $q_H = 0$, simulating a spherical K^+ ion, to an extreme anisotropic charge distribution of $q_N = -1$ and $q_H = 0.5$. The distribution of the ionic charge affects the interaction energies of each atom of NH_4^+ with the dipole of the ligand. However, the total ion–dipole and ion-induced dipole interaction energies are nearly constant due to canceling effects of the individual interaction energies. Reproduced with permission from ref 89. Copyright 1991 American Chemical Society.

resonance, and the loss of this stabilization energy makes the overall bond formation less exothermic. This occurs when

protonated acids such as $\text{CH}_3\text{C}(\text{OH})_2^+$ bond to a neutral CH_3COOH molecule to form the dimer ion in $(\text{CH}_3\text{COOH})\text{H}^+\cdot\text{CH}_3\text{COOH}$. In this case, ΔH°_D is lower by about 2 kcal/mol than in protonated dimers of alcohols and ketones.⁵⁰

In anions, weaker bonding energies were observed in the complexes of ROOH and $\text{C}_6\text{H}_5\text{OH}$ versus ROH donors in their complexes with a common anionic hydrogen acceptor, even when the relative acidities of the components were similar. The decreased bond energies with the ROOH and $\text{C}_6\text{H}_5\text{OH}$ donors suggest that IHB formation increases the negative charge on the bonding oxygens of the ligands, which decreases their resonance stabilization.^{57,82a} Resonance effects can also affect the IHB strength of heterocyclic aromatics.⁷³

2.3.3. Steric Hindrance. The components of gas-phase dimers can usually assume optimized geometries and free rotation about the IHBs, but bulky substituents may impose constraints. The effects of steric hindrance were examined in bulky alkylamines and alkylpyridines,⁹¹ and ΔG°_D was found to decrease systematically with increasing steric hindrance.

However, this was found to be an entropy rather than enthalpy effect, and even in dimers of bulky 2,6-dialkylpyridines, ΔH°_D remained constant at about 23 kcal/mol, similar to other $\text{NH}^+\cdot\text{N}$ bonds. The optimal bonding energy suggested that the $\text{NH}^+\cdot\text{N}$ bonds could reach their optimal lengths. Space-filling models confirmed this but showed that substituents on the two component molecules interfere with each other within the volumes of rotation of the alkyl groups. Correspondingly, the entropy of dimer formation changes from $-28.2 \text{ cal}/(\text{mol K})$ in $(\text{pyridine})_2\text{H}^+$ to -33.2 , -37.4 , and $-48.4 \text{ cal}/(\text{mol K})$ in the dimers of the protonated 2,6-di-Me, 2,6-di-Et, and 2,6-di-*i*-Pr-pyridine compounds.

In the amine dimers $(\text{R}_3\text{N})_2\text{H}^+$, the bonding energy first decreases from 25.2 kcal/mol in $(\text{NH}_3)_2\text{H}^+$ to 22.2 kcal/mol in $(\text{Me}_3\text{N})_2\text{H}^+$, but the trend reverses, and the bonding energy increases again to 23.8 kcal/mol in $((\text{Et})_3\text{N})_2\text{H}^+$ and 24.4 kcal/mol in $((n\text{-Bu})_3\text{N})_2\text{H}^+$, possibly due to attractive dispersion forces between the interacting alkyl substituents of the two components. While the bonding energies change little, interference between the rotational volumes of the alkyl groups of the two components results in very large negative entropies of dimer formation, from $-32.0 \text{ cal}/(\text{mol K})$ in $(\text{Me}_3\text{N})_2\text{H}^+$ to $-41.0 \text{ cal}/(\text{mol K})$ in $(\text{Et}_3\text{N})_2\text{H}^+$ and $-56.5 \text{ cal}/(\text{mol K})$ in $((n\text{-Bu}_3\text{N})_2\text{H}^+$.

Even bonding to the small H_2O molecule can interfere with large alkyl rotors. From $(\text{pyridine})\text{H}^+\cdot\text{H}_2\text{O}$ to $(2,6\text{-}(di-t\text{-Bu})\text{pyridine})\text{H}^+\cdot\text{H}_2\text{O}$, the entropy of dimer formation changes from -27 to $-41 \text{ cal}/(\text{mol K})$, and from $\text{Me}_3\text{NH}^+\cdot\text{H}_2\text{O}$ to $(n\text{-But})_3\text{NH}^+\cdot\text{H}_2\text{O}$, the entropy of association changes from -24.1 to $-36.4 \text{ cal}/(\text{mol K})$. The small H_2O ligand molecule seems to interpose between the large alkyl groups and inhibit their rotations (Figure 18). The low basicity of 2,6-(di-*t*-Bu)-pyridine in solution may be due therefore to the unfavorable entropy of hydration of the protonated ion.^{91a} Similarly, steric interference with methyl groups and NH_3 leads to nonlinear IHBs in complexes with methylated pyrazoles and imidazoles.

2.4. Carbon-Based Bonds

A special class of IHBs involves bonds where the acceptor or donor groups are carbon-based. The first carbon-based hydrogen bond was identified in 1937 by Glasstone in $(\text{CH}_3)_2\text{CO}\cdot\text{HCCl}_3$.⁹² In ionic systems, the donors may be alkyl hydrogens in $\text{CH}^{\delta+}\cdots\text{O}$, N , or S bonds and in $\text{CH}\cdots\text{O}^-$, N^- , S^- , or halide $^-$ bonds. The acceptors may be π -electrons of olefins or aromatics in $\text{BH}^+\cdot\pi$ complexes or the π -systems of aromatic anions in $\text{BH}\cdots\pi^-$ bonds,

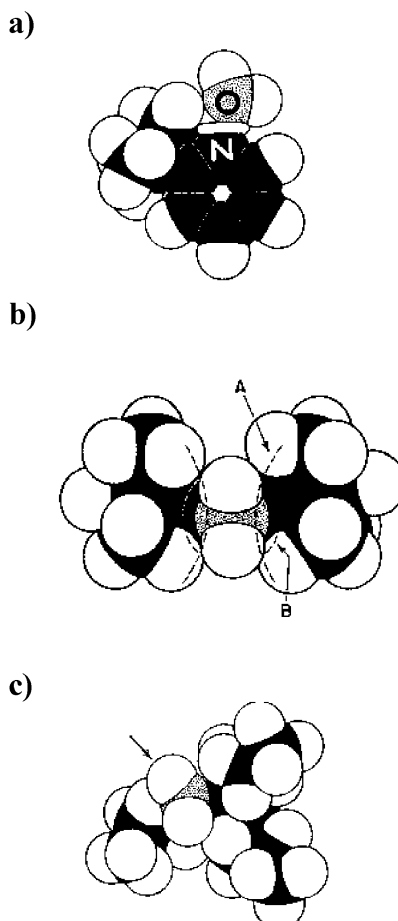


Figure 18. Steric interference between the rotations of the alkyl groups in complexes (a) $(2\text{-}tert\text{-butylpyridine})\text{H}^+\cdot\text{H}_2\text{O}$, (b) $2,6\text{-}(di\text{-}tert\text{-butylpyridine})\text{H}^+\cdot\text{H}_2\text{O}$, and (c) $(n\text{-But})_3\text{NH}^+\cdot\text{H}_2\text{O}$. The water molecule (gray oxygen) interferes with the volumes of rotation of the alkyl groups leading to large negative entropies of association. Reproduced with permission from ref 91a. Copyright 1983 American Chemical Society.

or carbon lone pairs in $\text{BH}^+\cdot\text{CNR}$ (isonitrile) bonds. In some complexes both the acceptor and donor may be carbon-based, as in $\text{CH}^{\delta+}\cdot\pi$ bonds. Several of these bond types appear in biological systems.

In the first thermochemical studies on ionic $\text{CH}\cdot\text{X}^-$ systems, Larson and McMahon studied a large number of complexes of F^- and Cl^- with hydrocarbon CH donors.^{7,57} In cations, Meot-Ner and Deakyne,^{93a} and more recently Prell and Williams,^{93b} studied unconventional carbon-based IHBs in complexes of quaternary ammonium ions, and in π -complexes of protonated amines with aromatic molecules.^{94a} Recently, Blades, Klassen, and Kebarle studied bonds where doubly charged quaternary ions served as donors.⁹⁵ Table 3 shows the available thermochemical data. Some unconventional IHBs have biological roles, for example, in the interactions of acetylcholine neurotransmitters that contain a quaternary amine group binding with aromatic hydrogen-bond receptors in a $\text{CH}\cdots\pi$ (carbon donor–carbon receptor) hydrogen bond (see ref 124).

2.4.1. Cationic Complexes with CH Donors. A theoretical study by Uggerud found that CH_3^+ can serve as a hydrogen donor for IHB interactions with NH_3 and H_2O molecules.^{96a} Experimentally, $\text{CH}^{\delta+}\cdot\text{B}$ bonds were investigated in complexes of quaternary ammonium ions, carbonium ions,

Table 3. Thermochemistry of Unconventional Carbon-Based Ionic Hydrogen Bonds

ion	ligand	ΔH°_D ^a	ΔS°_D ^a	refs
$\text{CH}^+ \cdots \text{B}$ bonds				
Me_3C^+	H_2O^b	11.2 [11] ^c	22 [35] ^d	132
	MeOH^b	15.1 ^e [24.9] _{cond} ^c [29.1] _{cond} ^f	21.1 ^e [54.0] ^f	123
	EtOH^b	20.4 ^e [35.6] _{cond} ^c [38.6] _{cond} ^f	27.6 ^e [72.9] _{cond} ^f	123
	Me_2O^b	23.2 ^e [33.2] _{cond} ^f	36.0 ^e [62.1] _{cond} ^f	123
	Et_2O^b	33.7 ^e [46.3] _{cond} ^f	52.4 ^e [86.4] _{cond} ^f	123
	Me_2CO^b	19.2 ^d [33.5] _{cond} ^e	24.2 ^d [54.4] _{cond} ^e	123
	MeCN^b	20.4 ^e [35.0] _{cond} ^f	20.5 ^e [45.4] _{cond} ^f	123
	HCN	16.3 [24.4] _{cond} ^g [30.9] _{cond} ^h	25.0	102
MeCHOMe^+	H_2O^b	11.2 [7] _{cond} ^c	19 [31] _{cond} ^d	100
	MeOH^b	13.1 [14] _{cond} ^c	21 [40] _{cond} ^d	100
Me_2COMe^+	H_2O^b	10.8 [4] _{cond} ^c	23 [31] _{cond} ^d	100
Me_4N^+	H_2O	9.0	21.5	93a
	H_2O (2) ⁱ	9.4		93a
	MeOH	9.8	23.2	93a
	MeOH (2) ⁱ	9.2	24.0	93a
	Me_2CO	14.6	24.7	93a
	Me_2CO (2) ⁱ	13.0	29.2	93a
	Me_2CO (3) ⁱ	11.7		93a
	$\text{MeO}(\text{CH}_2\text{CH}_2\text{O})_2\text{Me}$	20.6	28.7	93a
	$\text{MeO}(\text{CH}_2\text{CH}_2\text{O})_3\text{Me}$	24.2	33.8	93a
	MeCONMe_2	18.0	21.6	93a
	MeNH_2	8.7	17.0	93a
	Me_3N	9.9	20.6	93a
	MeCO-gly-OMe	20.1	29.4	93a
Et_4N^+	H_2O	7.0		93a
	Me_2CO	12.4	26.7	93a
Me_3O^+	Me_2O	13.0	28.4	93a
MeCNMe^+	H_2O	10.0	22.0	42
$\text{Me}_3\text{N}(\text{CH}_2)_2\text{NMe}_3^{+2}$	H_2O	12.7	19.3	95
	H_2O (2) ⁱ	12.2	19.8	95
$\text{Me}_3\text{N}(\text{CH}_2)_3\text{NMe}_3^{+2}$	H_2O	11.0	16.5	95
	H_2O (2) ⁱ	10.7	19.0	95
$\text{MeOCH}_2\text{CH}_2\text{NMe}_3^+$ (acetylcholine)	H_2O	8.0	22.0	124
	Me_2CO	13.2	21.7	124
$(c\text{-C}_4\text{H}_4\text{O})\text{H}^+$	H_2O	10.2	19.7	101
MeNCH^+	H_2O	14.8	19.7	42
	MeOH	19.0	23.2	42
	Me_2O	21.2	21.9	42
	MeCN	19.1	18.7	42
$c\text{-C}_3\text{H}_3^+$	H_2O	11.7	18.8	96c
	H_2O (2)	10.3	17.2	96c
$\text{C}_6\text{H}_6^{\bullet+}$	H_2O	9.0	19.5	117d
	H_2O (2) ⁱ	8.0	18.9	117d
	H_2O (3) ⁱ	8 (7.8) ^j		117d
	H_2O (4) ⁱ	10.3 (7.5) ^j	22.4	117d
	H_2O (5) ⁱ	8.6	18.1	117d

Table 3. continued

ion	ligand	ΔH°_D ^a	ΔS°_D ^a	refs
$\text{CH}^+ \cdots \text{B}$ bonds				
	H_2O (6) ⁱ	7.8	15.1	117d
$\text{BH}^+ \cdots \text{C}$ and $\text{CH}^+ \cdots \text{C}$ bonds (isocyanide ligands)				
NH_4^+	MeNC	24.0	20.2	42
MeNH_3^+		23.8	22.7	42
Me_2NH_2^+		20.6	21.5	42
Me_3NH^+		19.5	20.7	42
MeNH_3^+	EtNC	23.8	24.3	42
MeNCH^+	MeNC	25.2	24.7	42
EtNCH^+	EtNC	25.2	23.8	42
$\text{BH}^+ \cdots \pi$ bonds				
NH_4^+	C_2H_4^b	10 [26] _{cond} ^c		94a
	C_6H_6	19.3	23.3	94a
	$\text{C}_6\text{H}_5\text{F}$	14.4	18.0	94a
	$1,3,5\text{-C}_6\text{H}_3\text{Me}_3$	21.8	21.2	94a
MeNH_3^+	C_6H_6	18.8	25.1	94a
	$c\text{-C}_6\text{H}_{10}$	11.6	16.9	94a
	$c\text{-C}_4\text{H}_4\text{N}$	18.6	21.0	94a
EtOH_2^+	C_6H_6	21		94a
Me_3NH^+	C_6H_6	15.9	27.7	94a
PyridineH⁺	C_6H_6	13.4	25.1	118b
NH_4^+	phenylalanine	40.0		94b
	tyrosine	40.6		94b
	tryptophan	44.2		94b
$\text{CH}^+ \cdots \pi$ bonds				
Me_4N^+	C_6H_6	8.6	18.4	124
	$\text{C}_6\text{H}_5\text{CH}_3$	9.5	20.3	93a
$\text{MeOCH}_2\text{CH}_2\text{NMe}_3^+$ (acetylcholine)	$\text{C}_6\text{H}_5\text{CH}_3$	8.1	15.5	124
$\text{X}^- \cdots \text{HC}$ bonds				
$\text{CH}_3\text{C}(\text{CH}_2)\text{O}^-$	CH_3CN	15.3	18.9	58
CH_2CN^-		12.8	13.4	58
CH_2NO_2^-	CH_3NO_2	15.9	25	114
CH_3NO_2^-		15.2		114
CH_3NO_4^-		13.0	22	114
F^-	HCN	39.5		57
	CH_2CO	35.3		57
	$\text{C}_2\text{F}_5\text{H}$	30.4		57
	CF_3H	27.1		57
	Me_3CCHO	24.6		57
	$\text{C}_6\text{H}_5\text{CH}_2\text{F}$	24.4		57
	$t\text{-C}_4\text{H}_9\text{F}$	22.3		57
	H_2CCH_2	8.8	14	113
	CH_3CHCH_2	9.8	16	113
Cl^-	HCN	21.0		7
	CH_3F	11.5		7
	CH_3CN	15.8		7
	CH_3Cl	12.2		7
	CH_2Cl_2	15.8		7
	CHF_3	16.7		7
	C_6H_6	9.9		7
	MeCHO	14.4		7
	Me_3CCHO	15.0		7
	Me_2CO	14.8		7
	$(\text{Me})(\text{Et})\text{CO}$	14.8		7
	Et_2CO	14.1		7
	CH_3NO_2	15.6	21.4	114
	H_2CCH_2	5.4	18	113
	CH_3CHCH_2	5.9	16	113
Br^-	H_2CCH_2	4.7	15	113
	CH_3CHCH_2	5.5	15	113

Table 3. continued

ion	ligand	ΔH°_D ^a	ΔS°_D ^a	refs
$X^- \cdots HC$ bonds				
I ⁻	H ₂ CCH ₂	3.7	14	113
	CH ₃ CHCH ₂	4.6	15	113
NO ₂ ⁻	CH ₃ NO ₂	14.5	22.5	114
$C^- \cdots HO$ and $\pi^- \cdots HO$ bonds				
HCC ⁻	H ₂ O	16.2	18.6	58
	MeOH	21.6	33.6	125
	CF ₃	19.3	28.9	126
c-C ₅ H ₅ ⁻	H ₂ O	15.7	17.5	58
	H ₂ O (2) ⁱ	10.0	17.4	58
	MeOH	13.2	21.1	58
	t-BuOH	17.0	32.1	58
c-C ₄ H ₄ N ⁻	H ₂ O	15.7	23.1	58
	MeOH	18.6	27.5	58
$\Pi^- \cdots HC$ bonds				
c-C ₅ H ₅ ⁻	Me ₂ CO	13.5	21.8	58
	MeCN	15.5	22.8	58
c-C ₄ H ₄ N ⁻	Me ₂ CO	13.1	20.5	58
	MeCN	15.8	23.4	58

^a ΔH°_D values are in kcal/mol, and ΔS°_D are in cal/(mol K). ^bIn these systems, covalent bonds with larger ΔH°_D and ΔS°_D are also possible.

^cEnthalpies of condensation reactions calculated from thermochemical data of refs 127 and 128. ^dEntropies of condensation reactions as estimated in the references for the cited reactions. ^eThermochemistry of association reactions to form cluster ions at high temperatures, usually above 400–450 K.

^fThermochemistry of association reactions to form covalent adducts, usually below 400–450 K.¹²³ ^gBond dissociation energy (ΔH°_D) corresponding to the condensation reaction to form t-C₄H₉NCH⁺ as estimated from data for isocyanides.^{127,128} ^hBond dissociation energy (ΔH°_D) corresponding to the condensation reaction to form t-C₄H₉CNH⁺ from the thermochemistry in refs 127 and 128. ⁱShorthand for second or higher ligand molecule.

^jThe measured binding energies of C₆H₆^{•+}(H₂O)₃ and C₆H₆^{•+}(H₂O)₄ may be perturbed by the deprotonation reaction, and the computed values in parentheses may be more reliable.

and aromatic hydrocarbon cations with N and O lone pair acceptors.^{93a–96a} The bond strengths range between 9 and 20 kcal/mol. The bond strength of 9 kcal/mol seems to be typical for CH^{δ+}·H₂O bonds as this value is observed for diverse ions such as C₃H₃⁺, C₆H₆^{•+}, and N(CH₃)₄⁺ (Table 3). Ab initio calculations showed that, in the complex (CH₄)₄N⁺·OH₂, where ΔH°_D is 9.4 kcal/mol, the most stable conformation involves a cavity formed by three H atoms of two methyl groups that accommodate the ligand molecule (Figure 19). The second water molecule seems to bond preferentially to the first water molecule in an outer position forming a conventional OH^{δ+}·O hydrogen bond. This may account for the anomaly that the second bond is slightly stronger than the first bond. An isomeric structure where the two H₂O molecules bond directly to two cavities formed by the methyl groups of the ion is less stable, although only by 1.2 kcal/mol, and the two isomers may be present in the observed equilibrium populations.^{93a}

However, in complexes of (CH₃)₄N⁺ with blocked ligands such as Me₂CO, both the first and second ligand molecules could form only weak CH·O bonds with the ion and with each other. Here the second molecule is indeed bonded more weakly than the first, the first two bonds being 14.6 and 13.0 kcal/mol, respectively.^{93a}

The main feature in N(CH₃)₄⁺(H₂O)_n is that a water molecule is bonded in a pocket of three methyl hydrogens from two methyl groups, and a second water molecule is attached to the first water molecule, rather than directly to the ion.^{93a} These features were confirmed and extended by IR spectroscopy and quantum chemical computations for clusters of N(CH₃)₄⁺(H₂O)_n with up to 8 H₂O molecules. The water molecules in these clusters are attached to each other, and the ion is attached on the outside and does not perturb significantly the structure of the attached water cluster.^{93b}

Complexes of doubly charged diquaternary ions were measured recently.⁹⁷ Bond strengths in the complexes (CH₃)₃N(CH₂)_pN(CH₃)₃²⁺·H₂O, *p* = 2 and 3, are 11–13 kcal/mol. These bonds are somewhat stronger than the bond of H₂O to the singly charged (CH₃)₃N⁺ ion, which is 9.0 kcal/mol, because Coulomb interactions between the two charge groups increase the positive charge on the bonding methyl hydrogen of each group in the doubly charged ion. These electrostatic interactions between the ionic groups decrease with increasing separation between the charged groups, and as the charges on the bonding end methyl group hydrogens decrease from *p* = 2 to 3, the bonding energies to the H₂O molecules decrease from 12.7 to 11.0 kcal/mol. The bonding energies of the first and second water molecules to these ions are similar, which indicates that consecutive H₂O molecules add alternately to the two functional groups. However, the ΔS° values observed for *p* = 3 suggest that here the second H₂O molecule may bond to the first H₂O molecule rather than to the second quaternary amine group.⁹⁵

Recently, Hiraoka and co-workers studied the clusters CH₃(N₂)_n⁺. The thermochemistry and ab initio calculations showed covalent bonding to the first N₂ molecule, a 3-fold shell structure in H₃CN₂⁺(N₂)₃ with *n* = 4, and the 4-fold shell structure (N₂)H₃CN₂⁺(N₂)₄ with *n* = 6.⁹⁸

In complexes of C₂H₅⁺ with CO₂ and N₂O, the nonclassical proton-bridged structure of the ion rearranged to the classical structure in the complexes. The s-C₃H₇⁺ and t-C₄H₉⁺ ions bonded to these ligands only by 4–5 kcal/mol due to hyperconjugation.⁹⁹

Complexes with CH^{δ+}·B bonds in (furan)H⁺·H₂O, (pyrrole)H⁺·H₂O, and (thiophene)H⁺·H₂O were also investigated.^{100,101} The furan and thiophene complexes have small bonding energies, 10.2 kcal/mol. The H₂O molecules bond to the acidic

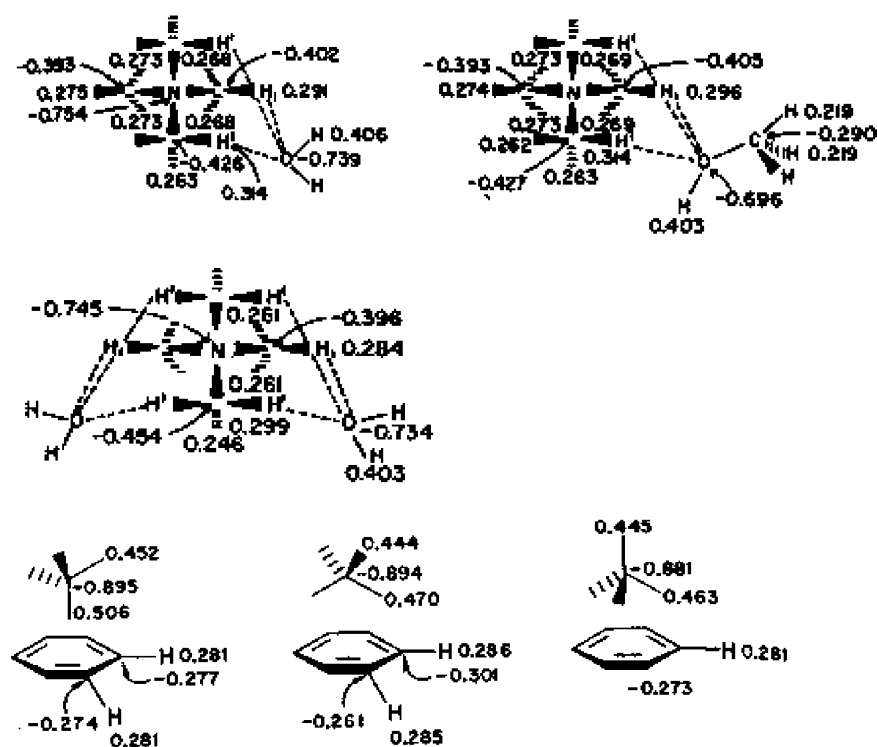


Figure 19. The top panel (from ref 94a) shows the structures of $(\text{CH}_3)_4\text{N}^+\cdot\text{H}_2\text{O}$ and $(\text{CH}_3)_4\text{N}^+\cdot\text{CH}_3\text{OH}$ where the oxygen functions fit in a cavity formed by three hydrogens on two methyl groups. The center panel (from ref 93a) shows the structure of $(\text{CH}_3)_4\text{N}^+\cdot 2\text{H}_2\text{O}$ where both H_2O molecules are bonded to cavities formed by the methyl groups. This isomer is less stable by 1.2 kcal/mol than a structure where the second water molecule is bonded to the first by an $\text{OH}^{\delta+}\cdot\text{O}$ bond. The bottom panel (from ref 93a) shows the structure of the $\text{NH}_4^+\cdot\text{C}_6\text{H}_6$ complex in three orientations of NH_4^+ showing $\text{NH}_4^+\cdot\pi$ interactions. Reproduced from refs 93a and 94a with permission. Copyright 1985 American Chemical Society.

proton on the unprotonated α -carbon. In comparison, $(\text{pyrrole})\text{H}^+$ is also ring-protonated, but the N–H hydrogen is strongly acidic, and it is the most strongly hydrogen-bonding site. Weak $\text{CH}^{\delta+}\cdot\text{OH}_2$ bonds may also form in the complexes of the radical ions of these heterocyclic aromatics, such as in $(\text{furan})^{\bullet+}\cdot\text{H}_2\text{O}$ ($\Delta H^\circ_D = 9.8 \text{ kcal/mol}$) and $(\text{thiophene})^{\bullet+}\cdot\text{H}_2\text{O}$ ($\Delta H^\circ_D = 9.5 \text{ kcal/mol}$), where the charge is delocalized and the charge densities on the bonding CH sites are smaller than those in the protonated analogues.¹⁰¹ The complexes of the $(\text{benzene})^{\bullet+}$ ion discussed below also belong to this group.

Bonds with CH donors may also occur in the blocked clusters ($\text{CH}_3\text{CNH}^+\cdot\text{NCCH}_3\cdot\text{CH}_3\text{CN}$)¹⁰² and ((CH_3)₂ OH^+ · $\text{O}(\text{CH}_3)_2\cdot(\text{CH}_3)_2\text{O}$)¹⁰³ where the third molecule is bonded relatively weakly (9.3 and 10.1 kcal/mol, respectively), suggesting that the third ligand is bonded by weak CH-N- or CH-O- hydrogen bonds. Alternatively, these complexes may have T-shaped geometries with a long second H⁺-N or H⁺-O bond.

Bonds of CH-N type occur in the linear protonated clusters of HCN, that is, in $\cdots\text{HCN}\text{-HCNH}^+\text{-NCH}\cdots$. The cyanide CH groups are efficient hydrogen donors because of the carbon acidity of the sp carbon hydrogen.¹⁰² In these complexes, the core HCNH^+ ion is both an –NH and a –CH donor. Similar CH-N bonds occur in complexes of protonated isocyanides with amines, $\text{RNCH}^+\text{-NR}_3$. The intrinsic strengths of these $\text{CH}^{\delta+}\text{-N}$ bonds are shown in the correlation parameters in Table 2. Complexes of CH donors were investigated also spectroscopically^{104,105,106a} and as reaction intermediates.^{94a,107–111}

2.4.2. Anionic Complexes with Carbon-Based Bonds. Carbon CH donors can also bond to neutral or anionic halide

acceptors. In ionic systems, the Kebarle group reported $\text{CH}\cdots\text{Cl}^-$ complexes with an inverse correlation between $\Delta H^\circ_{\text{acid}}$ of the carbon acid and the $\Delta H^\circ_{\text{D}}$ value.⁴¹ As another example, $\text{CN}^-(\text{H}_2\text{O})$ involves a $\text{C}^-\cdots\text{HO}$ bond, and cyclic structures involving $\text{CH}\cdots\text{Cl}^-\cdots\text{HC}$ and $\text{CH}\cdots\text{CN}^-\cdots\text{HC}$ bonds were indicated by the thermochemistry in $\text{Cl}^-((\text{CH}_2)_x\text{O})^8$ (Figure 20).

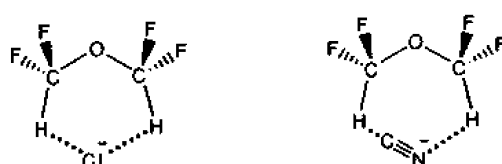


Figure 20. Bidentate cyclic structures with CH donors in the complexes of $(CHF_2)_2O$ with Cl^- and CN^- anions. Reproduced with permission from ref 8. Copyright 1987 American Chemical Society.

In a series of complexes of CH_3CN , $(\text{CH}_3)_2\text{CO}$, CH_3NO_2 , and $\text{C}_6\text{H}_5\text{Cl}$ with Cl^- , Sieck found an inverse correlation between ΔH°_D and the $\Delta \Delta H^\circ_{\text{acid}}$ of these carbon acids.^{83a}

Hydrogen bonds between alkyl CH donors and anion receptors can also form as intramolecular bonds. Evidence for CH...O⁻ internal bonds were observed in carboxylate anions with long-chain hydrocarbon substituents such as in *n*-CH₂(CH₂)₆COO⁻ anions.¹¹²

The thermochemistry of further anionic systems with CH₄ donors was investigated recently by Hiraoka and co-workers. In clusters of halide anions with C₂H₄ and CH₃CHCH₂, the bonding energies were <10 kcal/mol. Shell-filling effects were observed in complexes of the smaller halide ions F⁻(C₂H₄)_n.

and $\text{Cl}^-(\text{CH}_3\text{CHCH}_2)_3$ but not in the complexes of the larger halide anions.¹¹³ In other anionic systems, Wincel studied the binding energies of CH_3NO_2 to Cl^- , NO_2^- , CH_2NO_2^- , CH_3NO_2^- , and CH_3NO_4^- by $\text{CH}\cdots\text{X}^-$ bonds.¹¹⁴

2.4.3. Complexes of Carbon Lone-Pair Acceptors. Carbon lone pairs of isocyanides and of some anions can serve as hydrogen acceptors in ionic hydrogen bonds. Such complexes form, for example, between protonated amines and neutral isocyanides. These complexes have bonding energies comparable with the analogous complexes of cyanides, where the cyanide nitrogen lone pairs are the hydrogen acceptors. The correlation parameters in Table 2 show that the intrinsic strengths of $\text{NH}^+\cdots\text{CNR}$ bonds are significantly smaller (25.7 kcal/mol) than those of $\text{NH}^+\cdots\text{NCR}$ bonds (35.3 kcal/mol). Although the isocyanide complexes are weaker, the charge transfer and the stretching of the donor bonds are greater in these complexes. The electrostatic and delocalization components are different in the cyano and isocyanide complexes, and the covalent contributions are larger when the acceptors are the carbon lone pairs of the isocyanides.⁴² In a special case, $\text{CH}^+\cdots\text{C}$ bonds form in the complexes of protonated and neutral isocyanides. In such a complex, $\text{CH}_3\text{NCH}^+\cdot\text{CNCH}_3$, the bonding is weaker, but only by 4 kcal/mol, than in the analogous $\text{CH}_3\text{CNH}^+\cdot\text{NCCH}_3$ cyanide complex.

In anions, bonds with carbon lone-pair acceptors occur in $\text{HCC}^-\cdot\text{H}_2\text{O}$ ($\Delta H^\circ_D = 14.6$ kcal/mol)⁵⁸ and possibly in $\text{CN}^-\cdot\text{H}_2\text{O}$, where the second H_2O molecule may attach to the carbon lone pair. Anionic complexes of the $\text{CH}\cdot\text{C}^-$ type with carbon-based acceptors and donors also occur, but these bonds are expected to be weak according to electronegativity considerations.⁸ For example, the $\text{CH}_3\text{CN}\cdot\text{CH}_2\text{CN}^-$ dimer with ΔH°_D of 12.8 kcal/mol is relatively weakly bonded.

2.4.4. Complexes of π -Acceptors. Examples of unconventional bonds between cations and π -acceptors were investigated in gas-phase complexes^{94a} and, more extensively, in solution,¹¹⁵ and these cation– π interactions were reviewed.¹¹⁵

In complexes of protonated amines with benzene derivatives, the bonding energies range from 13.4 kcal/mol for the pyridine $\text{H}^+\cdot\text{C}_6\text{H}_6$ complex (in agreement with the calculated 14.8 kcal/mol),^{118a,b} 15.9 kcal/mol for the bonding of the large, charge-delocalized ion Me_3NH^+ to C_6H_6 , to 19.3 kcal/mol for $\text{NH}_4^+\cdot\text{C}_6\text{H}_6$ and 21.8 kcal/mol for the bonding of the small NH_4^+ ion to the efficient acceptor 1,3,5- $\text{C}_6\text{H}_3(\text{CH}_3)_3$ complexes.^{94a} The bonding energies of these $-\text{NH}^+\cdots\pi$ complexes are inversely related to the proton affinity differences of the components, as observed also for other ionic hydrogen bond complexes.

In the most stable conformation of $\text{NH}_4^+\cdots\text{C}_6\text{H}_6$, two hydrogen atoms point toward the benzene; 0.066 of a unit charge is transferred to the aromatic ligand, compared with 0.055 in $\text{NH}_4^+\cdot\text{H}_2\text{O}$ and 0.094 in $\text{NH}_4^+\cdot\text{NH}_3$. The bonding enthalpies of these complexes are also comparable, 19.3, 20.6, and 24.4 kcal/mol, respectively. The extent of charge transfer in these cation– π complex is comparable to the extent of charge transfer in complexes with lone-pair acceptors that have similar bond energies. The bonding energies of NH_4^+ to up to 4 C_6H_6 molecules were found to be similar to the respective K^+ bonding energies, which shows that NH_4^+ behaves essentially as a spherical ion in these complexes.⁸⁹ In $\text{Me}_2\text{NH}_2^+\cdot\text{C}_6\text{H}_6$ two and in $\text{MeNH}_3^+\cdot\text{C}_6\text{H}_6$ three hydrogens point toward benzene, and in $\text{Me}_3\text{NH}^+\cdot\text{C}_6\text{H}_6$ the ammonium proton points toward the center of the benzene ring. The distances from the nitrogen to the benzene centroid are 2.91–3.01 Å, and the distances from the bonding hydrogens to the aromatic plane are 2.0–2.3 Å.^{116a}

The proton gains positive charge, but the changes in the charge density and geometry of the hydrogen donor are small.^{116a} The $\text{NH}_4^+\cdot\text{C}_6\text{H}_6$ complex,^{94a,116a} bonded by cation– π interactions, can be compared with the adducts of NH_4^+ with aromatic amino acids. The bonding energies of NH_4^+ to phenylalanine, tyrosine, and tryptophan are 40.0, 40.6, and 44.2 kcal/mol, respectively,^{94b} much higher than the 19.3 kcal/mol to benzene. In these complexes the proton is transferred from the amino acids to ammonia, although its PA is lower, to form NH_4^+ that is stabilized by 3.3, 3.7, and 3.6 kcal/mol by three hydrogen bonds, respectively, to the amine group, the carboxylic carbonyl, and the aromatic ring of the amino acids. In comparison, an $\text{Na}^+\cdot\pi$ bond contributes 7.0, 7.8, and 6.8 kcal/mol in complexes of Na^+ with these amino acids, respectively.^{94b}

In other complexes both the donor and acceptor may be carbon-based. For example, a complex of the $\text{CH}^+\cdots\pi$ type $\text{N}(\text{CH}_3)_4^+\cdot\text{C}_6\text{H}_6$ has a bonding energy of 9.0 kcal/mol. In its most stable conformer, one hydrogen from each of three methyl groups bonds to three different C–C bonds of the benzene molecule. The distance from the methyl carbons to the aromatic center is 4.22 Å, and that from the bonding hydrogens to the benzene plane is 2.6 Å.^{116a} Further $\text{CH}^+\cdots\pi$ complexes were observed also in $\text{C}_6\text{H}_6^+\cdots(\text{C}_2\text{H}_2)_n$ clusters with the benzene hydrogens as proton donors and the acetylene π electrons as acceptors, with bonding energies of 3–4 kcal/mol for the first 4 C_2H_2 molecules.^{116b} Electrostatic $\text{NH}\cdots\pi$ and $\text{CH}\cdots\pi$ interactions and exchange repulsion $\pi\cdots\sigma^*$ interactions are both important in these $\text{NH}^+\cdots\pi$ and $\text{CH}^+\cdots\pi$ complexes.^{94a,116a}

A stronger $\text{CH}^+\cdots\pi$ bond forms in the T-shaped isomer of the $(\text{C}_6\text{H}_6)_2^{+*}$ radical dimer cation. A CH group on one component is bonded to the center of the partially negative carbon ring of the other component with a calculated bond energy of 15.2 kcal/mol. However, an isomer where the benzene rings are parallel is bonded more strongly, by a calculated 17.4 kcal/mol (experimental 17.8 kcal/mol), due to charge-transfer interactions between the components.^{117a,b}

The π -bond system of aromatic anions can also serve as a hydrogen acceptor. Such $\text{OH}\cdot\pi$ bonds occur in complexes of C_5H_5^- with H_2O and alcohols. The bond strengths of $\text{ROH}\cdot\text{C}_5\text{H}_5^-$ show a linear correlation with $\Delta\Delta H^\circ_{\text{acid}}$ (Table 2) with an intercept of 24.4 kcal/mol, which shows intrinsically strong interactions. Nevertheless, the bonds are weaker by 4 kcal/mol than a localized $\text{OH}\cdots\text{C}^-$ bond in $\text{HCC}^-\cdots\text{H}_2\text{O}$, which has a similar $\Delta\Delta H^\circ_{\text{acid}}$ demonstrating the difference between the delocalized π -acceptor and the localized C^- acceptors.⁵⁸

Bonds between carbon π -acceptors and CH donors occur in complexes of C_5H_5^- with CH_3CN and CH_3COCH_3 . Despite the expected weak $\text{CH}\cdots\pi$ interactions, these complexes have fairly strong bonds of 15.5 and 13.1 kcal/mol, respectively, which may imply multiple hydrogen bonds between the methyl groups and the π -ring.⁵⁸

Spectroscopic studies of unconventional IHBs of aromatic molecules were summarized recently.^{119a} Bonds of $\text{OH}\cdots\pi$ type were found in radical ion complexes of phenol with acetylene, ethylene, and benzene. In $(\text{benzene/water})^{+*}$ and $(\text{benzene/methanol})^{+*}$ clusters, the spectra showed evidence of $\text{CH}\cdots\text{OH}_2$ bonds, where one ligand molecule bonds to one or two benzene hydrogen atoms, while further ligand molecules form ligand–ligand bonds.^{119a,b,120} Spectroscopic evidence for $\text{OH}\cdots\pi$ interactions was found also in complexes of benzene with acetic acid.¹²¹ A novel IHB was found in $1,2\text{-CH}_3\text{C}_6\text{H}_4\text{OH}^+$ and $1,2\text{-C}_2\text{H}_5\text{C}_6\text{H}_4\text{OH}^+$ ions where the alkyl groups serve as hydrogen acceptors.¹²²

2.4.5. Hydrogen-Bonded Isomers of Covalent Ions. Some noncovalent hydrogen-bonded adducts can form even

when covalently bonded isomers are also possible. The noncovalent hydrogen-bonded adducts may be more stable, having lower free energies than the covalent adducts due to a combination of enthalpy and entropy effects. Hydrogen-bonded complexes may also form even when they are less stable than the covalent adducts when there are energy barriers to the formation of the covalent adducts.

In the hydrogen-bonded complexes, the reactants retain free rotation and low-frequency vibrations about the hydrogen bond, while in covalent adducts, this internal freedom is absent. Correspondingly, the value of ΔS°_D is usually about 20–25 cal/(mol K) for the loose noncovalent complexes but over 35 cal/(mol K) for covalent adducts. Because of the $T\Delta S^\circ$ contributions, ΔG° can favor the loose noncovalent adduct at high temperatures, even if the covalent bond is somewhat stronger. **Hydrogen-bonded isomers can form in the addition of carbonium ions to O and N lone-pair donors to form $\text{CH}^+ \cdots \text{N}$ or $\text{CH}^+ \cdots \text{O}$ complexes, or to unsaturated molecules forming $\text{BH}^+ \cdots \pi$ complexes, or by forming weak electrostatically bonded complexes.**

The first example was observed by Hiraoka and Kebarle in the complex of C_2H_5^+ with H_2 . The van't Hoff plot had two sections, corresponding to a noncovalent adduct at low temperatures and the C_2H_7^+ protonated ethane at high temperatures where the complex can overcome an activation barrier to form covalent bonds.^{129a}

Carbonium ions can add to nitrogen and oxygen bases to form either noncovalent $\text{CH}^+ \cdots \text{N}$ or $\text{CH}^+ \cdots \text{O}$ adducts or covalent protonated alcohols or ethers. For example, the CH_3^+ cation can form ionic hydrogen bonds with NH_3 and H_2O molecules to form hydrogen-bonded isomers CH_3NH_3^+ and CH_3OH_2^+ , respectively.^{96a} Similarly, CH_3^+ adds to CH_3OH and $(\text{CH}_3)_2\text{O}$ to form either hydrogen-bonded isomers or $(\text{CH}_3)_2\text{OH}^+$ and $(\text{CH}_3)_3\text{O}^+$ ions, respectively.^{96b} Also, the small aromatic cation $c\text{-C}_3\text{H}_3^+$ forms $\text{CH}^{\delta+} \cdots \text{O}$ bonds in hydrated $\text{C}_3\text{H}_3^+ \cdots (\text{OH}_2)_n$ complexes, rather than a covalent adduct, as suggested by the −18.8 cal/(mol K) entropy of association characteristic to cluster ions.^{96c}

Noncovalent adducts are especially competitive with covalent adducts when the reactants are highly stabilized carbonium ions such as $t\text{-C}_4\text{H}_9^+$ or oxocarbonium ions. The stabilities of the ions weaken the covalent bonds to oxygen or nitrogen bases, and their strengths become comparable to $\text{CH}^{\delta+} \cdots \text{B}$ bonds, while entropy favors the hydrogen-bonded isomers. In such cases, the hydrogen-bonded complex may be favored at high temperatures and the covalent adduct at low temperatures.

In early examples, covalent condensation was indicated in $s\text{-C}_3\text{H}_7^+ + \text{HCN} \rightarrow s\text{-C}_3\text{H}_7\text{NCH}^+$ with $\Delta H^\circ_D = 30.8$ kcal/mol and $\Delta S^\circ_D = 32$ cal/(mol K). On the other hand, noncovalent adducts were indicated in $t\text{-C}_4\text{H}_9^+ + \text{HCN}$, where the values of $\Delta H^\circ_D = 16.3$ kcal/mol and $\Delta S^\circ_D = 25$ cal/(mol K) are too small for covalent addition. The thermochemistry suggests a loose complex where the ligand is hydrogen-bonded to methyl hydrogens of the $t\text{-C}_4\text{H}_9^+$ ion rather than forming the covalent $t\text{-C}_4\text{H}_9\text{CNH}^+$ or $t\text{-C}_4\text{H}_9\text{NCH}^+$ adducts, the ΔS°_D of which can be estimated as 35 cal/(mol K) (see Table 3).¹⁰²

A system with oxygen acceptors is $t\text{-C}_4\text{H}_9^+\cdot\text{H}_2\text{O}$ for which Hiraoka and Kebarle measured a binding energy of 11.2 kcal/mol.¹³² This small binding energy may correspond to a covalent or noncovalent adduct. The formation of a $\text{CH}^{\delta+} \cdots \text{OH}_2$ type noncovalent adduct rather than the $t\text{-C}_4\text{H}_9\text{OH}_2^+$ covalent adduct was suggested by Meot-Ner and co-workers on the basis of the small $\Delta S^\circ_D = 22$ cal/(mol K), and this was confirmed by

the collisional dissociation mass spectrum of the adduct, which was different than that of $t\text{-C}_4\text{H}_9\text{OH}_2^+$.¹⁰⁰ The adducts of the oxocarbonium ions $\text{CH}_3\text{CHOCH}_3^+$ and $(\text{CH}_3)_2\text{COCH}_3^+$ with H_2O and CH_3OH in Table 3 also appear to be noncovalent complexes rather than unstable protonated hemiacetals or acetals.¹⁰⁰

Subsequently, the analogous adducts of $t\text{-C}_4\text{H}_9^+$ with CH_3OH , $\text{C}_2\text{H}_5\text{OH}$, $(\text{CH}_3)_2\text{O}$, $(\text{C}_2\text{H}_5)_2\text{O}$, $(\text{CH}_3)_2\text{CO}$, and CH_3CN were investigated by Norrman and McMahon.¹²³ The van't Hoff plots were curved between 360 and 670 K (Figure 21), and the thermochemistry suggested the covalent adducts at low

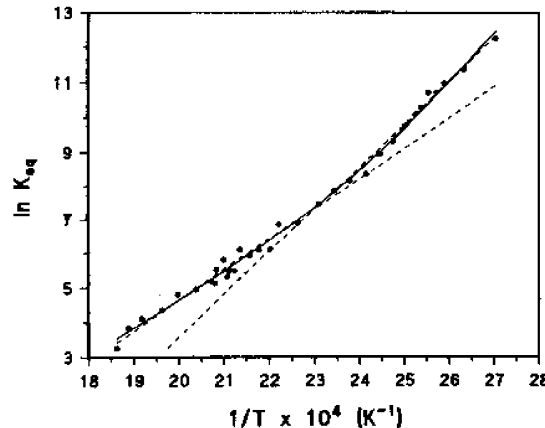


Figure 21. van't Hoff plot for the association of $t\text{-C}_4\text{H}_9^+$ with CH_3OH . The plot shows two areas, below 440 K corresponding to the formation of $t\text{-C}_4\text{H}_9\text{OCH}_3\text{H}^+$ and above 440 K corresponding to the formation of $t\text{-C}_4\text{H}_9^+ \cdots \text{CH}_3\text{OH}$. The solid line represents an exponential fit over the temperature range according to calculated equilibrium between the two dimers, and the dashed line represents equilibrium independently for the two types of complexes. Reproduced with permission from ref 123. Copyright 1996 American Chemical Society.

temperatures and hydrogen-bonded $\text{CH}^+ \cdots \text{O}$ complexes at higher temperatures (Table 3).

Hydrogen-bonded isomers of covalent ions can be also formed in the association of protonated ions with N, O, or π donors. In some of these adducts the hydrogen-bonded and covalent adducts may have similar energies, such as $\text{C}_2\text{H}_5\text{OH}_2^+ \cdots \text{NO}_2$ and the covalent $\text{C}_2\text{H}_5\text{ONO}_2\text{H}^+$ ions.^{129b} However, the hydrogen-bonded adducts may form even when the covalent adducts are more stable. For example, the observed bonding energy of 11.5 kcal/mol of $\text{H}_3\text{O}^+ \cdots \text{CO}$ indicates a hydrogen-bonded cluster rather than forming protonated formic acid ($\text{HCOOH})\text{H}^+$ that would be exothermic by 18.6 kcal/mol.^{129c} Also, protonated amines such as CH_3NH_3^+ bond weakly to CO_2 to form hydrogen-bonded cluster isomers of protonated amino acids, in this case, a hydrogen-bonded isomer of protonated glycine.

Other examples of IHB isomers include protonated ethyl compounds $\text{CH}_3\text{CH}_2\text{BH}^+$ ($\text{B} = \text{H}_2\text{O}, \text{Cl}, \text{Br}, \text{I}$) where a nonclassical protonated ion $(\text{H}_2\text{C}=\text{CH}_2)\text{H}^+$ is formed with a hydrogen bond to the neutral BH residue.^{109,110,130,131} Protonated ions can bond to $\text{H}_2\text{C}=\text{CH}_2$ to form a $\text{BH}^+ \cdots \pi$ complex, such as in $\text{NH}_4^+ \cdots \text{C}_2\text{H}_4$,^{94a} which is bonded by 10 kcal/mol although the formation of $\text{C}_2\text{H}_5\text{NH}_3^+$ would be exothermic by 26 kcal/mol (see Table 3). In this case, the noncovalent adduct persists because of an activation barrier to forming the covalent ion. Another example of a hydrogen-bonded

adduct of ethylene is the complex with HCNH^+ , which is an intermediate in the rearrangement between $\text{CH}_3\text{CH}_2\text{CNH}^+$ and $\text{CH}_3\text{CH}_2\text{NCH}^+$.¹¹¹

In summary, hydrogen-bonded complexes may be formed in the association of carbonium ions and protonated ions with N, O, and lone-pair donors of π -electron donors. The hydrogen-bonded isomers may be more stable than the covalent isomers due to a combination of enthalpy and entropy effects. However, hydrogen-bonded complexes may form even if there are more stable covalent adducts, because of energy barriers to the formation of the covalent adducts.

2.5. Radical Ions and Distonic Dimers

2.5.1. Reaction Intermediates and Distonic Dimers.

Ionic hydrogen bonds occur also in open-shell radical ions. Such systems can be generated in the ionization of clusters, for example, to generate $(\text{H}_2\text{O})_n^{\bullet+}$ or $(\text{NH}_3)_n^{\bullet+}$ or other clusters with $\text{OH}^{\bullet+}\cdots\text{O}$ or $\text{NH}^{\bullet+}\cdots\text{N}$ bonds.

The thermochemistry of these clusters can be obtained from the ionization energies of the neutral clusters, which were measured for clusters of N, O, and S bases, and also for neutral clusters containing $\text{CH}\cdots\text{O}$, $\text{CH}\cdots\text{N}$, $\text{NH}\cdots\pi$, or $\text{CH}\cdots\pi$ bonds. For example, the bonding energy of the presumably hydrogen-bonded complex $(\text{C}_6\text{H}_6\cdot\text{HCl})^{\bullet+}$ was measured as 7.3 ± 1.2 kcal/mol.¹³³ Note however that adiabatic ionization energies and the bonding energies of the neutral clusters are needed to calculate the hydrogen-bond energies of the cluster ions, but these data are often hard to obtain.

Hydrogen-bonded complexes can also occur as reaction intermediates, as discussed later.^{134–140} Complexes formed from a radical ion and a neutral molecule can undergo internal proton transfer to form a distonic hydrogen-bonded complex where the radical and charged sites are different. For example, we observed a strongly bonded complex $\text{C}_6\text{H}_6^{\bullet+}\cdot\text{C}_5\text{H}_5\text{N}$ in the benzene/pyridine system.^{118b} The complex does not undergo exchange with an additional $\text{C}_5\text{H}_5\text{N}$ molecule to form the protonated pyridine dimer $(\text{C}_5\text{H}_5\text{N})_2\text{H}^+$ + C_6H_5 , although the overall process $\text{C}_6\text{H}_6^{\bullet+} + 2\text{C}_5\text{H}_5\text{N} \rightarrow (\text{C}_5\text{H}_5\text{N})_2\text{H}^+ + \text{C}_6\text{H}_5$ would be exothermic by 32 kcal/mol. Theory and ion mobility suggested that the adduct $\text{C}_6\text{H}_6^{\bullet+}\cdot\text{C}_5\text{H}_5\text{N}$ is covalently bonded. However, it also has stable hydrogen-bonded $\text{C}_5\text{H}_5\text{NH}^+\cdot\text{C}_6\text{H}_5^{\bullet}$ distonic isomers with calculated dissociation energies of 9.0 kcal/mol when the NH^+ function points to the center of the $\text{C}_6\text{H}_5^{\bullet}$ ring, or 16.6 kcal/mol when it points to the radical carbon atom.^{118b}

The thermochemistry of the rearrangement of radical dimer ions to form the distonic hydrogen-bonded dimers, reaction 11a, can be calculated from thermochemical relations as eq 11b.



$$\begin{aligned} \Delta H_{11a}^{\circ} = & \Delta H_D^{\circ}(\text{B}^{\bullet+}\cdot\text{RH}) - \Delta H_D^{\circ}(\text{BH}^+\cdot\text{R}^{\bullet}) \\ & + \text{BDE}(\text{R}-\text{H}) + \text{IE}(\text{H}) - \text{IE}(\text{B}) - \text{PA}(\text{B}) \end{aligned} \quad (11b)$$

The second term on the right-hand side (RHS), the hydrogen-bond energy of a proton donor to a carbon lone pair of a radical ($\Delta H_D^{\circ}(\text{BH}^+\cdot\text{R}^{\bullet})$), is expected to be substantial. In comparison, the bond energies, $\Delta H_D^{\circ}(\text{B}^{\bullet+}\cdot\text{RH})$, with $\text{CH}\cdots\text{O}$ or $\text{CH}\cdots\text{N}$ bonds are expected to be weaker, and the sum of the first two terms on the RHS side of eq 11b should be negative. The sum of the other terms is negative for most oxygen and nitrogen bases if the bond dissociation energy, $\text{BDE}(\text{R}-\text{H})$, is less than 110 kcal/mol, which applies for most hydrocarbons. Therefore

proton transfer from hydrocarbons to most ionized O and N bases is usually exothermic. Such proton transfer in the complexes forms even-electron hydrogen-bonded dimers with protonated $-\text{OH}^+$ or NH^+ donors and carbon lone-pair radical acceptors. These distonic dimers are generally more stable than the electrostatically bonded radical dimer ion isomers with $\text{CH}\cdots\text{O}$ or N bonds.

2.5.2. Complexes of Ionized Aromatics: Solvation of the Benzene and Pyridine Cations. Carbon-based $\text{CH}^{\delta+}\cdots\text{O}$ bonds appear in the solvation of ionized aromatics, such as the solvated benzene ion $\text{C}_6\text{H}_6^{\bullet+}(\text{H}_2\text{O})_n$. The binding energies of H_2O molecules to $\text{C}_6\text{H}_6^{\bullet+}$ were measured by equilibrium studies in a mobility cell,^{117d,e} with a binding energy of 9.0 kcal/mol for the first H_2O molecule, in agreement with 9.4 kcal/mol from spectroscopy.^{117c} The results in Table 3 show that $\Delta H_{n-1,n}^{\circ}$ for the first six H_2O molecules are nearly constant, possibly because the water molecules bond to individual benzene hydrogens, causing little charge delocalization from the remaining benzene hydrogens. However, the binding energies are also close to the water–water bonds, and the results may suggest that a water network builds up attached to the benzene ion.

IR spectroscopy and ab initio calculations showed that the first solvent molecule forms IHBs with two adjacent protons of $\text{C}_6\text{H}_6^{\bullet+}$. The spectra with 2–4 H_2O or 2 CH_3OH molecules showed isomers where each water molecule is bonded directly to the benzene ion (“inner solvation”) and isomers where the benzene ion is attached to a cluster of solvent molecules (“external solvation”).^{119a,120,141} Both types of isomers were present in equilibrium, consistent with ab initio calculations that showed them to have similar energies.^{117e}

In relation to these structures, the IR dissociation spectra of $\text{C}_6\text{H}_5^{\bullet}(\text{H}_2\text{O})_n\text{H}^+$ clusters after $n = 4$ was very similar to the spectra of $(\text{H}_2\text{O})_n\text{H}^+$ clusters, indicating that internal proton transfer formed a protonated water cluster attached to the phenyl radical.¹⁴¹ On the other hand, isotope-exchange experiments under thermal ion mobility conditions showed that $\text{C}_6\text{H}_6^{\bullet+}(\text{D}_2\text{O})_n$ ($n = 2$ –8) did not exchange a proton with D_2O to yield a $\text{C}_6\text{H}_5^{\bullet}(\text{D}_2\text{O})_n\text{D}^+$ ion, although this would be expected for the $\text{C}_6\text{H}_5^{\bullet}(\text{D}_2\text{O})_n\text{H}^+$ structure. It is possible that the intracluster proton transfer has an energy barrier that cannot be overcome in thermal systems below 280 K in the ion mobility experiments.^{117d,e}

With the addition of 3–4 H_2O molecules, proton transfer from $\text{C}_6\text{H}_6^{\bullet+}$ to form a $(\text{H}_2\text{O})_n\text{H}^+$ cluster ion becomes energetically possible.^{117d,e} This can result in intracluster rearrangement to form a $\text{C}_6\text{H}_5^{\bullet}(\text{H}_2\text{O})_n\text{H}^+$ cluster with an $\text{OH}\cdots\pi$ bond to the phenyl radical (Figure 22). Alternatively, the intracluster proton transfer may be dissociative and produce protonated water clusters.^{117d,e}

Similarly, the solvated ions $\text{C}_3\text{H}_3^+(\text{H}_2\text{O})_n$ with $n = 1$ –5 were observed, with binding energies slightly higher than in the analogous $\text{C}_6\text{H}_6^{\bullet+}(\text{H}_2\text{O})_n$ complexes, due to the smaller, more charge-localized ion. Similar to the $\text{C}_6\text{H}_6^{\bullet+}(\text{H}_2\text{O})_n$ system, deprotonation of $\text{C}_3\text{H}_3^+(\text{H}_2\text{O})_n$ to form $(\text{H}_2\text{O})_n\text{H}^+$ clusters becomes exothermic for $n = 4$ and 5, and these reactions were observed.^{96c}

The deprotonation of C_3H_3^+ and $\text{C}_6\text{H}_6^{\bullet+}$ by 3–6 H_2O molecules requires the formation of multibody complexes, which is strongly facilitated with decreasing temperatures. Correspondingly, the rate coefficients of these reactions showed uniquely large negative temperature coefficients, with pseudo-second-order rate coefficients varying as $k = cT^{-63\pm 4}$ and

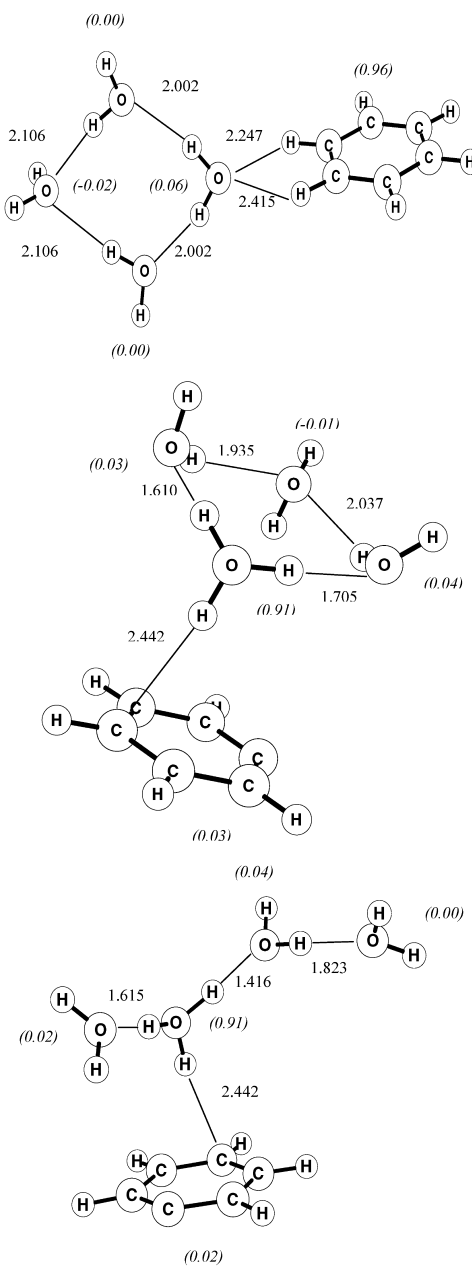


Figure 22. Stable structures of the $\text{C}_6\text{H}_6^{\bullet+}(\text{H}_2\text{O})_4$ cluster. The top panel shows a ring structure with bifurcated $\text{CH}^{\delta+}\cdots\text{O}$ bond; the center and bottom panels show ring and linear isomers of $\text{C}_6\text{H}_5^{\bullet}(\text{H}_2\text{O})_4\text{H}^+$ after proton transfer to water with $\text{OH}^{\bullet}\cdots\pi$ bonds to the phenyl radical. In the latter two, the proton is located on the water bonded to the phenyl radical. The lengths of hydrogen bonds and Mullikan group charges (in parentheses) are shown. Note that in $\text{C}_6\text{H}_6^{\bullet+}(\text{H}_2\text{O})_4$, 0.96 of the charge remains on benzene, while in $\text{C}_6\text{H}_5^{\bullet}(\text{H}_2\text{O})_4\text{H}^+$, 0.91 of the charge is on the H_3O^+ center. Total bonding energies versus $\text{C}_6\text{H}_6^{\bullet+} + 4\text{H}_2\text{O}$ monomers, from ROHF/6-31+G* calculations were, for the isomers from top to bottom, -43.6, -41.0, and -41.3 kcal/mol. The calculations suggest that intraccluster proton transfer is slightly endothermic in this cluster but becomes exothermic in larger clusters.^{117d,e}

$cT^{-67\pm 4}$ in the hydrated C_3H_3^+ and $\text{C}_6\text{H}_6^{\bullet+}$ systems, respectively.^{96c,117d,e} We also observed recently the radical pyridine $^{\bullet+}(\text{H}_2\text{O})$ cluster ion, bonded by 15.6 kcal/mol, similar to the $\text{NH}^{\bullet}\cdots\text{OH}_2$ hydrogen bond in $\text{pyridineH}^+(\text{H}_2\text{O})$, rather than the weaker $\text{CH}^{\delta+}\cdots\text{O}$ bonds of 11.7 and 9.0 kcal/mol in

$\text{C}_3\text{H}_3^+(\text{H}_2\text{O})$ and $\text{C}_6\text{H}_6^{\bullet+}(\text{H}_2\text{O})$. The further solvation steps were also similar to $\text{pyridineH}^+(\text{H}_2\text{O})_n$ (Table 4). Also, pyridine $^{\bullet+}$ was not deprotonated by gas-phase water molecules, unlike the C_3H_3^+ and $\text{C}_6\text{H}_6^{\bullet+}$ ions. These observations suggest that pyridine $^{\bullet+}$ is not solvated through $\text{CH}^{\delta+}\cdots\text{O}$ bonds that form in $\text{C}_3\text{H}_3^+(\text{H}_2\text{O})_n$ and $\text{C}_6\text{H}_6^{\bullet+}(\text{H}_2\text{O})_n$ but through an $\text{NH}^{\bullet}\cdots\text{OH}_2$ bond in a $\text{C}_5\text{H}_4\text{NH}^+(\text{H}_2\text{O})_n$ complexes of the distonic $\text{C}_5\text{H}_4\text{NH}^+$ pyridine radical cation. This is an example where cluster binding energies can identify a distonic ion.^{117f}

3. LARGER CLUSTERS AND HYDROGEN-BOND NETWORKS

3.1. Neat Aggregates and Solvation Sequences

Beyond dimers, further ligand molecules can be added stepwise to ionic clusters. In principle, the process can be carried up to forming condensed-phase aggregates. In practice, equilibrium measurements cover in most cases 4–8 and in some instances 10–18 ligand molecules,^{142–146} and collisional dissociation measurements were applied up to 26 solvent molecules.^{147,148}

The thermochemistry of the clusters gives valuable information about the inner solvent shells where ionic forces are most significant. Data on the inner-shell interactions allows quantification of the physical factors in ion solvation.³⁵

The thermochemistry also gives structural indications. Do distinct solvent shells form? How closely do the ligand-binding energies and IHB networks resemble the condensed phase? Is the ion inside or on the surface of the incipient solvent? Where is the proton in clusters? This information is indicated by the thermochemistry and can be tested further by computation, reactivity, ion chromatography, collisional dissociation, and photodissociation spectroscopy.

3.1.1. Thermochemical Studies of Stepwise Solvation.

Thermochemical studies have been applied to many solvation sequences. Hydration studies by 4 or more water molecules were applied to NH_4^+ ,^{149–151} a set of oxonium, ammonium, and derivatized amino acid ions,^{5,150} protonated amides^{48,150} and alcohols,¹⁵³ and polyfunctional ions such as protonated polyethers¹⁵⁴ and diamines.^{95,155} In the solvation of anions, hydration sequences were measured for OH^- ,^{52,156,157} the halide ions,^{158–160} HCO_3^- ,¹⁶¹ CN^- ,¹⁶² NO_2^- ,^{158,163} O_2^- ,^{52,158} Cl^- and other halide ions,^{159,160,164–166} and polyfunctional anions such as $\text{O}_3\text{S}_n\text{O}_3^{2-}$,¹⁶⁷ PO_3^{2-} ,¹⁶⁸ diacids,¹⁶⁷ diphosphate,¹⁶⁹ and adenosine 5'-diphosphate,¹⁶⁹ as well as other biomolecules discussed later.

Hydrogen bonding occurs also in the outer hydration shells of both hydrogen-bonding and non-hydrogen-bonding ions including the metal ions Li^+ ,¹⁷⁰ Na^+ ,^{171,172} K^+ ,¹⁷³ Rb^+ ,¹⁷¹ Ag^+ ,¹⁷⁴ Bi^+ ,¹⁷⁵ Ca^+ ,¹⁷⁶ Cu^+ ,¹⁷⁴ Pb^+ ,¹⁷² and Sr^+ .¹⁷⁷ Solvation series were studied also with nonaqueous solvents. Studies covering at least 4 solvent molecules were extended to solvation by CH_3OH of CH_3OH_2^+ ,^{103,178} $(\text{CH}_3)_2\text{OH}^+$,¹⁵² $(\text{CH}_3\text{OCH}_2\text{CH}_2\text{OCH}_3)\text{H}^+$,¹⁵⁴ Na^+ ,¹⁷⁹ K^+ ,⁷⁷ CH_3O^- ,^{180b} and the halide ions,¹⁶⁴ solvation series by the higher alcohols EtOH , $n\text{-PrOH}$, and $n\text{-PeOH}$ including the solvation of ROH_2^+ ,^{178,181} and of the halide ions.¹⁶⁴ Solvation by formic acid was observed in $\text{HCOO}^-\cdot n\text{HCOOH}$ and in $\text{Cl}^-\cdot n\text{HCOOH}$ clusters,¹⁸² as well as by acetic acid in cationic $(\text{CH}_3\text{COOH})\text{H}^+\cdot n\text{CH}_3\text{COOH}\cdot m\text{H}_2\text{O}$ and anionic $\text{CH}_3\text{COO}^-\cdot n\text{CH}_3\text{COOH}\cdot m\text{H}_2\text{O}$ ^{178,183} clusters. As in most mixed solvent/water clusters, the stability of each cluster of rank $r = m + n$ increases with increasing mole fraction of the larger, more polarizable acetic acid. The aggregation of acetic acid in these clusters may model fatty

Table 4. Thermochemistry of Stepwise Gas-Phase Hydration

n^b	hydration $\text{BH}^+(\text{H}_2\text{O})_n$												refs			
	$-\Delta H^\circ_{n-1,n}{}^a$								$-\Delta S^\circ_{n-1,n}{}^a$							
	1	2	3	4	5	6	7	8	cond ^c	1	2	3	4	5	6	
alcohols, ethers, ketones, acids																
H_3O^+	32.1	20.4	17.2	12.2	11.6	11.2	11.2	9.8	10.5	26.4	21.3	27.8	24.0	24.5	27.8	d
CH_3OH_2^+	26.4	20.4	14.4	11.6	9.4	9.2			10.5	26.2	28.1	25.5	22.6	19.6	21.2	d
$\text{C}_2\text{H}_5\text{OH}_2^+$	24.0	19.0	13.8	11.9	9.7				10.5	26.0	27.4	25.2	24.4	20.9		5
$n\text{-C}_3\text{H}_7\text{OH}_2^+$	23.9	17.9	11.0	9.5	8.8				10.5	28.0	26.3	22.9	20.7	20.8		153
CH_3CHOH^+	25.0	16.8	17.0	11.3	9.4	9.3			10.5	27.6	25.2	27.9	21.4	18.8	21.7	49
$(\text{CH}_3)_2\text{OH}^+$	23.3	15.4	13.4	10.2					10.5	27.6	28.2	24.2	19.0			49, 152, 200
$(\text{CH}_3)_2\text{COH}^+$	20.5	13.6	12.7	10.3	10.3				10.5	26.0	23.2	21.9	20.2	23.5		49
$(\text{CH}_3\text{COOH})\text{H}^+$	20.4	17.8	12.9	10.8					10.5	23.0	26.4	23.2	20.4			183
amines and pyridine																
NH_4^+	20.2	14.2	13.1	11.5	10.2	9.1	8.4		10.5	23.9	22.0	23.7	25.2	24.7	22.0	d
CH_3NH_3^+	17.8	14.6	12.4	10.3	8.5				10.5	24.2	25.4	25.2	22.0	20.9		201, 49
$\text{C}_2\text{H}_5\text{NH}_2^+$	17.5	14.7	13.2						10.5	25.9	29.7	30.8				201, 202
$(\text{CH}_3)_2\text{NH}_2^+$	15.0	13.5	11.3	10.5	9.4	8.4			10.5	22.9	24.7	24.4	25.2	24.4	21.2	49
$(\text{CH}_3)_3\text{NH}^+$	14.5	11.4	10.0						10.5	24.2	24.8	24.9				91, 49, 203b
$\text{C}_5\text{H}_5\text{NH}^+ (\text{PyrH}^+)$	15.0	9.6	8.3							25.5	19.6	19.6				40a
$\text{C}_5\text{H}_4\text{NH}^+ (\text{disticone Pyr}^{*+})$	15.2	9.9	8.8	7.1						33.1	19.0	20.2	15.3			117f
doubly charged diamines																
$\text{H}_3\text{N}(\text{CH}_2)_6\text{NH}_3^{2+}$	17.8	17.3								21.0	23.1					95
$\text{H}_3\text{N}(\text{CH}_2)_8\text{NH}_3^{2+}$	16.9	16.8								21.5	23.8					95
$\text{H}_3\text{N}(\text{CH}_2)_{10}\text{NH}_3^{2+}$	16.8	16.8								22.8	25.2					95
$\text{H}_3\text{N}(\text{CH}_2)_{12}\text{NH}_3^{2+}$	15.7	15.7	13.4	13.6						20.1	23.2	21.5	24.5			95
nitriles, sulfide																
HCN^+	27.4	21.4	17.2						10.5	29.6	25.3	26.2				199
CH_3CNH^+	22.5	16.2	15.6	11.2	10.4	10.1			10.5	24.5	25.1	24.8	21.8	23.4	25.5	49, 199, 204
H_3S^+	21.2	20.3							10.5	24.5	21.8					132

^aUnits are as follows: $\Delta H^\circ_{n-1,n}$ (kcal/mol); $\Delta S^\circ_{n-1,n}$ (cal/(mol K)). ^bIn the hydration series, $\Delta H^\circ_{n-1,n}$ corresponds to the addition of the n th H_2O molecule to the core ion. ^cBulk condensation enthalpy of water. ^dAverage of acceptable literature values in the NIST tables.²⁹

acids in biological membranes, where anionic and neutral carboxylic acid headgroups can form IHB networks to stabilize the membranes.^{178,183}

Further acid/water clusters were studied by Lovejoy and co-workers in relation to atmospheric nucleation, with clusters $\text{HSO}_4^-(\text{H}_2\text{SO}_4)_m(\text{HNO}_3)_n$ (m up to 5 and n up to 3), hydrated $\text{HSO}_4^-(\text{H}_2\text{SO}_4)_s(\text{H}_2\text{O})_w$ (s up to 6 and w up to 10), and in $\text{HS}_2\text{O}_7^-(\text{H}_2\text{SO}_4)_s$ (s up to 3) that contain SO_3 . The bonding energy of 41.8 kcal/mol in $\text{HSO}_4^-(\text{H}_2\text{SO}_4)$ is one of the strongest IHBs observed.^{184a-d} The thermochemistry of cationic $\text{H}^+(\text{H}_2\text{SO}_4)_s(\text{H}_2\text{O})_w$ clusters (s up to 3 and w up to 16) was also measured. It was observed that H_2O molecules tend to displace H_2SO_4 in these clusters, which indicates that nucleation through clusters containing sulfuric acid may not occur in the atmosphere.^{185a,b}

Other mixed clusters include the solvation of ammonia by nitrogen bases, studied by the Castleman group;^{77,174} the solvation of protonated amines by neutral amines;¹⁷⁸ the clustering of HCN molecules about NH_4^+ ,¹⁸⁶ HCN^+ ,¹⁰² CN^- ,^{43a,162,187} CH_3COO^- ,^{43a} and halide ions,^{43a,188} and CH_3CN molecules about NH_4^+ ,⁸⁹ which were also investigated theoretically as to $\Delta \text{PA}/\text{bond strength}$ correlations;¹⁸⁹ and also association of CH_3CN with alkali cations¹⁹⁰ and halide anions,^{160,191,192a} and protonated amino acids,^{192b} was also studied. A few studies addressed hydrogen-bonded clusters involving the hydrides of heavier elements such as $\text{H}_3\text{S}^+(\text{H}_2\text{O})_n$,^{61,64a} and $\text{PH}_4^+(\text{PH}_3)_n$.⁶⁵

3.1.2. Effects of Stepwise Solvation on Charge Distributions and Hydrogen-Bond Lengths.

The changes in structures and charge distributions with increasing cluster size can be illustrated by protonated neat water clusters and water/ammonia mixed clusters that were studied both experimentally and theoretically.³⁶ Figure 23 shows the structures and atomic charges in $\text{H}_3\text{O}^+(\text{H}_2\text{O})_n$ clusters. In

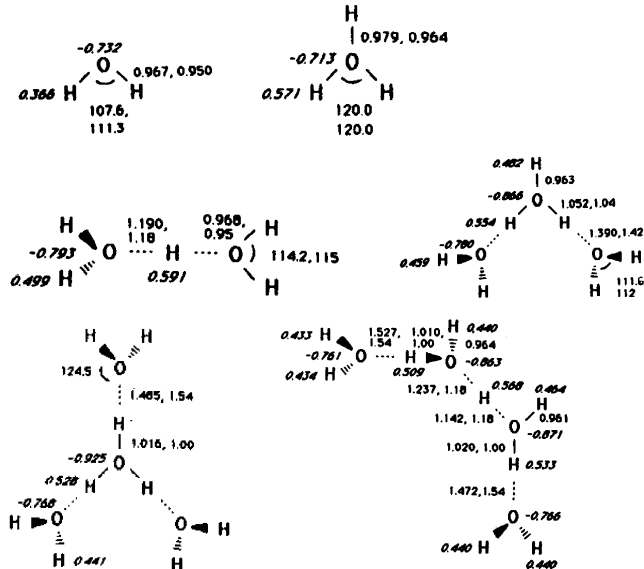


Figure 23. Structures and atomic charges in $\text{H}_3\text{O}^+(\text{H}_2\text{O})_n$ clusters. Reproduced with permission from ref 36. Copyright 1986 American Chemical Society.

forming the dimer, the bonding proton becomes more positive because the electronegative oxygen of the ligand attracts electron density away from the proton. However, on addition of further solvent molecules, the positive charge dissipates and the bonding proton or protons of the H_3O^+ core ion become less positive. When 1–3 water molecules are added in the inner shell, the ligands attach directly to the core ion as in Figure 23. The charge on the bonding protons changes from 0.571 to 0.591, 0.554, and 0.528, while the overall charge on the central H_3O^+ ion changes from 1.000 to 0.796, 0.724, and 0.659 unit charge. Even when the inner solvent shell is filled by three H_2O molecules, 66% of the charge remains on the core ion.

Similar trends were observed in $\text{NH}_4^+(\text{NH}_3)_n$ clusters. With inner-shell solvation as n changes from 0 to 3, the charge on the bonding proton changes from 0.488 to 0.535, 0.521, and 0.507 while the charge on the NH_4^+ core ion changes from 1.000 to 0.906, 0.858, and 0.832 unit charge. Again, a large fraction of the charge, 83%, remains on the core ion. Anionic clusters behave similarly. Calculations on $\text{OH}^-(\text{H}_2\text{O})_n$ showed that 75% of the charge remains on the hydroxyl anion.^{193,194}

In these clusters, the protonated core species and ligands were identical. More commonly, a core ion is solvated by a different solvent, especially water. This is illustrated in Figure 24 by $\text{NH}_4^+(\text{H}_2\text{O})_n$ clusters in the ammonia/water system. The charge on the bonding proton increases again at the first solvation step and decreases in the further steps as n changes from 1 to 4, changing from 0.488 to 0.542, 0.527, 0.513, and 0.499, while the charge on the core NH_4^+ ion changes from 1.000 to 0.945, 0.908, 0.881, and 0.861 as n increases. In all clusters, most of the charge remains on the protonated core ion even after the inner solvent shell becomes filled.

These examples concerned clusters where the solvent molecules are bonded directly to the core ion. Figures 23 and 24 also show isomers in which ligand molecules bond to inner ligand molecules in the outer shell before the inner shell is filled. In either case, charge delocalization to the solvent increases with added solvent molecules, but less additional charge becomes delocalized in each solvation step. Adding further ligand molecules in the outer shells should have even smaller effects, which suggests that most of the charge remains on the protonated core ion even in bulk solution.

The above trends are physically sensible although the charge densities were derived from Mullikan population analysis based on relatively low-level 6-31G* calculations. Higher-level calculations are needed, especially on the larger clusters.

Generally, when consecutive ligand molecules are attached directly to a protonated core ion, the following changes occur in charge distributions: as more solvent molecules are attached to the core ion, the positive charge q_H on each of its bonding protons decreases, although it is always larger than that in the unsolvated ion. The charge becomes dispersed, and the charge remaining on the core ion decreases. The total charge transferred to the solvent increases, but the charge on each solvent molecule decreases.

In parallel, structural changes occur: the B–H⁺ bond lengths of the donor become less extended. With increasing cluster size, individual hydrogen bonds in the assembly weaken and become more extended.

In addition, especially in larger clusters, the following are possible: shell filling may occur. Isomeric clusters of similar energies may be possible and may coexist in equilibrium. Cyclic and clathrate hydrogen-bonded systems may form.

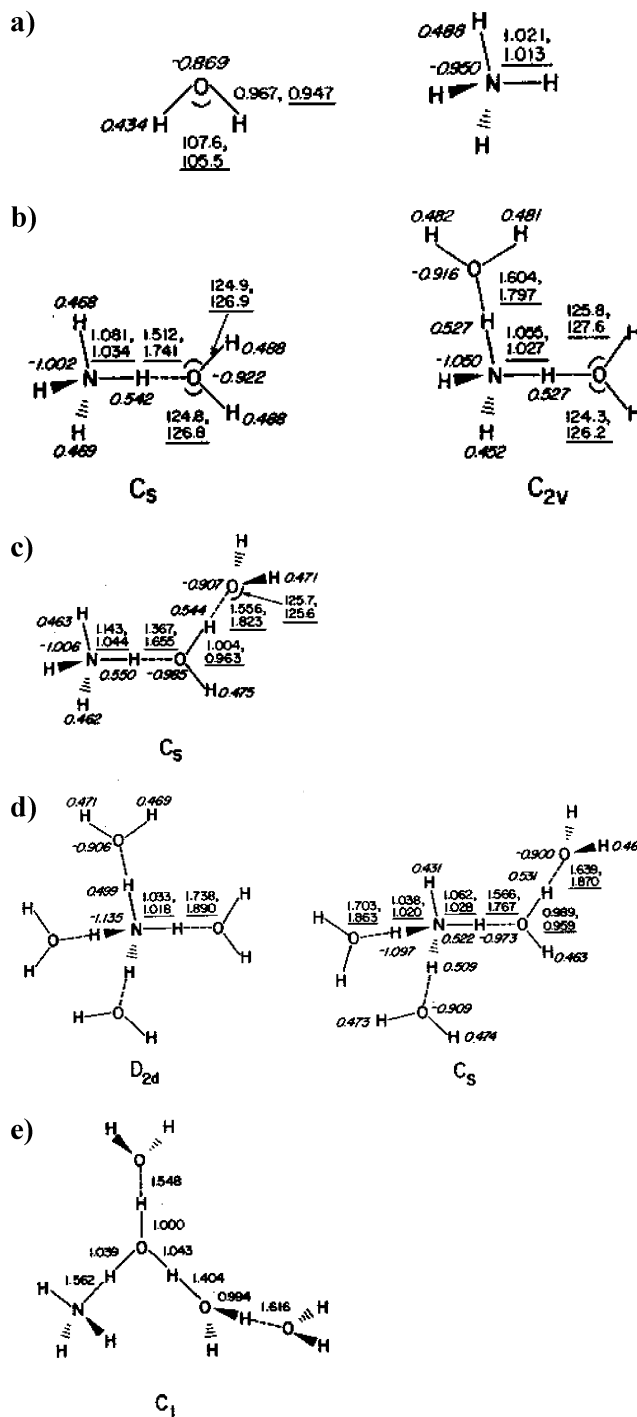


Figure 24. Geometries of $\text{NH}_4^+\cdot n\text{H}_2\text{O}$ clusters from 3 to 21G and 6-31G* (underlined) optimizations. Atomic charges from population analysis using 6-31G* basis set are given in italics. Reproduced with permission from ref 36. Copyright 1986 American Chemical Society.

Anionic clusters show similar trends, because they form IHB bonds that are shorter than those in neutral clusters and similar to cationic IHBs. For example, the calculated ab initio bond lengths in the anionic $\text{OH}^-(\text{H}_2\text{O})_3$ clusters were similar to those in the $\text{H}_3\text{O}^+(\text{H}_2\text{O})_3$ cationic clusters.¹⁹⁴

The individual IHBs usually weaken with increasing cluster size when the ion is surrounded by solvent molecules. However, the IHB may strengthen when the ion is solvated externally, as in comparing the $\text{NH}_4^+(\text{H}_2\text{O})$ and $\text{NH}_4^+(\text{H}_2\text{O})_2$

(C_s) clusters in Figure 24, where upon the attachment of outer-shell solvent molecules, q_H on the bonding hydrogen increases, $r(N-H)$ increases, $r(H\cdots O)$ shortens, and the inner-shell hydrogen bond strengthens. However, this effect is balanced by the weak bonding of the outer-shell molecule, making the inner-shell solvated C_{2v} ion more stable than the mixed inner-and-outer shell C_s ion by 1–4 kcal/mol depending on the level of calculation.

In summary, the charge on the bonding protons decreases with increasing solvation. Some of the charge dissipates from the protonated core ion, but it retains most of the charge even in large clusters, suggesting that this applies even in solution. In parallel, ionic hydrogen bonds become longer and weaker with increasing cluster size. Thermochemical studies can be extended recently to the solvation of doubly charged ions, such as diprotonated diamines,⁹⁵ and to biological ions, as discussed below.

3.1.3. Consecutive Bonding Energies and Some Predictive Relations. With increasing cluster size, the consecutive bonding energies, $\Delta H^\circ_{n-1,n}$, should decrease due to repulsion among the ligand molecules and charge delocalization. This trend has been observed in most solvation sequences. A classic example is the enthalpy sequence in H₃O⁺(H₂O)_n, which was measured by several authors by equilibrium measurements^{157,181,195–197} and by collisional dissociation.^{14,147,148} Figure 25 illustrates the long series of

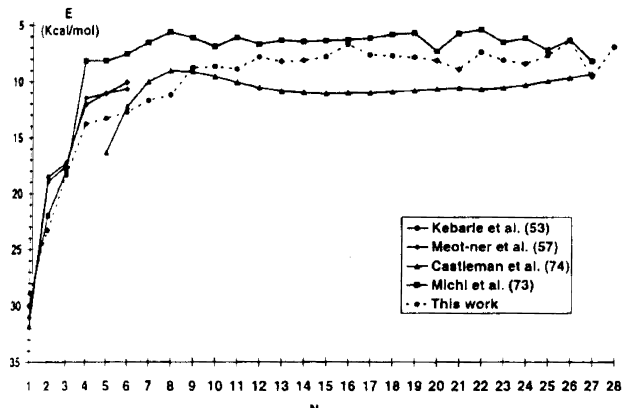


Figure 25. Consecutive bonding energies in the series H₃O⁺(H₂O)_{n-1} + H₂O → H₃O⁺(H₂O)_n. The references cited are as follow: Kellarie and co-workers, refs 196 and 197; Meot-Ner and Speller, refs 199 and 157; Michl and co-workers, ref 147; Castleman and co-workers, ref 148. “This work” refers to computational results of Kelterbaum and Kochanski, ref 198. Reproduced from ref 198 with permission. Copyright 1995 American Chemical Society.

IHB clusters measured by dissociation methods. Figure 26 illustrates the variation in bonding energies, $\Delta H^\circ_{n-1,n}$, in hydration sequences.

Figures 25 and 26 and the data in Tables 4 and 5 illustrate the following thermochemical trends upon adding ligand molecules. The bonding energies, $-\Delta H^\circ_{n-1,n}$, decrease, usually by similar factors of 0.7 in each consecutive clustering step, in many solvation sequences. Shell filling may be followed by a drop of 1–4 kcal/mol in the bonding energy of the next step. The bonding energies and entropies approach the condensation thermochemistry of the bulk solvent ($\Delta H^\circ_{\text{condensation}}$ and $\Delta S^\circ_{\text{condensation}}$) often already after 4–6 solvation steps.

The absolute solvation energies decrease with each additional solvent molecule as illustrated in Tables 4–6 and in

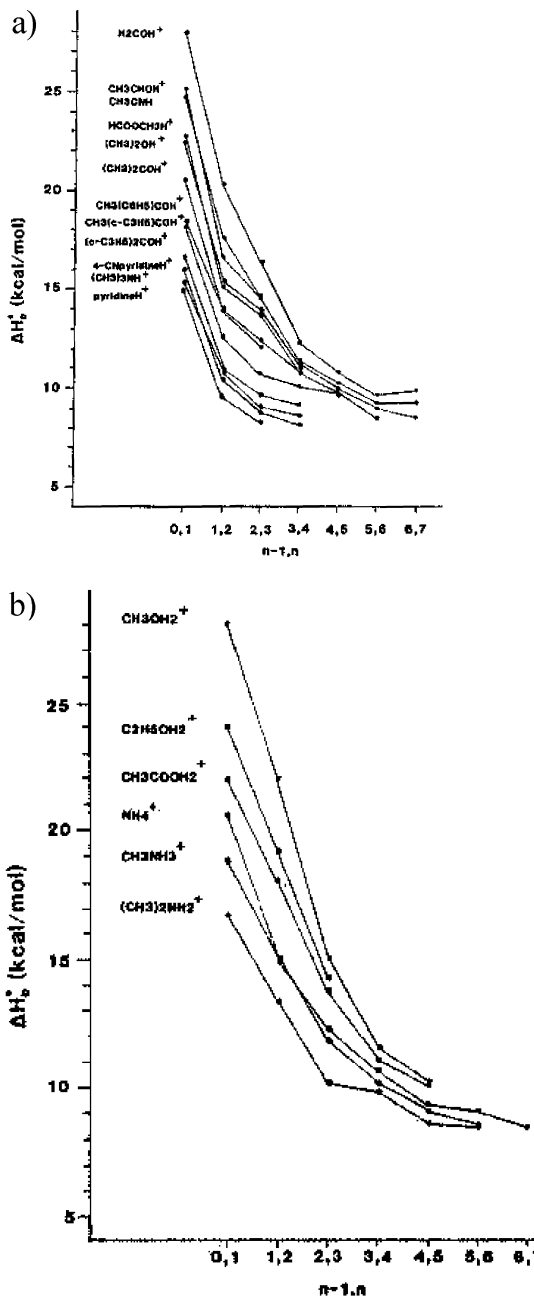


Figure 26. Bonding energies in hydration sequences of (a) monoprotic and (b) polyprotic ammonium and oxonium ions. Reproduced with permission from ref 49. Copyright 1984 American Chemical Society.

Figures 25 and 26. This trend continues until $\Delta H^\circ_{n-1,n}$ reaches, in some cases after undershooting, the limiting macroscopic $\Delta H^\circ_{\text{condensation}}$, which is often reached surprisingly already after 4–6 solvation steps. There exist no accurate thermochemical data on larger hydrated clusters, but some theoretical considerations will be discussed below.

The structural changes upon sequential clustering should be different for various core ions and solvent molecules. Nevertheless, the clustering energies for each consecutive step decrease by similar factors in various clustering sequences, so each step can be predicted from the preceding step, starting from the first step, $\Delta H^\circ_{0,1}$. These relations can be used to estimate the partial and bulk hydration energies based on the proton affinity of a base, PA(B), and $\Delta H^\circ_{\text{condensation}}(\text{H}_2\text{O})$

Table 5. Thermochemistry of Neat Clusters

<i>n</i> ^b	-Δ <i>H</i> ^o _{<i>n</i>-1,<i>n</i>} ^a								-Δ <i>S</i> ^o _{<i>n</i>-1,<i>n</i>} ^a							
	1	2	3	4	5	6	7	8	cond ^c	1	2	3	4	5	6	refs
neat clusters B _{<i>n</i>} H ⁺																
H ₃ O ⁺	32.1	20.4	17.2	12.2	11.6	11.2	9.8	10.5	26.4	21.3	27.8	24.0	24.5	27.8	<i>d</i>	
(CH ₃ OH) _{<i>n</i>} H ⁺	32.5	21.2	15.1	12.4	11.4	10.6	10.5	9.4	8.4	28.8	27.0	26.4	25.0	27.3	28.1	<i>d</i>
(C ₂ H ₅ OH) _{<i>n</i>} H ⁺	32.1								10.0	28.5						205, 50
(n-C ₃ H ₇ OH) _{<i>n</i>} H ⁺	31.0	20.2	14.3	11.8	10.9	11.1			11.2	28.5	27.2	24.6	23.9	25.4	28.8	50, 181, 178
((CH ₃) ₂ O) _{<i>n</i>} H ⁺	31.4	10.1								30.8	27.9					103, 152
((CH ₃) ₂ CO) _{<i>n</i>} H ⁺	30.7	12.2	8.5							29.9	23.0	17.0				181
(CH ₃ COOH) _{<i>n</i>} H ⁺	28.1	18.5	12.7	12.1					12.8	28.3	24.5	21.1				183
amines																
(NH ₃) _{<i>n</i>} H ⁺	25.2	16.6	14.9	12.2	7.8	6.2	5.0	4.0	5.6	26.3	24.4	26.0	26.2	21.9		
(CH ₃ NH ₃) _{<i>n</i>} H ⁺	23.6	16.0	13.4	7.8						25.5	27.2	26.1	22.5	22.5		39, 178
((CH ₃) ₂ NH ₂) _{<i>n</i>} H ⁺	22.5	16.4	9.9	7.9	6.3				26.9	27.2	26.1	22.5	22.5		178	
((CH ₃) ₃ N) _{<i>n</i>} H ⁺	22.2	6.5	8.3	8.8	7.4				5.2	28.8						39, 207, 203b, 178
nitriles, sulfide, phosphide																
(HCN) _{<i>n</i>} H ⁺	28.1	13.8	11.8	9.2					6.0	27.5	23.0	25.0	26.0			102, 199
(CH ₃ CN) _{<i>n</i>} H ⁺	30.0	9.3	7.3	6.5	5.5				7.9	26.4	19.9	18.4	15.0			199, 204
(H ₂ S) _{<i>n</i>} H ⁺	15.1	8.2	8.4	6.7	6.1				4.5	20.3	19.1	24.5	24.7			132, 61
(PH ₃) _{<i>n</i>} H ⁺	11.5	9.2	7.3	6.5					25.9	22.3	18.4	15.0				65

^aUnits are as follows: Δ*H*^o_{*n*-1,*n*} (kcal/mol); Δ*S*^o_{*n*-1,*n*} (cal/(mol K)). ^bIn the neat cluster series, Δ*H*^o_{*n*-1,*n*} corresponds to the addition of the *n*th neutral molecule to the protonated core ion. ^cBulk condensation enthalpy of the neutral ligand. ^dAverage of the acceptable literature values in the NIST tables.²⁹

Table 6. Thermochemistry of Stepwise Hydration and Neat Clusters of Anions

n^b	$-\Delta H^\circ_{n-1,n}{}^a$								cond ^c	$-\Delta S^\circ_{n-1,n}{}^a$						refs
	1	2	3	4	5	6	7	8		1	2	3	4	5	6	
hydration $A^-(H_2O)_n$																
OH ⁻	26.6	17.6	15.4	12.0	11.5	11.2	10.4	9.8	10.5	22.5	21.3	24.4	21.1	24.1	23.2	d
CH ₃ O ⁻	24.6	19.2	14.8	11.0					10.5	22.9	25.3	24.4	20.0			180b
HCOO ⁻	16.0	13.8							10.5	23.0	24.0					55
CH ₃ COO ⁻	16.1	12.8	12.0						10.5	21.4	19.8	20.0				55, 79, 167
CN ⁻	13.7	11.7	10.7	9.8					10.5	19.2	18.1	19.8	20.0			162
F ⁻	27.4	17.9	14.5	13.7	12.8	10.9	10.4	11.2	10.5	20.1	20.5	21.7	26.8	28.4	29.8	159
Cl ⁻	14.1	12.7	11.8	10.6	9.5	8.6	8.1		10.5	19.8	20.9	22.6	29.4	21.7	21.2	d
HS ⁻	14.2	12.6	11.7						10.5	18.7	20.4	23.5				79, 56
neat clusters $A^- \cdots nA$																
CH ₃ O ⁻ ...nCH ₃ OH	28.8	21.4	15.0	11.4					8.4	20.8	27.8	26.3	22.4			180b
CH ₃ COO ⁻ ...nCH ₃ COOH	29.3	19.6	12.5						12.8	29.6	28.6	22.7				55, 183
CN ⁻ ...nHCN	21.2	16.4	12.6	10.9	9.8	8.5			6.0	20.6	21.8	21.2	24.8	20.2	20.4	8, 43
F ⁻ ...nHF	45.8															208
Cl ⁻ ...nHCl	23.5 ^d	14.6	11.7	10.3						23.1 ^d	22.4	23.4	26.7			188
HS ⁻ ...nH ₂ S	13.2								4.5	19.7						79

^aUnits are as follows: $\Delta H^\circ_{n-1,n}$ (kcal/mol); $\Delta S^\circ_{n-1,n}$ (cal/(mol K)). ^bIn the hydration series, $\Delta H^\circ_{n-1,n}$ corresponds to the addition of the n th H_2O molecule as shown. In the neat cluster series, $\Delta H^\circ_{n-1,n}$ corresponds to the addition of the n th neutral molecule to the protonated or deprotonated core ion. ^cBulk condensation enthalpy of the neutral ligand. ^dAverage of the acceptable literature values in the NIST tables.²⁹

alone. As we saw above, $\Delta H^\circ_{0,1}$ can be estimated from the ΔPA correlations in eqs 4–7 and Table 2, which can be reformulated in eqs 12 and 13 using $PA(H_2O) = 165$ kcal/mol.

For OH⁺·OH₂ bonds,

$$\Delta H^\circ_{0,1} = 80 - 0.30PA(B) \text{ kcal/mol} \quad (12)$$

For NH⁺·OH₂ bonds,

$$\Delta H^\circ_{0,1} = 73 - 0.26PA(B) \text{ kcal/mol} \quad (13)$$

The cumulative integrated hydration enthalpies by n H_2O molecules, $\Delta H^\circ_{0,n}$, are remarkably constant multiples of the first step, $\Delta H^\circ_{0,1}$, and their value can be predicted by eqs 14–17 on this basis.

$$\Delta H^\circ_{0,2} = (1.8 \pm 0.1)\Delta H^\circ_{0,1} \quad (14)$$

$$\Delta H^\circ_{0,3} = (2.3 \pm 0.1)\Delta H^\circ_{0,1} \quad (15)$$

Oxonium and monoprototonic ammonium ions:

$$\Delta H^\circ_{0,4} = (2.8 \pm 0.1)\Delta H^\circ_{0,1} \quad (16)$$

Polyprototonic ammonium ions:

$$\Delta H^\circ_{0,4} = (3.1 \pm 0.1)\Delta H^\circ_{0,1} \quad (17)$$

These relations were found to apply in the hydration sequences of 22 onium ions, as well as of the alkali ions, and they apply even in solvation sequences with CH₃OH, NH₃, H₂S, and CH₃CN ligand molecules.⁴⁹

The integrated enthalpy of solvation by four H_2O molecules, $\Delta H^\circ_{0,4}$, can be estimated by eqs 16 and 17 usually within ± 1 kcal/mol, which is well within the cumulative experimental error of the four solvation steps. The relation between $\Delta H^\circ_{0,1}$ and $\Delta H^\circ_{0,4}$, combined with the correlation between $\Delta H^\circ_{0,1}$ and ΔPA above, yields accurate estimates, within ± 2 kcal/mol, of the four-molecule hydration energy, $\Delta H^\circ_{0,4}$, based on PA(B) alone.

Oxonium ions ($ROH_2^+(H_2O)_4$ and $R_2OH^+(H_2O)_4$ clusters):

$$\Delta H^\circ_{0,4} = 0.84PA(B) - 224 \text{ kcal/mol} \quad (18)$$

Primary and secondary ammonium ions

($RNH_3^+(H_2O)_4$ and $R_2NH_2^+(H_2O)_4$ ions):

$$\Delta H^\circ_{0,4} = 0.81PA(B) - 226 \text{ kcal/mol} \quad (19)$$

For pyridinium and substituted pyridinium ions, pyridinium- $H^+(H_2O)_4$, a somewhat different relation, $\Delta H^\circ_{0,4} = 0.64PA(B) - 185$ kcal/mol, applies.

Surprisingly, these relations can be extended to predict the bulk solvation enthalpies of most ions. The 4-fold hydrated clusters, $BH^+(H_2O)_4$, can be transferred into liquid water to form the BH_{aq}^+ hydrated ion. The experimental data show that the enthalpies of hydration of the clusters, $\Delta H^\circ_{g\text{-}aq}(BH^+ \cdot 4H_2O)$ are a constant -70 ± 3 kcal/mol for diverse ions. Combined with eqs 18 or 19 and eq 38, and the observation that the enthalpies of solvation of the $BH_4^+(H_2O)_4$ clusters are a constant -70 kcal/mol for diverse ions (Table 11), the bulk solvation energies, $\Delta H^\circ_{g\text{-}aq}(BH^+)$, can be predicted on the basis of PA(B) alone. These relations can be expressed by eqs 20a and 20b.

Alkyloxonium ions:

$$\Delta H^\circ_{g\text{-}aq}(BH^+) = 0.84PA - 252 \text{ kcal/mol} \quad (20a)$$

Alkylammonium ions:

$$\Delta H^\circ_{g\text{-}aq}(BH^+) = 0.81PA - 254 \text{ kcal/mol} \quad (20b)$$

A similar general equation $\Delta H^\circ_{g\text{-}aq}(BH^+) = 0.84PA(B) - a$ can be applied to both alkyloxonium and alkylammonium ions. When constant a of 252 kcal/mol for alkyloxonium ions and 262 kcal/mol for alkylammonium ions is used, this equation predicts the solvation energies ranging from 63 to 101 kcal/mol for diverse ions with an SD of ± 2 kcal/mol (Table 11, columns 8 and 9). It is surprising that the complex energetics of ion solvation can be reduced to such a simple relation. This results

from a canceling variation of solvation terms as described below.

As noted above, after the fourth step $\Delta H_{n-1,n}^\circ$ approaches the limiting bulk-phase value of $\Delta H_{\text{condensation}}^\circ(\text{H}_2\text{O}) = -10.5$ kcal/mol within ± 1 kcal/mol in most hydration sequences (Figures 25 and 26 and Tables 4 and 5). This suggests that the strong ionic interactions are contained mostly in the bonding energies of the first four solvent molecules.

The fact that the effects of solvation are concentrated in the first few solvent molecules is born out also by solvation effects on the structures of the core ions themselves. Ab initio calculations showed that bond lengths and charge distributions in the cluster change less with each additional solvent molecule (Figures 23 and 24). Solvation effects on the structure of the core ion are also largest for the first inner-sphere solvent molecules. For example, the first four H_2O molecules have the largest effect on stretching the C–C bond by 0.026 Å in $\text{CH}_3\text{COO}^-(\text{H}_2\text{O})_6$, and the effects of additional H_2O molecules are small enough to expect that structures of CH_3COO^- in this cluster and in bulk solution are similar.²⁰⁹

For anion clusters, Larson and McMahon calculated the consecutive clustering energies of Cl^- with H_2O , HCl , and CH_3CN molecules and of F^- by H_2O and HF up to four ligand molecules, using eq 10 above, by first recalculating the acid dissociation energy of the solvated ions using eq 21.

$$\begin{aligned}\Delta H_{\text{acid}}^\circ((\text{RH})_n\text{A}^-\text{H}^+) &= \Delta H_{\text{acid}}^\circ(\text{A}^+\text{H}^-) \\ &+ \sum \Delta H_{j-1,j}^\circ \quad (j = 1 \text{ to } n-1)\end{aligned}\quad (21)$$

The calculated $\Delta H_{\text{acid}}^\circ$ of the clustered anion can then be inserted into eq 21 to calculate the bonding energy of the next ligand molecule. Larson and McMahon found that this procedure predicted the binding energies of 16 clusters with a standard deviation of ± 1.6 kcal/mol.⁸

As noted above, equilibrium measurements on hydrated clusters are limited to 6–8 H_2O molecules, as the bonding energies approach $\Delta H_{\text{condensation}}^\circ(\text{H}_2\text{O}) = -10.5$ kcal/mol, and these clusters can be observed only near the temperature where water vapor condenses. However, near this temperature, the distribution of clusters broadens and shifts to larger clusters. It can be shown that, in the equilibrium populations of large clusters the thermochemistry of which reached the limiting value of $\Delta G_{n-1,n}^\circ \approx \Delta G_{\text{condensation}}^\circ$ the maximum population of the n th cluster is a fraction $n^n/(n+1)^{n+1}$ of the total population. The result is that any cluster containing 10 or more H_2O molecules constitutes less than 3.5% of the total cluster population under any equilibrium condition. Furthermore, it is also observed experimentally and can be shown mathematically that clusters of increasingly larger sizes can be observed by equilibria over increasingly more narrow temperature ranges. These effects limit the clusters accessible to equilibrium measurements and the accuracies of the measurements.¹⁷⁸

In summary, empirical relations allow estimation of the partial solvation enthalpies by 1–4 H_2O molecules and even the bulk solvation enthalpies, based on the proton affinity alone, to within the experimental accuracy of ± 2 kcal/mol for diverse ions. These relations can be useful for estimating the thermochemistry of hydration of protonated ions and protonated functional groups of biomolecules.

3.1.4. Shell Filling, Magic Numbers, and Ring and Cage Structures. a. Thermochemical Effects of Shell Filling.

In some clustering series, the bonding energies drop after a

shell is filled at step $n = s$, and the next ligand molecule starts an outer shell at $n = s + 1$. Entropy effects are also observed as ΔS_D° increases before shell filling due to the increasing steric interference of ligand molecules and then decreases at the beginning of an outer shell due to the unhindered rotation of the first molecule in a new shell.

These thermochemical effects can lead to magic numbers in clustering series. The shell-filling effect was first noted in the series $\text{NH}_4^+(\text{NH}_3)_n$ at $s = 4$ solvent molecules.^{36,149,210–213} Similar thermochemical effects may occur by the formation of rings and three-dimensional cages, cryptands, and clathrates. Without shell filling at the s th ligand molecule, the value of ΔH_D° decreases monotonically, and the difference between each consecutive step becomes smaller. However, the drop in the bonding energy after the shell-filling step s introduces a larger decrease in the bonding energy at this step than in the preceding step ($s-1$) or following step ($s+1$), and this leads to eq 22.¹⁵⁷

$$\begin{aligned}(\Delta H_{(s-2,s-1)}^\circ - 2\Delta H_{(s-1,s)}^\circ + \Delta H_{(s,s+1)}^\circ) &< 0 \text{ no shell} \\ &> 0 \text{ shell filled}\end{aligned}\quad (22)$$

A difficulty with thermochemical evidence for shell filling is that the effects are often within the error limits of the measurements, because three clustering steps, each with its usual associated uncertainty of ± 1.5 kcal/mol, must be compared.

Shell effects are illustrated in clustering sequences in Figure 27, where three ligand molecules complete the first shell, and in

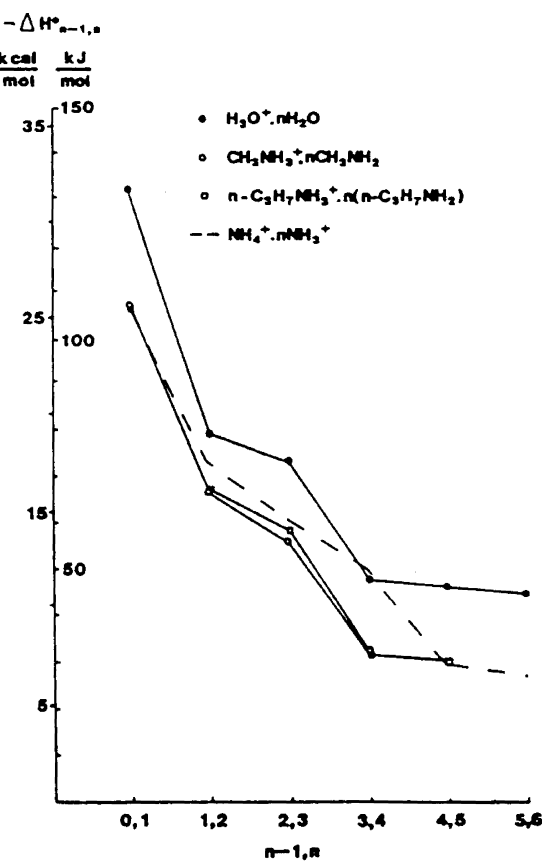


Figure 27. Enthalpy sequences for neat clusters about core ions with three bonding hydrogens with shell filling at the 2,3 step. For comparison, the clustering series for $\text{NH}_4^+\cdot\text{nNH}_3^+$, where shell filling occurs at the 3,4 step, is also shown. Reproduced with permission from ref 178. Copyright 1992 American Chemical Society.

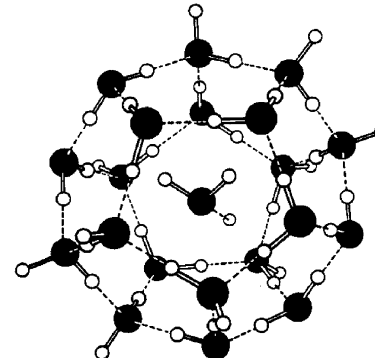
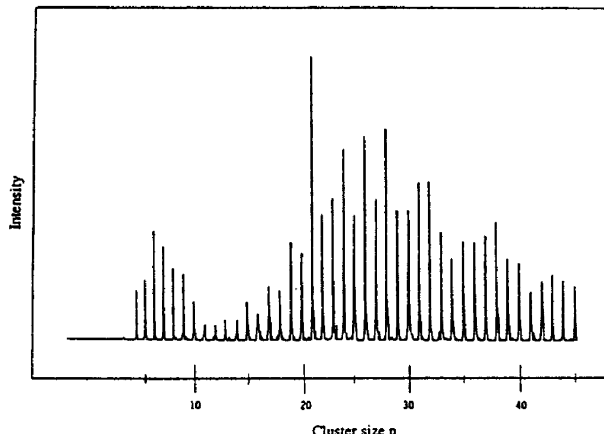


Figure 28. Pentagonal didodecahedral hydrogen-bonded structure of $(\text{H}_2\text{O})_{21}\text{H}^+$ with a central engaged H_3O^+ ion. Reproduced from ref 218b with permission. Copyright 1996 American Chemical Society.

some of the clustering sequences in Figure 26, where three water molecules complete the second shell. A review of solvation sequences by H_2O , CH_3OH , HCN , CH_3CN , NH_3 and alkylamines, H_2S , and $(\text{CH}_3)_2\text{SO}$ showed that shell-filling effects according to eq 22 are observed in 10 of 61 known clustering series. Shell-filling effects after the s th solvent molecule were observed in $\text{H}_3\text{O}^+\cdot n\text{H}_2\text{O}$ ($s = 3$), $\text{NH}_4^+\cdot n\text{NH}_3$ ($s = 4$), $\text{CH}_3\text{OH}_2^+\cdot n\text{H}_2\text{O}$ ($s = 2$), and $\text{CH}_3\text{OH}_2^+\cdot n\text{CH}_3\text{OH}$ ($s = 2$) and in the hydration of CH_3CHOH^+ , $(\text{CH}_3)_2\text{OH}^+$, and CH_3CNH^+ ($s = 3$, second shell), as well as in $\text{K}^+\cdot \text{CH}_3\text{CN}$ ($s = 3$), $\text{K}^+\cdot (\text{CH}_3)_2\text{SO}$ ($s = 2$), $\text{K}^+\cdot n(\text{H}_2\text{N}(\text{CH}_2)_2\text{NH}_2)$ ($s = 2$), and $\text{OH}^-\cdot n\text{H}_2\text{O}$ ($s = 3$)¹⁵⁷ and later also in the neat cluster series $\text{CH}_3\text{NH}_3^+\cdot n\text{CH}_3\text{NH}_2$, $n\text{-C}_3\text{H}_7\text{NH}_3^+\cdot n(\text{n-C}_3\text{H}_7\text{NH}_2)$, and $(\text{CH}_3)_2\text{NH}_2^+\cdot n(\text{CH}_3)_2\text{NH}$.¹⁷⁸

The thermochemical effects are illustrated in Figure 27. Interestingly, the shell-filling effects in each series are comparable, about a drop of 3–5 kcal/mol in ΔH°_D below the extrapolated value from the preceding steps, although shell filling occurs at different steps. An interesting effect is that shell filling occurs after three H_2O molecules both about H_3O^+ and OH^- , the latter suggesting hydrogen bonds of water molecules to each of the three oxygen lone pairs in the hydroxyl anion. Similarities in geometries and shell-filling effects in the clusters of H_3O^+ and OH^- were confirmed by ab initio calculations.¹⁹⁴

Shell-filling effects can be observed by other methods such as the metastable fragmentation of cluster ions, which was used to study hydrated adenine and thymine cations. Both exhibited well-defined hydration shell structures with the first hydration shell complete with four water molecules.²¹⁴

Shell effects may not be observed by equilibrium measurements when the bonding energies approach the limiting condensation energies already before shell filling occurs. In these cases, the bonding energy cannot drop further significantly. For example, in Figure 26, three monoprotic oxonium ions show the filling of the second shell after $n = 3$, but other monoprotic ions do not show this effect, because for these clusters $-\Delta H^\circ_{2,3}$ is <12 kcal/mol, close to the 10.5 kcal/mol condensation enthalpy of water. The bonding energy cannot become significantly smaller after shell filling.

Another factor that can obscure shell filling is the possible formation of open-shell and closed-shell isomers of comparable energies. This can cause the observed lack of shell effects in $\text{NH}_4^+(\text{H}_2\text{O})_n$,¹⁹⁹ in $\text{HCN}(\text{NH}_3)_m\text{H}^+$, and in $(\text{HCN})_n(\text{NH}_3)\text{H}^+$ clusters.¹⁸⁶

However, large shell effects occur in methyl-blocked clusters. For example, in $(\text{CH}_3)_2\text{O}\text{H}^+$, $((\text{CH}_3)_2\text{CO})_n\text{H}^+$, $(\text{CH}_3\text{OCH}_2\text{CH}_2\text{OCH}_3)_n\text{H}^+$, and $(\text{CH}_3\text{CN})_n\text{H}^+$, the first IHB of the dimers is strong, 30–32 kcal/mol, but the second bond must form through weaker CH-X bonds or a long T-shaped hydrogen bond, and ΔH°_D drops to <12 kcal/mol. An intermediate case occurs in $(\text{HCN})_n\text{H}^+$, where CH-N bonds are present in the HCN-HCN-H⁺-NCH-NCH chain, but these do not block bonds strongly since HCN is a relatively efficient hydrogen donor. Shell filling in clusters with blocked ligands was observed in mixed clusters of NH_4^+ solvated by NH_3 and CH_3CN , CH_3CHO , and $(\text{CH}_3)_3\text{N}$ ligands.^{207,215,216a,b}

Thermochemical shell effects in non-hydrogen-bonded clusters were investigated experimentally and theoretically by Hiraoka and co-workers in $(\text{N}_2)_n^+$,¹⁴⁵ $(\text{N}_2)_n\text{H}^+$,¹⁴⁴ $(\text{CO})_n^+$,¹⁴⁶ $(\text{CO})_n\text{H}^+$,¹⁴⁴ $(\text{CO}_2)_n^+$,¹⁴² and $(\text{CO}_2)_n\text{H}^+$.¹⁴⁴ This group also investigated bonding and shell effects in the clusters with weak CH···X bonds in $\text{CH}_3\text{N}_2(\text{N}_2)_n^+$ at $n = 3, 6$, and 8 ,⁹⁸ in complexes of C_2H_5^+ , $s\text{-C}_3\text{H}_7^+$, and $t\text{-C}_4\text{H}_9^+$ with CO_2 and N_2O ,⁹⁹ and in the complexes $\text{F}^-(\text{C}_2\text{H}_4)_4$ and $\text{Cl}^-(\text{CH}_3\text{CH}_2)_3$.¹¹³

b. Shell-Filling Effects in Cluster Distributions and Magic Numbers. Shell filling causes “magic numbers” in cluster distributions generated under nonequilibrium conditions by supersonic beam expansion. For example, $(\text{Me}_3\text{N})_m(\text{H}_2\text{O})_n\text{H}^+$ and $(\text{Me}_3\text{N})_m(\text{NH}_3)_n\text{H}^+$ clusters showed maximum intensities when the number of outer blocked ligands was equal to the number of free hydrogens on the protonated cores. The number of Me_3N molecules that filled shells about $(\text{H}_2\text{O})_n\text{H}^+$ and $(\text{NH}_4)_n\text{H}^+$ suggested that the IHBs in the cores formed cyclic structures^{207,216a,b} and that in larger clusters rings can merge into stable cryptands and clathrates such as in $(\text{H}_2\text{O})_{21}\text{H}^+$, where H_3O^+ may be on the surface with an engaged H_2O in the center as suggested by Searcy and Fenn,^{217a} or H_3O^+ may be engaged in the center (Figure 28). In the vibrational predissociation spectroscopy of $(\text{H}_2\text{O})_{21}\text{H}^+$ and also $\text{NH}_4^+(\text{H}_2\text{O})_{20}^+$, the observation of free OH bands verifies the structure with $\text{H}_3\text{O}^{+217b,c}$ or NH_4^+ on the surface of the clusters.^{217d} These structures could be identified by titrating the ligands attached to the core. The related literature was reviewed recently.^{218a,b} Other examples of the reduced reactivities of closed-shell clusters were observed in the slow reactions of alkyl blocked dimers, $(\text{MeCN})_2\text{H}^+$, $(\text{Me}_2\text{O})_2\text{H}^+$, and $(\text{Me}_2\text{CO})_2\text{H}^+$, and in mixed clusters, $(\text{EtOH})(\text{MeCN})_2\text{H}^+$ and $(\text{HCOOH})(\text{MeCN})_2\text{H}^+$.^{53,220–224}

How large a thermochemical effect is needed to cause magic numbers in cluster distributions? In mixed clusters formed in supersonic beam expansion, peaks corresponding to shell-filled $(\text{CH}_3\text{CN})_2(\text{CH}_3\text{OH})_n\text{H}^+$ or $(\text{CH}_3)_3\text{N}_{m+2}(\text{H}_2\text{O})_m\text{H}^+$ clusters were larger than peaks formed by adding further CH_3CN or $(\text{CH}_3)_3\text{N}$ ligands in blocked positions even when the difference between the total bonding energies was only 2–3 kcal/mol. The observed clusters are formed by the dissociation of larger clusters in the beam, and the observations suggest that the final dissociation steps occur in cold clusters where small energy differences can have large kinetic effects. Therefore, the distributions of clusters generated by supersonic beams are sensitive probes of even small energy effects of shell filling.^{203a,b}

Effects similar to shell filling may be caused also by the formation of rings and three-dimensional cage structures.^{219a–f} Protonated water clusters of all sizes may have Eigen structures centered on $\text{H}_3\text{O}^+(\text{H}_2\text{O})_3$ or Zundel structures centered on $\text{H}_2\text{O}-\text{H}^+-\text{OH}_2$ cores.^{219c–f} Both cores form cyclic structures in clusters that contain 5 H_2O molecules or more and multi-ring or three-dimensional cage structures for 6 or more H_2O molecules.^{219b,c} Typically, many open, cyclic, and cage isomers of similar energy exist for clusters with over 4–6 H_2O molecules, and several may be present in equilibrium populations.

For other solvated ions, Seward and co-workers measured the thermochemistry of anionic $\text{Cl}^-(\text{H}_2\text{O})_n$, $\text{Br}^-(\text{H}_2\text{O})_n$, $\text{I}^-(\text{H}_2\text{O})_n$ with $n = 8, 7$, and 5 H_2O molecules, respectively,^{219b} and also protonated $\text{H}_3\text{O}^+(\text{H}_2\text{O})_n$, $\text{H}_3\text{O}^+(\text{H}_2\text{O})_m(\text{H}_2\text{S})_n$, $\text{NH}_4^+(\text{H}_2\text{O})_m(\text{H}_2\text{S})_n$, and $\text{H}_3\text{S}^+(\text{H}_2\text{O})_m(\text{H}_2\text{S})_n$ clusters, in relation to geochemical environments.^{219c,d} In the anionic clusters they observed nonmonotonic successive hydration enthalpies, reflecting the number of hydrogen bonds formed in each step, that varies according to the formation of cyclic and cage structures.^{219b} For example, in the cationic clusters $\text{H}_3\text{O}^+(\text{H}_2\text{O})_n$, these workers observed an increase in $-\Delta H^\circ_{n-1,n}$ and in $-\Delta S^\circ_{n-1,n}$ when adding the sixth H_2O molecule,^{219d} although these effects were not observed in earlier measurements.^{195–197} If verified, the increased values may reflect the formation of three-dimensional clathrates at this cluster size.

The preferred isomers may also depend on the temperature. In the anions, clusters with halide ions on the exterior have lower enthalpies, but interior clusters are favored by entropy at higher temperatures.^{219b} In solvated ammonium, cyclic $\text{NH}_4^+(\text{H}_2\text{O})_5$ and $\text{NH}_4^+(\text{H}_2\text{O})_6$ are preferred at low temperatures, but entropy effects lead to open structures at high temperatures as indicated by thermochemistry,^{219c} as well as spectroscopy and computation.^{219e,f}

Three-dimensional clathrates with hydrogen-bonded rings were also found spectroscopically in sulfate dianions solvated by 6 H_2O molecules.^{219g} Further IR photodissociation spectroscopic studies showed that the effects of the sulfate dianions on water structure extend up to the third solvation shell, whereas free surface O–H bands appear for clusters with more than 44 H_2O molecules, corresponding to intrinsic water structure at the surfaces of these large clusters.^{219h}

However, equilibrium measurements on such large clusters are difficult because the cluster populations are spread out over many sizes at the required low temperatures, and the clusters of each size have a small population and low signal intensity. These large clusters are observable only over a narrow temperature range of 10–20 degrees before condensation, which limits the spans of the corresponding van't Hoff plots. Also, neutral water dimers and clusters may be present in the gas phase at the required low temperatures. These factors limit

the sizes of the accessible clusters and decrease the accuracy of the equilibrium measurements. Large clusters are also hard to handle computationally, because the numerous isomers preclude global minima conformational searches with high level ab initio calculations. Therefore structural inferences from anomalous ΔH° and ΔS° effects measured near the condensation temperatures must be made with caution.

We may ask whether there is a relation between solvent shells in gas-phase clusters and in solution. Intermediate between the gas phase and bulk water are $(\text{H}_2\text{O})_n\text{H}^+$ ions in nonaqueous solvents that contain trace water. In dichloroethane and benzene with carborane counterions, IR spectroscopy suggested neither Eigen structures with H_3O^+ cores nor Zundel ions with H_5O_2^+ cores, but clusters with H_7O_3^+ cores where the excess proton is localized between three oxygen atoms, and further water molecules are attached to this core. The difference from the gas phase may be due to the effects of the counterions in these mixed solvents.^{225a}

Turning to bulk water, several theoretical papers addressed the structure about H_3O^+ ions. Tunon and co-workers studied H_3O^+ and OH^- with a hydration shell of three H_2O molecules in the gas phase or in bulk solvent. They found that the central H_3O^+ ion retains 0.796 of the charge and an inner shell of three H_2O solvent molecules, even in the presence of nine solvent molecules. The OH^- ion also retained –0.782, –0.592, and –0.676 charge in the presence of three or six discrete solvent molecules or three H_2O molecules and a continuum solvent, respectively. Bulk solvation changed the most stable conformation from one in which the three H_3O inner shell dipoles point away from the OH^- dipole to one where they are almost parallel to this dipole, reversing a 5.2 kcal/mol energy difference. Further solvation increased the geometrical changes caused by the first solvent shell, but both H_3O^+ and OH^- retained a distinct inner shell of three H_2O molecules upon higher solvation in these models.^{194,225b} Monte Carlo calculations showed that the inner shell effects about H_3O^+ can be discerned even in the presence of 40–50 H_2O molecules.¹⁹⁸

3.1.5. The Evolution of Hydrogen-Bond Networks and Thermochemical Effects of Isomeric Clusters.

Pertinent to shell filling is the fact that outer shells can start before an inner shell is completed (similar to shell filling in atoms). Clusters with 6–8 or more solvent molecules usually have IHB networks with isomeric noncyclic, cyclic, and three-dimensional clusters with similar energies that may coexist in equilibrium.

The addition of each solvent molecule increases the number of possible structural isomers. Typically, several structures with similar energies are separated by small barriers and they may interconvert in thermal populations, providing low-energy pathways for proton transfer. Isomeric clusters can affect shell filling, participate in the formation of covalent or noncovalent adducts, and affect thermochemical and spectroscopic measurements. Early ab initio studies of Newton and Ehrenson on isomeric protonated water clusters found cyclic structures comparable in energy to open isomers.^{226,227}

The fact that isomers may coexist in equilibrium in thermal cluster populations was discussed by Meot-Ner and Speller,¹⁵⁷ and Deakyne and co-workers calculated the energies of isomers with filled shells or mixed inner/outer shells in $(\text{H}_2\text{O})_n\text{H}^+$, $(\text{NH}_3)_n\text{H}^+$, $(\text{NH}_3)_m(\text{H}_2\text{O})_n\text{H}^+$, $(\text{HCN})_m(\text{H}_2\text{O})_n\text{H}^+$, and $(\text{MeCN})_m(\text{H}_2\text{O})_n$ clusters.^{36,228} More recently, cluster distributions and IR spectroscopy of clusters at 170 ± 20 K identified coexisting isomers with five- and six-membered rings and cage structures of $(\text{H}_2\text{O})_n\text{H}^+$ clusters,²³⁰ H_3O^+ and

CH_3OH_2^+ centered isomers and cyclic structures in mixed methanol–water clusters,²³¹ and cyclic structures blocked by acetonitrile in methanol–water–acetonitrile clusters.²³² Isomers with or without intramolecular IHBs were observed in $(\text{H}_2\text{NCH}_2\text{CH}_2\text{NH}_2)(\text{H}_2\text{O})_3\text{H}^+$ clusters,^{233a} isomers with a H_3O^+ core or a protonated dimer core in protonated water/ketone clusters,¹⁰⁴ and isomers with water bonded directly to $\text{C}_6\text{H}_6^{•+}$ or with hydrogen-bonded water rings were found computationally in ionized benzene/water clusters.¹²⁰ The energy differences between isomeric clusters are often small, and enthalpy and entropy differences often compensate each other since tightly bound low-energy isomers tend to have smaller entropies, which decreases the free energy differences.

The presence of isomeric clusters can affect equilibrium measurements of association reactions. A lower cluster B_nH^+ may be in equilibrium with a mixture of B_{n+1}H^+ isomers each with a different $\Delta H^\circ_{n-1,n}$ and $\Delta S^\circ_{n-1,n}$ value. The results can yield apparent van't Hoff plots that do not represent exactly any of the isomers.¹⁵⁷ For example, if $\Delta H^\circ_{n-1,n}$ for one product is -15.0 kcal/mol and $\Delta S^\circ_{n-1,n}$ is $-23.0 \text{ cal}/(\text{mol K})$, then the presence of isomers with $\Delta H^\circ_{n-1,n}$ of $-19.0, -17.0, -13.0$, or -11.0 kcal/mol and the same $\Delta S^\circ_{n-1,n}$ will yield composite van't Hoff plots yielding apparent $\Delta H^\circ_{n-1,n}$ values of $-19.0, -16.8$ to -14.8 , and -15.0 kcal/mol , respectively. Such systems may yield broken or curved van't Hoff plots, but this is not detectable if the energies of the isomers are similar. The composite results are close to the more stable isomer, but they are not precise.¹⁵⁷ However, when one isomer is a weakly bonded cluster and the other isomer is a strongly bonded covalent adduct, the effects may be observed as broken van't Hoff plots such as the $\text{C}_2\text{H}_5^+ + \text{H}_2$ adducts^{129a} or as curved van't Hoff plots as in the association of $t\text{-C}_4\text{H}_9^+$ with various oxygen bases.¹²³

The presence of isomers affects the measured thermochemistry, for example, in the association of deprotonated glycine ($\text{Gly}-\text{H}^-$) with H_2O , CH_3OH , and $\text{C}_2\text{H}_5\text{OH}$ solvent molecules. Accounting for the thermochemistry of isomeric populations can lead to a close agreement between the experimental and computed thermochemistry.^{233b,c}

These examples illustrate the effects of isomers on apparent thermochemical values from equilibrium measurements. However, the presence of isomers can affect not only the apparent but also the actual thermochemistry of equilibrium populations, by contributing a positive entropy of mixing, expressed as $\Delta S^\circ_{\text{mix}} = -R\sum x_i \ln(x_i)$, where x_i is the mole fraction of isomer i and the summation is over all isomers. In the case of N isomers of equal abundance, $\Delta S^\circ_{\text{mix}} = R \ln N$.^{233b,c} This can be significant in large clusters where conformation searches show hundreds of isomers with similar free energies, as in hydrated clusters with six or more H_2O molecules. For example, for 100 isomers, $\Delta S^\circ_{\text{mix}} = 9.2 \text{ cal}/(\text{mol K})$, and at 300 K, $RT\Delta S^\circ_{\text{mix}} = 2.8 \text{ kcal/mol}$. For 1 000 isomers, which are found computationally for $n = 8\text{--}10$ clusters, $\Delta S^\circ_{\text{mix}} = 13.8 \text{ cal}/(\text{mol K})$, and at 300 K $RT\Delta S^\circ_{\text{mix}} = 4.1 \text{ kcal/mol}$.

Examples of filled and open-shell structures with similar energies within 2 kcal/mol are $\text{NH}_4^+(\text{H}_2\text{O})_n$ and in $(\text{NH}_3)_n(\text{HCN})_m\text{H}^+$ clusters containing more than four molecules.^{36,186} These results were confirmed by more recent high-level calculations and spectroscopy on the $\text{NH}_4^+(\text{H}_2\text{O})_n$ clusters ($n = 0\text{--}5$), which found an isomer with closed-shell and cyclic and noncyclic isomers of similar energies at $n = 4$ and a four-membered ring and a fifth double acceptor H_2O molecule at $n = 5$.^{234,235}

Similar effects of many isomeric clusters of comparable energies were shown by molecular mechanics calculations on large protonated water clusters¹⁹⁸ and by spectroscopy and theoretical calculations on water/methanol clusters.²³⁶ In some low-energy clusters outer shells start before an inner shell is completed, as may be common in large clusters.

Isomeric clusters of similar energies occur also in solvated anions. For example, ab initio calculations on $\text{I}^-(\text{H}_2\text{O})_n$ ($n = 1\text{--}6$) found flexible potential surfaces in particular for $n = 5$ and 6 with four nearly isoenergetic conformers for $n = 6$. These conformers have surface and near-surface structures with coordination numbers of 4 H_2O molecules about the ions.²³⁷

3.1.6. Location of the Ion: Interior-Ion and Exterior-Ion Structures. As the solvent shell grows, solvent molecules may fill a shell about the core ion and keep building up shells about it with the ion inside the solvent cluster (internal solvation or interior-ion structures). Alternatively, outer solvent molecules can attach to the first inner molecule and build a solvent cluster to which the ion is attached on the outside (external solvation or exterior ion structures). (Note on terminology: Internal solvation is often used for intramolecular IHBs in polyfunctional ions, and external solvation is used for the attachment of solvent molecules to these ions. To avoid ambiguity, ions inside a solvent cluster may be called interior, and ions on the outside, or on the surface of solvent cluster, may be called exterior ion structures.)

Isomers of either form and close in energy were found in early calculations on $\text{NH}_4^+(\text{H}_2\text{O})_n$ clusters,³⁶ and some of the isomers were observed later by spectroscopy.^{234,235} The solvent may even remove the proton, leaving the neutral solute on the outside, such as in $\text{MeCNH}^+(\text{H}_2\text{O})_n \rightarrow \text{MeCN}(\text{H}_2\text{O})_n\text{H}^{228}$ or in $\text{Me}_2\text{OH}^+(\text{H}_2\text{O})_n \rightarrow \text{Me}_2\text{O}(\text{H}_2\text{O})_n\text{H}^{230}$

The location of the ion was investigated extensively in the hydration of halide anions. The larger ions, Cl^- , Br^- , and I^- , are surface-solvated by water and methanol, while F^- is inside the hydrated cluster.^{88a} Recently, Seward and co-workers measured the thermochemistry of $\text{Cl}^-(\text{H}_2\text{O})_n$, $\text{Br}^-(\text{H}_2\text{O})_n$, and $\text{I}^-(\text{H}_2\text{O})_n$ clusters with 8, 7, and 5 H_2O molecules, respectively.^{219c} Computations suggested that clusters with external halide have lower enthalpies and would predominate at low temperatures, but entropy favors interior solvation at higher temperatures.^{219c} The observed clusters were mostly externally solvated or mixtures of externally and internally solvated isomers.^{219c}

External solvation of halide ions, but internal solvation of Na^+ , was also suggested by liquid-drop theory.²³⁸ The development of solvent structure in clusters about halide ions and implications about the inner solvent shell in solution were reviewed recently.⁸⁶

Halide anions and protonated alkylated cations often remain on the surface in small clusters but assume inner positions as the solvent surrounds the ions upon higher solvation.^{237,239} For example, in alkylated oxonium and ammonium ions, the first 6–8 H_2O molecules are expected to cluster about the ionized functional group, leaving the hydrophobic alkyl substituents on the outside. Indeed, water clusters appear to solvate alkylated ions such as protonated *n*-octylamine and 1-adamantylamine in this manner with the amine positioned on the surface of the water cluster. This was indicated by magic numbers in the solvating water clusters in studies using electrospray–Fourier transform ion cyclotron resonance (FTICR).

However, the alkyl groups become solvated when the cluster is transferred to bulk solution. Cluster thermochemistry separates the “inner” and “external” (hydrophobic) solvation

energies, allowing calculation of the various solvation terms, as discussed below.

3.1.7. Approach to Condensation. As the cluster size increases, the outer shells become increasingly shielded from the ionic charge, which remains concentrated mostly on the core ion. The structure assumes liquid-like characteristics with hydrogen-bonded networks including rings and three-dimensional cages. Also similar to liquids, where hydrogen bonds constantly break and reform, many isomeric clusters of comparable energies can be present in equilibrium. With these features, the bonding energies should approach $\Delta H^\circ_{\text{condensation}}$ of the bulk liquid.

In fact, the trends in bonding energies, $\Delta H^\circ_{n-1,n}$ with increasing cluster size have been measured in clustering sequences of many ligands and about many ions. In all cases, the binding energies converge to the respective bulk liquid $\Delta H^\circ_{\text{condensation}}$ already after a few, usually 4–6, solvent molecules. Remarkably, this convergence occurs for solvent molecules with a wide range of structures and condensation energies. It was observed for small molecules with $-\Delta H^\circ_{\text{condensation}}$ of 1–2 kcal/mol, such as Ar,^{240a} H₂,^{240b} CO,^{240c} and N₂,^{240d} that were measured up to 10–16 molecules by Hiraoka and co-workers. It was also observed in clustering series of hydrogen-bonding species such as (NH₃)_nH⁺ and (H₂O)_nH⁺ with $-\Delta H^\circ_{\text{condensation}}$ of 5–10 kcal/mol and in clustering series of more complex molecules, some with even larger condensation enthalpies, such as alcohols from CH₃OH to t-C₄H₉OH with $-\Delta H^\circ_{\text{condensation}}$ of 8.4–13.4 kcal/mol, and also for ions solvated by CH₃COOH, HCN, and CH₃CN and (CH₃)₃N with $-\Delta H^\circ_{\text{condensation}}$ of 5.5–12.8 kcal/mol.¹⁷⁸

In hydration sequences, the bonding energies converge to $\Delta H^\circ_{\text{condensation}}(\text{H}_2\text{O})$ regardless of the core ions, from the hydration of Na⁺, K⁺, and H₃O⁺ to larger core ions such as protonated alcohols and amines and also anions such as OH⁻, CH₃COO⁻, and halide anions. In each case, $\Delta H^\circ_{n-1,n}$ converges to –8 to –10 kcal/mol after 4–8 ligand molecules, close to the bulk $\Delta H^\circ_{\text{condensation}}(\text{H}_2\text{O}) = -10.5$ kcal/mol. The convergence of clustering sequences to the bulk limit was summarized.¹⁷⁸

The approach to bulk $\Delta H^\circ_{\text{condensation}}$ already after 4–8 steps implies that liquid-like structures form even in these small clusters. The strength of a single neutral OH···O bond is 5 kcal/mol, and the observed limiting value of $\Delta H^\circ_{n-1,n}$ of about –10 kcal/mol for $n > 4$ in hydration sequences implies that two net new hydrogen bonds form by the addition of each H₂O molecule. This requires liquid-like cyclic and three-dimensional hydrogen-bond structures. These conclusions from the thermochemistry were confirmed by the ab initio and spectroscopic results discussed later.

3.2. Mixed Clusters

3.2.1. Unlimited and Blocked IHB Networks. In clusters formed in natural processes such as atmospheric nucleation and in mixed liquids and solution, several different components usually aggregate into multicomponent hydrogen-bonded networks. Two main types of networks can be distinguished. In the first type, both components have bonding hydrogens, can serve both as acceptors and donors, and can therefore form indefinite hydrogen-bond networks. The thermochemistry of such clusters was measured in mixtures of H₂O with NH₃¹⁴⁹ and H₂S^{61,64a} and in both anionic and cationic clusters in mixtures of H₂O with CH₃OH,^{180a,b} CH₃COOH,¹⁸³ and H₂SO₄.^{241a,b}

In the second type of mixture, one component, usually water, can serve both as acceptor and donor and forms a strongly hydrogen-bonded protonated core surrounded by alkyl-blocked components that can serve only as acceptors. The thermochemistry of such clusters was measured in mixtures of H₂O with (CH₃)₂O,¹⁰³ (CH₃)₂CO,²⁴² CH₃OCH₂CH₂OCH₃,¹⁵⁴ HCN,^{199,186} and CH₃CN²²⁸ and also in nonaqueous mixtures of CH₃OH/(CH₃)₂O,¹⁰³ CH₃OH/CH₃CN,²⁴³ and HCN/NH₃.¹⁸⁶ Clusters containing HCN are intermediate between the two types because it can serve as a strong acceptor but also as a donor of CH···X type bonds.

3.2.2. The Location of the Proton. The nature of the IHB network, unlimited or blocked, affects the location of the proton in the clusters. The position of the proton in non-blocked clusters was investigated both by theory and spectroscopy. For example, ab initio calculations addressed ammonia/water clusters where the proton is usually on an NH₄⁺ core ion, consistent with the higher PA(NH₃) versus PA(H₂O). However, Figure 24 above shows a cluster where NH₄⁺ is attached to a (H₂O)₃ water cluster in an outer position. The proton affinity of H₂O (165 kcal/mol) plus the total binding energy of (H₂O)₃H⁺ is 207 kcal/mol, just above the proton affinity of NH₃ (204 kcal/mol). Correspondingly, the calculated structure shows that the proton is partially transferred to water. However, such structures with NH₃ in outer positions are high-energy isomers that may not exist in equilibrium mixtures.³⁶ In MeOH/H₂O clusters the proton tends to be located on MeOH₂⁺, but H₃O⁺-centered isomers can have comparable energies. Such a structure was proposed for (ROH)₉H₃O⁺ based on cluster size distributions in clusters of methanol, ethanol, n-propanol and 2-propanol, and water.^{244a} The structures of protonated NH₃/H₂O clusters^{234,235} and MeOH/H₂O clusters²³⁶ will be discussed in the spectroscopy section.

In mixed clusters of nonblocked and blocked components, the proton usually resides on the component with the higher proton affinity. However, a proton can reside on the weaker base due to two effects. The proton can form an H₃O⁺ core ion when blocked molecules with higher proton affinity attach to it and exert balancing attractions that keep the proton on the core ion. Second, several water molecules can form a (H₂O)_nH⁺ core where the strong IHBs stabilize the proton in this center. Figure 29 illustrates these effects in Me₂O/H₂O clusters as suggested first by Grimsrud and Kebarle.¹⁰³

The first study that showed a proton located on the component with the lower PA was performed by Meot-Ner, Deakyne, and co-workers on CH₃CN/H₂O clusters.²²⁸ This type of structure is shown in Figure 30 in MeCN(H₂O)₂H⁺ in which PA(H₂O) plus the binding energy of (H₂O)₂H⁺ is 198 kcal/mol, greater than PA(MeCN) (186.2 kcal/mol). Correspondingly, the proton is transferred from MeCN to a (H₂O)₂H⁺ dimer. A similar effect was observed spectroscopically in protonated Me₂O/H₂O clusters where the proton is transferred to a H₃O⁺ core ion in (Me₂O)(H₂O)₃H⁺.²³⁰

The Castleman group^{207,216a,b} examined the (CH₃)₂O/H₂O, (CH₃)₂CO/H₂O, (CH₃)₃N/H₂O, (CH₃)₃N/NH₃, and pyridine/NH₃ clusters by metastable and collisional induced dissociation (CID). They concluded that H₃O⁺ or NH₄⁺, respectively, are the core ions when the cluster size is large enough to form a closed hydrogen-bonded shell, even where the proton affinity of the core species (H₂O) is lower by 61.8 kcal/mol than that of the ligand (CH₃)₃N (Figure 31). In this type of structure, the maximum content of the blocked B molecule can be represented as (H₂O)_nB_{n+2}H⁺ or (NH₃)_nB_{n+2}H⁺.

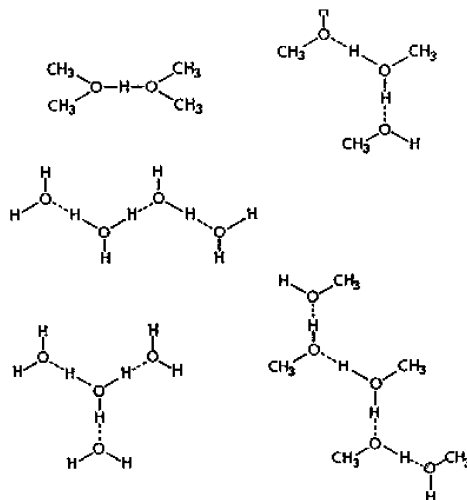


Figure 29. Structures of protonated water/dimethyl ether and methanol/dimethyl ether clusters with a protonated water or methanol core and, when dimethyl ether is present, a blocked dimethyl ether periphery. Reproduced with permission from ref 103. Copyright 1973 American Chemical Society.

with a protonated water or ammonia core of which the outer H atoms are all occupied by methyl-blocked ligands. These formulas apply as long as no cyclic hydrogen-bond networks are formed.

There is some evidence that blocked ligands may not always surround a H_3O^+ or NH_4^+ core ion. In $((\text{CH}_3)_2\text{CO})_2(\text{H}_2\text{O})\text{H}^+$ and $(\text{pyridine})_2(\text{NH}_3)\text{H}^+$, collision-induced dissociation (CID) yielded only the loss of H_2O and NH_3 molecules, respectively, suggesting that these were bound weakly to the $((\text{CH}_3)_2\text{CO})_2\text{H}^+$ or $(\text{pyridine})_2\text{H}^+$ dimers.^{207,216a,b} However, the clusters could have rearranged before dissociation. In fact, evidence for protonated cores surrounded by blocked ligands was observed in related systems by selected ion flow tube (SIFT) experiments and ab initio calculations. In such studies, Lifschitz and co-workers identified stable clusters where NH_4^+ ,

protonated amines, or MeOH_2^+ are surrounded by blocked CH_3CN or CH_3COCH_3 ligands.^{53,222–224,244b,245}

In $(\text{HCOOH})_n(\text{H}_2\text{O})\text{H}^+$, structures with a H_3O^+ core ion start to dominate at $n = 4$. For larger clusters, with $n = 5–8$, folded structures with a central H_3O^+ core ion and terminating with cyclic, neutral H-bonded $(\text{HCOOH})_2$ dimers (Figure 32) were calculated as more stable than linear structures terminated by H_2O and HCOOH , but only by a few kilocalories per mole. Experimentally, the coexistence of all of these structures is indicated because H_2O , HCOOH , and $(\text{HCOOH})_2$ loss channels all occur upon CID.²⁴⁶

The location of the proton on H_3O^+ surrounded by blocked bases was also confirmed by IR spectroscopy.^{104,230,247} Similar groupings of a central $(\text{H}_2\text{O})_n\text{H}^+$ unit between more basic polar groups can be formed also when the polar groups are located on a polyfunctional molecule. In biology, this allows the proton to move through a water chain that is surrounded by more basic groups in proteins.

An extreme example of a proton on a H_3O^+ center occurs in the cation-bridged, that is, salt-bridged, cluster $\text{CH}_3\text{COO}^- \cdot \text{H}_3\text{O}^+ \cdot \text{CH}_3\text{COO}^- \cdot \text{H}_2\text{O}$ where the H_2O molecule has a PA lower by 140 kcal/mol than each of the neighboring CH_3COO^- ions.¹⁸³ The low energy of the charge-separated intermediate results from the location of the proton between two negative charges that attract the proton in opposite directions. Such charge-separated isomers can constitute low-energy intermediates for proton transfer between carboxylic groups in biological systems.

In summary, the proton can be located in a protonated core stabilized by ionic hydrogen bonds, even when the core is formed by a weak base surrounded by stronger but blocked base molecules. Such structures were confirmed by various experiments and by calculations, and they play significant roles in biology.

3.2.3. Relations between Cluster Composition and Binding Energies. Figures 33 and 34 show the thermochemical data for IHB networks in mixed clusters as illustrated in the $\text{CH}_3\text{OH}/\text{H}_2\text{O}$ cationic and anionic clusters.

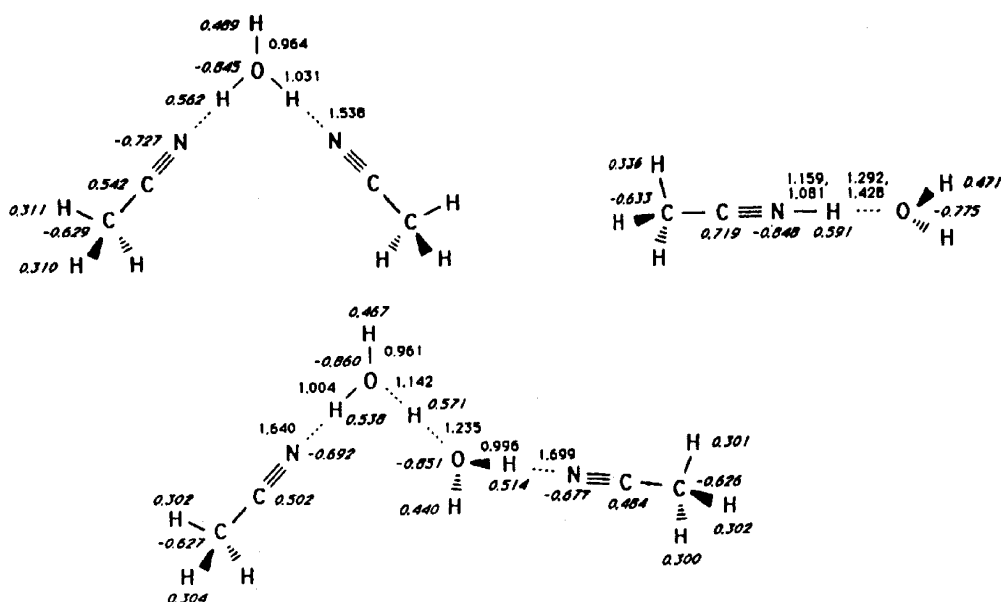


Figure 30. Calculated structures of $(\text{CH}_3\text{CN})(\text{H}_2\text{O})\text{H}^+$, $(\text{CH}_3\text{CN})_2(\text{H}_2\text{O})\text{H}^+$, and $(\text{CH}_3\text{CN})_2(\text{H}_2\text{O})_2\text{H}^+$, where in the latter two clusters the balancing attractions of two CH_3CN molecules keep the proton on a water core, despite the lower proton affinity of water. Reproduced with permission from ref 228. Copyright 1986 American Physical Society.

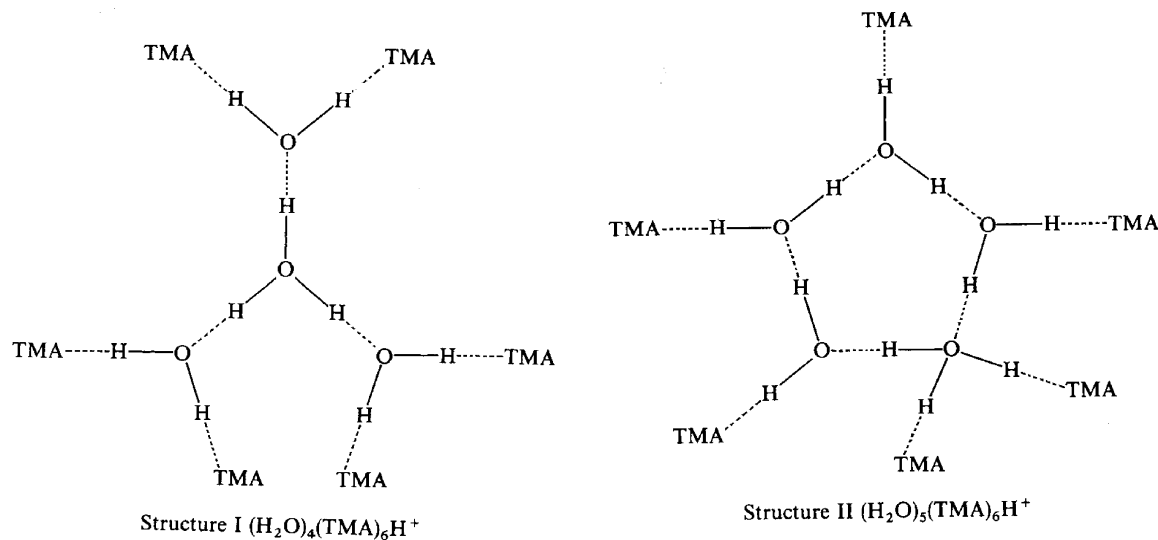


Figure 31. Structures derived from collisional dissociation of mixed protonated clusters of trimethylamine and water. The proton is located on a H_3O^+ core ion. Reproduced from ref 216b with permission. Copyright 1991 American Chemical Society.

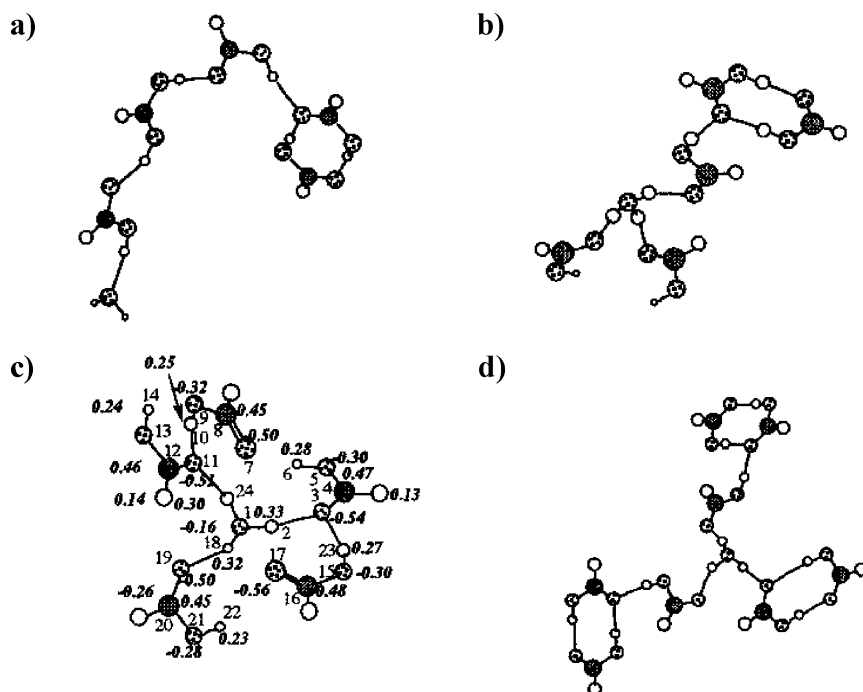


Figure 32. Structures indicated in (a–c) $(\text{HCOOH})_n(\text{H}_2\text{O})\text{H}^+$ clusters and (d) $(\text{HCOOH})_8(\text{H}_2\text{O})\text{H}^+$ clusters. The proton is located in a H_3O^+ core ion in structures b, c, and d. Reproduced with permission from ref 246. Copyright 1997 Elsevier.

The numbers under the formulas in Figures 33 and 34 indicate the stabilities of the ionic hydrogen-bond networks in terms of the energy required for dissociation to the highest-energy monomer ion and neutral components. The effects of increasing mole fraction of the organic component can be observed by proceeding vertically up a given column, comparing clusters of a constant rank, $m + n$. Note that the term “rank” may be more precise than “size” to describe the number of components, because various clusters with equal number of components may have different physical sizes.

The stabilities increase with increasing enrichment of the component with the higher PA or, in anion clusters, of the component with the greater gas-phase acidity. For example, the

trend of increasing stability of $(\text{MeOH})_m(\text{H}_2\text{O})_n\text{H}^+$ four-membered clusters with increasing MeOH content can be noted in Figure 33 and was also confirmed by ab initio calculations and spectroscopy.²³⁶ This is also the trend in protonated and in anionic clusters of acetic acid and water in Figure 35, even when complex geometries such as in Figure 36 arise because of two functional groups in the acetate ion. In these clusters, the strong $\text{OH}^+\cdots\text{O}$ or $\text{O}^-\cdots\text{HO}$ bonds that can form unlimited IHB networks and enrichment by the stronger base or acid always increase the stability.

However, when one of the components can form stronger IHBs, enrichment in this component may be stabilizing. This is the case in ammonia/water clusters (Figure 24) where some of

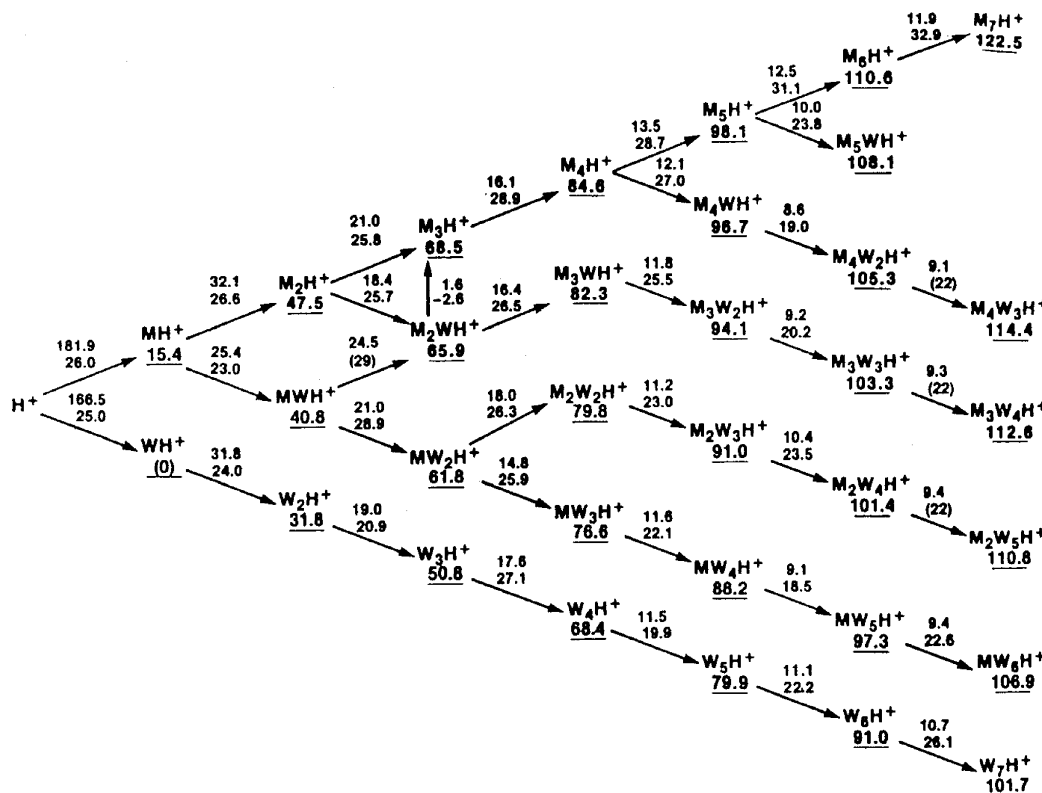


Figure 33. Thermochemistry of protonated hydrogen-bond networks in methanol/water mixed clusters, $(\text{CH}_3\text{OH})_m(\text{H}_2\text{O})_n\text{H}^+$. Numbers above arrows indicate $\Delta H^\circ_{\text{D}}$ (top) (kcal/mol) and $\Delta S^\circ_{\text{D}}$ (bottom) (cal/(mol K)) for the step indicated. Vertical arrows indicate ligand-exchange reactions. Numbers under formulas indicate enthalpies of dissociation to H_3O^+ and neutrals. Reproduced with permission from ref 180b. Copyright 1986 American Chemical Society.

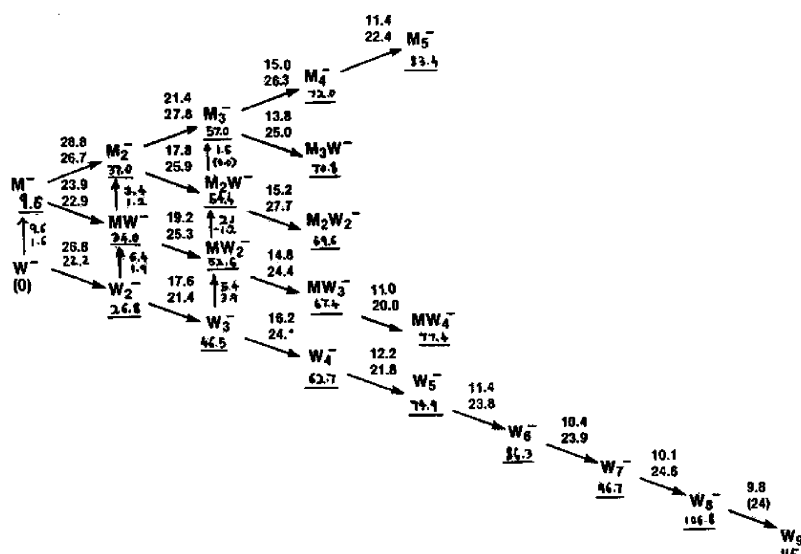


Figure 34. Thermochemistry of anionic hydrogen-bond networks in methanol/water mixed clusters $((\text{CH}_3\text{OH})_n(\text{H}_2\text{O})_m-\text{H})^-$. Numbers above arrows indicate $\Delta H^\circ_{\text{D}}$ (top) (kcal/mol) and $\Delta S^\circ_{\text{D}}$ (bottom) (cal/(mol K)) for the step indicated. Vertical arrows indicate ligand-exchange reactions. Numbers under formulas indicate enthalpies of dissociation to OH^- and neutrals. Reproduced with permission from ref 180b. Copyright 1986 American Chemical Society.

the bonds are $\text{OH}^+\cdots\text{O}$, some $\text{NH}^+\cdots\text{O}$, and some $\text{NH}^+\cdots\text{N}$. Although the proton affinity of NH_3 (204 kcal/mol) is much higher than that of H_2O (165 kcal/mol), the stabilities of the $(\text{H}_2\text{O})_n\text{H}^+$ clusters increase faster with increasing size than those of the $(\text{NH}_3)_n\text{H}^+$ clusters because of the stronger $\text{OH}^+\cdots\text{O}$ bonds in the former.

3.3. Effects of Partial Solvation on Acidities, Basicities, and on Ionic Aggregation

3.3.1. Effects of Partial Solvation on Basicities. Gas-phase ion chemistry made an important contribution to acid/base chemistry by measuring intrinsic solvent-free molecular acidities and basicities. Comparison with solution then shows

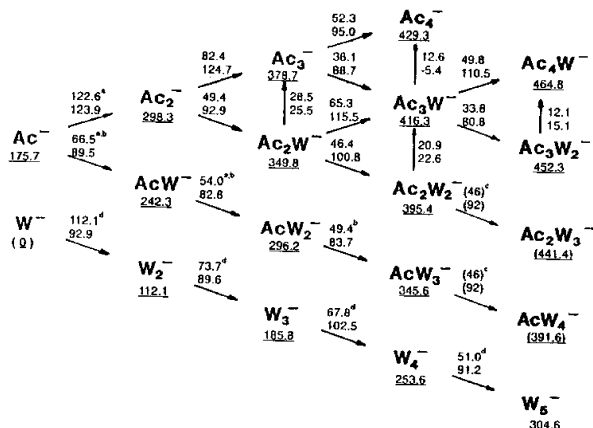


Figure 35. Thermochemistry of anionic hydrogen-bond networks in acetic acid/water mixed clusters. Numbers above arrows indicate ΔH°_D (top) (kJ/mol) and ΔS°_D (bottom) (J/(mol K)) for the step indicated. Vertical arrows indicate ligand-exchange reactions. Numbers under formulas indicate enthalpies of dissociation to OH^- and neutrals. Reproduced with permission from ref 183. Copyright 1999 American Chemical Society.

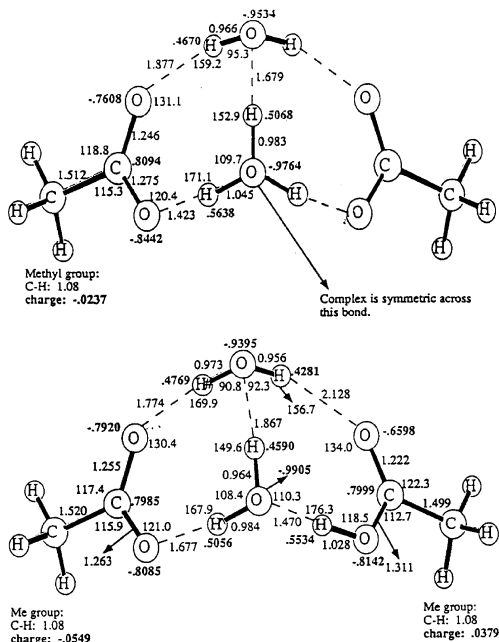


Figure 36. Water-bridged (bottom panel) and salt-bridged (top panel) geometries of some anionic acetic acid/water clusters calculated by the Gaussian 92 method, optimized at the SCF/4-31G level. Reproduced with permission from ref 183. Copyright 1999 American Chemical Society.

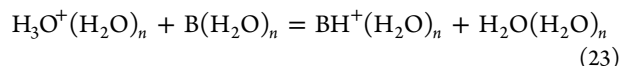
that ion solvation is as significant as the molecular properties themselves in determining the solution acidities and basicities. Solvation effects can compress, and sometimes reverse, the relative acidities and basicities. This was shown in early studies on the acidities of alcohols and the basicities of amines by Brauman and Blair,^{248,249} Kebarle,⁵ McIver and co-workers,²⁵⁰ and Bohme and co-workers.^{11,251,252}

Since these early measurements, the gas-phase acidities and basicities of thousands of compounds were compiled.^{27,30,128,253} These data allow an analysis of structural effects on molecular acidities and basicities, and comparison with solution then quantifies the solvation effects.²⁰

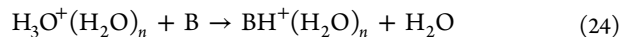
The solvation effects are illustrated by comparing the relative enthalpies of protonation in the gas phase and in solution (Table 11). Among the oxonium and ammonium ions listed, $\Delta H_{\text{prot},g}$ varies by 45.4 and 30.7 kcal/mol, while $\Delta H^\circ_{\text{prot},\text{aq}}$ varies only by 3.3 and 5.5 kcal/mol, respectively. In some cases solvation reverses the relative basicities.

The physical effects of stepwise solvation were investigated recently by ab initio calculations on the stepwise hydration of ammonia, methylamine, dimethylamine, and trimethylamine and their protonated ions. The first water molecules add distinctly, while larger numbers of water molecules form hydrogen-bond networks. The thermochemistry of solvation leads toward the anomalous basicities of ammonia and alkylamines in solution.²⁵⁴ Cluster studies show the stepwise buildup of these solvation effects.

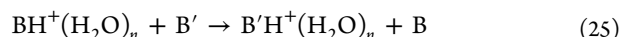
When a base B is protonated in water, the proton is transferred from a solvated $\text{H}_3\text{O}^+_{\text{aq}}$ ion to form a solvated BH^+_{aq} ion. The process also releases a solvated H_2O molecule and takes up a solvated B molecule. Equation 23 shows the cluster equivalent of this process.



The effects of stepwise solvation are reflected by the variation of the thermochemistry with n . The energies of the neutral clusters in eq 23 are usually not available, but for n lone-pair donor acids and bases, the energies of neutral hydrogen bonds are likely to be comparable. Most of the solvation effects in reaction 23 may be attributed therefore to ion solvation as in reaction 24, the thermochemistry of which can be calculated from proton affinities and from the thermochemistry of the $\text{H}_3\text{O}^+(\text{H}_2\text{O})_n$ and $\text{BH}^+(\text{H}_2\text{O})_n$ clusters.



Reaction 25 and the corresponding eq 26 show the effects of n -fold hydration on the relative heats of protonation. Using $\text{B}' = \text{H}_2\text{O}$ in eq 26 yields the enthalpy of proton transfer from water to base B as a function of n -fold solvation.



$$\Delta H^\circ_{25} = [\text{PA}(\text{B}) - \text{PA}(\text{B}')] + [H^\circ_{0,n}(\text{B}'\text{H}^+\cdot n\text{H}_2\text{O}) - \Delta H^\circ_{0,n}(\text{BH}^+\cdot n\text{H}_2\text{O})] \quad (26)$$

Analogous relations apply for anion clusters and relative acidities. Note that eq 26 neglects the relative clustering energies of the neutrals, that is, it corresponds to reaction 25. Figure 37 shows the results for several bases. The main observation is that increasing solvation compresses and in some cases reverses the differences between the intrinsic molecular basicities and acidities of molecules. For example, solvation by 6 H_2O molecules decreases the enthalpies of proton transfer from H_3O^+ to alkylamines from -40 to -60 kcal/mol to -12 to -20 kcal/mol, while further bulk solvation decreases these values by a much smaller factor, to -10 to -16 kcal/mol.

Solvation in the clusters decreases the differences between enthalpies of protonation because ions of stronger bases are solvated less efficiently than H_3O^+ , according to the $\Delta H^\circ_D/\Delta \text{PA}$ correlations. This trend carries over to aqueous solution where solvation causes the irregular basicities of alkylamines and compresses the differences between the basicities of oxygen and nitrogen bases (Figure 37). Similar effects also apply in anions, where solvation compresses the relative acidities of

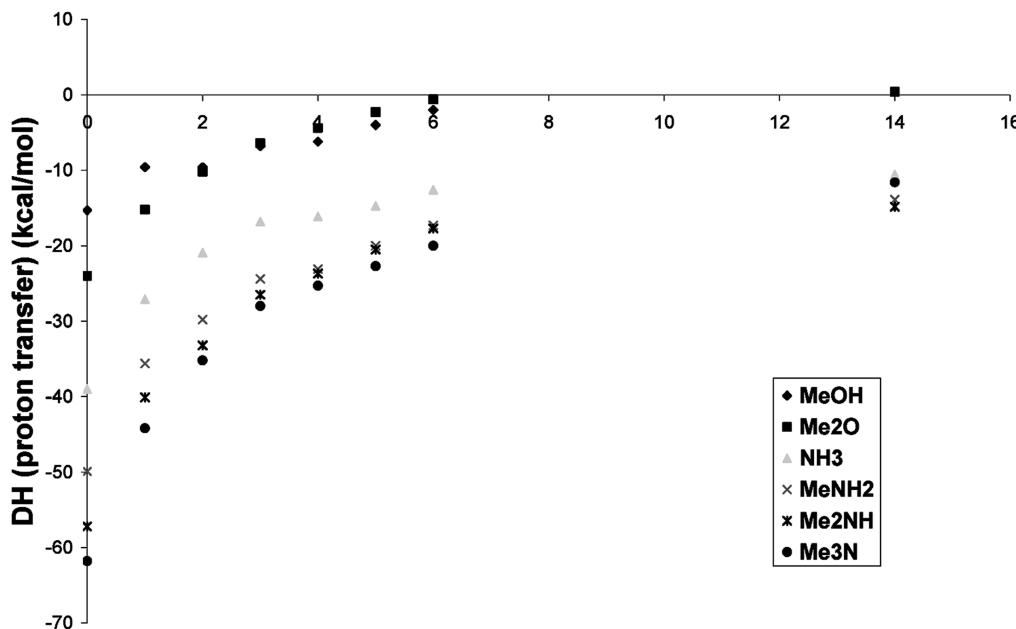
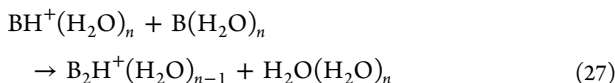


Figure 37. Enthalpies of proton transfer from water to base B as a function of n -fold ion solvation for $\text{H}_3\text{O}^+(\text{H}_2\text{O})_n + \text{B} \rightarrow \text{BH}^+(\text{H}_2\text{O})_n + \text{H}_2\text{O}$. The exothermicity decreases with increasing n as proton transfer from H_3O^+ to bases B becomes less exothermic with increasing solvation due to the strong hydration of the H_3O^+ ion. In general, proton transfer from weaker bases B to stronger bases B' (vertically down at each n) becomes less exothermic with increasing n due to the stronger hydration of the BH^+ ions. The relative values approach the relative heats of protonation in solution. The figure shows the compression of relative enthalpies of protonation (approximately, the relative basicities) with stepwise solvation toward the values in bulk water, represented by " $n = 14$ ". Values were calculated from eq 26 using cluster data from Table 4, enthalpies of ion hydration from Table 10, and proton affinities from Table 11.

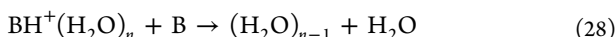
alcohols and carboxylic acids. This was shown by the classical studies of Brauman and Blair on the acidities of alcohols^{248,249} and by recent results on $\text{NH}_2^-(\text{NH}_3)_n$ ($n = 0-2$) where NH_2^- is a stronger base than H^- in the gas phase but two ammonia solvent molecules reverse this order.²⁵⁵

In conclusion, comparisons with gas-phase chemistry show that solvation effects can be as significant as intrinsic molecular parameters in determining relative acidities and basicities. Cluster studies show that most of the solvation effects, often 80% or more, result from solvation by the first 4–8 solvent molecules.

3.3.2. Effects of Partial Solvation on Ionic Aggregation. Equation 27 represents aggregation with solvent displacement of an n -fold solvated ion and neutral to form an ($n - 1$) solvated dimer ion.



Again, focusing on strong ion solvation and disregarding the effects of weaker and unknown bonding energies in the neutral clusters leads to reaction 28 to model the effects of ion solvation on aggregation.



The thermochemistry of reaction 28 is shown by the second step vertically up (from $\text{BH}^+(\text{H}_2\text{O})_n$ to $\text{B}_2\text{H}^+(\text{H}_2\text{O})_{n-1}$) in clustering energy diagrams such as in Figures 33–35. The reaction enthalpy is shown in Figure 38 for clusters with various degrees of solvation. Reaction 28 may be exothermic if the $\text{BH}^+\cdot\text{B}$ bond is stronger than the $\text{BH}^+\cdot\text{H}_2\text{O}$ bond, but this difference decreases as the number of H_2O molecules in the cluster increases and they solvate the monomer ion more

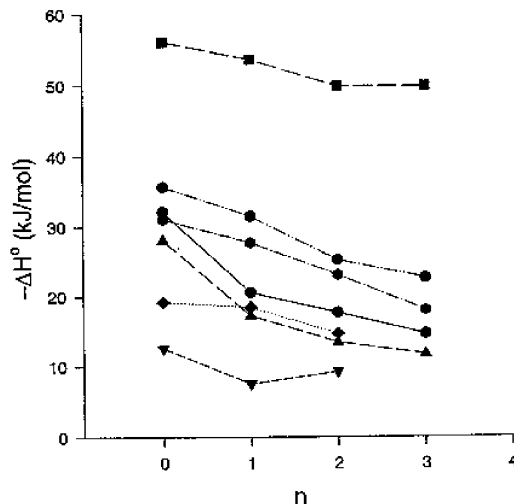


Figure 38. Enthalpies of dimer formation with solvent displacement for the reactions $\text{A}^-(\text{H}_2\text{O})_n + \text{AH} \rightarrow \text{A}_2^-(\text{H}_2\text{O})_n + \text{H}_2\text{O}$ in anionic and $\text{BH}^+(\text{H}_2\text{O})_n + \text{B} \rightarrow \text{B}_2\text{H}^+(\text{H}_2\text{O})_{n-1} + \text{H}_2\text{O}$ in cationic mixed clusters of water with (from top to bottom lines as they start at $n = 0$) acetate anion, dimethylamine cation, acetic acid cation, *n*-propylamine cation, methanol cation, ammonia cation, and methanol anion clusters. The figure shows that dimer formation with water replacement between carboxylate ions and carboxylic acids (top plot) is more exothermic at any degree of hydration than in the other systems. The exothermicity reflects the combination of the formation of a strong $\text{RCOO}^-\cdot\text{HOOCR}$ bond formed with the displacement of a weak $\text{RCOO}^-\cdot\text{HOH}$ bond. Preferential aggregation in the carboxylate/carboxylic acid system also applies in higher steps of aggregation; see Figure 39. This effect may contribute IHB networks in the formation of membranes by carboxylic acids. Reproduced with permission from ref 183. Copyright 1999 American Chemical Society.

efficiently. Consequently, increasing solvation decreases the exothermicity of aggregation with solvent displacement.

Solvation effects on higher aggregation steps with solvent displacement are represented by the cluster reaction 29, which corresponds to consecutive steps vertically up in clustering diagrams such as in Figures 33–35.

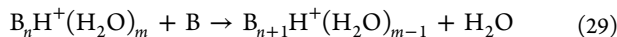


Figure 39 shows the enthalpy of reaction 29 for 4-membered mixed clusters. In general, the exothermicities are largest for the

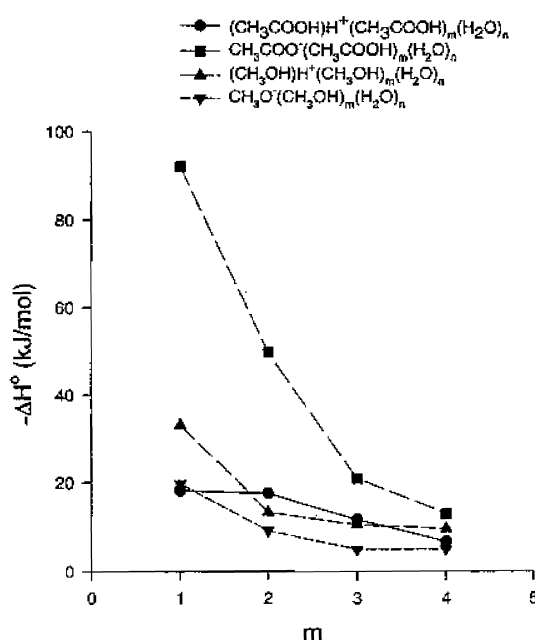


Figure 39. Enthalpies of stepwise aggregation with solvent displacement as modeled by clusters that contain four ligand molecules in anionic and cationic methanol/water and acetic acid/water clusters. The x-axis indicates that the m th molecule of the nonaqueous component is displaced by the m th water molecule. The figure shows that the aggregation of carboxylate ions/carboxylic acids (top plot) is more exothermic than that in the other systems because a strong $\text{RCOO}^- \cdot \text{HOOCR}$ bond replaces a weaker $\text{RCOO}^- \cdot \text{HOH}$ bond. The preference for aggregation by carboxylate/carboxylic acids versus other systems is strongest in the first aggregation steps. Reproduced with permission from ref 183. Copyright 1999 American Chemical Society.

first step of aggregation and decrease with adding each further acid or base molecule. The exothermicities of the aggregation steps decrease with increasing mole fraction of the organic component because each consecutive step becomes less significant in stabilizing further the already stabilized charge.

Figure 39 allows us to compare the thermochemistry of ionic aggregation of various acids and bases. As may be expected, aggregation with solvent displacement is favorable when a strong new $\text{BH}^+\cdot\text{B}$ bond (or $\text{A}^-\cdot\text{HA}$ bond in anions) displaces a weak $\text{BH}^+\cdot\text{H}_2\text{O}$ bond (or $\text{A}^-\cdot\text{H}_2\text{O}$ bond) to the solvent. This effect favors the ionic aggregation of oxygen bases and oxygen acids that form strong $\text{OH}^+\cdot\text{O}$ or $\text{O}^-\cdot\text{HO}$ bonds compared with the aggregation of nitrogen bases that form weaker $\text{NH}^+\cdot\text{N}$ bonds. These effects also favor the aggregation of strong acids or bases whose ions form weak bonds with the H_2O molecules that are easier to displace.

Figures 33–35 show that adding the stronger acid or base component binds to the clusters more strongly even in large

clusters. This shows that the correlations between hydrogen-bond energies and PA differences apply even in large clusters.

In conclusion, structures of mixed clusters were inferred first from thermochemistry and have been verified by ab initio calculations, dissociation methods, reactivity, and spectroscopy. The results show that nonblocked bases can form unlimited ionic hydrogen-bonded networks involving chains and rings, sometimes with distinct shells. The ionic effects are strongest in the inner shells of 4–6 molecules bonded to the core ions, which retain most of the charge even in large clusters and in solution.

In mixed clusters, where unlimited IHB networks are possible, the inner shell contains the component with the higher proton affinity. The stabilities of clusters of a given rank $m+n$ increase with the mole fraction of the component that has the higher PA or acidity. In mixtures of blocked and unblocked components, the proton can remain on the unblocked component even if it has the lower proton affinity, when this component forms a core of strong IHBs surrounded by a shell of the blocked components.

4. COMPLEX MOLECULES: INTRAMOLECULAR AND MULTIPLE BONDS

4.1. Intramolecular Hydrogen Bonds

4.1.1. Thermochemistry of Internal Hydrogen Bonds.

When polyfunctional molecules are protonated, strong internal ionic hydrogen bonds (iIHB's) can form with cyclic structures (Figures 40 and 41). The internal bonds stabilize the ions and increase the PAs of the parent molecules. However, internally bonded structures are constrained, and their formation results in negative entropy changes. Nevertheless, the overall free energy effects are usually stabilizing.

Intramolecular IHB formation was first observed by Bowers and co-workers in the increased basicities of diamines,^{258a} where they can lead to very high proton affinities, such as in the “proton sponge” (1,8-bis-(dimethylamino)naphthalene), where protonation causes a large shift of electron density toward the center of the molecule.^{258b} The enthalpy and entropy effects were investigated using temperature studies by Yamdagni and Kebarle and by Meot-Ner and co-workers in proton-transfer equilibria of diamines, triamines, and amino alcohols,^{39,259} protonated polyethers and crown ethers,^{260,261} and diketones.^{260,262} Studies by the McMahon and Stone groups found similar effects in dialcohols,^{262,263} amino alcohols, and methoxy alcohols.^{257,259} The cyclic internally bonded structures were confirmed by ab initio calculations on diamines, polyethers, methoxy alcohols,^{154,256,257} and other molecules^{s^{264–271}} and also were confirmed by H_2O and MeOH loss through metastable and collisional dissociation.²⁷²

A thorough study of iIHBs in aliphatic and alicyclic diamides, as models for peptides, was performed by Witt and Grutzmacher, using kinetic and thermokinetic method measurements of protonation thermochemistry.^{63a–c} The resulting PAs and apparent entropies of protonation showed ring-size effects on iIHB bond strengths, strain, and thermal stability similar to other series of compounds (Table 7). In sterically constrained diamides, only stereoisomers with the amide groups close to each other showed negative ΔS_{prot} indicative of iIHB formation. For example, in $\text{H}_2\text{NCOCH}=\text{CHCONH}_2$ only the cis but not the trans isomer showed such effects, and similar geometric effects were observed in alicyclic diamides.^{63b,c}

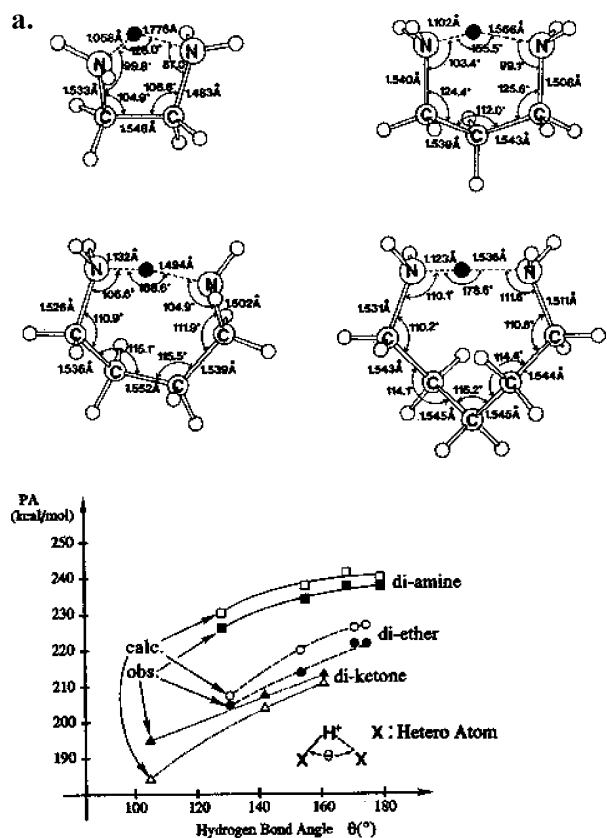


Figure 40. Calculated structures of protonated diamines at the RHF/3-21G level. Note that the bent $\text{NH}^+ - \text{N}$ angles approach linear geometry with increasing ring size. The bottom plot shows the correlation between the internal bond angle and the stabilization of the proton by the internal IHB as reflected in the proton affinities of difunctional compounds. With increasing approach to optimized 180° bond angle, the internal hydrogen bond formed upon protonation becomes stronger and the proton affinities of diamines increase correspondingly. Reproduced with permission from ref 256. Copyright 1992 American Chemical Society.

Cyclic iHIB structures and solvent effects thereon were confirmed also by recent IR predissociation spectroscopy studies, especially by the group of Y. T. Lee and co-workers.^{233a,247,273-276a} The thermochemistry of internal hydrogen bonds in polyfunctional ions was reviewed recently.^{276b,c}

Internal hydrogen bonds can also form involving CH donors. Figure 42 shows such structures with $\text{CH}\cdots\text{O}^-$ bonds in the *n*-decanoate anion that were studied by Norrman and McMahon.¹¹²

The thermochemistry of internal IHBs (iiHB's) can be evaluated by comparing the PAs of polyfunctional versus monofunctional bases, leading to the results in Table 7. These comparisons make the assigned iiHB strengths dependent on the chosen reference bases.^{39,258a,259} The internal bond strengths also can be obtained from theory by calculating the energies of the open and cyclized forms of the ions.²⁷²

4.1.2. Thermal Stabilities of Internal Hydrogen Bonds.

The overall stability of an iIHB was characterized by Meot-Ner and co-workers in terms of the temperature required to open the bond, $T_{\text{open}} = \Delta H^{\circ}_{\text{iIHB}} / \Delta S^{\circ}_{\text{iIHB}}$, at which half of the equilibrium population is open.²⁵⁹ Stabilities in these terms are listed in Table 7. Notably, the hypothetical ring-opening temperatures of most of the listed ions are near or >1000 K, exceeding those of stronger covalent bonds. The thermal stabilities of the hydrogen-bonded rings are much higher because the entropy gain of opening the internal bond is much smaller than that of pyrolyzing a covalent molecule into free fragments. Consequently, some stable internal bonds may never open thermally since at the required temperatures the ions may pyrolyze first. For these ions in Table 7, the internally hydrogen-bonded structure will always dominate. This is significant in the collisional dissociation of peptide ions that are often activated to effective temperatures of 400–800 K, where partial protonation by the internal hydrogen bonds activate the dissociation of amide links.

The thermochemical ring-opening effect was demonstrated experimentally by Norrman and McMahon in ions of some

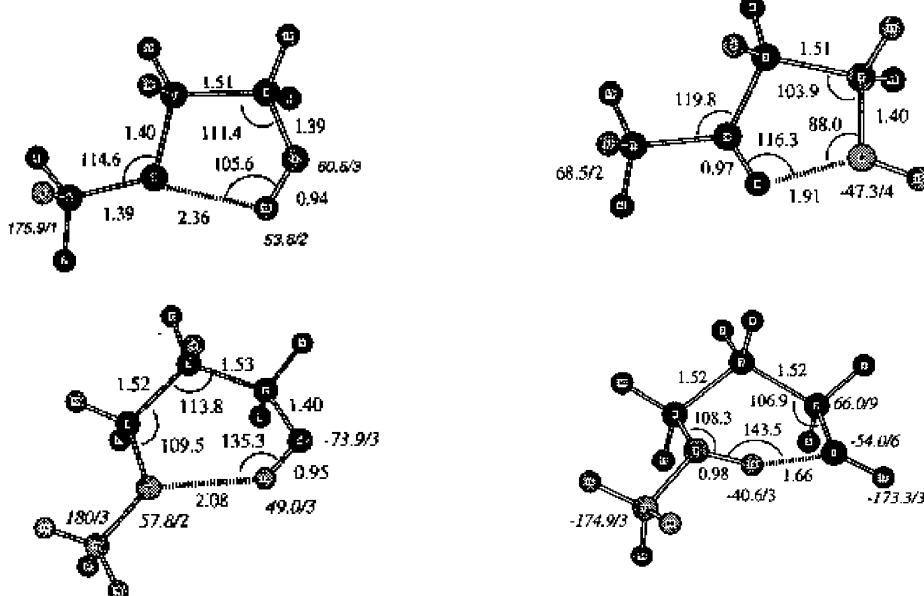


Figure 41. Calculated structures of neutral and protonated methoxy alcohols at the HF/6-31G* level. The internal bonds in the neutrals (left-side figures) are displaced by shorter, more optimized and stronger internal bonds in the ions. The internal hydrogen bond becomes more optimized with ring size. Reproduced with permission from ref 257. Copyright 1998 American Chemical Society.

Table 7. Enthalpies, Energies, Strain, and Stability of Intramolecular IHBs in Protonated Polyfunctional Ions BH^+ ^a

base (B)	PA ^b	$\Delta H^\circ_{\text{iIHB}}$ ^c	$\Delta H^\circ_{\text{strain}}$ ^d	$\Delta S^\circ_{\text{iIHB}}$ ^e	stability (T_{open}) ^f	refs ^g
diamines						
[CH ₃ (CH ₂) ₂ NH ₂]	219.4					
H ₂ N(CH ₂) ₂ NH ₂	227.4	8	16	11	727	259, 39
H ₂ N(CH ₂) ₃ NH ₂	235.8	16	8	17	942	259, 39
H ₂ N(CH ₂) ₄ NH ₂	240.3	21	3	18	1167	259, 39
triamines						
[(CH ₃ CH ₂ CH ₂) ₂ NH] ⁺	230.2					
H ₂ N(CH ₂) ₂ NH(CH ₂) ₂ NH ₂	237.5 ^h	7	17	7	1000	259
H ₂ N(CH ₂) ₃ NH(CH ₂) ₃ NH ₂	247.5 ^h	17	7	15	1134	259
amino alcohols						
[(CH ₃ (CH ₂) ₂ NH ₂] ⁺	219.4					
H ₂ N(CH ₂) ₂ OH	222.4	3	14			259
H ₂ N(CH ₂) ₃ OH	230.0	11	6	12	917	259
H ₂ N(CH ₂) ₄ OH	235.3	16	1	17	941	259
dialcohols						
[CH ₃ (CH ₂) ₂ OH]	188.0					
HO(CH ₂) ₂ OH	195.0	7	24	13	538	263
HO(CH ₂) ₃ OH	209.4	22	9	17	1294	263
HO(CH ₂) ₄ OH	218.8	31	0	23	1348	263
methoxy alcohols						
[CH ₃ O(CH ₂) ₂ CH ₃]	194.8					
CH ₃ O(CH ₂) ₂ OH	198.8 ⁱ	6.8 ⁱ	19.5	2.5 ⁱ	2720	263
CH ₃ O(CH ₂) ₃ OH	213.5 ⁱ	16.3 ⁱ	10.0	14.0 ⁱ	1164	263
CH ₃ O(CH ₂) ₄ OH	219.4 ⁱ	22.4 ⁱ	3.9	15.0 ⁱ	1493	263
CH ₃ O(CH ₂) ₅ OH	219.5 ⁱ	22.0 ⁱ	4.3	18.0 ⁱ	1222	263
diethers and polyethers						
[CH ₃ O(CH ₂) ₂ CH ₃]	194.8					
CH ₃ O(CH ₂) ₂ OCH ₃	205.1	10 ^j	21	4.3	2326	260
CH ₃ O(CH ₂) ₃ OCH ₃	214.4	20 ^j	11	6.0	3340	260
CH ₃ O(CH ₂) ₄ OCH ₃	222.6	28	3	16.8	1667	261
CH ₃ O(CH ₂) ₅ OCH ₃	222.6	28	3	17.3	1618	261
CH ₃ O(CH ₂) ₂ O(CH ₂) ₂ OCH ₃	219.6	25 ^j	6	13.8	1812	260
CH ₃ O(CH ₂) ₂ O(CH ₂) ₂ O(CH ₂) ₂ OCH ₃	226.2	31 ^j		18.6	1667	260
12-crown-4	221.6	27		8.3	3253	261
15-crown-5	225.6	31		11.1	2793	261
18-crown-6	231.1	36		22.0	1636	261
diketones						
[CH ₃ COCH ₂ CH ₃]	197.7					
CH ₃ COCOCH ₃	191.7	-6 ^k	30	2.6		260
CH ₃ COCH ₂ COCH ₃	208.8	1	30	3.6	278	260
CH ₃ COCH ₂ CH ₂ COCH ₃	213.2	6	25	7.0	857	260
diamides						
[CH ₃ CH ₂ CH ₂ CONH ₂]	210					63a
H ₂ NCOCH=CHCONH ₂ (trans)	206	-4				63b
H ₂ NCOCH=CHCONH ₂ (cis)	225	15	15	5	3000	63b
H ₂ NCO(CH ₂) ₂ CONH ₂	225	15	15	5	3000	63b
H ₂ NCO(CH ₂) ₃ CONH ₂	232	22	8	10	2200	63b
H ₂ NCO(CH ₂) ₄ CONH ₂	235	25	5	10	2500	63b
H ₂ NCO(CH ₂) ₈ CONH ₂	234	24	6	9	2600	63b
amino acid derivatives						
[CH ₃ CONHCH ₃]	212.7					
CH ₃ CONHCH ₂ COOCH ₃ (CH ₃ CO-Gly-OCH ₃)	223.7 ^l	11 ^l	20	12 ^l	917	150
CH ₃ CONHCH(CH ₃)COOCH ₃ (CH ₃ CO-Ala-OCH ₃)	224.7 ^l	12 ^l	19	15 ^l	800	150

^aUnits of $\Delta H^\circ_{\text{iIHB}}$ and $\Delta H^\circ_{\text{strain}}$ are in kcal/mol, those of $\Delta S^\circ_{\text{iIHB}}$ are in cal/(mol K), and those of T_{open} are in K. Monofunctional reference compounds are shown in brackets. ^bProton affinities from NIST tables²⁷ unless noted otherwise. ^cEnthalpies of opening of internal bonds obtained from $\Delta H^\circ_{\text{iIHB}} = \text{PA(B)} - \text{PA(B}_{\text{ref}})$ where B_{ref} is the reference compound shown in brackets. ^dStrain energies from the difference between $\Delta H^\circ_{\text{iIHB}}$ and $\Delta H^\circ_{\text{D}}$ of protonated dimer ions as reference: for diamines, symmetric NH⁺...N dimers, $\Delta H^\circ_{\text{D}} = 23$ kcal/mol; for amino alcohols, the CH₃NH₃⁺...CH₃OH dimer, $\Delta H^\circ_{\text{D}} = 17$ kcal/mol; for diols, diethers, and diamides, symmetric OH[−]...O dimers, $\Delta H^\circ_{\text{D}} = 30$ kcal/mol; for methoxy alcohols, the dimer (CH₃)₂OH[−]...CH₃OH, $\Delta H^\circ_{\text{D}} = 26.3$ kcal/mol.^{261,257} ^eEntropies of ring-opening of internal bonds as assigned in the original references. For the diamines, average values are from refs 39 and 259. ^fTemperatures of internal ring-opening calculated from $T_{\text{open}} = \Delta H^\circ_{\text{iIHB}} / \Delta S^\circ_{\text{iIHB}}$ (see text). ^gReferences for the original data. ^hFrom ref 259. ⁱValues assigned in ref 257. ^jFor the diethers and glymes, refs 260 and 261 give similar PAs and entropies of protonation. ^kThe reduced PA compared with the monofunctional reference ketone reflects the effects of the internal dipole. ^lData based on ref 150.

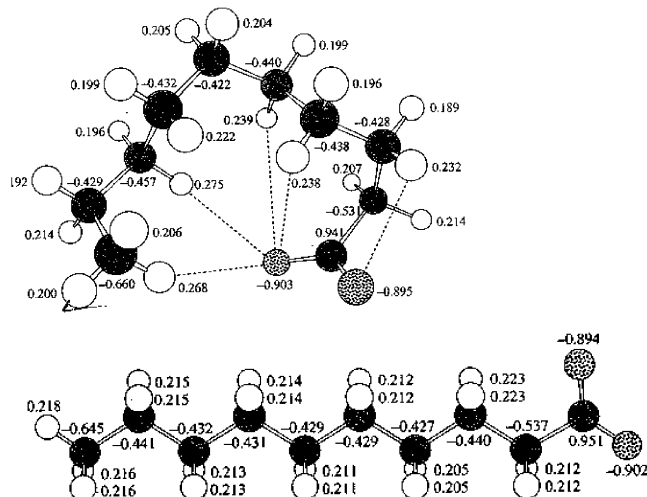


Figure 42. Internally hydrogen-bonded cyclic conformation of *n*-decanoate with five $\text{CH}\cdots\text{O}^-$ bonds, and the open isomer. Note increased positive charges on the bonding hydrogens and negative charges on the donor CH carbons and acceptor O^- atoms upon hydrogen-bond formation. Reproduced with permission from ref 112. Copyright 1999 American Chemical Society.

longer-chain acids that form unconventional $\text{CH}\cdots\text{O}^-$ intermolecular bonds as shown in Figure 42. Proton-transfer equilibria involving *n*-decanoic and 2-ethylhexanoic acids showed curved van't Hoff plots, which suggested an equilibrium population that contained folded and unfolded conformations. For example, 45% of the decanoate population was folded at 435 K, but only 4% was folded at 669 K because the iIHB opened at high temperatures because of entropy effects. The data lead to $\Delta H^\circ_{\text{iIHB}} = -7.3 \text{ kcal/mol}$ and $\Delta S^\circ_{\text{iIHB}} = -17.2 \text{ kcal/mol}$ for decanoate and $-16.8 \text{ cal}/(\text{mol K})$ 2-ethylhexanoate. For the shorter-chain *n*-butanoate, $\Delta H^\circ_{\text{iIHB}} = -0.7 \text{ kcal/mol}$ and $\Delta S^\circ_{\text{iIHB}} = -2.5 \text{ cal}/(\text{mol K})$ were calculated. The stabilities of the internal bonds calculated from these data in terms of T_{open} are 424, 435, and 280 K, respectively, consistent with weak $\text{CH}\cdots\text{O}^-$ internal bonds.¹¹²

4.1.3. Ring-Size and Strain Effects. The strain energies reflect constraints on the iIHB geometry imposed by the backbones that connect functional groups.^{39,257,259,263} With increasing ring size the strain decreases and the strengths of the internal bonds increase. The bonds become nearly linear and essentially fully optimized when four or more methyl groups separate the functional groups (Figures 40 and 41). This is observed in Table 7 where $\Delta H^\circ_{\text{strain}}$ decreases and the stabilization, as expressed by T_{open} , increases with increasing ring size. For a given ring size, the stability of intramolecular $\text{OH}^+\cdots\text{O}$ bonds is greater than that of $\text{NH}^+\cdots\text{N}$ bonds, in accordance with the relative intrinsic strengths of these bonds.

Table 7 shows that various bifunctional ions of equal chain length have comparable strain energies. The strain is largest for the smallest rings with two methylene groups between the substituents ($n = 2$), which form 5-membered rings containing the carbons, heteroatoms, and binding proton. These rings have comparable strain energies of 15–24 kcal/mol for the listed compounds with various functional groups that form the iIHB bonds. The strain energies are substantially smaller, 6–14 kcal/mol, for $n = 3$ structures, which form 6-membered rings, and become almost negligible within error limits, mostly 2–6 kcal/mol, for $n = 4$ and 5, which form 7- or 8-membered or larger rings.

Entropy effects vary correspondingly, with negative entropies of protonation increasing with increasing ring size. However, these effects level off for 6 members or larger rings, all of which allow optimized linear hydrogen-bond geometries. The consistency among various ions of equal ring size is encouraging, considering that assigning the iIHB strengths for various types of internal bonds ($\text{OH}^+\cdots\text{H}$, $\text{NH}^+\cdots\text{O}$, $\text{NH}^+\cdots\text{N}$) involves comparisons with different reference compounds.

Most internal hydrogen bonds were studied in protonated polyamines, polyethers, and diketones where all the heteroatoms are of the same type. However, Meot-Ner and co-workers also studied protonated amino alcohols where the functional groups are different,²⁵⁹ and Szulejko, McMahon, and co-workers extended subsequently experimental and theoretical studies to methoxy alcohols where the functional groups are also different.²⁵⁷

Table 7 shows some of these results. Figures 40 and 41 illustrate that the bond lengths and angles in diamines and methoxy alcohols optimize with increasing ring size. For example, the ab initio $\text{OH}^+\cdots\text{O}$ bond length in $(\text{MeO}-(\text{CH}_2)_n\text{OH})\text{H}^+$ decreases for $n = 2, 3$, and 4 from 1.91 to 1.66 and 1.53 Å, respectively, and the bond angle increases from 116.3° to 143.5° and 165.3° , approaching the optimal 180° conformation.

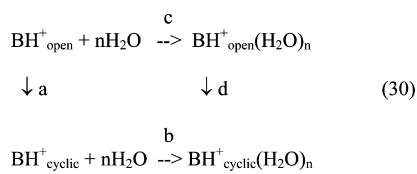
Additional polar groups in the ion can further stabilize the ion by forming multiple intramolecular hydrogen bonds and by additional electrostatic stabilization of the charge.²⁶¹ The protonation of the crown ethers in Table 7 involves large negative entropy changes, although the neutrals are already cyclic, as these structures stiffen upon protonation.^{260,261}

In protonated polyfunctional ions, the proton may be located on the site with the highest PA, but it may also be on a group with a lower PA if this leads to stabilization by stronger hydrogen bonds. For example, in the triamine $\text{H}_2\text{N}(\text{CH}_2)_2\text{NH}-(\text{CH}_2)_2\text{NH}_2$, the site with the highest PA is the central secondary amine group, the protonation of which can form a small ring ($n = 2$) with a terminal amine group. The other two primary amine groups have lower PAs, but their protonation could form a larger ring with an optimized bond. Therefore either location may be preferred. The increase in PA versus monofunctional primary or secondary amines would be consistent with either, but the entropy effect is small and suggests protonation on the central amine group, which is stabilized by forming a small hydrogen-bonded ring with one of the other amine groups.²⁵⁹ Protonation of the central amine group in the larger $\text{H}_2\text{N}(\text{CH}_2)_3\text{NH}(\text{CH}_2)_3\text{NH}_2$ diamine can form a more optimized ring, resulting in increased proton affinity (Table 7).

The strain energies cannot be evaluated in polyfunctional ions that have more than two polar groups. The increased iIHB energies for these compounds in Table 7 reflect stabilization of the charge by several polar groups,²⁶¹ and the overall energy effects cannot be factored reliably. However, in the triamines where the additional substituent is less polar, the strain energies are comparable to the diamines with $n = 2$ and 3, respectively. This also suggests that the proton is located on the central amine groups and is stabilized primarily by hydrogen bonding to one other amine group. Intramolecular iIHBs can also form in distonic radical ion reaction intermediates, such as in the decomposition of $(\text{CH}_3\text{OCH}_2\text{CH}_2\text{OH})^{\bullet+}$.^{277,278}

4.1.4. Mutual Effects of Intramolecular and External Solvation. The internal bond can be weakened or displaced by external solvent molecules.²⁵⁹ The effects of stepwise solvation

on the intramolecular bond may be calculated from the thermochemistry of clustering of water molecules on a protonated difunctional ion, compared with an analogous monofunctional ion (reaction 30).



The thermochemistry of reaction 30a can be found from comparing the protonation, and that of reactions 30b and 30c can be found from comparing the clustering thermochemistry of a bifunctional and an analogous monofunctional base. The cycle yields the thermochemistry of reaction 30d for ring-closure of the *n*-fold solvated bifunctional ion.

The effect of partial solvation on the stabilities of the internal bonds in protonated diamines is shown in Figure 43, where

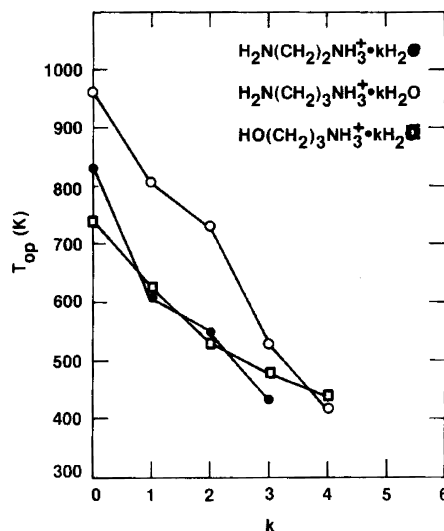


Figure 43. Effects of the stepwise solvation of protonated diamines on the stability of the internal hydrogen bond as expressed by the bond opening temperature, T_{open} , calculated from thermochemical cycle 30. Reproduced from ref 259 with permission. Copyright 1980 American Chemical Society.

four H_2O molecules decrease T_{open} almost to room temperature. The trend explains why intramolecular iIHBs may not form in protonated polyamines in bulk solution where full solvation may decrease T_{open} below the ambient temperature.

Conversely, internal hydrogen bonds weaken the external bonds to the solvent molecules. The internal functional group may be seen as the first ligand molecule, and the bond to the *n*th solvent molecule becomes equivalent to a bond to the (*n* + 1)th solvent molecule of an analogous monofunctional ion.²⁵⁹

Partially solvated ions with internal hydrogen bonds were investigated by IR spectroscopy studies of $\text{H}_2\text{NCH}_2\text{CH}_2\text{NH}_3^+(\text{H}_2\text{O})_n$ ^{233a} and of $(\text{MeCOCH}_2\text{COMe})(\text{H}_2\text{O})_n\text{H}^+$ (*n* = 0–3).²⁷⁵ Figure 44 illustrates the energy scheme of the unfolding steps that open the iIHB and the evolution of the two-water bridged isomers. This work illustrates the mechanism by which the water molecules help to open the internal bond. Adding water molecules delocalizes the charge, the water interposes between the functional groups, and the distance

between the bridged ketone oxygens increases. With addition of 0–3 water molecules, the energy difference between the most stable closed form and the open form decreases from 11.9 to 7.1, 3.8, and 3.6 kcal/mol, and the difference in the ketone O–O distance between the closed and open forms decreases in parallel. These changes decrease the barrier for ring-opening.

This work also showed that conformational changes that transfer the proton between the ketone groups are possible with relatively low activation energies. Similar water bridges may allow proton transfer with low activation energy through water channels in proteins.^{154,242} Recent studies by Bowers, Wyttenbach, and co-workers found similar relations between the internal and external solvation of protonated biomolecules,^{279a–d} as reviewed later.

4.2. Polydentate Bonding

4.2.1. Thermochemistry and Structures of Polydentate Complexes. Protonated ions can form strong hydrogen bonds to several functional groups of a polydentate ligand. Polydentate bonding increases the bond strengths of the complexes (increased ΔH°_D) but also leads to constrained structures with low entropies (increased ΔS°_D). Tables 8 and 9 present the thermochemistry of polydentate complexes and some monodentate complexes for comparison.

The first complexes with thermochemical evidence for polydentate IHB structures were reported by Meot-Ner and co-workers in protonated dimers of nucleic bases,^{280a} in polydentate complexes of protonated amines with polyethers and crown ethers,^{90,154,280b} and in the complexes of the glycine and alanine derivatives, $\text{CH}_3\text{CONHCH}(\text{R})\text{COOCH}_3$ ($\text{R} = \text{H}$ or CH_3).¹⁵⁰ Sharma and Kebarle also measured the thermochemistry of complexes of H_3O^+ and CH_3OH_2^+ with polyethers and crown ethers (Tables 8 and 9).²⁸¹ Some of these data were confirmed recently by Fourier transform ion cyclotron resonance mass spectrometry (FTICR).²⁸² Polydentate bonding in these complexes was confirmed theoretically.²⁸³ Similar polydentate structures are involved in complexes of metal ions with crown ethers and in molecular recognition.¹⁰ Structures with multiple IHBs were proposed even in simple systems such as the complexes of I^- with H_2O , HCOOH , and MeCOOH .⁷⁶

Polydentate bonding has significant thermochemical effects. The complexes of polyethers in Table 8 have greater bond strengths than those of a single ether or acetone ligand. The bonding energies of the proton and hydronium ion to polydentate ligands increase with the number of functional groups, as observed in comparisons of mono-, bi-, tri-, tetra-, and hexadentate complexes in Tables 8 and 9. However, the binding energies are affected by geometrical constraints. For example, in the tetradentate complexes of H^+ in Table 8, the total bond strengths are greatest when the complexes are assembled from four free Me_2CO molecules. The bonding energies decrease as the complexes are assembled from two G1 or one G3 or one 12-crown-4 molecule, where the functional groups are increasingly constrained on fewer ligand molecules.

While more ligand molecules or ligand groups increase the bonding energies, they also increase the entropy losses upon forming the complex. For example, the ΔH°_D values of the tetradentate complexes of H^+ in Table 8 vary by 20.2 kcal/mol, and those of ΔS°_D vary compensatingly by 62.9 cal/(mol K). As a result, the free energies of the complexes, ΔG°_D (298), remain nearly constant. Similar effects are observed in Table 8 for the complexes of H^+ and H_3O^+ with various ligands.

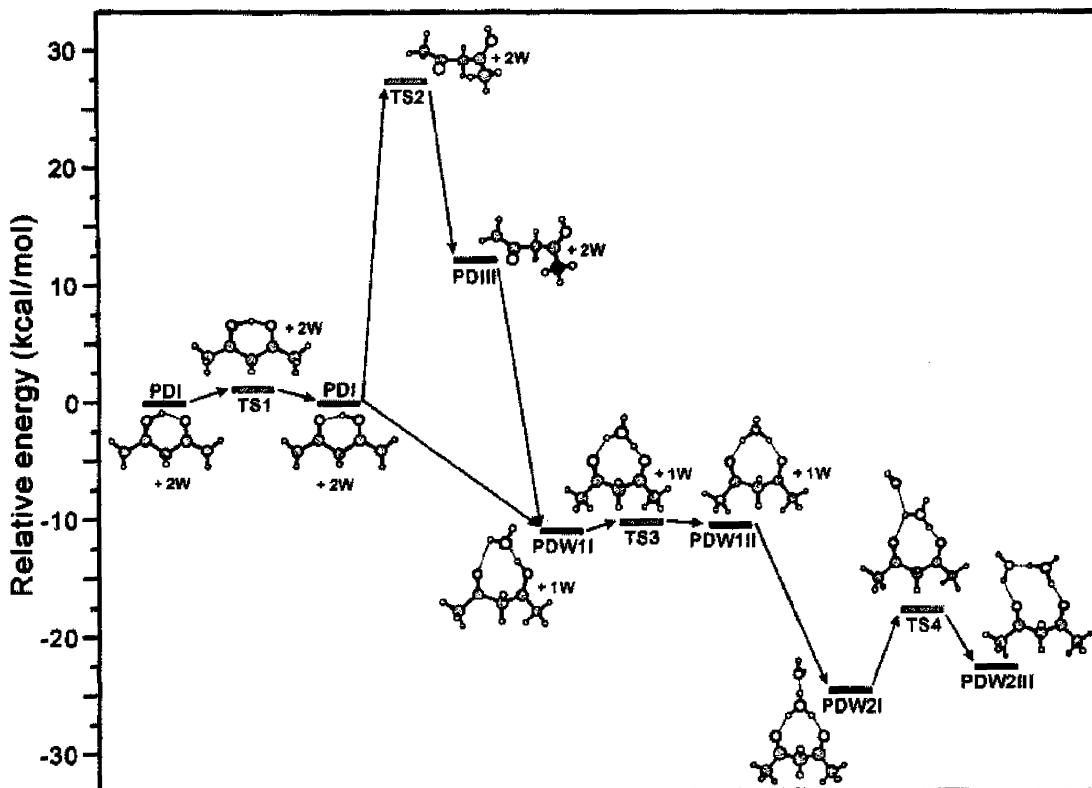


Figure 44. Energy relations between unsolvated and mono- and dihydrated clusters of $(\text{MeCOCH}_2\text{COMe})(\text{H}_2\text{O})_n\text{H}^+$, denoted as PDW, including transition-state energies between various conformations. The ab initio structures illustrate that the proton can be located on a H_3O^+ center that bridges between the ketone oxygens and that there are small barriers between conformations, allowing the proton to move between the ketone groups or along the water chain. Reproduced from ref 275 with permission. Copyright 2003 Taylor and Francis (www.tandf.co.uk).

The excess stabilization energy due to multiple bonding denoted by $\Delta H^\circ_{\text{MB}}$ can be assigned by comparing the dissociation energy of a complex of a polydentate ligand with that of a reference monodentate ligand. A suitable reference monodentate ligand for polyethers is Me_2CO , the PA of which is comparable to MeOEt , the structural unit of glymes and crown ethers. The excess polydentate stabilization energies of the three ions H^+ , H_3O^+ , and NH_4^+ by a given ligand are similar (Tables 8 and 9), especially in the larger complexes, although the absolute bonding energy of H^+ to a given ligand is greater by about 150 kcal/mol than that of H_3O^+ and by 170 kcal/mol than that of NH_4^+ . The data in Tables 8 and 9 show that the excess bonding energies ($\text{PA(B)} - \text{PA}(\text{Me}_2\text{CO})$) of the polyethers to H^+ , H_3O^+ , and NH_4^+ are as follows: G1, 14, 9, 10; G2, 28, 23, 18; 2G1, 42, 34, 33; 3G1, 52, 48, 47; 2G2, 51, 50, 49; and 18-crown-6, 40, 39, 42 kcal/mol, respectively. This supports the suggestion of Sharma and Kebarle that the excess polydentate stabilization is due to nonspecific electrostatic interactions.²⁸¹ Otherwise, multiple hydrogen bonding to H^+ would involve weaker “bifurcated bonds”,²⁸⁴ while H_3O^+ and NH_4^+ could form several stronger IHBs with the polar groups of these ligands, which would result in significantly different excess stabilization energies of these ions.

Ion–dipole interactions in polydentate complexes were also shown by ab initio calculations. For example, the B3LYP DFT method gave good agreement with the experimental binding energies of the complexes of $\text{CH}_3\text{OCH}_2\text{CH}_2\text{OCH}_3$ (glyme (G1)), glyme dimer (2G1), and 12-crown-4 (12c4) with the H^+ , MeOH_2^+ , NH_4^+ , MeNH_2^+ , Me_2NH^+ , and Me_3NH^+ ions.

The B3LYP/4-21G(*) geometries of several complexes are shown in Figure 45. The complexes with H^+ , that is, the

protonated species, are stabilized by internal hydrogen bonds, forming a five-membered ring in G1H^+ . In the protonated dimer $(\text{G1})_2\text{H}^+$, the proton is bound by two short 1.2 Å bonds to an oxygen of each glyme molecule and is stabilized additionally by two long 2.6 Å ion–dipole bonds with the other two oxygens. Similarly, in (12-crown-4) H^+ the proton is stabilized by short hydrogen bonds with two opposite oxygens and is stabilized further by two long 2.4 Å ion–dipole bonds with the other two oxygens.²⁸³

In the complexes of MeOH_2^+ , NH_4^+ , MeNH_3^+ , and Me_2NH_2^+ with $\text{CH}_3\text{OCH}_2\text{CH}_2\text{OCH}_3$, the ions form two short 1.6–1.7 Å IHBs with two ether oxygens, while Me_3NH^+ forms one short strong hydrogen bond of 1.6 Å and one long 2.9 Å ion–dipole bond. In complexes with two glyme molecules, MeOH_2^+ forms two short IHBs and two long ion–dipole bonds, while NH_4^+ forms four hydrogen bonds that involve all the available oxygens. In the complex of 12-crown-4 with MeOH_2^+ , similar to the complex with the proton, there are two 1.5 Å strong hydrogen bonds with two opposite oxygens of the crown ether, while with NH_4^+ there are two unequal bonds of 1.6 and 2.6 Å. The monoprotonic Me_3NH^+ ion gives a different structure without any short IHBs but with four longer bonds of 2.2–2.6 Å of the proton to each oxygen that together stabilize the structure.²⁸³ Figure 45 shows some of these structures.

In these complexes, the proton is located on the small core molecule even when the PAs of the surrounding ether groups are much higher. This is supported by the ab initio structures of complexes of H_3O^+ and NH_4^+ with $\text{CH}_3\text{OCH}_2\text{CH}_2\text{OCH}_3$, a ligand that is similar to the structural units of the crown ethers, where the proton also remains on the H_3O^+ core ion.^{90,154,283}

Table 8. Thermochemistry of Complexation of H^+ , H_3O^+ , and MeOH_2^+ by Polydentate Ligands^a

	H^{+b}		H_3O^{+c}		MeOH_2^{+d}	
	$\Delta H^\circ_{\text{D}}$, $\Delta S^\circ_{\text{D}}$	$\Delta G^\circ_{\text{D}}$ (298)	$\Delta H^\circ_{\text{D}}$, $\Delta S^\circ_{\text{D}}$	$\Delta G^\circ_{\text{D}}$ (298)	$\Delta H^\circ_{\text{D}}$, $\Delta S^\circ_{\text{D}}$	
monodentate						
Me ₂ O	189.0, 21.1	182.7	49.8, 30.0	40.9	35.0, 24.7	
Me ₂ CO	194.0, 23.8	186.9	49.5, 26.0	41.8		
bidentate						
2Me ₂ O	220.4, 51.9	204.9	63.3, 56.3	46.5	55.0, 54.5	
2Me ₂ CO	224.0, 53.1	208.2	73.7, 56.9	56.8		
MeCO-Gly-OMe	223.7, 38.2	212.3				
MeCO-Ala-OMe	224.7, 41.1	212.5	72.1, 42.6	59.4		
G1 ^e	208.4, 32.4	198.7	58.6, 30.0	49.7		
tridentate						
3Me ₂ O	230.5, 79.8	206.7	80.0, 82.9	55.3		
3Me ₂ CO	235.5, 75.2	213.1	92.2, 87.0	66.3		
G2 ^e	222.0, 40.3	210.0	72.0, 49.8	57.2		
tetradentate						
4Me ₂ CO	245.2, 97.2	216.2	(100), (112) ^f	(67) ^f		
2G1 ^d	236.0, 60.7	217.9	83.2, 63.1	64.4		
G3	230.0, 44.6	216.7	83.9, 59.7	66.1		
12-crown-4	225.0, 34.3	214.8			58.3, 40.6	
hexadentate						
6Me ₂ CO		(116), (162) ^f		(68) ^f		
3G1 ^d	246.2, 85.8	220.6	97.9, (89.3)	71.3		
2G2 ^d	244.9, 77.5	221.8	99.0, 87.2	73.0		
18-crown-6 ^c	233.8, 48.0	219.5	88.5, 55.8	71.9	67.6, 50.0	

^aUnits are as follows: ΔH° and ΔG° in kcal/mol; ΔS° (in italics) in cal/(mol K). ^bThe complexation energy of the proton, calculated from PA and GB values from ref 27. Entropies of protonation include the loss of entropy of the free proton (26.0 cal/(mol K) at 298 K). Thermochemical data for polyethers and crown ethers as listed in ref 154, based on data in refs 260 and 261. ^cData for H_3O^+ complexes from refs 154 and 242. ^dData for complexes of MeOH_2^+ and of 18-crown-6 from ref 281. The data for complexes of H_3O^+ and MeOH_2^+ with polyethers were obtained from the association equilibria of (polyether) H^+ with H_2O or MeOH and thermochemical cycles. ^eG1 = glyme ($\text{MeO}(\text{CH}_2)_2\text{OMe}$), G2 = diglyme ($\text{MeO}(\text{CH}_2)_2\text{O}-(\text{CH}_2)_2\text{OMe}$). ^fEstimated values in parentheses are based on usual cluster trends, considering that after three Me₂CO ligands the further ligands are bonded weakly in the outer sphere.

As in mixed unblocked/blocked clusters, the central proton is balanced by opposing attractions of the surrounding polar groups.

4.2.2. Solvent Bridges in Polydentate Complexes. In protonated complexes of polydentate molecules, water can form bridges between the functional groups. The thermochemical effects in Figure 46 show an anomalous enthalpy sequence for the hydration of $(\text{CH}_3\text{OCH}_2\text{CH}_2\text{OCH}_3)\text{H}^+$ compared with the hydration of a monofunctional ether. The exothermicity of adding the first H_2O molecule to the protonated diether is decreased because forming the bond requires disrupting the internal hydrogen bond. The second H_2O molecule creates a $(\text{H}_2\text{O})_2\text{H}^+$ bridge between the ether groups. The bonding energy of the third H_2O molecule drops since it starts an outer shell.

The calculated geometries in Figure 47 are consistent with the thermochemical indications. Similar to mixed blocked clusters, the proton is located on the central core ion although the proton affinity of water is smaller than that of the ether groups. In $(\text{MeO}(\text{CH}_2)_2\text{OMe})(\text{H}_2\text{O})_2\text{H}^+$ the two water

molecules constitute a protonated water bridge between the functional groups of the polydentate ligand.

Solvent-bridged structures can form also in clusters of protonated diketones and H_2O molecules, although rigid small diketones, such as that in $(\text{MeCOCH}_2\text{COMe})\text{H}^+(\text{H}_2\text{O})_2$, may not be able to accommodate the water bridge.²⁷⁵ When bridged structures form, they can provide low-energy pathways for proton transfer between functional groups, by switching hydrogen bonds through the water chain.

5. SPECTROSCOPY OF HYDROGEN-BONDED CLUSTERS

The structures of hydrogen-bonded cluster ions were often inferred from the thermochemistry and theoretical computations in early work as discussed in the above sections. However, spectroscopy has been used increasingly in more recent research to obtain structural information, often confirming the earlier postulated structures.

The vibrational predissociation spectroscopy of cluster ions can be obtained with powerful laser IR spectroscopy. Excitation of modes associated with the hydrogen bond leads to the loss of a ligand or a weakly bonded probe molecule attached to the cluster, such as Ar or H_2 , which is detected by mass spectrometry. Comparison with ab initio computed spectra for various ion geometries allow identifying cluster structures such as the location of the proton, solvent shells, and intramolecular hydrogen bonds.

The infrared spectra of $(\text{H}_2\text{O})_n\text{H}^+$ clusters were obtained first by Schwartz in 1977,²⁸⁵ using vibrational assignments from ab initio calculations by Newton^{226,227} and followed by many higher-level calculations.²⁸⁶ Spectra of the H_3O^+ core ions helped to assign spectra of larger clusters.^{287–291}

The IR studies of clusters using probe molecules and OPO lasers were advanced in particular by Y. T. Lee and co-workers.^{236,292a–c} The Lee group produces low-temperature, 170 ± 20 K, clusters by corona discharge followed by supersonic expansion and storage in an ion trap. The clusters are irradiated with IR photons from pulsed lasers, and the fragments are detected. The power-normalized vibrational predissociation spectra of the clusters are compared with spectra calculated by ab initio theory. The absorption bands of X–H bonds are shifted when they form hydrogen bonds, and this shift allows identification of the hydrogen-bonding sites. Alternatively, CO₂ lasers or more recently powerful free electron lasers dissociate cluster ions, as detected by ion trap or FTICR mass spectrometry.^{292d–g,293} The IR vibrational predissociation spectroscopy of clusters has been applied with success since 1985, and the spectroscopic methods for cluster ions were reviewed.^{294a–d,295,296} Another method, photoelectron spectroscopy, has been applied to probe the structures of anionic clusters.^{218b,255,297} This section will illustrate some of the results that complement the thermochemical studies.

5.1. Spectroscopy of Dimers and Correlations Between Bond Energies and Proton Affinities

The thermochemical relationships among the relative PAs, the IHB bond strengths, and proton sharing, which were obtained earlier from thermochemistry and computation as discussed above, were confirmed more recently by spectroscopy.^{40b–g} In dimers of protonated ethers, the low-frequency O–H⁺···O stretch in homodimers, where the proton moves easily between the components, shifted to higher energies in heterodimers

Table 9. Thermochemistry of Polydentate and, for Comparison, Some Monodentate Complexes^a

ligands	monoprotonic ions			triprotonic ions		tetraprotic ion
	pyridineH ⁺	pyridazineH ⁺	Me ₃ NH ⁺	MeNH ₃ ⁺	c-C ₆ H ₁₁ -NH ₃ ⁺	NH ₄ ⁺
monodentate						
Me ₂ CO	(22, 25)	(23, 25)	19.5, 29.4	25.9, 26.0	(22, 25)	28.3, 26.4
Et ₂ O	22.5, 32.9	(23, 25)	(23, 25)	22.0, 25.0	22.0, 31.8	(27, 25)
bidentate						
2Me ₂ CO				(44, 50)	(37, 50)	48.6, 51.3
MeOCH ₂ CH ₂ OMe (G1) ^b	25.4, 31.4		26.7, 34.8	30.1, 30.1	29.4, 35.5	38, 36
MeO(CH ₂) ₃ OMe	26.5, 35.8		25.5, 33.1	31.2, 32.0	28.4, 35.0	
MeCONHCH(Me)COOMe (MeCO-Ala-OMe)			29.7, 27.6	40.1, 35.1	37.8, 40.9	
tridentate						
3Me ₂ CO					(48, 75)	64.4, 77.3
G2 ^b	31.5, 36.5	32.4, 36.1	32.8, 40.0		39.7, 44.6	46.6, 35.7
tetridentate						
4Me ₂ CO						77.5, 101.7
2G1 ^b						61.2, 69.5
G3 ^b	34.7, 38.3		34.6, 40.0		43.3, 44.8	
12-crown-4	36.1, 40.0	37.0, 40.8	35.8, 41.5		37.2, 34.8	
15-crown-5	41.0, 42.6				42.3, 36.5	
pentadentate						
hexadentate						
6Me ₂ CO						(96), (145)
3G1 ^b						75.6, 96.8
2G2 ^b						77.3, 86.6
18-crown-6	42, 44	42, 44	41, 40		46, 38	(70)
nucleic base dimers						
pyridineH ⁺ .pyridine	23.7, 28					
adenineH ⁺ .adenine	30.3, 39					
cytosineH ⁺ .cytosine	38.3, 37					

^aUnits are as follows: ΔH°_D in kcal/mol; ΔS°_D (in italics) in cal/(mol K). Data from ref 260, except for complexes of NH₄⁺ from ref 90 and nucleic bases from ref 280a. Data in parentheses were estimated from PA correlations and from clustering trends. ^bG1 = glyme (MeO(CH₂)₂OMe), G2 = diglyme (MeO(CH₂)₂O(CH₂)₂OMe), G3 = triglyme (MeO(CH₂)₂O(CH₂)₂O(CH₂)₂OMe).

where it is held more strongly by the more basic component and needs higher energy to displace.^{40b,c}

Anionic complexes were studied with Ar vibrational predissociation spectroscopy. In X⁻·HOH dimers that are formally X⁻··H⁺··OH⁻ complexes of the Br⁻, Cl⁻, F⁻, O⁻, and OH⁻ anions, the hydrogen bond grows stronger and the barrier to proton transfer between the components along the hydrogen-bond axis decreases, as the proton affinities of X⁻ get closer to that of the OH⁻ anion. Correspondingly, the anion charge becomes increasingly delocalized to water and the vibrational frequency of the shared proton becomes increasingly red-shifted. The identity of water is preserved in the complexes with Br⁻ and Cl⁻, but the interaction evolves toward a three-center covalent bond as the proton affinity of the anion increases toward forming a symmetric (HO··H··OH)⁻ ion with an equally shared proton.^{40d,e}

Similarly, there is only a small barrier to proton transfer in NH₄⁺·NH₃ and other protonated homodimers.^{40f} In a further series of protonated dimer cations, in 16 dimers involving Ar, Xe, CO₂, water, alcohols, and ethers, the vibrational bands of the shared proton along the hydrogen-bond axis shift to lower energies as the proton affinities of the components get closer.^{40g}

5.2. Spectroscopic Effects of Shell Filling and Isomers, and the Location of the Proton

5.2.1. Clusters of Water, Alcohols, and Amines with Unlimited IHB Networks. The spectroscopy of the (H₂O)_nH⁺ dimer ion was investigated by several groups.^{292a-c,e,f} The

structures of larger (H₂O)_nH⁺ clusters were investigated by the spectroscopy of hydrogen-bonded and free O-H stretches. Eigen structures centered on H₃O⁺ were identified for n = 3, 4, 5, 10, and 11, and Zundel structures centered on a symmetric (H₂O)₂H⁺ were observed for n = 2, 6, 7, and 8 clusters, with the Zundel structure incorporated in a 5-membered ring in the 7 and 8 clusters.²⁹⁶ Several (H₂O)_nH⁺ isomers including a 5-membered ring, 6-membered rings, and three-dimensional cage structures were identified with the 5-membered ring favored by a combination of enthalpy and entropy effects.²²⁸ The spectra of the larger clusters are consistent with a highly polarizable Zundel excess proton in bulk water.²⁹⁶

Similarly, in methanol clusters, (MeOH)_nH⁺, with n = 4, a linear isomer was found, while for n = 5, linear and cyclic isomers were identified with the proton localized on one or delocalized between two methanol units.²³⁰ In methanol–water mixed clusters, (MeOH)(H₂O)_nH⁺, at n = 2, methanol and the water dimer can equally share the proton. At n = 3 and 4, distinct methanol-centered MeOH₂⁺(H₂O)₃ and water-centered H₃O⁺(MeOH)(H₂O)₂ isomers were identified. In larger clusters, the structures become similar to protonated water clusters, including, at n = 5, the formation of a 5-membered ring.²³¹

For example, a typical recent study addressed 4-membered clusters of water and methanol, (MeOH)_n(H₂O)_{n-4}H⁺. Figure 48 illustrates the results for (H₂O)₄H⁺ and (MeOH)₃(H₂O)H⁺. The spectra support structures with a MeOH₂⁺ core ion, a chain of MeOH molecules, and H₂O molecules attached at the end. This is reasonable energetically because MeOH has a

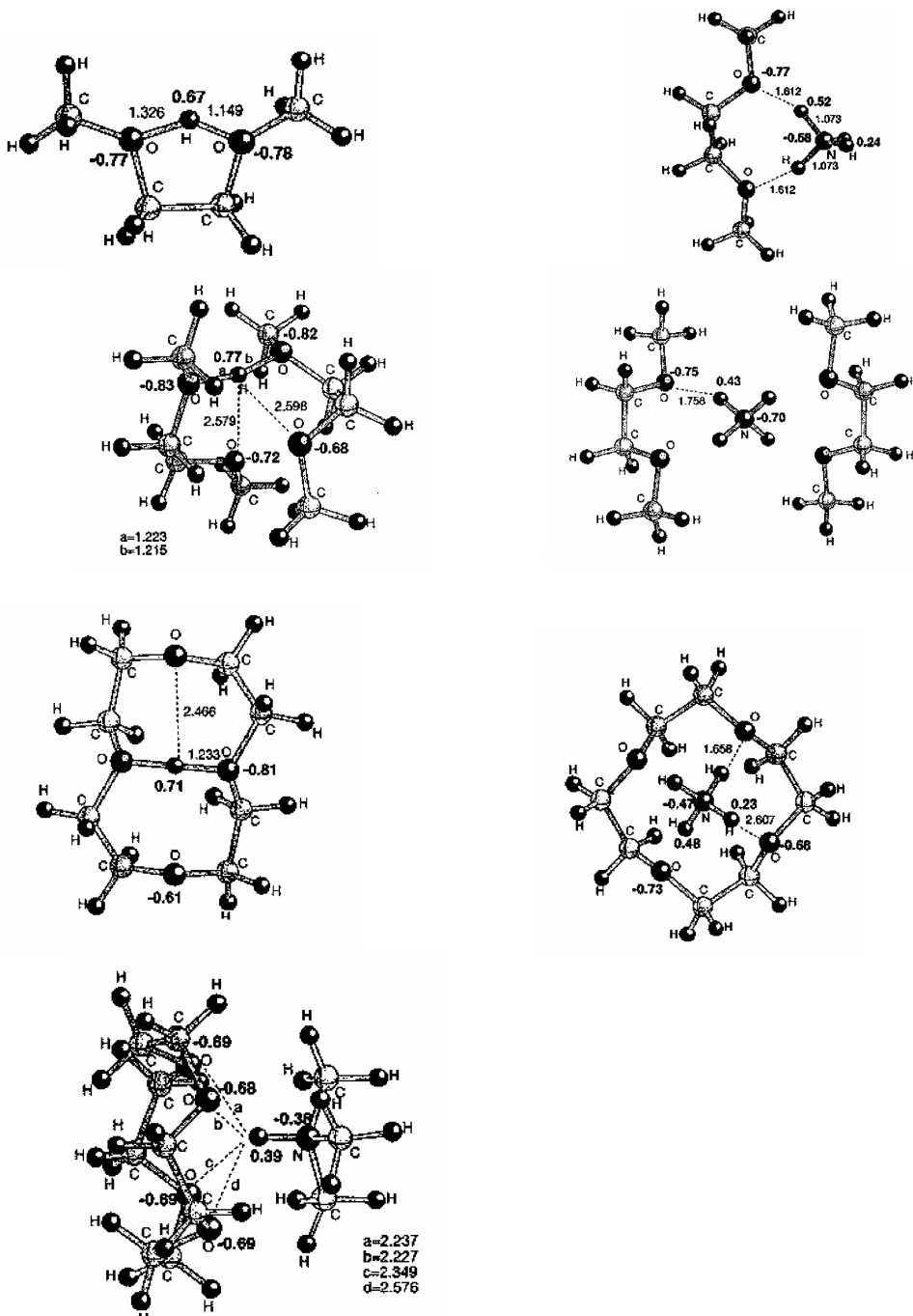


Figure 45. Geometries and atomic charges of complexes of $\text{MeOCH}_2\text{CH}_2\text{OMe}$ (glyme or (G1)), two G1 molecules and 12-crown-4 with H^+ and NH_4^+ , and 12-crown-4 with Me_3NH^+ calculated by B3LYP/4-21G(*) density functional theory methods. Reproduced from ref 283 with permission. Copyright 1998 American Chemical Society.

higher PA than H_2O . However, ab initio calculations for each mixed cluster gave several isomers with similar energies within a range of 2 kcal/mol, and these isomers may be in equilibrium in a thermal population. The ab initio studies also confirmed the thermochemical results that the cluster stabilities increase with increasing MeOH mole fraction.²³⁶

The protonated ethanol dimer ion was also investigated spectroscopically. The IR photodissociation spectrum of $(\text{EtOH})_2\text{N}_2\text{H}^+$ is consistent with a Zundel type $\text{EtO}(\text{H})\cdots\text{H}^+\cdots\text{O}(\text{H})\text{Et}$ core.^{106b} Comparison with $\text{H}_2\text{O}\cdots\text{H}^+\cdots\text{OH}_2$ show that the ethyl substituents have only small effects on the properties of the $\text{O}\cdots\text{H}^+\cdots\text{O}$ core and on the proton-transfer potential,^{106b} consistent with the

similar binding energies of symmetric protonated dimers of alcohols, esters, ethers, and ketones.^{62,178} In larger clusters $(\text{EtOH})_n\text{H}^+$, Eigen type EtOH_2^+ centers are observed spectroscopically for $n = 1$ and 3 while Zundel-type clusters with $\text{EtO}(\text{H})\cdots\text{H}^+\cdots\text{O}(\text{H})\text{Et}$ centers are observed for $n = 2$ and 4. However, asymmetric microsolvation by N_2 ligands can switch the Zundel cores to Eigen cores.^{106c} Comparing $(\text{MeOH})_n\text{H}^+(\text{N}_2)_m$ and $(\text{EtOH})_m\text{H}^+(\text{N}_2)_n$ clusters shows that the terminal OH groups in the EtOH clusters are more acidic, and correspondingly, the bonding to N_2 ligands is stronger, according to the usual $\Delta\text{PA}/\text{bond strength}$ correlations.^{106c}

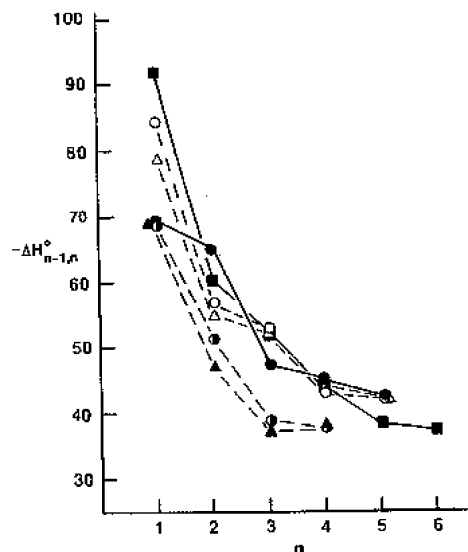


Figure 46. Effects of internal hydrogen bonds on the hydration of ions, as reflected in the enthalpies of stepwise hydration of protonated ketones, ethers, and diethers (kJ/mol): (○) $(\text{CH}_3)_2\text{COH}^+$; (open upward-facing triangle) $(n\text{-C}_3\text{H}_7)_2\text{OH}^+$; (filled left open right circle) $\text{CH}_3\text{N}(\text{CH}_3)_2\text{COH}^+$; (■) $(c\text{-C}_3\text{H}_5)_2\text{COH}^+$; (●) $(\text{CH}_3\text{OCH}_2\text{CH}_2\text{OCH}_3)\text{H}^+$ all solvated by H_2O molecules; (■) solvation of $(\text{CH}_3\text{OCH}_2\text{CH}_2\text{OCH}_3)\text{H}^+$ by CH_3OH molecules. The hydration of the protonated diether is anomalous as the first step disrupts the internal bond in the $(\text{CH}_3\text{OCH}_2\text{CH}_2\text{OCH}_3)\text{H}^+$ ion, while the increased bond strength in the second step suggests forming two hydrogen bonds in a solvent-bridged structure. The third water molecule bonds to the water bridge in an outer position, resulting in a large drop of bonding energy. See Figure 47 for structures. Reproduced from ref 154 with permission. Copyright 1994 American Chemical Society.

Alcohol clusters $(\text{ROH})_2\text{H}^+$ can dissociate following IR excitation to give $(\text{ROH})\text{H}^+$ monomer ions, or by S_N2 reaction to give protonated ether R_2OH^+ ions.^{292g,293} Low-power CO_2 laser photodissociation of methanol, ethanol, and isopropanol dimers gave exclusively the ether products, while *n*-propanol dimer gave simple bond cleavage and the ether and ether–water cluster products.²⁹³ Similarly, in dimers of methanol, ethanol, and propanol, weak absorption gave the S_N2 ether products whereas strong absorption gave bond cleavage in the free electron laser (FEL) studies.^{292g}

Recent high-level calculations and spectroscopy of the $\text{NH}_4^+(\text{H}_2\text{O})_n$ clusters ($n = 0\text{--}5$) found that at $n = 4$ the closed-shell isomer has the lowest energy, but cyclic and noncyclic isomers were both observed by IR spectroscopy in a supersonic jet at about 170 K.²³⁴ The calculated lowest-energy isomer at $n = 5$ contained a 4-membered ring, and the fifth H_2O molecule acted as a double-proton acceptor. This calculated structure was confirmed spectroscopically.²³⁵ The cluster $\text{CH}_3\text{NH}_3^+(\text{CH}_3\text{NH}_3)_3$ with a closed solvent shell was also identified spectroscopically.²⁹⁸

5.2.2. Spectroscopy of Mixed Clusters of Nonblocked and Blocked Components. As discussed above, in protonated mixed clusters of nonblocked and blocked components such as ethers or nitriles with water, the proton may be located on an H_3O^+ core ion even though the proton affinity of H_2O is lower than the blocked components, as postulated first for $(\text{Me}_2\text{O})_n(\text{H}_2\text{O})\text{H}^+$ clusters¹⁰³ and shown computationally first $(\text{MeCN})_n(\text{H}_2\text{O})\text{H}^+$ clusters.²²⁸

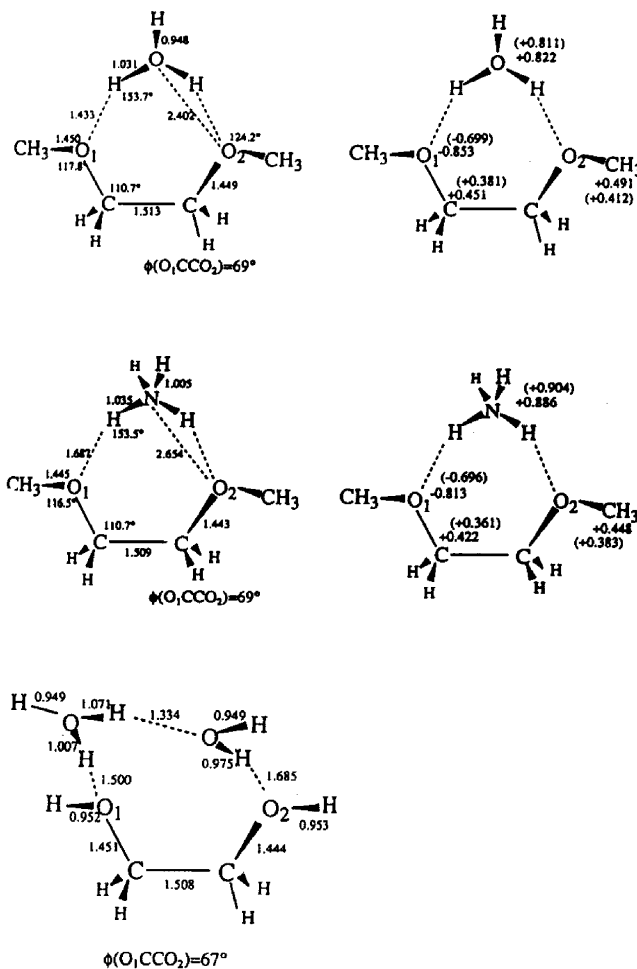


Figure 47. Top figures show the calculated geometries and atomic and group charges in the polydentate complexes of $\text{MeOCH}_2\text{CH}_2\text{OMe}$ with H_3O^+ , of $\text{MeOCH}_2\text{CH}_2\text{OMe}$ with NH_4^+ , and of $\text{HOCH}_2\text{CH}_2\text{OH}$ with $(\text{H}_3\text{O}^+\cdot\text{OH}_2)$, all using the 4-31G basis set and Gaussian 88, 90, and 92 methods. The bottom figures show proposed polydentate complexes of three bidentate glyme and two tridentate diglyme molecules with H_3O^+ based on thermochemistry. Reproduced from refs 90 and 154 with permission. Copyright 1996 and 1994 American Chemical Society, respectively.

To follow up, a recent study addressed mixed $(\text{Me}_2\text{O})_n(\text{H}_2\text{O})\text{H}^+$ clusters. The spectroscopic and ab initio results, illustrated in Figure 49, indicated that the proton is located on the ether when it is solvated by one H_2O molecule. With two H_2O molecules, the proton is shared by the ether and the water dimer, and with three or more H_2O molecules, the proton is

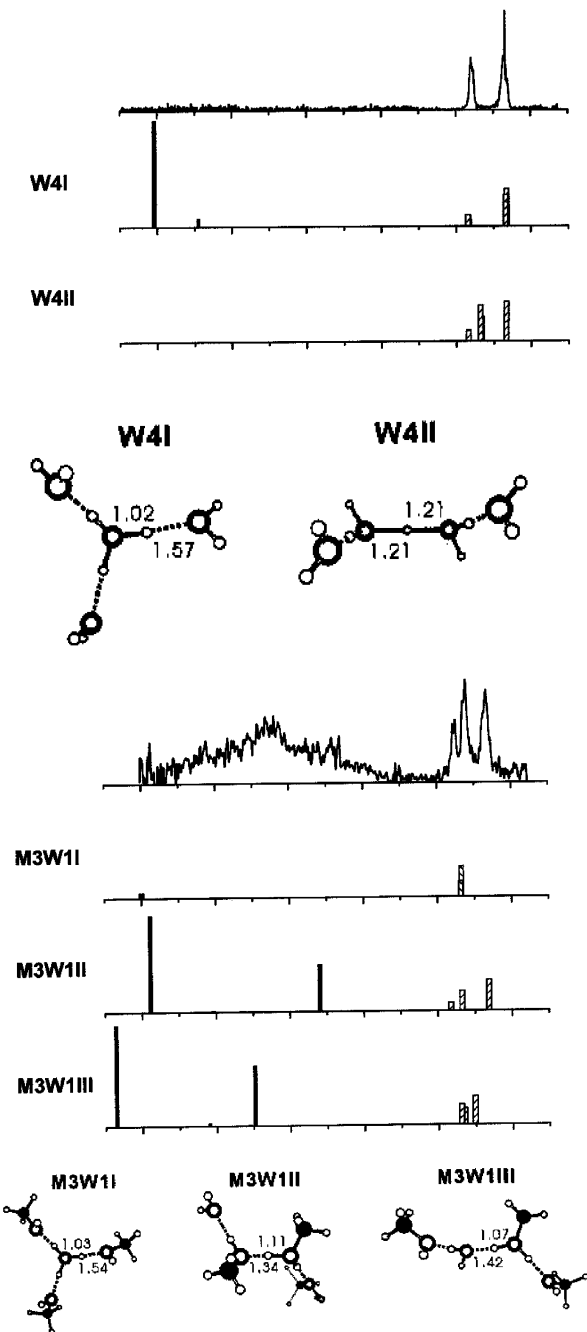


Figure 48. Top panel shows experimental and theoretical IR vibrational predissociation spectra and structures of $(\text{H}_2\text{O})_4\text{H}^+$. The spectra support the Eigen structure W4I with a central H_3O^+ core ion. The bottom panel shows the $(\text{MeOH})_3(\text{H}_2\text{O})\text{H}^+$ spectra and structures. The spectra support the structure M3W1III with a linear MeOH chain centered about a MeOH_2^+ core ion with H_2O attached to a MeOH molecule at the end of the chain. Reproduced from ref 236 with permission. Copyright 2004 American Chemical Society.

transferred completely to water. However, at $n = 2$ and 3, the calculations showed several isomers with comparable energies within 2 kcal/mol, where the position of the proton was affected by hydrogen cooperativity and zero-point energy effects.²³⁰

The location of the proton on H_3O^+ that is surrounded by blocked bases was confirmed further by IR spectroscopy in clusters of H_3O^+ with two molecules of dimethyl ether, methyl ethyl ether, acetone, acetaldehyde,¹⁰⁴ and formamide.²⁴⁷ Mixtures

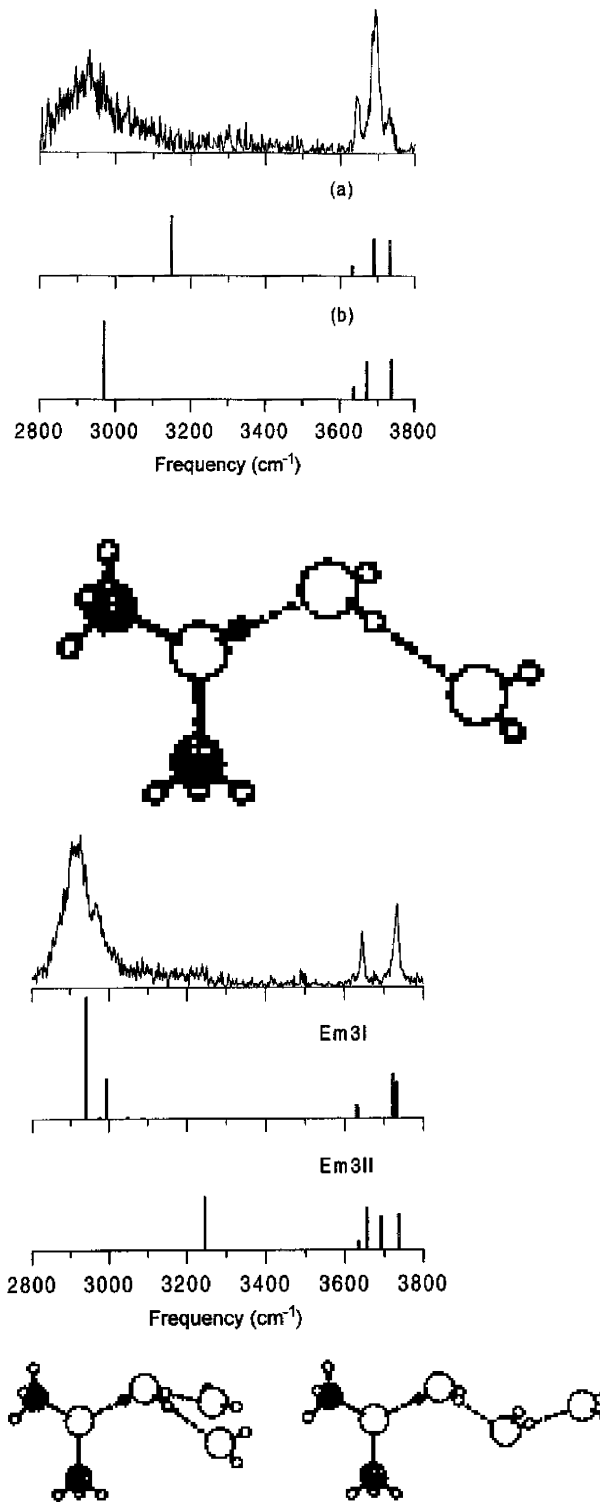


Figure 49. Top panel shows experimental and theoretical IR vibrational predissociation spectra and structures of $((\text{Me}_2\text{O})(\text{H}_2\text{O})_2)\text{H}^+$ showing the proton on Me_2O . The bottom panel shows spectra and structures of $(\text{Me}_2\text{O}(\text{H}_2\text{O})_3)\text{H}^+$ showing the proton on a $(\text{H}_3\text{O})^+$ core ion, consistent with the symmetric structure Em3I (top theoretical spectrum, left structure) rather than the linear Em3II structure (bottom theoretical spectrum, right structure). Reproduced from ref 230 with permission. Copyright 1999 American Chemical Society.

of isomers were present in clusters formed by supersonic expansion and studied by IR spectroscopy in mixed clusters of water with dimethyl ether, methyl ethyl ether, acetone, and

acetaldehyde. The proton can be located on a H_3O^+ core surrounded by the blocked ligands or the blocked components can form a hydrogen-bonded dimer, and water is attached by $\text{CH}\cdots\text{O}$ bonds to the methyl groups. These isomers displayed different OH stretching spectra.¹⁰⁴

The location of the proton was also investigated spectroscopically in protonated formamide and in the neat clusters. The spectra confirmed protonation on the oxygen atom of the amide group.²⁷³ In the hydrated clusters, $\text{H}_2\text{NCH}_2\text{COH}^+(\text{H}_2\text{O})_n$ ($n = 3$) isomers protonated on the formamide oxygen and isomers with water-protonated H_3O^+ centers were identified from NH and OH stretching spectra; similar to blocked clusters, at $n = 4$ the proton shifted to water, producing a H_3O^+ ion core.²⁴⁷

The free electron laser IR multiphoton dissociation (FEL IRMPD) spectroscopy of ethers confirmed the correlations between ΔPA , IHB bond energies, and proton sharing. For example, in the homodimer $\text{Me}_2\text{OH}^+\cdot\text{Me}_2\text{O}$ ($\Delta\text{PA} = 0$), the IHB bond energy is 31.4 kcal/mol whereas in the heterodimer $\text{THF}^+\cdot\text{Me}_2\text{O}$ ($\Delta\text{PA} = 7.5$ kcal/mol) the estimated IHB bond strength is 27.4 kcal/mol. The proton is closer to tetrahydrofuran (THF) in the heterodimer, with a computed $\text{THF}-\text{H}^+$ bond length of 1.100 Å versus 1.328 Å for the weaker $\text{Me}_2\text{O}\cdots\text{H}^+$ bond. Correspondingly, the $\text{O}-\text{H}\cdots\text{O}$ stretch shifts from $\sim 800 \text{ cm}^{-1}$ in the homodimers to 1586 cm^{-1} in the $\text{THF}^+\cdot\text{Me}_2\text{O}$ heterodimer, where more energy is needed to remove the proton from the protonated THF^+ site to the neutral $(\text{CH}_3)_2\text{O}$ ligand. Similar to the homodimers, a symmetric $\text{O}-\text{H}^+-\text{O}$ stretch vibration of $\sim 760 \text{ cm}^{-1}$ was observed for protonated diglyme that contains a symmetric internal hydrogen bond.^{40b} Similar relations apply for other homodimers versus heterodimers.^{40c}

The relation between relative acidities and proton sharing was also illustrated for anions. In $\text{Cl}^-\cdot\text{H}_2\text{O}$, the water molecule is intact and bonded to the anion by a single hydrogen bond through a shared proton, with a vibrational frequency of a bound proton stretch. In contrast, in $\text{OH}^-\cdot\text{H}_2\text{O}$ a shared proton configuration $(\text{HO}\cdots\text{H}\cdots\text{OH})^-$ is observed with large charge delocalization, and in spectroscopy a single OH stretch with a 1090 cm^{-1} band for the excitation of the proton verifies the symmetric sharing of the proton.^{40d}

5.3. Spectroscopy of Carbon-Based Hydrogen Bonds

Complexes of CH donors were investigated by vibrational predissociation spectroscopy and DFT ab initio calculations on $(\text{Me}_2\text{O})_2\text{H}^+\cdot\text{H}_2\text{O}$ ions produced by supersonic expansion. Two types of isomers, one with water bonded by a $\text{CH}^\delta^+\cdots\text{O}$ bond to the methyl groups of the $(\text{Me}_2\text{O})_2\text{H}^+$ dimer and a H_3O^+ -centered isomer, were identified by different hydrogen-bonded and non-hydrogen-bonded OH stretches of the water molecule. Similar observations were made in analogous clusters of Et_2O , Me_2CO , and MeCHO . The H_3O^+ -ion-centered isomers are likely to be the most stable ones because they were identified in collisional dissociation experiments as discussed below.¹⁰⁴

Spectroscopic studies by Dopfer and co-workers on complexes of cyclic C_3H_3^+ and linear H_2CCCH^+ with N_2 showed evidence for planar C_3H_3^+ ions and linear $\text{CH}\cdots\text{NN}$ bonds.¹⁰⁵ In another study, the IR dissociation spectra of clusters of protonated benzene C_6H_7^+ with Ar , N_2 , CH_4 , and H_2O ligands indicated weak bonds, 9.5 kcal/mol with N_2 and 11.5 kcal/mol with CH_4 , where the ligands perturbed only slightly the aliphatic and aromatic CH vibrations of the ion. Evidence for σ -bonded and π -bonded structures were discussed.

In the complexes with Ar , N_2 , and CH_4 , the proton remains on C_6H_7^+ even when up to four ligand molecules are present.^{106a}

5.4. Spectroscopy of Carbon-Based Bonds in Ionized Aromatics

Unconventional IHBs can involve aromatic molecules that can serve as π -acceptors or CH donors. The group of Fujii, Mikami, and co-workers studied several such systems by the IR spectroscopy of clusters and recently summarized this work.^{119a}

Results on the benzene–water system were described previously in the section on radical ions. Several isomers were observed in the benzene cation solvated by several water and methanol ligands. With one ligand molecule, the IR spectrum showed only an isomer in which the oxygen of the first ligand molecule forms two IHBs with adjacent protons of $\text{C}_6\text{H}_6^\bullet^+$ in the aromatic plane. In contrast, the spectra of clusters with 2–4 H_2O and 2 CH_3OH ligands provided evidence for isomers where each ligand molecule forms separate H-bonds to the central cation or where at least 1 ligand forms a hydrogen bond to a second ligand.^{119a,b,120}

The benzene–water system with 1–6 H_2O molecules was observed also in the OH and CH stretching vibrational region and by ab initio DFT calculations. This work also found that in the $n = 1$ cluster cation the water oxygen is in the benzene plane and forms two identical IHBs with two adjacent benzene hydrogens. The IR spectra of the $n = 2$ cluster showed two isomers, one with 2 H_2O molecules bonded to benzene and one in which they bonded to each other, which also applied in the $n = 3$ cluster. Higher clusters showed spectra that were very similar to that of protonated water clusters $(\text{H}_2\text{O})_n\text{H}^+$, indicating that the proton was transferred from benzene to water to form $\text{C}_6\text{H}_5^\bullet\cdot(\text{H}_2\text{O})_n\text{H}^+$ clusters.¹⁴¹

Isomeric structures were observed also in the complex of $\text{C}_6\text{H}_6^\bullet^+$ with CH_3COOH by vibrational and electronic spectra and ab initio calculations. A band was assigned to the O–H stretching vibration of the cis-isomer of acetic acid in the hydrogen-bonded complex (horizontal cis-isomer), and another band was assigned to the vertical trans-isomer where the acetic acid interacts with the π -electron system of the benzene cation. The spectra also showed intermolecular charge transfer between a carbon atom of benzene and the carbonyl oxygen atom of acetic acid.¹²¹

Complexes of phenol were also investigated by spectroscopy. Bonds of $\text{OH}\cdots\pi$ -type were found in $(\text{phenol/benzene})^\bullet^+$, $(\text{phenol/C}_2\text{H}_2)^\bullet^+$, and $(\text{phenol/C}_2\text{H}_4)^\bullet^+$ complexes. The hydrogen bonds in the neutral complexes were enhanced significantly by ionization. The nature of the π -bond, whether an olefin or aromatic ligand, did not affect strongly the spectral shifts.

The phenol–water system was investigated also by two-photon ionization and fluorescence spectroscopy by Kleiner-manns and co-workers. They found that with 1 and 2 water molecules no proton transfer occurs in $\text{C}_6\text{H}_5\text{OH}^\bullet^+(\text{H}_2\text{O})_n$ clusters, but with $n = 4$, linear and solvated isomers were observed. The latter, where the phenol ion is solvated, shows proton transfer to form $\text{C}_6\text{H}_5\text{O}^\bullet^+(\text{H}_2\text{O})_n\text{H}^+$ clusters. With $n = 8$, two filled shells and the beginning of a new shell were observed.²⁹⁹ With n up to 20, the water forms bi-, tri-, and tetracoordinated hydrogen-bonded structures similar to water and ice surfaces.³⁰⁰ In complexes of phenol with 1–4 NH_3 ligand molecules, the high proton affinity of the ligand causes proton transfer to occur already to the first NH_3 ligand molecule or to several NH_3 molecules to form $\text{C}_6\text{H}_5\text{O}^\bullet(\text{NH}_3)_n\text{H}^+$ clusters.^{301,302}

5.5. Spectroscopic Consequences of Intramolecular and External Solvation

The group of Y. T. Lee investigated the relation between intramolecular and external solvation in the diketone hydrates ($\text{MeCOCH}_2\text{COMe}(\text{H}_2\text{O})_n\text{H}^+$ ($n = 0-3$)). The calculations showed that the unsolvated ion contains an internal ionic hydrogen bond (iIHB), which is replaced by a H_3O^+ bridge in the monosolvated ion. Further replacement of the iIHB occurs with two H_2O molecules. After 3 or more water molecules, the proton is transferred to water, and the water bridges between the ketone groups can open. The IR spectra in Figure 44 showed evidence both for open and water-bridged isomers.²⁷⁵

A new type of unconventional intramolecular IHB was observed in the *cis* conformation of the ortho isomers of the $\text{CH}_3\text{C}_6\text{H}_4\text{OH}^{•+}$ and $\text{C}_2\text{H}_5\text{C}_6\text{H}_4\text{OH}^{•+}$ radical cations. Here the alkyl groups act as hydrogen acceptors, rather than in their usual roles as donors.¹²²

Intermolecular bonds in complexes of diamines were investigated in $(\text{H}_2\text{NCH}_2\text{CH}_2\text{NH}_2)(\text{H}_2\text{O})_3\text{H}^+$; the IR spectra indicated a bicyclic structure assisted by an internal IHB. This isomer coexists with monocyclic open isomers at 150 K, and the relative abundances of the isomers were consistent with a combination of enthalpy and entropy effects.^{233a}

An internal IHB was observed spectroscopically in the ethanolamine component of the (phenol–ethanolamine) $^{•+}$ complex.³⁰³ These spectroscopic studies confirmed the earlier conclusions from thermochemistry about the relations between external solvation and intramolecular IHBs.²⁵⁹

5.6. Spectroscopy of IHB Networks about Anions

The formation of ionic hydrogen bonds causes a red shift of the stretching modes of the hydrogen-bonding proton, both in anions and in cations.^{219a,255,297} For example, the frequencies of the OH stretching mode in the vibrational spectrum of the complex $\text{OH}^-\cdot\text{H}_2\text{O}$ were found to be red-shifted.³⁰⁴ The ion–molecule stretching vibrational frequencies in the binary complexes $\text{X}^-\cdot\text{H}_2\text{O}$ ($\text{X} = \text{Cl}, \text{Br}, \text{I}$) were investigated via argon predissociation spectroscopy.³⁰⁵ Larger clusters were observed through the 3200–3800 cm^{-1} vibrational IR predissociation spectra of the Br^- and I^- clustered by up to 6 H_2O molecules. The spectra of these anionic clusters become increasingly similar after 3 or more water molecules, which displayed a very wide unresolved band reminiscent of the bulk water spectrum. A blue shift with increasing solvation suggested the strengthening of the interwater hydrogen-bonding network at the expense of the hydrogen bonds to the halide.³⁰⁶

In solvation by water, F^- undergoes internal solvation, remaining on the inside of the solvent clusters, but Cl^- , Br^- , and I^- undergo external or surface hydration, being on the surface of the cluster. This also applies in the solvation of Cl^- and I^- by methanol.^{88a}

External solvation of halide ions was also shown by liquid-drop and statistical theories.²³⁸ A recent review covered hydration shells about halide ions, discussing how clusters can elucidate the behavior of the inner water molecules in contact with the anion. For example, vibrational predissociation spectroscopy showed the morphology of the small water networks attached to anions. Charge transfer in the binary interaction and its effects on the structures of the larger hydrogen-bond networks were discussed.⁸⁶

Solvation of F^- anion by MeOH was investigated by vibrational predissociation spectroscopy. The strong hydrogen bond between the anion and the hydroxyl group shifted some

O–H stretching frequencies into the C–H stretch region. Ab initio calculations combined with experiment showed that the fluoride anion is on the surface of the methanol solvent cluster, which starts to form methanol–methanol hydrogen bonds after 4 or more methanol molecules.

Spectroscopy was applied by Bieske and co-workers to clusters that involve unconventional $\text{CH}\cdots\text{X}^-$ bonds such as the $\text{Cl}^-\cdots\text{CH}_4$ dimer³⁰⁷ and halide anions clustered by acetylene with a coordination number of four. The spectra of these anions was reviewed recently.^{308a} Unconventional $\text{CH}\cdots\text{Cl}^-$ dimers of alcohols may also serve as intermediates in $\text{S}_{\text{N}}2$ reactions, but photodissociation spectroscopy showed that complexes of Cl^- with H_2O , CH_3OH , and $\text{C}_2\text{H}_5\text{OH}$ are bonded by $\text{Cl}^-\cdots\text{HOR}$ bonds with ground-state frequencies of $\sim 700 \text{ cm}^{-1}$.^{308b}

Photoelectron spectroscopy has been applied to many anionic clusters, especially by K. H. Bowen and co-workers. For example, solvent effects on acidities/basicities were studied in $\text{NH}_2^-(\text{NH}_3)_n$ ($n = 1$ and 2). The spectra implied that the clusters consist of intact amide ions solvated by ammonia, the geometry of which is distorted from that of a free ammonia molecule due to the hydrogen bond. The gas-phase basicities showed that, while NH_2^- is a stronger base than H^- in the gas phase, the addition of only 2 ammonia solvent molecules reverses these relative basicities.²⁵⁵

Similar studies were applied to the methylated species $\text{Me}_2\text{N}^-(\text{Me}_2\text{NH})$.³⁰⁹ Photoelectron spectra to IHB systems include measurements of the binding energies of NO^- to H_2O , NH_3 , and H_2S .³¹⁰

An interesting case of IHB formation was found in anions formed by electron attachments to uracil–glycine and uracil–phenylalanine complexes. The most stable structure of (uracil–glycine) $^{•-}$ was a distonic anion dimer ($\text{H}_2\text{C}(\text{NH}_2)\text{COO}^-$)–(uracil H^{\bullet}), formed by barrier-free proton transfer in the anionic complex.³¹¹

5.7. Summary of Spectroscopic Studies

In summary, spectroscopic studies of hydrogen-bonded clusters can be based on shifts in vibrational frequencies caused by the formation of hydrogen bonds. Spectroscopy confirmed the relation among proton affinity differences, bonding energies, and the degree of proton transfer in dimer ions. In larger clusters, spectroscopy can identify cluster structures, such as noncyclic and cyclic isomers, and the location of the proton.

In relation to isomers, spectra show distinct cluster structures that sometimes coexist in equilibrium. For example, spectroscopy can identify $\text{CH}^{\delta+}\cdots\text{O}$ bonded clusters that may be in equilibrium with $\text{OH}^{\delta+}\cdots\text{O}$ isomers. In polyfunctional ions, spectroscopy can identify internal hydrogen bonds, the insertion into solvent molecules in the internal bonds, and the displacement of the internal bonds by external solvation.

For ions solvated by several solvent molecules, spectra can identify structures where the solvent molecules are bonded directly to the core ion, which is inside the solvent cluster. In special cases, the proton is located on an H_3O^+ core ion even when it is surrounded by blocked ligands that are stronger bases. Alternatively, the solvent molecules can be attached to each other, and the ion is attached to one of the solvent molecules on the outside of the solvent cluster. In this case the solvent cluster has neutral-like structure and spectra.

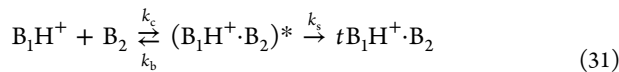
For ions with internal strong hydrogen bonds, the surrounding solvent molecules can loosen or open the internal bond or form a protonated solvent bridge between functional groups. When 2–4 H_2O molecules are present, the proton

often shifts to form a strongly hydrogen-bonded $(\text{H}_2\text{O})_n\text{H}^+$ cluster that is hydrogen-bonded to a deprotonated ligand or radical. In the clusters, the solvent tends to form cyclic or three-dimensional structures. Spectroscopy confirms these structural features that were inferred previously from thermochemistry and predicted by ab initio studies.^{228,259}

6. KINETICS OF HYDROGEN-BOND FORMATION AND DISSOCIATION

6.1. Formation and Dissociation of Hydrogen Bonds

6.1.1. Formation of Hydrogen-Bonded Clusters. The formation of IHBs occurs mostly by association reactions (eq 31). An excited complex $(\text{B}_1\text{H}^+\cdot\text{B}_2)^*$ forms with collision rate k_c (between B_1H^+ and B_2) and becomes stabilized also near the collision rate k_s (between $(\text{B}_1\text{H}^+\cdot\text{B}_2)^*$ and a third-body molecule) to form the adduct, or dissociates with unimolecular rate coefficient k_b back to reactants.



The overall forward rate coefficient, $k_f = k_c(k_s/(k_b + k_s))$ depends on the relation between the rate of stabilization, k_s , and the rate of back-dissociation, k_b . In particular, the rate of back-dissociation, k_b , which competes with product formation, decreases with increasing IHB bond strength, with increasing number of degrees of freedom of the complex, and with decreasing temperature. These factors therefore increase the rate of formation of the complex.

The temperature dependence of the rate coefficient k_f of the overall association reactions 31 may be expressed in the form $k_f = AT^{-n}$.³¹² Temperature coefficients of T^{-2} to T^{-4} are usually observed in small ions and molecules. In a sequence of clustering reactions, the rate coefficients k_f tend to increase at higher steps where the number of degrees of freedom in the complex is larger, and as a result, equilibrium may be achieved faster in higher steps than in lower steps. For example, Kebarle and co-workers observed such effects in a detailed study of the $(\text{H}_2\text{O})_n\text{H}^+$ system.¹⁹⁷

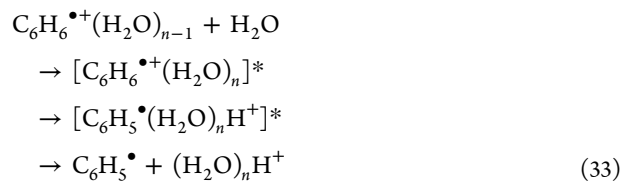
6.1.2. Reactions Driven by Hydrogen-Bond Formation: Associative Proton-Transfer Reactions. Noncovalent association to form a strong hydrogen bond of 20–30 kcal/mol can drive ionic reactions. Such reactions occur, for example, when molecules associate to form a protonated cluster by extracting a proton from a radical ion in reaction 32. These reactions may be called associative proton transfer (APT) reactions.



The first examples were reported in 1970 by Sieck and Searles³¹³ who observed the extraction of a proton from radical ions of butane, pentane, and hexane isomers in termolecular reactions with two H_2O molecules to form the $(\text{H}_2\text{O})\text{H}^+$ dimer. More recently, Meot-Ner, El-Shall, and co-workers observed reaction 32 between $\text{RH}^{\bullet+} = \text{C}_6\text{H}_6^{\bullet+}$ and $\text{C}_6\text{H}_5\text{CH}_3^{\bullet+}$ formed by resonant two-photon ionization and $\text{B} = \text{MeOH}$, EtOH , MeCOOEt , or MeCN , to form the respective protonated dimers.³¹⁴ These reactions are rendered exothermic by the formation of the hydrogen bond in B_2H^+ . The formation of the hydrogen bond must occur in the three-body reaction intermediate $\text{RH}^{\bullet+}(\text{B}_2)$ concerted with proton transfer to make the reactions energetically feasible.

Associative proton-transfer reactions can require >2 neutral molecules to extract the proton. For example, when $\text{C}_6\text{H}_6^{\bullet+}$

reacts with n H_2O molecules, the enthalpy change of reaction 32 is 46, 14, -7, and -25 kcal/mol for $n = 1$ –4, respectively. The overall reaction is exothermic for $n = 3$, but it proceeds with the stepwise buildup and stabilization of the $\text{C}_6\text{H}_6^{\bullet+}(\text{H}_2\text{O})_n$ cluster followed by reaction 33 of which the enthalpy change is 46, 23, 10, 0, and -3 kcal/mol for $n = 1$ –5, respectively.

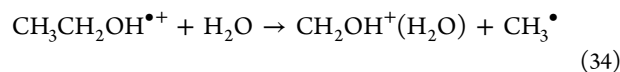


At $n = 4$, the reaction becomes thermoneutral and energetically feasible. The reaction is a five-body process, and the enthalpy assembling the reactive complex from $\text{C}_6\text{H}_6^{\bullet+} + 4\text{H}_2\text{O}$ molecules into the $\text{C}_6\text{H}_6^{\bullet+}(\text{H}_2\text{O})_4$ complex is -35 kcal/mol. Correspondingly, this reaction shows an unprecedentedly large negative activation energy of -34 ± 1 kcal/mol, expressed alternatively as $k = AT^{-67 \pm 4}$. In general, high-order associative transfer reactions that require the assembling of multibody complexes are expected to have unusually large negative temperature coefficients.^{117d,e}

In the above systems the reaction occurs between a gas-phase ion and neutral molecules that cluster stepwise onto the ion. Similar processes can occur in preassembled clusters formed by supersonic beam expansion. Such associative transfer reactions with the formation of a strong hydrogen bond were observed following the resonance two-photon ionization of clusters of toluene with H_2O , MeOH , Me_2O , and NH_3 molecules. The reaction onset is with 1 NH_3 , 2 CH_3OH , and 3 H_2O molecules in the cluster, depending on the PAs of the proton acceptor bases and the strengths of the IHB networks in the product protonated clusters.^{315,316a} Intracluster proton transfer reactions involving hydrogen-bonded cluster ions were reviewed.^{316a,b}

Such reactions can be therefore significant in astrochemical environments at low temperatures, where they may proceed at collision rate. For example, ionized aromatics in interstellar clouds and solar nebulae can serve as nuclei for the attachment of water and other polar molecules. The solvated aromatics, or the product protonated clusters, can form centers for nucleation to form interstellar grain particles.

Several other kinetic effects of IHBs were observed. Associative reactions can be driven by the formation of ionic hydrogen bonds to eliminate a radical, reaction 34.



Analogous reactions occur between $\text{C}_2\text{H}_5\text{OH}^{\bullet+}$ and CH_2O or CH_3OH and between $(\text{C}_2\text{H}_5)_2\text{O}^{\bullet+}$ and H_2O , $\text{C}_2\text{H}_5\text{OH}$, $(\text{CH}_3)_2\text{O}$, $(\text{CH}_3)_2\text{CO}$, $(\text{C}_2\text{H}_5)_2\text{O}$, or CH_3CN .^{108,317a} Hydrogen-bonded dimers are reaction intermediates in the association of $\text{CH}_3\text{OCH}_2^+$ with alcohols.^{317b} The formation of a hydrogen-bond network also contributes to the reaction $\text{NO}^+(\text{H}_2\text{O})_n + \text{H}_2\text{ON} \rightarrow \text{NO}^+(\text{H}_2\text{O})_{n+1} = (\text{HONO})\text{H}^+(\text{H}_2\text{O})_n \rightarrow \text{HNO}_2 + (\text{H}_2\text{O})_n\text{H}^+$ that becomes essentially thermoneutral for 4 water molecules.^{318a–f}

Ionic hydrogen bonds can also affect the kinetics by solvating the ions. For example, the reactivity of the hydroxyl anion was observed to be affected by solvation by H_2O molecules.³¹⁹

6.1.3. Reactions Driven by Hydrogen-Bond Formation or Dissociation and Entropy-Driven Reactions. The exothermic formation of an internal hydrogen bond can provide the driving force for proton-transfer (PT) reactions

to polyfunctional molecules. Conversely, the positive entropy change upon dissociating the internal bond can also drive or accelerate the deprotonation of polyfunctional ions.

Most exothermic PT reactions proceed near the collision rate. This includes PT reactions to polyfunctional molecules that are made exothermic by the formation of internal hydrogen bonds in the product ion. Without formation of the internal bond, proton transfer to a single functional group of the molecule may be endothermic and slow.

In the reverse direction, the dissociation of an internal hydrogen bond releases a constrained cyclic structure, which leads to a positive entropy change. In some of these reactions, ΔH° is positive but ΔG° is negative. Reactions were observed that are endothermic by up to 8 kcal/mol and would normally be too slow to observe, but they are fast and proceed near the collision rate with near unit efficiency because ΔG° is negative.^{206a,b,259}

These reactions are “intrinsically fast” because they are not slowed by barriers, and the kinetics are controlled only by the overall thermochemistry. The one-intermediate, single-well mechanism is similar to reaction 31, with k_s representing the product formation rate coefficient, and with a reverse reaction forming the complex at collision rate k_{cr} . This mechanism yields forward and reverse reaction efficiencies $r_f = k_s/(k_b + k_s)$ and $r_r = k_b/(k_s + k_b)$, yielding $r_f + r_r = 1$. The sum of the forward and reverse reaction efficiencies is unity, which defines “intrinsically fast” reactions.^{206a,b} The reaction efficiency in either direction is then determined only by the equilibrium constant K in that direction, as $r = K/(1 + K) = (\exp(-\Delta G/RT))/(1 + \exp(-\Delta G/RT))$.^{206a,b} For significantly exergonic reactions ($\Delta G^\circ \ll 0$ and $K \gg 1$), this relation gives $r \approx 1$ and the reaction that proceeds near unit efficiency, even if the reactions are endothermic but the positive entropy change of opening the internal IHB renders ΔG° negative. In these reactions, the formation or dissociation of internal hydrogen bonds affects the kinetics directly through their effects on the thermochemistry.^{206a,b} Because of the direct relation of rates to thermochemistry, this type of reaction can be used for bracketing the gas-phase basicities of molecules. Fast proton transfer to a reference base indicates that the molecule has lower basicity than the reference base and vice versa.³²⁰

In reactions where the formation or opening of an IHB drives a proton-transfer reaction, it affects the energy and density of states of the transition state, and therefore, the formation of opening of the internal bond must be concerted with the intermolecular proton-transfer process. The first examples of such “entropy-driven reactions” including IHB formation were observed in reactions of diamines.²⁵⁹ The kinetics were generalized and analyzed for other reactions with significant entropy changes.^{206a,b} Similar effects were observed also in biomolecules, such as proton transfer from (lysine) H^+ , the increased PA of which can be attributed to an internal IHB.⁹ Internal hydrogen bonds and their entropy effects are common in polyfunctional biomolecules, and their kinetic effects are also expected to be common in the reactions of biomolecules.

6.2. Hydrogen-Bonded Complexes as Reaction Intermediates

Hydrogen-bonded complexes may be intermediates in the dissociation of protonated or radical ions. These intermediates may involve lone-pair bases or unconventional carbon-based IHBs.

An example of an $OH^+ \cdots O$ hydrogen-bonded complex, $(H_2O \cdots H \cdots O=C-OH)^{+\bullet}$, was identified by metastable and collision-induced dissociation and theory in the dissociation of ionized dihydroxyfumaric acid ($HOOCC(OH)=C(OH)COOH$)^{+\bullet}

leading to $(H_2O \cdots H \cdots OCO)^{+\bullet}$ and H_3O^+ products.¹⁴⁰ The ΔH°_D versus PA correlations gave 24.4 kcal/mol for the bond strength of this complex, but it remains to be shown whether these relations apply in complexes of radical ions.

Complexes with carbon-based IHBs were identified in numerous reaction intermediates. For example, such complexes occur in the reactions of CH_3^+ and $CH_4^{+\bullet}$ ions. An early example of $CH^+ \cdots O$ bonded complexes was identified by Smith and Futrell in the hydride-transfer reaction $CH_3^+ + CH_3OH \rightarrow CH_2OH^+ + CH_4$,¹⁰⁷ and more recently, ICR studies and ab initio calculations showed such complexes in the reactions of CH_4^+ with H_2O , CH_3OH , and $(CH_3)_2O$.¹⁰⁸

In other reactions, theory showed $CH_3CNR^+\cdot OH_2$ and $CH_3CN\cdot ROH^+$ with $CH \cdots O$ and $CH \cdots N$ bonds as intermediates in the dissociation and rearrangement of $CH_3CNH^+ \cdots ROH$ complexes.^{321a} The complex $H_2O \cdots H_2CCO^{+\bullet}$ with a calculated bonding energy of 14 kcal/mol occurs in the decomposition of $(HOCH_2)CO^{+\bullet}$.¹³⁵⁻¹³⁷ The $c-C_3H_6^{+\bullet} \cdots H_2O$ complex in the dissociation of $n-C_3H_7OH^{+\bullet}$ may be a T-shaped bidentate complex with a bonding energy of 10.4 kcal/mol.^{138,139}

Complexes with hydrogen bonds between protonated functional groups and olefinic or aromatic π -bonds were also observed. For example, theory showed a complex involving a hydrogen bond between NH_4^+ and the π -bond in $H_2C=CH_2$.⁹⁴ An analogous complex, $(H_2O)H^+(C_2H_4)$, with an energy about 12 kcal/mol above $C_2H_5OH_2^+$ was also demonstrated.

Hydrogen-bonded complexes can be intermediates in isomerization and proton-transport catalysis. An early example was the conversion of $HCN^{+\bullet}$ to the lower-energy $HNC^{+\bullet}$ by reaction with CO , and CO_2 reacted similarly.^{321b} Schematically the reaction may proceed through the intermediates $NCH^{+\bullet} + CO \rightarrow NCH^{+\bullet} \cdots CO \rightarrow NC \cdots HCO^+ \rightarrow CN \cdots HCO^+ \rightarrow HNC^{+\bullet} \cdots CO \rightarrow HNC^{+\bullet} + CO$, and CO_2 reacted similarly.^{321b} Other examples are the isomerization from $CH_3CHO^{+\bullet}$ to the distonic ion $CH_2CHOH^{+\bullet}$, catalyzed through a $CH^+ \cdots O$ complex with CH_3OH ,^{321c} and proton-transport catalysis affected by water between isomers of protonated theophylline.^{321d}

A complex of $HCNH^+\cdot C_2H_4$, with a CH^+ or NH^+ donor group bonded to the olefin π -bond, was observed in the isomerization $CH_3CH_2CNH^+ \leftrightarrow CH_3CH_2NCH^+$.¹¹¹ Complexes with a hydrogen bond between an OH^+ group and a double bond were also indicated in the loss of methanol from protonated methoxyhexenes.^{322a} Hydrogen exchange between an OH group and a double bond in this intermediate can facilitate hydrogen transfer between the leaving methanol and the remaining hydrocarbon ion.

Hydrogen-bonded complexes also serve as intermediates in S_N2 reactions. These reactions are affected by microsolvation by a few solvent molecules^{322b-k} that interact with the complexes through hydrogen bonding. Generally, solvation increases the barrier heights because the charge is more delocalized in the transition state and it is solvated less efficiently than the ground-state reactant complex.

Examples of such systems are the complexes of halide ions with halogenated hydrocarbon CH donors, with $Cl^- \cdots HR$ bonds of 12–18 kcal/mol and $Br^- \cdots HR$ bonds of 10–15 kcal/mol. The bond energies of the S_N2 complexes to one further $MeOH$, $MeCN$, Me_2CO , and CH_3CF_2H molecule were investigated recently, and one solvent molecule affected significantly these reactions.^{322l,m}

7. IONIC HYDROGEN BONDS IN BIOMOLECULES

Ionic hydrogen bonds are ubiquitous in biology. IHBs contribute to the solvation of ionized groups by water and

by polar groups in desolvated protein interiors. These IHB interactions contribute to protein folding and aggregation, enzyme energetics,³²³ molecular recognition, neurotransmitters, and receptors, as well as in membranes and photosystems.^{324,325}

The energetics of individual IHBs cannot be isolated in complex biosystems, but they can be inferred from similar interactions in clusters. For example, IHB bond strengths involving N and O functional groups in biomolecules can be estimated from proton affinity/bond strengths correlations in clusters (Table 2).^{48,53–56} Studies on sufficiently volatile biomolecules such as amino acid esters and intramolecular bonds¹⁵⁰ (Table 7) and nucleic bases and polydentate bonding^{280a,b} (Tables 8 and 9) can also serve as biological models.

Actual biomolecules can now be studied in the gas phase using electrospray³²⁶ coupled with HPMS¹⁵⁵ or mobility cells,³²⁷ collisional dissociation,¹⁴ blackbody infrared radiative dissociation ZETRID/BIRD^{15,18} or Fourier transform ion cyclotron resonance (FTICR),^{9,10,18,328} and IR photodissociation spectroscopy.^{236,292a} These studies confirm that the effects observed earlier in model molecules, such as intramolecular and polydentate IHBs, are indeed significant in biomolecules. New IHB interactions, such as the formation of zwitterions and salt bridges,^{329–331} were observed. Solvation by nonaqueous solvents, such as acetonitrile, was also studied.^{331b} The following sections and Table 10 review these results.

7.1. Intramolecular Solvation and Conformation

Studies of peptides and proteins show trends that were observed first in model molecules. For example, internal IHBs can form in functionalized amino acids such as in protonated lysine.³³² Internal IHBs also contribute to the gas-phase basicities of peptides that increase with peptide size and allow better internal solvation. The basicities for multiple protonation decrease with increasing charge due to Coulomb repulsion between the protonated functions.^{333–335} The PAs and GBs of amino acids, peptides, and proteins were reviewed.³³⁶ As to conformations, long chains, low charge states, and low temperatures favor compact geometries.

7.1.1. Amino Acids and Derivatives. Before the new methods of volatilization, IHB interactions in proteins were modeled by the sufficiently volatile amino acid derivatives $\text{CH}_3\text{CONHCH}_2\text{COOCH}_3$ ($\text{CH}_3\text{CO-Gly-OCH}_3$) and $\text{CH}_3\text{CONHCH}(\text{CH}_3)\text{COOCH}_3$ ($\text{CH}_3\text{CO-Ala-OCH}_3$). The two carbonyl groups in these molecules are positioned similarly to adjacent amide groups in peptides. Protonation forms an intramolecular IHB, and the thermochemistry suggests an internal bond of 11–12 kcal/mol between these groups,¹⁵⁰ less than the 30 kcal/mol of unconstrained $\text{OH}^+\cdots\text{O}$ bonds, due to constrained geometries. The 7-membered ring includes the proton, 2 $-\text{C}=\text{O}$ bonds, and 5 single bonds with flexible bond angles. The strain of 18–19 kcal/mol is similar to 5-membered IHB rings ($\text{XCH}_2\text{CH}_2\text{X}$) H^+ in ions that also contain 5 single bonds including the hydrogen bond (Table 7).

The proton affinities of further N-acetylated amino acid methyl esters of glycine, leucine, phenylalanine, proline, glutamic acid, and arginine have been calculated and characterized at B3LYP/6-31++G(d,p) level, and proton affinities of 15 similarly derivatized amino acids have been measured experimentally. The proton is attached to the carbonyl group in most cases. The proton affinities of all N-acetyl amino acid methyl esters are higher than those of the corresponding underivatized amino acids, reflecting stabilization of the ions by intramolecular hydrogen bonding.^{337a} The intramolecular bond $-\text{NH}_3^+\cdots\text{O}=\text{C}-$ between

the protonated amine and the carbonyl oxygen of protonated glycine and alanine methyl esters was confirmed by free electron laser IR multiphoton dissociation (FEL IRMPD) spectroscopy,^{337b} extending earlier studies on glycine and alanine derivatives,¹⁵⁰ and similarly for bonding between the protonated side-chain amine and carbonyl oxygen in ArgH^+ and ArgOMeH^+ .^{337c}

Longer chains between functional groups allow more optimized intramolecular IHBs. For example, Lebrilla and co-workers found that the gas-phase basicities of β -alanine and β -alanine–glycine are higher by 7 kcal/mol than analogous derivatives of α -alanine, because the longer chain and larger hydrogen-bonded ring in the protonated β -isomers allows more optimized IHB angle and more stable iIHBs. The gas-phase basicity (GB) of *N*-acetylglycine amide is higher by 5 kcal/mol than that of *N*-acetylglycine itself because a stronger iIHB forms between the two amide groups of similar PAs in the amide, in accordance with ΔH°_D versus ΔPA correlations. The increased GB of *N*-acetylglycine amide is similar to that of triglycine, and the iIHB simulates interactions between adjacent amide groups in peptides.^{338a}

7.1.2. Peptides. Intramolecular hydrogen bonds involving polar amide links and functional groups in peptides and proteins can stabilize the ions, leading to increased proton affinities and gas-phase basicities. Internal IHBs may remain stable even at high temperatures up to 600–1000 K where covalent bonds of the ions would dissociate, as noted previously for protonated diamines. This may be significant in the mass spectrometry of protonated peptides where internal ionic hydrogen bonds can activate the dissociation of peptide bonds of ions at high effective temperatures.^{338b}

Because of intramolecular bonds, the gas-phase basicities of polyglycines increase with size. The proton is localized on the terminal amine group, and the proton affinity increases with increasingly efficient internal solvation.^{333–335,339} Semiempirical AM1 and PM3 calculations reproduced the trend observed in Figure 50 and showed that the increasing PA from Gly_1 to Gly_5 is caused by internally solvated conformations, whereas in extended conformations the PA would remain constant. For example, internal solvation of the charged site in Gly_5H^+ accounted for 83% of the increase of its PA relative to glycine.³⁴⁰

Recently, these structural effects in $(\text{Gly}_{1–5})\text{H}^+$ were confirmed by FEL IRMPD spectroscopy, complemented by ab initio computation.^{341a,b} These studies showed that in the lowest energy isomers of GlyH^+ and Gly_2H^+ the proton is located on the amine nitrogen, with a hydrogen bond to carboxylic acid carbonyl oxygen. In Gly_3H^+ , and also in Ala_3H^+ ,^{341a} the proton is bonded to the amide oxygen at the N terminus, stabilized by an IHB to the second amide oxygen and two additional IHBs. In Gly_4H^+ and Gly_5H^+ the proton is on the amine at the N-terminus, stabilized by hydrogen bonds to carbonyl oxygens, and the ions are stabilized further by additional hydrogen bonds. Protonated peptides have isomers with energies within 1–3 kcal/mol of the lowest energy structures. In Gly_3H^+ the amine-protonated and carbonyl-protonated isomers were both observed.^{341a,b}

Internally solvated structures were identified experimentally by ion mobility in $(\text{Ala-Ala-Arg-Ala-Ala})\text{H}^+$ and its N-acetylated and $-\text{COOCH}_3$ derivatives. These ions had similar binding energies to H_2O molecules, which supported a common structure. However, a salt-bridged structure also became energetically accessible as a transition state for H/D exchange in the monohydrated ion.^{279c}

Table 10. Thermochemistry of Biomolecules and Clusters^a

Proton Affinity and Gas-Phase Basicity							refs
	PA	$\Delta S^\circ_{\text{prot}}$	GB	method ^b	comments		refs
glycine	212 ^c		204 ^c	PHPMS, ICR			372, 373, 334, 335, 27
(Gly) ₃	231 ^c		219 ^c	CID			333, 334, 335, 27
(Gly) ₄	233 ^c		222 ^c	CID			333, 334, 335, 27
(Gly) ₆			227 ^c				334, 335, 27
(Gly) ₈			237 ^c		increasing PA, GB with <i>n</i> due to internal solvation		334, 335, 27
alanine	216		207				27
B-Ala			211				338a
Ala-Gly			211				338a
β -Ala-Gly			218				338a
MeCO-Gly-OMe	217	-12	206		$\Delta S^\circ_{\text{prot}}$ indicates internal IHB		150
MeCO-Ala-OMe	224	-15	212		$\Delta S^\circ_{\text{prot}}$ indicates internal IHB		150
valine	218		210				27
leucine	219		211				27
lysine	238		227		increased PA, GB due to internal solvation		27
Gramicidin S			>243				16
(gramicidin S)H ⁺			215		decreased GB vs uncharged protein due to Coulomb repulsion		16
Clusters							
hydration							
ion	ligand	$\Delta H^\circ_{\text{D}}$	$\Delta S^\circ_{\text{D}}$	$\Delta G^\circ_{\text{D}}$	method ^b	comments	refs
GlyH ⁺	H ₂ O			9.7	ES/HPMS		155
	2H ₂ O			7.2	ES/HPMS		155
	3H ₂ O			5.4	ES/HPMS		155
(Gly) ₂ H ⁺	H ₂ O			8.8	ES/HPMS		155
	2H ₂ O			6.2	ES/HPMS		155
(Gly) ₃ H ⁺	H ₂ O			6.7	ES/HPMS		155
	2H ₂ O			5.8	ES/HPMS		155
(Gly) ₄ H ⁺	H ₂ O			5.8	ES/HPMS	weaker bonding to H ₂ O in larger peptides due to internal solvation	155
GlyH ⁺	H ₂ O	15.4	20.4		PHPMS		348b
GlyH ⁺	2H ₂ O	13.9	22.4		PHPMS		348b
GlyH ⁺	3H ₂ O	12.8	24.8		PHPMS		348b
GlyH ⁺	4H ₂ O	10.6	22.2		PHPM		348b
AlaH ⁺	H ₂ O	14.8	20.6		PHPMS		348b
PheH ⁺	H ₂ O	14.0	21.8		PHPMS		348b
ProH ⁺	H ₂ O	14.8	24.2		PHPMS		348b
CH ₃ COO ⁻ CH ₂ -CH ₂ N-(CH ₃) ₃ ^{+d}	H ₂ O	8.0	22.0	1.5	PHPMS	weak interaction in CH ^{δ+} ...OH ₂ bond	124
CH ₃ CONCH-(CH ₃)COOCH ₃ ^{-e}	H ₂ O	15.2	20.9	9.0	PHPMS		187
	2H ₂ O	13.0	19.8	7.1	PHPMS		187
(Ala) ₃ H ⁺	H ₂ O	12.3	23.3	5.4	mobility	solvation of -NH ₃ ⁺ group	279b
	2H ₂ O	11.3	22.6	4.6	mobility	solvation of -NH ₃ ⁺ group	279b
	(3-5) H ₂ O	8.7-7.6			mobility	solvation of -NH ₃ ⁺ group	279b
(Ala) ₃ H ⁺	H ₂ O	10.5	21.3	4.2	mobility	internal solvation weakens bond to water	279b
	(2-4) H ₂ O	8.5-9.0			mobility		279b
(Ala-Ala-Arg-Ala-Ala)H ⁺	H ₂ O	10.2	23		mobility		279b
	2H ₂ O	8.4	18		mobility		279b
((Gly) ₂ -H) ⁻	H ₂ O	11.0	14.5		mobility	solvation of -COO ⁻ group	349
	2H ₂ O	9.5	15.2		mobility	solvation of -COO ⁻ group	349
	3H ₂ O	8.2	14.4		mobility	solvation of -COO ⁻ group	349
	4H ₂ O	7.4	13.7		mobility	solvation of -COO ⁻ group	349
((Ala) ₂ -H) ⁻	H ₂ O	11.7	17.1		mobility	solvation of -COO ⁻ group	349
	2H ₂ O	9.6	16.0		mobility	solvation of -COO ⁻ group	349
	3H ₂ O	8.6	15.6		mobility	solvation of -COO ⁻ group	349
	4H ₂ O	7.1	13.0		mobility	solvation of -COO ⁻ group	349
(BPTI + 6H ⁺) ⁶⁺	H ₂ O	21.3	62	2.8	mobility	large ΔS indicates locking of protein by inserted H ₂ O	13

Table 10. continued

hydration							
ion	ligand	ΔH°_D	ΔS°_D	ΔG°_D	method ^b	comments	refs
(cytochrome <i>c</i> + 5H ⁺) ⁵⁺	2H ₂ O	16	42	3.5	mobility		13
	3H ₂ O	14	34	4.0	mobility		13
	(1–5)H ₂ O			3.5	mobility	$\Delta G_{n-1,n}$ approximately constant for <i>n</i> = 1–5	359
	(cytochrome <i>c</i> + 7H ⁺) ⁷⁺	H ₂ O		4.4	mobility		359
		(2–7)H ₂ O		4.3–3.8	mobility	$\Delta G_{n-1,n}$ decreases slightly for <i>n</i> = 1–7	359
Clusters							
ion	ligand	PA or ΔH°_D	$\Delta S^\circ_{\text{prot}}$ or ΔS°_D	GB or ΔG°_D	method ^b	comments	refs
bioions + organic ligands							
ValH ⁺	NH ₃	20.9		28.8	8.4	PHPMS	ΔS° indicates no bridging of –NH ₃ ⁺ and –COOH by ligand
ValH ⁺	CH ₃ NO ₂	19.8		27.8	12.4	PHPMS	
CH ₃ COOCH ₂ – CH ₂ N(CH ₃) ₃ ⁺ ^d	Me ₂ CO	13.2		21.7	6.7	PHPMS	
	3-CH ₃ C ₆ H ₄ OH	12.8	(24)	5.6	PHPMS		124
	C ₆ H ₅ CH ₃	8.1		15.5	3.5	PHPMS	124
CH ₃ CONCH(CH ₃) ₂ – COOCH ₃ [–] ^e	MeOH	18.0	(25)	10.6	PHPMS		187
biomolecule dimers							
ValH ⁺	Val	20.7			PHPMS		374
ProH ⁺	Pro	20.0			PHPMS		374
GlyH ⁺	Gly	26.5			BIRD	–NH ₃ ⁺ …NH ₂ and –NH ₃ ⁺ …CO multiple bonds	18
AlaH ⁺	Ala	25.8			BIRD		18
GlyH ⁺	Ala	26.5			BIRD		18
LysH ⁺	Lys	26.5			BIRD		18
((Gly) ₂ – H) [–]	(Gly) ₂	32.2			mobility	ΔH°_D from <i>E</i> _a (dissociation)	349
((Ala) ₂ – H) [–]	(Ala) ₂	34.9			mobility	ΔH°_D from <i>E</i> _a (dissociation)	349
leucine enkephalin H ⁺ (YGGFL)H ⁺	leucine enkephalin	46.5 (36.6); 36.9			ES thermal dissoc, using log <i>A</i> = 21.7 (or 17.2); BIRD	multiple IHBs indicated	364
adenineH ⁺	adenine	30.3	39	18.7		large ΔH°_D and ΔS°_D indicates two IHBs in the dimers	280a
thymineH ⁺	thymine	30.1	37	19.1		large ΔH°_D and ΔS°_D indicates two IHBs in the dimers	280a
cytosineH ⁺	cytosine	38.3	37	27.3		large ΔH°_D and ΔS°_D indicates three IHBs in the dimers	280a

^aUnits are as follows: PA, GB, ΔH°_D , and ΔG°_D in kcal/mol; $\Delta S^\circ_{\text{prot}}$ and ΔS°_D in cal/(mol K). ^bMethods are as follows: PHPMS, pulsed high-pressure mass spectrometry; ICR, ion cyclotron resonance; CID, collisional-induced dissociation threshold measurements; ES/HPMS, electrospray high-pressure mass spectrometry; mobility, variable temperature ion mobility equilibrium measurements; BIRD, blackbody IR dissociation. ^cData from several sources; evaluated values cited from ref 27. ^dAcetylcholine. ^e(MeCO-Ala-OCH₃–H)[–].

Counterman and Clemmer studied the effects of peptide size and multiple protonation on the conformation of polyprolines [Pro_{*n*} + *z*H]^{*z*+} (*n* = 3–56; *z* = 1–6) using ion mobility and molecular modeling calculations. Protonation at the N-termini allowed hydrogen bonds to backbone carbonyl groups of the second and third proline residues. Singly charged ions favored more compact globular and hairpin-like conformers. The shorter and low protonation state peptides with *n* = 5–11 and *z* = 1 and *n* = 10–22 and *z* = 2 and highly charged *z* = 3–6 ions favored relatively extended conformations, but as the polymer size increased, the higher charge state ions become more compact.³⁴²

These authors also studied quadruply protonated polyalanines ([Ala_{*n*} + 4H]⁴⁺, *n* = 29–49). The results indicated that [Ala_{*n*} + 4H]⁴⁺ favors stretched helices, stabilized by *i* → *i* + 3 and *i* → *i* + 4 hydrogen bonding, where the latter increases with polymer length, constituting about 65% of the interactions in *n* = 36 and 85% in *n* = 48 peptides.³⁴³ In the triply charged

polyalanines (*n* = 27–39, *z* = 3) at room temperature, extended helical structures and compact hinged helix-coils were observed, but these conformations unfolded at higher temperatures, and the peptides adopted extended helical structures. The activation energies for the transition increased by about 1 kcal/mol per residue from *n* = 27–39, because the increased size allowed more efficient hydrogen bonds that must be released in the transition.^{344,345}

7.1.3. Proteins. Many biomolecules are multiply protonated in solution and biological environments, and electrospray can also generate multiply charged states in the gas phase. The multiply charged ions assume extended conformations because of Coulomb repulsion,^{16,17,331,346} and the ionized state decreases the gas-phase basicity for adding further protons. For example, the GB of gramicidin S is >243 kcal/mol, whereas the GB of (gramicidin S)H⁺ is only 215 kcal/mol. This difference suggested a Coulomb energy of >28 kcal/mol and a dielectric polarizability of <1.2 in this ion.¹⁶

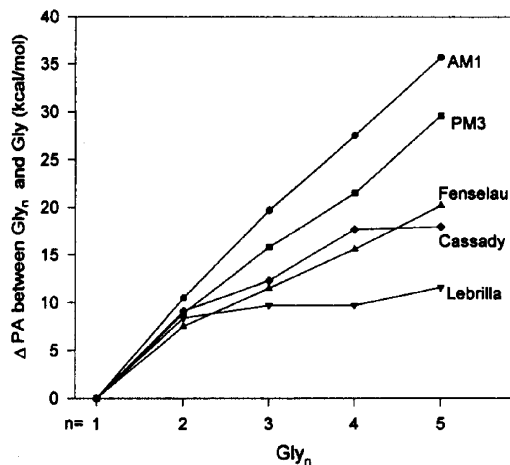


Figure 50. Proton affinities of polyglycines as a function of chain length. Reproduced from ref 340 with permission. Copyright 1995 American Chemical Society.

7.2. Stepwise Solvation of Biological Ions and Mutual Effects of Intramolecular and External Solvation

Early studies used protonated polyfunctional compounds to model ion–solvent interactions in biomolecules. The models showed the following:

- Internal hydrogen bonds decrease the bonding energies to external solvent molecules, as the internal bonds acts as the first solvent molecule (observed in diamines²⁵⁹ and in amino acid derivatives¹⁵⁰).
- Conversely, external solvation weakens, and may ultimately open, the internal bonds²⁵⁹ (observed in diamines).
- Solvent molecules insert into internal hydrogen bonds to form water bridges between the ionized and neutral polar groups (computational results in polyethers,¹⁵⁴ diketones,²⁴² amino acid derivatives,¹⁵⁰ and acetic acid/water clusters¹⁸³).
- Solvent molecules can facilitate the formation of salt bridges (computations on acetic acid/water clusters¹⁸³).
- Stepwise solvation and ionic aggregation can have comparable thermochemistry (thermochemical analysis of acetic acid/water clusters¹⁸³).

These interactions were confirmed subsequently in actual biological ions generated by ESI or MALDI methods. These studies include the stepwise solvation of protonated,^{348a,b} sodiated,^{348c} potassium,^{348d} and deprotonated amino acids,^{348e} as well as ionized peptides, proteins, and nucleotides and other ion–molecule interactions of biomolecules,^{12d,e} as reviewed in the following sections.

7.2.1. Stepwise Solvation of Amino Acids and Peptides and the Effects of Internal Solvation. We observed in early studies in protonated diamines that the internal hydrogen bonds can be weakened by external solvation and, conversely, bonding to solvent molecules is weakened by the internal hydrogen bonds.²⁵⁹ Similarly, the internal bond in the protonated dipeptide analogue ($\text{CH}_3\text{CO}-\text{Ala}-\text{OCH}_3$) $^+$ reduces the binding energy of this ion to H_2O to 13 kcal/mol, instead of the 16 kcal/mol expected from ΔPA correlations. This effect results because internal solvation provides the first solvent group and H_2O becomes in effect the second solvent molecule of the protonated group.¹⁵⁰ Similar relations may be expected in the stepwise solvation of ions of biomolecules.

The solvation of amino acids and derivatives was subject to early studies by PHPMS equilibrium studies^{150,374} and has been extended recently by Bowers and co-workers, applying ion mobility apparatus,^{347a,b} and by Wincel, applying electrospray ionization–PHPMS equilibrium studies to the solvation of protonated,^{348a,b} sodiated,^{348c} potassium,^{348d} and deprotonated amino acids.^{348e} The solvation of ValH^+ , GluH^+ , and MetH^+ and the (Ala-Ala) $^+$, (Glu-Met) $^+$, and (Met-Glu) $^+$ dipeptides by 1 and 2 H_2O molecules,^{348a} and of GlyH^+ , AlaH^+ , PheH^+ , and ProH^+ by 1–4 H_2O molecules,^{348b} was also studied. The binding energies of the ions to the first H_2O molecule are mostly 14.0–15.8 kcal/mol, except for GluH^+ with 13.1 kcal/mol.

The binding energies of $\text{GlyH}^+\cdot\text{H}_2\text{O}$, $\text{ValH}^+\cdot\text{H}_2\text{O}$, and $\text{ProH}^+\cdot\text{H}_2\text{O}$ were 15.4, 15.1, and 14.8 kcal/mol, respectively,^{348a,b} whereas ΔPA correlations for $\text{NH}^+\cdots\text{OH}_2$ bonds in Table 2 predict slightly higher binding energies of 17.8, 16.3, and 15.7 kcal/mol, respectively. In these systems weak internal bonds in the unsolvated ions, such as in GlyH^+ ,^{341b} may decrease slightly the H_2O binding energies, but the effects are within the error limits. Similar effects were observed also for the hydration of ArgH^+ and LysH^+ .^{347b}

The binding energy of PheH^+ , TrpH^+ , and TyrH^+ to the first H_2O molecules are also similar, 13.3, 13.2, and 13.6 kcal/mol, respectively, and decrease from ~11 to 7 kcal/mol for the second to fifth H_2O molecules. The protonated ammonium groups and the neutral carboxylic hydroxyl bond to the first H_2O molecule with similar strength. After filling the first solvation shell, further water molecules bind to the amino acid side-chain in tyrosine or start a second shell about the protonated amine groups.^{347a} With ArgH^+ and LysH^+ the binding energy of the first water molecule is smaller, 10.3 and 10.9 kcal/mol, respectively, due to internal hydrogen bonds in the ions. The binding energies of further water molecules decrease to 6–7 kcal/mol for the fourth and fifth water molecules, and the higher solvation steps form water bridges between the originally hydrogen-bonded functional groups. With the seventh water molecule the energies of the charge-solvated and salt-bridged structures become comparable.^{347b} The mutual effects of internal and external solvation in ArgH^+ and LysH^+ are similar to such effects observed earlier in protonated diamines.²⁵⁹

The binding energies of the first H_2O molecules to protonated amino acids are similar to the binding energies to protonated amines, and the binding energies of the subsequent H_2O molecules also decrease similarly stepwise in amines and amino acids. This suggests that the first water molecules solvate the protonated amine group, possibly with further hydrogen bonds to the carboxylic acid and other functional groups. With ProH^+ the first H_2O molecule binds to the neutral carboxylic acid OH group at low temperatures but transfers to the protonated amine function at high temperatures due to favorable entropy effects.^{348f} The binding energies of the first water molecule to the protonated amino acids correlates inversely with the gas-phase basicities,^{348b} and to deprotonated amino acids with the gas-phase acidities of the amino acids,^{348e} as expected from such correlations.

Kebarle and co-workers studied the hydration of protonated amino acids and small peptides. They found that the dissociation free energy, ΔG°_D , of $\text{Gly}_n\text{H}^+\cdots\text{H}_2\text{O}$ decreased from 9.8 to 8.8, 6.7, and 5.7 kcal/mol for $n = 1–4$, respectively, with increasing peptide size because of increasingly efficient internal solvation in the larger peptides,¹⁵⁵ similar to the trend found earlier in protonated diamines ($\text{H}_2\text{N}(\text{CH}_2)_n\text{NH}_2$) $^+$.²⁵⁹ Similarly, internal IHBs in LysH^+ and (Gly-Lys) $^+$ decreased the free energy of hydration by H_2O molecules.¹⁵⁵

Bowers and co-workers measured the H₂O binding energies of small protonated peptides as 7–15 kcal/mol. Small 2–3 residue peptides bonded water more strongly than larger peptides that are solvated more strongly internally.^{279b} Similarly, in protonated lysine containing peptides, *n* internal hydrogen bonds decrease the binding energy to water molecules similarly as *n* preceding water molecules bonded to a protonated amine group.^{279d}

Also, water molecules bind more strongly to peptides in higher charge states because of the higher charge densities of the binding protons and possibly because of their more extended, less internally solvated conformations.^{279b} In anions, the binding energy of the deprotonated (glycine–H)[–] and (alanine–H)[–] anions of 12 kcal/mol is expected for a free carboxylate anion.³⁴⁹ The solvation energies of the internally solvated deprotonated dipeptides, (Gly·Gly–H)[–], 11.0 kcal/mol, and (Ala·Ala–H)[–], 11.7 kcal/mol, are similar to this value,³⁴⁹ but internal solvation in the dipeptide anions (iIHBs) may weaken the bond to the first H₂O molecule. The binding energies of the next water molecules decrease, to 7.4 kcal/mol in (Gly·Gly–H)[–] and 7.1 kcal/mol for N(Ala·Ala–H)[–] where the first 4 H₂O molecules solvate primarily the anionic carboxylate function with one bridging IHB to the terminal amine group.³⁴⁹ The stepwise solvation of peptides was reviewed recently.³⁵⁰

7.2.2. Stepwise Solvation of Amino Acids and Peptides, and the Formation of Zwitterions and Salt Bridges. The formation of zwitterions is of long-standing interest. The internal and external solvation of the ionic groups, involving IHB interactions, is critical for forming zwitterions in amino acids and peptides. The question of how much solvation is needed to form zwitterions has been addressed by numerous workers. In GlyH⁺·*n*H₂O computations show that with *n* = 2 the zwitterion is higher in energy,^{351a} but with *n* = 3 it is comparable in energy to the nonzwitterion.^{351b}

Complexing by alkali metal cations, combined with hydration, also stabilizes zwitterions. For example, Williams and co-workers found from BIRD dissociation and water-binding energies that in ValLi⁺ and ValNa⁺ formation of a zwitterion requires 3–6 H₂O molecules.^{351c,d} The ValLi⁺·3H₂O zwitterion is stabilized by hydrogen bonds of 2 H₂O molecules to the protonated amine and the carboxylate functions of valine.^{351d} In GluLi⁺, GluNa⁺, and GluLi⁺(H₂O) the lowest energy isomers are nonzwitterionic whereas for GluNa⁺(H₂O) the nonzwitterionic and zwitterionic isomers have similar energies.^{351e} However, in contrast to the indirect BIRD evidence, the IR spectroscopy of ValH⁺ and ValLi⁺ suggested nonzwitterion structures upon solvation by up to 4 H₂O molecules.^{351f}

In ValH⁺·*n*H₂O the first 3 H₂O molecules hydrate the protonated amine group filling a solvent shell, whereas 4 H₂O molecules may form a cyclic water structure. In ValLi⁺·*n*H₂O the first H₂O is bonded to Li⁺ while further H₂O molecules are also hydrogen-bonded to each other and to the carboxylic Val oxygens.^{351f}

Similar to GluNa⁺, in LysLi⁺ the zwitterion is higher in energy by 6.9 kcal/mol, but in LysLi⁺·H₂O by only 1.7 kcal/mol, than the nonzwitterion form.^{351g} These examples illustrate that in favorable systems even solvation by 1 or a few water molecules can make the zwitterions comparable in energy to nonzwitterion isomers. The zwitterions are stabilized by water molecules by hydrogen bonding to the ionized groups and to each other.

In complexes of larger biomolecules zwitterions can form even in the absence of solvent molecules. For example, protonated

arginine dimer ArgH⁺(Arg), an increased binding energy compared with other amino acid dimers, suggested a zwitterion structure.³²⁹ Similarly, increased bond energies for complexes of protonated betaine (CH₃)₃NCH₂COOH⁺ with molecules of higher gas-phase basicity indicated a zwitterion structure with a strong ion–dipole interaction.³³⁰

For protonated bradykinine, a salt bridge between the protonated Arg groups and deprotonated C-terminal carboxylate anion was suggested by a decrease of the activation parameters for dissociation when the carboxylic acid was methylated.^{352a} For ArgH⁺(Arg),³²⁹ and for protonated bradykinin, ab initio calculations supposed that an internal ion–zwitterion (or salt-bridge) structure is the most stable conformation. For ArgH⁺(Arg) this was further confirmed by IRMPD spectroscopy, for a structure where the two protonated side-chain amine groups are hydrogen-bonded to the anionic carboxylic oxygens.^{352c}

In other peptides, zwitterions were not the most stable forms of polyglycine,³⁵³ but mobility studies suggested compact zwitterionic forms, stabilized by internal solvation, in the protonated (serine)₈H⁺ octapeptide.^{354a} In addition to solvation by water, the effects of nonaqueous solvents such as acetonitrile^{192b} and of amines on the relative energies of nonzwitterion and zwitterions isomers^{354b–h} were also studied. Although the zwitterion of glycine is higher in energy by 20–22 kcal/mol than nonzwitterionic glycine,^{354b} glycine and other amino acids can form zwitterions in protonated complexes with amines and amino acids.^{354c–f}

In such complexes, the binding enthalpies of GlyH⁺ with the first and second NH₃ molecules were 23.2 and 18.3 kcal/mol, and of (Gly)₂H⁺ with NH₃ was 19.1 kcal/mol. Computations showed that in GlyH⁺·NH₃ the proton shifts to ammonia although PA(glycine) is higher by 8 kcal/mol. The NH₄⁺·Gly dimer is stabilized by an IHB between NH₄⁺ and the carbonyl oxygen of Gly. However, such proton transfer does not occur in (Gly)₂H⁺·NH₃ where the proton is stabilized by the strong ionic hydrogen bond between the Gly molecules.^{354c,d}

In the complex with NH₄⁺ the glycine zwitterion and nonzwitterion are similar in energy, because the H₃⁺NCH₂COO[–]·NH₄⁺ hydrogen bond stabilizes the zwitterion.^{354c,d} More generally, in protonated complexes of amino acids GlyH⁺, AlaH⁺, ValH⁺, SerH⁺, and ProH⁺ with NH₃, CH₃NH₂, (CH₃)₂NH, and (CH₃)₃N, the stabilities of the zwitterions increase as the PA of the amino acid increases and decrease as the PAs of the amines increase.^{354e} Accordingly, the amino acid with a secondary amine, Pro, has an increased tendency to form zwitterions. Evidence for the (Pro(zwitterion)·CH₃NH₂)H⁺ complex was shown by the association enthalpy of 26.6 ± 0.5 kcal/mol in good agreement with the computed 25.7 kcal/mol for forming the Pro(Zwitterion)·CH₃NH₃⁺ complex, and also by IR multiphoton dissociation spectroscopy.^{354f}

Similarly to amines, interactions with a neutral amino acid molecule can stabilize zwitterions. This was not observed in (glycine)₂H⁺, but in (proline)₂H⁺ the zwitterions were present in equilibrium with conventional isomers, as shown by FEL IRMPD spectroscopy, with a 1396 cm^{–1} band of the symmetric stretching of the carboxylate group characteristic to gas-phase zwitterions.^{354g}

However, in contrast to earlier spectroscopy and computations, more recent IRMPD studies showed that protonated complexes of Val with alkylamines are not zwitterionic.^{354h} The

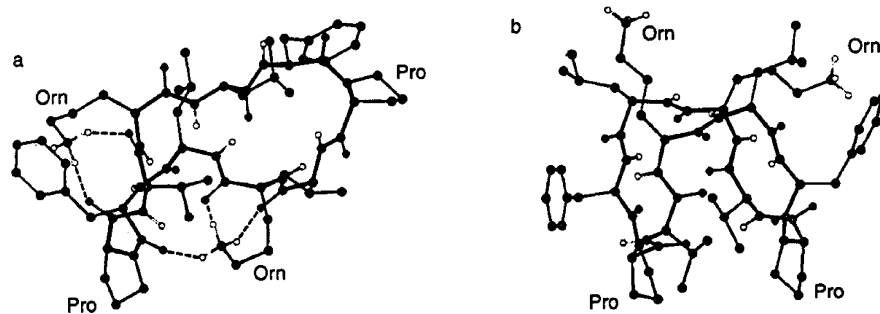


Figure 51. Representative low-energy structures of gramicidin S ($M + 2H$) $^{2+}$ ions in (a) a vacuum and (b) water obtained by molecular modeling using dielectric constants of 1.0 and 78, respectively. Intramolecular hydrogen bonding is indicated by dashed lines in the gas-phase ion. Reproduced from ref 328 with permission. Copyright 1997 Elsevier.

stabilization of zwitterions by protonated amines and amino acids, if confirmed, may help form zwitterions in biology.^{354c–g}

Both a $\text{COO}^- \cdots \text{H}_3\text{O}^+ \cdots \text{OOCCH}_3$ salt bridge in the $\text{CH}_3\text{COO}^-(\text{CH}_3\text{COOH})(\text{H}_2\text{O})_2$ cluster (Figure 36)¹⁸³ and a salt bridge in $(\text{Ala-Ala-Arg-Ala-Ala})\text{H}^+$ and in its $\text{Ac}-$ and $-\text{OMe}$ derivatives solvated by one H_2O molecule^{279c} serve as transition states in proton transfer. The salt bridge can also be the most stable structure, as in $\text{ArgH}^+(\text{Arg})$,^{329,352c} protonated bradykinine,^{352a} and $\text{ArgH}^+(7\text{H}_2\text{O})$ and $\text{LysH}^+(7\text{H}_2\text{O})$ clusters.^{347b}

7.2.3. Stepwise Hydration of Peptides. Jarrold and co-workers measured the binding energies of an H_2O molecule to protonated dipeptides, and their calculations found that both the unsolvated and solvated peptides have multiple conformations. The water molecule causes conformational changes by creating a bridge or by the loss of internal cation···π interactions.³⁵⁵

These workers also studied the effects of conformation, charge, and composition on binding a water molecule to alanine-based peptides. More association was found in globular peptides than in helical ones, and this difference was used to establish that the globular to helix transition occurs at eight residues.³⁵⁶

The ability to establish a network of hydrogen bonds to several different hydrogen-bonding partners emerged as a critical factor for the ability to bind water molecules. Another important factor is the shielding of the ionic site that binds the water molecule. For example, peptides containing a protonated histidine, the charge of which is delocalized and not shielded well, binds water more strongly than peptides that contain a protonated lysine, of which the localized charge is shielded more effectively.³⁵⁷

7.2.4. Thermochemical and Structural Effects of Stepwise Hydration. In conformationally extended multiply protonated ions, the separated ionized groups interact individually with solvent molecules. As models, the Kebarle group generated the diprotonated diamine ions $\text{H}_3\text{N}(\text{CH}_2)_p\text{NH}_3^{2+}$ in a high-pressure mass spectrometer source and measured the binding energies to water molecules. The results are illustrated in Table 4 above. The clusters $(\text{NH}_3^+(\text{CH}_2)_p\text{NH}_3^+)(\text{H}_2\text{O})_n$ for $p = 5–12$ and $n = 1–6$ showed hydration enthalpies larger by 2 kcal/mol than analogous protonated monoamines. For example, for $\text{NH}_3^+(\text{CH}_2)_6\text{NH}_3^+(\text{H}_2\text{O})$, $\Delta H^\circ_{0,1} = 17.3$ kcal/mol compared with 15.2 kcal/mol for the monoamine. The solvation enthalpies decrease slowly with increasing chain length p to 15.7 kcal/mol for $p = 12$. Extrapolating the curve of $\Delta H^\circ_{0,1}$ versus p suggests that, for $p = 1–4$, the bond energy may be

20–30 kcal/mol, much larger than that for singly charged ammonium ions.

These trends can be understood in terms of the Coulomb interaction between the protonated groups. In contrast to monoprotonated ions where $\Delta H^\circ_{n-1,n}$ decreases monotonically with n , in the diamines the binding of the first and second, third and fourth, and fifth and sixth H_2O molecules are comparable, showing that the water molecules attach alternately to the protonated end-groups and each has little effect on the charge densities on the other end group.⁹⁵

Going to actual proteins, in $(\text{gramicidin S} + 2\text{H})^{2+}(\text{H}_2\text{O})_n$, electrospray produces clusters with up to 50 H_2O molecules. In this molecule, two protonated ornithine residues can hydrogen bond to carbonyl oxygens of the peptide backbone as shown in Figure 51. The internal hydrogen bonds are displaced by external solvation when about 24 or more water molecules solvate each protonated group, and the ion assumes a structure similar to that in solution.³²⁸ At electrospray capillary temperatures of 435–455 K where some solvent from the clusters evaporates, magic numbers are observed at $n = 8, 11$, and 14 , which indicate particular stability. Solvation by <6 H_2O molecules was insufficient to displace the internal bonds, and these clusters had low abundances, while a magic number at 11 H_2O molecules indicated a water bridge. A magic number at $n = 40$ H_2O molecules suggested that two water clathrates of 20 molecules attach to the protonated ornithine groups, opening up the folded unsolvated structure.³⁵⁸ The magic numbers are due to the solvation of charged ornithine residues by 3–4 H_2O molecules and the formation of additional $-\text{NH}^+\text{OH}_2 \cdots \text{OH}_2 \cdots \text{OC}^-$ solvent bridges. At higher capillary temperatures, the unsolvated ions dominate as each protonated ornithine side chain becomes internally solvated by three peptide CO groups.³²⁸ Internal solvation is even more efficient in the singly protonated ion, where the absence of Coulombic repulsion allows optimal folding and 5 amide CO groups solvate the protonated ornithine amine group, causing an increase in the gas-phase basicity to >243 kcal/mol, compared with 222.5 kcal/mol for an isolated ornithine residue.¹⁶

Jarrold and co-workers examined protein hydration using ion mobilities in a drift cell. Attachment thermochemistry of the first solvent molecule to the 58-residue bovine pancreatic trypsin inhibitor ($\text{BPTI} + 6\text{H}$) $^{6+}$, $\Delta H^\circ_{0,1} = -21.3$ kcal/mol and $\Delta S^\circ_{0,1} = -62$ cal/(mol K), indicates four IHBs of the first H_2O molecule to cysteine and tyrosine residues, which can order the formation of a pocket, resulting in a large conformational constraint. The 5 further H_2O molecules have $\Delta H^\circ_{n-1,n}$ of -13 to -16 kcal/mol and entropy changes, $\Delta S^\circ_{n-1,n}$ of -38 to

$-42 \text{ cal}/(\text{mol K})$, close to the values for the initial hydration of solid protein films. Some of these may be the 3 structural H_2O molecules that are known to form a cluster hydrogen-bonded to 5 amino acid residues.¹³

Further, binding free energies in solvated (*cytochrome c + nH*)ⁿ⁺(H_2O)_m with a broad distribution of charge states showed that the $\Delta G^\circ_{n-1,n}$ (271 K) values for solvation by 1–5 H_2O molecules are -4.5 to -3.6 kcal/mol for the $+5$ state and -3.6 to -3.4 kcal/mol for the $+7$ state, showing stronger solvation for the lower charge state.³⁵⁹ The results show that, at 253 K and $P(\text{H}_2\text{O}) = 0.73$ Torr with an increase in charge state from 4 or 5 to 7–13, the conformation opens from folded to linear and the number of solvent molecules decreases from ~ 50 to ~ 30 . These data show that the lower charge state folded conformation is better solvated, probably because of cooperative effects, such as multiple IHBs to water molecules in pockets and water bridges between charged groups. The $+7$ charged state requires 29 water molecules for partial folding. Apomyoglobin gave similar results.³⁶⁰

Internal solvation of the charged group was also indicated by molecular dynamics simulation of the 9-residue protonated bradykinin.^{361a} The first results on the internal and external solvation of protonated peptides and proteins were reviewed recently.^{361b}

These studies illustrate that the gas-phase hydration of biological ions can identify and quantify the role of water biological structure. External solvation can also favor the formation of salt bridges. For example, the pentapeptide (Ala-Ala-Arg-Ala-Ala) H^+ and its Ac- and $-\text{OMe}$ derivatives are internally solvated, but adding a H_2O molecule facilitates a salt-bridge structure that can serve as a transition state for H/D exchange in a relay mechanism.^{279c}

The gas-phase solvation of biological ions can form isomers with similar energies in a population of mixed isomers, as demonstrated in the association (glycine- H)⁻ anions with H_2O , CH_3OH , and $\text{C}_2\text{H}_5\text{OH}$ molecules. Accounting for the isomeric populations leads to a close agreement between the experimental and computed thermochemistry.^{361c}

7.3. Intermolecular Association and Polydentate Bonding in Biological Ions

Biomolecules associate in many natural processes. The complexes may involve simple IHBs or internal, external, and multiple IHBs. In simple biomolecules, protonated dimer ions of amino acids were studied by PHPMS and BIRD methods. Recent PHPMS and BIRD thermal photodissociation showed bonding energies of 26–28 kcal/mol in several amino acid dimer ions and amino acid methyl ester ions.^{18,329,352b,c,362a-d,363} These bonding energies are similar to protonated amine dimer ions,³⁹ suggesting that the amino acid dimer ions are also bonded by a single IHB. Figure 52 shows the structures of these dimers.¹⁸ For example, the lowest-energy isomer of $(\text{Gly})_2\text{H}^+$ is bonded by an IHB between a protonated amine group of GlyH^+ and the carbonyl oxygen of Gly. They also suggest that internal hydrogen bonding does not affect the bond strength of the dimers.

In somewhat more complex systems we observed complexes of polyprotic ions such as MeNH_3^+ with the dipeptide-like MeCO-Ala-OMe molecule. Table 9 shows that, compared with a monoprotic Me_3NH^+ ion, which can form only one IHB, the binding energy of the polydentate complex with MeNH_3^+ increases from 29.7 to 40.1 kcal/mol and the complexation entropy changes from -27.6 to $-35.1 \text{ cal}/(\text{mol K})$.¹⁵⁰ Dimers

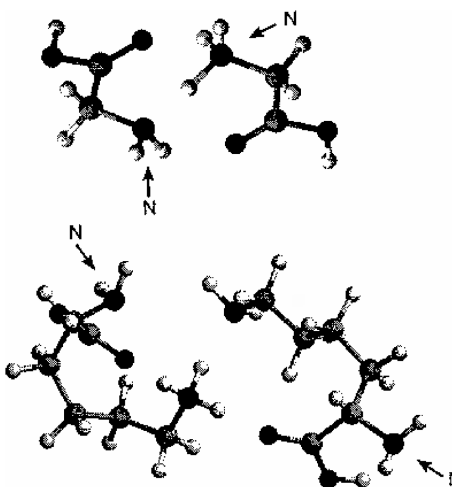


Figure 52. Protonated dimers of glycine and lysine. Reproduced from ref 18 with permission. Copyright 1997 American Chemical Society.

of protonated and neutral MeCO-Ala-OMe were also measured by BIRD thermal photodissociation.³⁶³

In dimers of dipeptides, a dissociation energy of 24.3 kcal/mol was calculated for $(\text{Ala-Ala}-\text{H})^- \cdots (\text{Ala-Ala})$ dissociating to the components in their minimum-energy conformations, but $\sim 35 \text{ kcal/mol}$ was calculated if the components separate and retain the same geometries as in the dimer. The latter agreed with the experimental activation energy for dissociation, suggesting a dimer-like transition state.³⁴⁹ The complexing energy of the deprotonated $(\text{Gly-Gly}-\text{H})^-$ and $(\text{Ala-Ala}-\text{H})^-$ by the respective neutral dipeptides was found to be comparable to solvation by 4 H_2O molecules.

The binding energy of the dimer of the pentapeptide leucine enkephalin, $(\text{YGGFL})_2\text{H}^+$, was equated to the 46.5 kcal/mol activation energy for its thermal dissociation ($k_{507} = 24.5 \text{ s}^{-1}$) in the electrospray capillary.³⁶⁴ This large binding energy and an unusually large $\log A = 21.7$ ($\log \text{s}^{-1}$), due to a high-entropy transition state, suggest a constrained multiply bonded dimer, but the complex desolvation/dissociation processes in electrospray makes these values only approximate. The same rate coefficient, using a more conventional $\log A = 17.2$ obtained from a blackbody IR dissociation (BIRD), gives an activation energy, $\Delta H^\circ_D(E_a)$, of 36.6 kcal/mol, in very good agreement with the $\Delta H^\circ_D(E_a)$ of 36.9 kcal/mol from the BIRD study of this dimer.³⁶⁵ These binding energies are stronger than that for a single IHB, especially if it is weakened by internal solvation in the protonated monomer. The results therefore indicate multiple IHB interactions.

The dissociation energies of alanine and glycine peptides were also studied using thermally activated dissociation kinetics. Activation energies and entropies were determined for dissociation of the diprotonated $\text{Ac-(GA)}_2\text{K} \cdots \text{Ac-A(GA)}_2\text{K} + 2\text{H}^+$ (Ac = acetyl, G = glycine, A = alanine, and K = lysine) dimer with the dominant conformation of a V-shaped helical dimer and for the dissociation of the $(2\text{Ac-(GA)}_2\text{K}) \cdots \text{Ac-A(GA)}_2\text{K} + 3\text{H}^+$ pinwheel-shaped helical trimers. The activation energies were 22 kcal/mol for the dissociation of the dimer and 17 and 18 kcal/mol for the trimers. The mobility method yielded high-pressure limiting activation energies that may be equated with the intermolecular bonding energies. In addition, the mobility also yields information on the conformations of the dissociating complexes. Therefore, ion mobility may be the method of

choice for measuring bonding energies based on dissociation of adducts.^{366a}

Ion mobility was applied also to the association of protonated polyalanine peptides. Mixtures of helix-forming monomers were found to form V-shaped helical dimers and pinwheel-shaped helical trimers tethered together by lysine residues and stabilized by cooperative interaction of the combined charge with the helix dipoles. Mixtures of globular monomers were found to form mainly globular multimers.^{366b} The first results on unsolvated and partially solvated proteins and peptides were reviewed recently.^{361b}

Polydentate bonding was proposed in reaction intermediates. Beauchamp and co-workers studied H/D exchange between polyglycine and D₂O and proposed two polydentate IHB structures, NH₃⁺···OD₂···OC⁻ → -H₂N···HDO···H⁺OC⁻, as a relay mechanism for the H/D exchange reaction. They also studied exchange reactions with ND₃ and found a mechanism suggestive of a -H₂N···NH₄⁺···OC⁻ complex. These authors also examined zwitterionic salt bridges in oligopeptides and presented evidence for a salt bridge in the IHB complex between protonated betaine and ND₃ in the reaction (CH₃)₃N⁺CH₂COOH···ND₃ → (CH₃)₃N⁺CH₂COO⁻·HND₃.³⁴⁰

Intermolecular association of larger protonated and deprotonated protein–ligand complexes was studied by Klassen and co-workers in numerous systems, using black-body infrared radiative dissociation. Various intermolecular interactions are possible in these large complexes, and hydrogen-bonding contributions were identified in some cases. For example, hydrogen bonds were identified in complexes of a single-chain variable fragment monoclonal antibody Se155-4^s with its native trisaccharide ligand Galα[Abe]Man involving the His^{101H} residue and Man C-4 OH group,^{367a} and in multiply protonated +10, +11, and +12 charge-state complexes of a single-chain variable fragment of the monoclonal antibody Se155-4^t with trisaccharide ligands,^{367b} as well as in complexes of a cationic protonated single-chain fragment of a monoclonal antibody and a trisaccharide ligand,^{367c} and anionic deprotonated complexes of β-lactoglobulin–fatty acid (7-) ions.^{367d} Evidence for the hydrogen-bonding interactions were obtained in these experiments from substitution of hydrogen-bonding amino acids with other amino acids.

Conformational changes, aggregation, solvation, and noncovalent supramolecular association of complex ionized biomolecules have been studied by ion mobility mass spectrometry by Bowers and co-workers.^{367e,f} Ionic hydrogen bonds must be significant in these processes, but identifying and quantifying these bonds is usually not possible in these complex systems.

7.4. Ionic Hydrogen Bonds in Nucleic Bases, Nucleosides, and Nucleotides

Nucleic bases are strong intrinsic acids and bases. The acidities are enhanced by the presence of multiple nitrogen atoms in the rings, and these molecules are as acidic as possible without undergoing acid dissociation in the DNA interiors. These acidic hydrogens can serve as strong hydrogen-bond donors in both ionic and neutral hydrogen bonds.^{68,69} Correlations between intrinsic acidities and hydrogen-bond energies suggest that ~1 kcal/mol, or 20%, of the hydrogen-bond strengths between DNA base pairs may be contributed by the enhanced acidities of the nucleic bases. Without this factor DNA base pairs may not be stable under biological conditions. These enhanced

hydrogen-bond strengths may explain why heterocyclic molecules with multiple nitrogen atoms encode genetic information through hydrogen bonding.^{368a} The nucleic bases are also strong bases in the gas phase, with possible tautomers protonated on the ring or on substituents.^{368b} However, in solution their enthalpies of protonation are attenuated by 32 kcal/mol more than the solvation effect on the enthalpy of protonation of ammonia.

In the gas phase, their protonated ions can form strongly hydrogen-bonded dimers, and the increased ΔH°_D and ΔS°_D of the dimers versus (pyridine)₂H⁺ indicates two hydrogen bonds bind (adenine)₂H⁺ and (thymine)₂H⁺ and three bonds bind (cytosine)₂H⁺, in planar bonding arrangements similar to the neutral base pairs.^{280a}

In complexes with ammonia, computations showed that the proton is transferred to ammonia partially in NH₄⁺···cytosine and fully in the NH₄⁺···uracil and NH₄⁺···thymine complexes, although the PA of ammonia is lower than that of the nucleic bases. The NH₄⁺ ion is stabilized in the complexes by hydrogen bond to carbonyl oxygens. However, in NH₄⁺···adenine that does not contain oxygen, the proton remains on an adenine ring nitrogen. In NH₄⁺···thymine and NH₄⁺···uracil the ammonia proton transport catalysis may facilitate conversion between tautomers protonated at various sites. The thermochemistry yields binding energies of 44.7, 28.6, and 32.8 kcal/mol between NH₄⁺ and cytosine, thymine, and uracil, respectively.^{368b} These binding energies agree with correlations between the proton affinities and IHB energies.^{48,368b}

Beyond nucleic bases, electrospray and matrix-assisted laser desorption ionization (MALDI) allow gas-phase studies of nucleotides and polynucleotides, whose conformations are affected by ionic hydrogen bonds, as found by Bowers and co-workers using ion mobilities and computation.^{369a–c} In deprotonated mononucleotides, hydrogen bonding occurs between a sugar OH group and the anionic phosphate oxygen, whereas in protonated mononucleotides, in dAMP⁺ it occurs between a protonated ring nitrogen and a phosphate oxygen and in dTMPH⁺ it occurs between the protonated phosphate and a ring oxygen.^{369b}

In thymine–guanine deprotonated dinucleotides dTG⁻ and dGT⁻, in π-stacked conformations, hydrogen bonding occurs between the -NH₂ group of guanine and a carbonyl oxygen in thymine, and in open conformations, it occurs between a phosphate oxygen and a sugar OH group.^{369a} A survey of the conformations of all 16 possible deprotonated dinucleotides showed open and folded conformations with isomerization barriers of 0–5 kcal/mol. The degree of hydrogen bonding in a given conformation was the primary determinant of the energy.^{369a}

The conformations of trinucleotides were also examined by ion mobilities and showed nonzwitterionic and zwitterionic isomers, with various hydrogen-bonding interactions.^{369c} The bonding in deprotonated nucleotide dimers were also investigated by BIRD thermal dissociation. The results showed that the dissociation energy in the guanosine–cytosine dimer anion is much higher than in other combinations, suggesting that Watson/Crick base pairing is maintained in the gas phase. Further, the dissociation energies of doubly deprotonated oligonucleotide heptamers were also studied, and the activation energies were found to depend on the identity of the leaving nucleic base.^{370,371a}

The stepwise solvation of ionized nucleotides, nucleic bases, and nucleosides was also investigated.^{371b,c} On the basis of the correlations between proton affinities and hydrogen-bond

energies, the stepwise solvation energies are expected to be similar to those of protonated pyridine and alkylpyridines, about 12–14 kcal/mol for the first water molecule and 8–11 kcal/mol for the second to fourth water molecules.^{40a,62b} In fact, the binding energies of the first water molecules to the protonated nucleic bases were all similar, 12.4–13.1 kcal/mol, and those of the second water molecule were 11.2–11.5 kcal/mol, whereas for protonated nucleosides, the binding energies of the first water molecules were 11.7–13.3 kcal/mol.

The binding energies of the first water molecule to the deprotonated anionic nucleotides were between 10.1 and 11.5 kcal/mol, bound to phosphate, and for further water molecules ($n = 2–4$), all were ~9 kcal/mol, bound to phosphate or various sites. Binding energies of the first water molecule for the protonated mononucleotides were from 10.5 to 13.5 kcal/mol, bound to the charged groups, except in the self-solvated dAMP H^+ , and for further water molecules were from 8.1 to 9.7 kcal/mol, bound to various sites.^{371b}

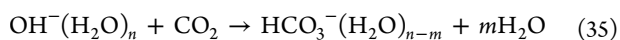
In summary, a rapidly advancing literature deals with biological ions in the gas phase. The interactions are similar to those observed earlier in model organics: internal and external solvation in which IHBs play significant roles; the presence of isomeric structures with comparable energies; association of ions and molecules through multiple IHBs; and the formation of solvent bridges. The advent of electrospray allows measurement of the thermochemistry of these interactions in the gas phase. These studies give insight into fundamental bioenergetics, such as the interrelations between internal and external solvation and their effects on conformation. The energy contributions of specific IHBs cannot be determined directly, but they can be estimated from cluster models as described in the next sections.

7.5. Cluster Models of Bioenergetics

Many biological processes are controlled by ionic intermediates. The intermediates may be stabilized by hydrogen bonds to polar groups in proteins more than they are stabilized by water. This decreases the activation energies of reactions through these intermediates.³²³

Cluster models can help to quantify these interactions. Both clusters and protein interiors are unsolvated or partially hydrated environments. In both environments, peptide amide NH groups are strong acids and CO groups are strong bases, which allows them to form strong IHBs. Cluster models allow evaluation of these contributions, keeping in mind that the geometrical constraints of biopolymers and the surrounding dielectric solvent are absent in the model clusters and the large biomolecules are replaced by more simple molecules.

7.5.1. Enzymatic Hydration of CO_2 . In a reaction catalyzed by carbonic anhydrase, OH^- reacts with CO_2 to produce HCO_3^- with a rate constant of $7.5 \times 10^7 \text{ M}^{-1} \text{ s}^{-1}$ (or $1.2 \times 10^{-13} \text{ cm}^3 \text{ s}^{-1}$), faster by about 4 orders of magnitude than the reaction in aqueous solution, where $k = 8.5 \times 10^3 \text{ M}^{-1} \text{ s}^{-1}$. The catalytic mechanism was proposed to strip the OH^- from its solvation sphere, assuming that the desolvated ion is more reactive.³⁷⁵ To test this proposal, Yang and Castleman³⁷⁶ examined the reactions of the IHB-bonded clusters $\text{OH}^-(\text{H}_2\text{O})_n$ with CO_2 . They observed mostly dissociative reactions (eq 35).



For combinations of $n = 0–5$ and $m = 0–3$, the reactions are exothermic by 34–88 kcal/mol, with the exothermity somewhat decreasing with increasing size n and with increasing

dissociation m . Rate coefficients, measured at 130 K where large clusters are stable, were found to decrease with increasing cluster size and became slow, below $0.80 \times 10^{-10} \text{ cm}^3 \text{ s}^{-1}$, that is, collision efficiencies below 0.1, for $n > 10$, as shown in Figure 53. However, at low solvation, the reaction becomes

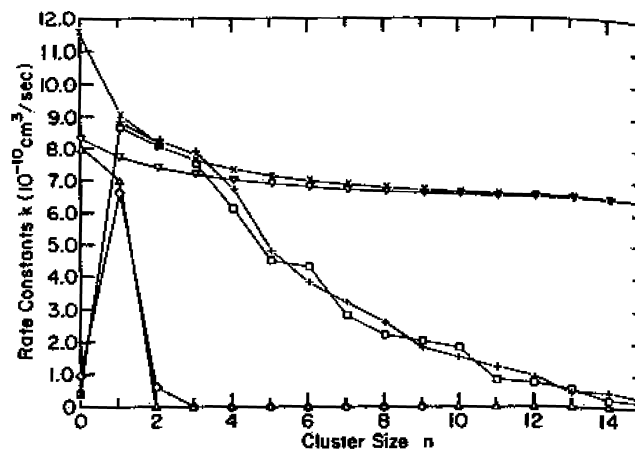


Figure 53. Rate constants of the reaction $\text{OH}^-(\text{H}_2\text{O})_n + \text{CO}_2 \rightarrow \text{HCO}_3^-(\text{H}_2\text{O})_{n-m} + m(\text{H}_2\text{O})$ as a function of solvation. Reproduced with permission from ref 376. Copyright 1991 American Chemical Society.

faster and approaches unit collision efficiency. This supports the proposed role of the enzyme to provide an environment where the OH^- ion is only partially solvated.

7.5.2. Enzyme Energetics: Ionic Hydrogen Bonds to Backbone Peptide Links. Proteolytic enzymes such as trypsin dissociate the peptide bonds of substrates. The active site is illustrated in Figure 54. Four IHB interactions are present in the resting state in Figure 54a. Two of these are $\text{COO}^- \cdots \text{HNimidazole}$ and $\text{COO}^- \cdots \text{HOR}$ bonds that can be modeled by the bonding of CH_3COO^- to imidazole and CH_3OH , respectively. The bonds between RCOO^- and protein amide NH groups are modeled by the bonding of CH_3COO^- to the amide NH function in the dipeptide analogue $\text{CH}_3\text{CONHCH}(\text{CH}_3)\text{COOCH}_3$ (i.e., $\text{CH}_3\text{CO-Ala-OCH}_3$), with a bonding energy of 30.2 kcal/mol for the first and 21.2 kcal/mol for the second molecule. Considering the mutual effects of the ligands, the total IHB interaction in the resting state is estimated as 65 kcal/mol.¹⁸⁷

The essential step is proton transfer from a serine OH group to imidazole that creates an anionic “tetrahedral intermediate”. This intermediate can hydrogen bond to NH groups of neighboring protein amide links (right-hand side of Figure 54b). The hydrogen bonds in the resting state and transition state are modeled by the cluster interactions shown in Figure 54c. Interactions in the $\text{CH}_3\text{COO}^- \cdot \text{CH}_3\text{CO-Ala-OCH}_3$ complex suggest that these additional hydrogen bonds of the tetrahedral intermediate to the peptide backbone amide groups can contribute a driving force of 32 kcal/mol to the formation of the transition state. Additional driving force is provided by the formation of the salt bridge between the (imidazole) H^+ cation and a carboxylate group. The strong IHBs between the amide NH groups and carboxylate ions result from the large intrinsic acidities of the protein amide groups.^{368a}

7.5.3. Formation of Biological Membranes. Figures 38 and 39 showed that the formation of $\text{RCOO}^- \cdots \text{HOOCR}$ bonds between ionized and neutral carboxylic acids is more exothermic than the formation of other types of IHBs.¹⁸³

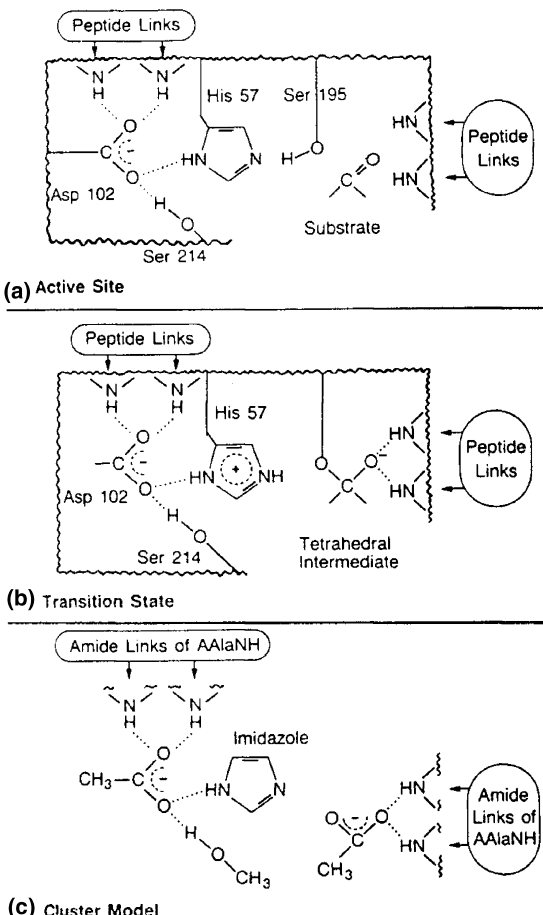


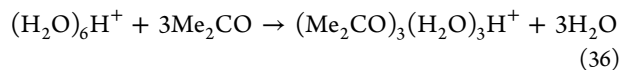
Figure 54. Panel (a) depicts the resting state of the active site of trypsin with four IHB bonds. Panel (b) depicts the reactive intermediate with a salt bridge and new IHBs to the peptide backbone. Panel (c) shows a cluster model of the active site. The ionic hydrogen bonds to the peptide backbone are represented in the model by bonds to amide groups in the dipeptide analogue $\text{CH}_3\text{CO}-\text{Ala}-\text{OCH}_3$, that is, $(\text{CH}_3\text{CONHCH}(\text{CH}_3)\text{COOCH}_3)$. Reproduced with permission from ref 187. Copyright 1988 American Chemical Society.

The exothermicity reflects the formation of a strong $\text{RCOO}^- \cdots \text{HOOCR}$ bond while displacing a weak $\text{RCOO}^- \cdots \text{H}_2\text{O}$ bond. Membrane formation in solutions of carboxylic acids would be favored when such IHB networks can form, when both ionized and neutral carboxylic groups are present at pH values near the pK_a of the acids.¹⁸³ This was indeed observed in the formation of membrane-bound vesicles from C_8 and higher carboxylic acids. The addition of alcohols also facilitated membrane formation, presumably because the ROH groups can also hydrogen bond strongly to the RCOO^- functional groups. The cluster data can therefore explain why carboxylate functions are efficient for forming membranes in solution.³⁷⁷

7.5.4. Proton Transport in Membranes. The membrane channel in gramicidin is spanned by a water chain that conducts protons by a fast “hopping” mechanism through shifting $\text{OH}^+ \cdots \text{O}$ bonds. This mechanism raises some interesting questions. How can the proton, well solvated in water, enter the less efficient, two-dimensional water chain? How can it move across the chain without being trapped by the surrounding protein amide groups that are strong bases?

In the protein channel, the proton is stabilized by strong ionic hydrogen bonds between the protonated water chain and the surrounding peptide amide CO groups. Proton entry from

aqueous solution is simulated by transfer from neat water clusters to mixed acetone–water clusters as in reaction 36.



Cluster thermochemistry shows that this reaction is exothermic by 19 kcal/mol due to the stabilizing effects of the strongly basic polar CO groups. The amide CO groups in the membrane may facilitate similarly the entry of protons from bulk water.

The mixed clusters of water and blocked ligands discussed above, such as the thermochemistry of acetone/water clusters, suggest that a central H_3O^+ unit is surrounded by more basic Me_2CO molecules. The central proton is stabilized by opposing attractions of the surrounding dipoles.

Similarly, the protonated water chain can bridge between the amide CO groups of the protein, and the proton can remain in the water chain due to the opposing attractions of the surrounding protein amide dipoles. In protonated diketone/water clusters, the second H_2O molecule showed anomalously strong bonding, and ab initio calculations showed that this is due to a $\text{H}_3\text{O}^+ \cdots \text{H}_2\text{O}$ bridge between the polar groups. Similarly, the proton remains in the water chain in the membrane due to the balance of opposing dipoles of more basic protein amide groups. The proton can be transferred between the polar groups with an energy barrier of only a few kcal/mol by shifting bonds in the $\text{H}_3\text{O}^+ \cdots \text{H}_2\text{O}$ bridge.²⁴²

As discussed above, the proton in clusters can remain in a water core even when it is surrounded by more basic blocked ligands. Links surrounding a water chain in a protein channel can facilitate the entry of a proton from solution, allow the proton to remain in the water chain, and provide a low-energy bridged pathway for proton transport.

7.5.5. Acetylcholine Neuroreceptors. Acetylcholine (ACh^+) is a neurotransmitter cation in which a quaternary amine group and an ester group can form an intramolecular hydrogen bond (Figure 55). To reach the receptor site, the ACh^+ molecule must enter from aqueous solution to a 20 Å deep groove lined with aromatic residues and transit this groove. The quaternary amine group of ACh^+ can interact by $\text{CH}^+ \cdots \pi$ hydrogen bonds with aromatic residues that line the groove. These bonds must stabilize acetylcholine sufficiently to allow entry from water where it is fully solvated, but they must interact weakly enough to avoid trapping it. Comparison between solvation by H_2O or the aromatic groups is made possible by the energetics of the $\text{ACh}^+(\text{H}_2\text{O})$, $\text{ACh}^+(\text{C}_6\text{H}_6)$, and $\text{ACh}^+(\text{C}_6\text{H}_5\text{CH}_3)$ complexes. All have weak bonding energies of 9.0, 8.6, and 9.5 kcal/mol, respectively. This suggests that the aromatic residues provide stabilizing interactions similar to that of water. This allows acetylcholine to enter the groove in the receptor lined by aromatic groups, and this allows the reactions to proceed.¹²⁴

Ab initio calculations supported the existence of an internal bond in ACh^+ . This internal bond may be weakened by hydration when the ion is in water. With two H_2O molecules, the formation of a solvent bridge favors the open conformation shown in Figure 55a in solution. Upon desolvation, acetylcholine can form an internally hydrogen-bonded conformation shown in Figure 55b that is stabilized by about 4.5 kcal/mol compared with an open conformation. This internal solvation and nonconventional $\text{CH}^+ \cdots \pi$ bonds with the aromatic residues in the channel can compensate for the loss of aqueous solvation when the ion enters the channel. The aromatic groups

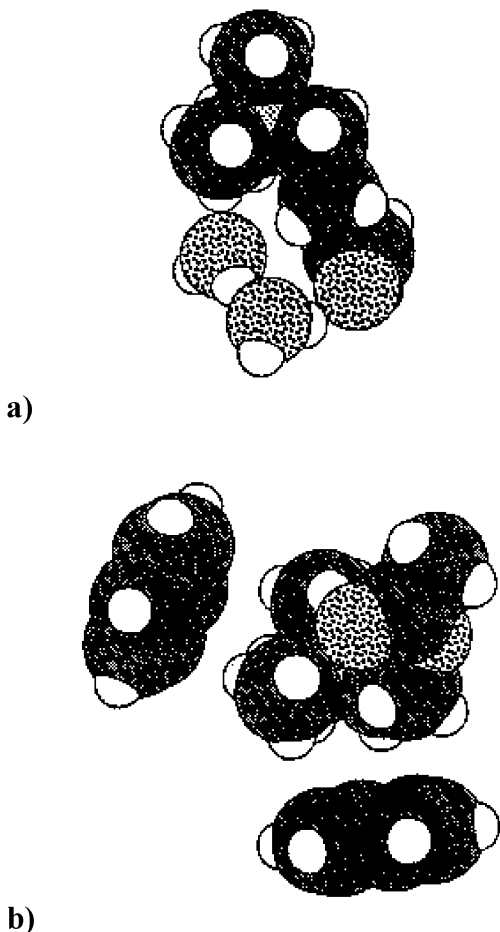


Figure 55. Panel (a) shows the open isomer of acetylcholine bridged by two water molecules. Panel (b) shows the internally hydrogen-bonded structure of acetylcholine interacting with two benzene molecules. The clusters simulate the conformational change of acetylcholine upon entry from water into a groove lined by aromatic residues in transit to the neuroreceptor. Reproduced from ref 124 with permission. Copyright 1999 American Chemical Society.

can also lower the energy barrier to the formation of the all-trans ACh⁺ conformation required at the receptor site.¹²⁴

In summary, cluster models provide the energetics of specific ion–neutral interactions in enzymes, membranes, and neuroreceptors, which cannot be measured in the complex biological systems themselves. These models show that polar protein groups can form strong IHBs with ions, which facilitate reactions that proceed through ionic intermediates.

8. IONIC HYDROGEN BONDS IN THE CONDENSED PHASE

Parallel with the gas-phase IHB studies, IHBs in solution also have been investigated, and the subject was reviewed.^{32b,c} The subject was investigated especially by the group of George Zundel, using IR continuum absorption to identify IHB networks. These studies show that many IHB effects in the gas phase have analogies in solution. The work was reviewed recently.³⁷⁸ This section will summarize solution results that parallel the gas-phase behavior.

8.1. Dimers, Intramolecular Bonds, and IHB Chains

8.1.1. Homodimers and Heterodimers. The first studies dealt with homoconjugated hydrogen bonds (i.e., symmetric

dimers or homodimers) in membranes of polystyrene sulfonic acid. Upon hydration, these solutions showed an IR continuum absorption between 1800 and 3400 cm⁻¹ due to the release of a proton and the formation of the H₅O₂⁺ ion.³⁷⁹

Observations with other concentrated acids showed that this absorption band develops when 2 or more H₂O molecules are available per free proton, confirming the H₅O₂⁺ assignment.³⁸⁰ The continuum absorption was assigned to fast proton fluctuation between the two H₂O components. Calculations identified a double minimum proton potential in the IHB, where a small potential can admix the ground and first excited states and allow rapid proton motion between the minima (about 10¹³ Hz), leading to a polarizability larger by 2 orders of magnitude than normal electron polarizabilities.³⁸¹ This assignment was confirmed by field and salt effects and temperature and deuteration effects.^{382,383} The absorption continuum requires interaction with the polar solvent. If the IHB is polarized by local fields, the proton polarizability decreases considerably.

Symmetric OH⁺···O bonds were found in solution of alcohols, NH⁺···N bonds in imidazole, and OH···O⁻ bonds in H₃O₂⁻ in concentrated aqueous KOH and in CH₃OK/CH₃OH. Similar to the gas phase, the IR studies showed intramolecular IHBs in ionized polyfunctional molecules, such as in protonated diamines and deprotonated diols.

In the gas phase, the IHB bond strength in alkylpyridine homodimers was 24 ± 1 kcal/mol, independent of alkyl substitution and of the basicities of the monomers. Similarly, in solution, the barriers, force constants, proton polarizabilities, and barriers of proton vibration and the bonding strengths were found to be independent of the pK_a for protonated pyridine homodimers.

Heteroconjugated bonds of the type OH···N → O⁻···H⁺N were also observed in solution, for example, in interactions of carboxylic acid and phenol donors with nitrogen base acceptors. In analogy with the gas-phase relations between PA differences and bond strengths, these condensed-phase systems can be viewed as heterodimers in which the extent of proton transfer and the bond strength depend on the proton affinity difference of the O⁻ and N proton acceptors (or the pK_a difference of the OH and NH⁺ donors). In fact, it was shown that the gas-phase $\Delta H^{\circ D}/\Delta PA$ correlations can be extended continuously to these pairs, even though the gas-phase ΔPA values of the O⁻ and N acceptors extend over 100 kcal/mol.^{384,385} In solution, the free energy required to form the ionized forms is much smaller (ΔG° proton transfer = 1.0–3.2 kcal/mol) because of the solvation of the ionized forms. Polar solvents, especially water, shift the proton transfer equilibria in the hydrogen bonds strongly to the charge-separated forms^{386a} and, in the extreme, can dissociate the hydrogen bonds,^{386b} similar to the weakening of IHBs in the gas phase by solvent molecules.

8.1.2. Intramolecular and Polydentate Bonds. In parallel to the gas phase, intramolecular IHBs were demonstrated by IR absorption continuum in OH···O⁻ bonds in diols,³⁸⁷ NH···N⁻ bonds in diamines,³⁸⁸ OH⁺···O bonds in protonated dinitroso compounds,³⁸⁹ and NH⁺···N bonds in protonated dipyradinyll alkanes.³⁹⁰

The IR spectra showed a polarizable proton that can move among several minima in protonated crown ethers,³⁹¹ consistent with polydentate complexing of the proton. However, the proton became fixed when it was complexed by an amine group.³⁷⁸

These observations are consistent with the polydentate complexing of the proton and the hydronium ion by crown

ethers and polyethers in the gas phase. The IR evidence leaves open the possibility that in solution also a H_3O^+ ion or a protonated structure with several H_2O molecules and a proton, rather than the proton itself, is complexed by the ethers. This can add further polarizability to the proton.

Polarizable bonds where the ion can move between several minima are also observed in systems where metal ions such as Li^+ , Na^+ , or K^+ replace H^+ in the bond.^{392–396a} Hydrogen-bond networks in bulk water rearrange on picosecond time-scales, at rates that are affected by the proximity of ions. For example, network randomization slows from 2.6 ps in pure water to 6.7 ps in 6 M NaBr solution.³⁹⁶

8.1.3. Hydrogen-Bond Chains. Theoretical studies of proton shifts in multiple-minima IHB systems in $\text{HCOO}^- \cdots \text{H}_2\text{O} \cdots \text{HCOOH}$ chains found increasing proton polarizability with increasing hydrogen bond chain length.^{397–399} These systems are similar to the $\text{CH}_3\text{COO}^- \cdots \text{H}_2\text{O} \cdots \text{H}_2\text{O} \cdots \text{CH}_3\text{COOH}$ clusters that were investigated in the gas phase experimentally and theoretically.¹⁸³

Hydrogen-bond chains can form also intramolecularly between several substituents on the same molecule. For example, evidence for large proton polarizabilities was found also in aromatic systems with mixed carboxylate and phenolic substituents.³⁷⁸

Large proton polarizabilities were observed in polylysine or poly(glutamic acid) + NaH_2PO_4 systems, due to hydrogen bonds of $\text{NH}_3^+ \cdots \text{H}_2\text{PO}_2^{2-} \cdots \text{H}_2\text{PO}_2^- \cdots \text{NH}_2$ bridged systems. Another IHB chain system was demonstrated by IR continuum in deprotonated poly(hydroxy pentacene) derivatives and in substituted Mannich bases. In these systems, the protons may move in a three-well system or be localized in any of the minima, according to the relative $\text{p}K_a$ values.³⁷⁸

The condensed-phase studies show large proton polarizabilities, indicating that the proton can move through hydrogen-bond chains in water between end-groups, even when the end-groups have higher proton affinities than water. This is similar to gas-phase results that showed that the proton can remain on central solvent molecules even when they are between molecules with higher proton affinities.

8.2. Biological Systems

An important class of ionic hydrogen bonds was observed in amino acid polymers that model proteins. Evidence for homoconjugated $\text{NH}^+ \cdots \text{N}$ bonds between amino acid side-chains was shown in polyhistidine films,^{400,401} for $\text{OH} \cdots \text{O}^-$ bonds in poly(glutamic acid), and for $\text{SH} \cdots \text{S}^-$ bonds in polycysteine films.^{402,403} The IR absorbance continuum in poly(glutamic acid) is at a pH where half of the carboxylic groups are ionized. This is similar to the formation of vesicles in aliphatic carboxylic acid solutions, which also appear at pH values where mixtures of ionized and neutral groups are present.⁴⁰⁴ Homoconjugated bonds were also observed in $(\text{Asp-Asp})^-$, $(\text{Cys-Cys})^-$, $(\text{Glu-Glu})^-$, $(\text{Tyr-Tyr})^-$, $(\text{His-His})^+$, and $(\text{Lys-Lys})^+$.

Also significant are heteroconjugated bonds with large proton polarizability that can conduct protons, which were observed between side-chain groups in Asp-His, Cys-Lys, Glu-His, Tyr-Arg, and Tyr-Lys hydrogen bonds.^{405,406} In mixtures with hydrogen acceptors or donors, water can shift the proton-transfer equilibrium toward the ionized forms, and at high hydration, the solvent can dissociate these bonds.^{405,406} These effects demonstrate the significance of partially hydrated regions in protein interior regions where ionic hydrogen

bonds are needed, such as in membrane proton wires and at enzyme active sites. For example, bridged systems involving carboxylate ions, tyrosine residues, and a Schiff base are active in the proton pump of bacteriorhodopsin.^{378,407,408}

The IR continuum also indicated a mobile polarizable proton in ATP synthetase, where the proton pathway starts with a carboxylic group of alanine and involves phenolic tyrosine, carboxylic glutamate, histidine, carboxylic lysine, and amine arginine groups and probably bridging structural water molecules along a 60 Å long path.^{402,403,406,409}

Serine proteases, modeled in the gas phase, were also examined for IHB effects in solution. Both studies considered the transition state with a protonated His57 imidazole and with a network of IHB interactions involving the Asp102 COO^- and the tetrahedral oxyanion groups, according to the model of Warshel and Russell, who pointed out the energetic significance of the IHBs.³²³ The gas-phase model suggested that the IHBs of the Asp102 shown in Figure 54 contribute up to 65 kcal/mol to help proton transfer to the histidine and the IHBs of the tetrahedral oxyanion intermediate contribute up to 32 kcal/mol to help proton transfer from Ser195 to histidine by stabilizing the resulting oxyanion intermediate. In the solution study, difference spectra between trypsin and anhydrotrypsin supported the protonated imidazole intermediate and the existence of polarizable IHBs around it, resulting in an IR absorption continuum.⁴¹⁰

In addition, IR spectroscopic studies also demonstrated an IHB network of two carboxylates and a H_2O molecule as providing the catalytic action in pepsin-like aspartate proteases.⁴¹¹ An IR continuum showed that the proton wire in the gramicidin channel involves a pathway of hydrogen bonds with high proton polarizability,⁴¹² in agreement with the gas-phase ketone/water cluster models of this system.²⁴²

Ionic hydrogen bonds allow the proton to move with little barrier between several minima in a large volume, resulting in very large proton polarizabilities, which are largest along, or nearly along, the direction of the bond. Because of the large polarizability, the bonds are affected strongly by electric fields caused by the surrounding solvent, by other polarizable IHBs, and by ions in the solution.

As a result, the hydrogen bonds are controlled easily by neighboring charged groups. This allows biological systems to control the movement of charges by controlling IHB chains that conduct and pump the charges.

8.3. Ionic Hydrogen Bonds in Solids

Ionic hydrogen bonds affect crystal structure.³ As in solution, the energy contributions of IHBs in solids cannot be isolated, but gas-phase data can give indications about their energy contributions. At least, the gas-phase bond strengths provide upper limits, because geometry and continuum effects decrease the strengths of ionic hydrogen bonds in solids. This section will note a few examples that show analogy in solids with gas-phase interactions in homodimers, heterodimers, anionic IHBs, carbon-based IHBs, and intramolecular bonds.

Homoconjugated $\text{NH}^+ \cdots \text{N}$ bonds were investigated in aminopyridine and in quinuclidinium–quinuclidine crystals⁴¹³ and $\text{OH} \cdots \text{O}^-$ bonds in carboxylate–carboxylic acid crystals,⁴¹⁴ which showed intense continuum absorption with light polarized along the hydrogen bond. Heteroconjugated $\text{OH} \cdots \text{N} \leftrightarrow \text{O}^- \cdots \text{H}^+\text{N}$ bonds were shown by IR absorbance in phenol + amine crystals.⁴¹⁵

Extensive networks of anionic IHBs were observed in crystals of deprotonated phthalic acid, $C_6H_4\text{-}1,2\text{-}(COOH)_2$, upon self-assembly of the anions into honeycomb superstructures held together by neutral O–H…O and charged O–H…O[−] hydrogen bonds. The crystals also accommodate organometallic cations via charge-assisted C–H^{δ+}…O^{δ−} hydrogen bonds. The formation of IHBs helps the assembly of hydrogen-bonded networks, and IHBs to water molecules stabilize the crystal structures.⁴¹⁶

Intramolecular hydrogen bonds in Schiff bases in the solid state were shown by crystallography and by ab initio calculations. Both neutral and ionic internal bonds were observed. In this case, geometry effects made the ionic NH…O[−] bonds weaker than the neutral hydrogen bonds.⁴¹⁷

These are just a few examples of charge-assisted ionic hydrogen bonds that were observed in solids. Recent reviews cover the roles of ionic hydrogen bonds in the solid state,⁴¹⁸ including CH…O bonds⁴¹⁹ and hydrogen bonds involving organometallics⁴²⁰ and metal ions.⁴²¹ The roles of IHBs in crystal engineering were also reviewed recently.^{3,422,423}

9. RELATIONS BETWEEN CLUSTERS AND BULK SOLVATION: A CLUSTER-BASED ANALYSIS OF ION SOLVATION ENERGIES AND FACTORS

9.1. Relations between Clusters and Bulk Solvation

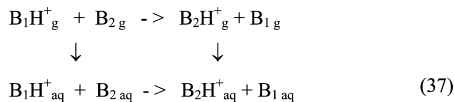
9.1.1. Overview of the Thermochemical Results.

Solvated clusters include the strong inner-shell interactions of ions with solvent molecules, but the small clusters lack other bulk solvation factors. Comparing clusters and bulk solvation can quantify and identify the major factors in ion solvation.

Solvation enthalpies of diverse alkali metal, oxonium, and ammonium ions (from Na⁺, Cs⁺, and NH₄⁺ to CH₃OH₂⁺ and (C₂H₅)₃NH⁺) range over 42 kcal/mol (Table 11 below). Remarkably, partial solvation by only 4 H₂O molecules reproduces these *relative* solvation enthalpies although the small (BH⁺·4H₂O) clusters lack major bulk continuum and hydrophobic solvation factors.

In other words, the further solvation enthalpies from 4 H₂O molecules to bulk solvation are equal for these diverse ions. This further solvation introduces cavity, dielectric charging, and hydrophobic solvation factors that vary substantially among the ions, but they vary almost exactly compensatingly, although they arise from independent physical forces.

These results are based on *relative* ion solvation energies from the well-established thermochemistry of solvation and protonation of neutral bases (eq 37). In particular, these results



$$\delta\Delta H^\circ_{\text{g}\rightarrow\text{aq}}(BH^+) = \Delta H^\circ_{\text{g}\rightarrow\text{aq}}(B_2H^+) - \Delta H^\circ_{\text{g}\rightarrow\text{aq}}(B_1H^+) = \delta\Delta H^\circ_{\text{g}\rightarrow\text{aq}}(B) + \delta\Delta H^\circ_{\text{prot(aq)}} - \delta\Delta H^\circ_{\text{prot(g)}}$$

do not involve any absolute single-ion solvation energies. However, accepted absolute single-ion solvation energies quantify the extra solvation energy beyond 4 H₂O molecules solvation as a constant -70 ± 3 kcal/mol for diverse ions (Table 11, column 11).

The measured bonding energies of the first 4 H₂O molecules include the strong ionic inner-shell hydrogen bond interactions.

These data, combined with the bulk solvation energies and calculated continuum terms, quantify all the ion solvation factors in simple, physically reasonable terms. For example, each CH hydrogen contributes -2.5 kcal/mol and each protic hydrogen contributes -10 kcal/mol to the bulk solvation enthalpies of alkylammonium ions.

Solvation beyond 4 H₂O molecules can occur stepwise through large clusters. The -70 ± 3 kcal/mol energy of this process is then the total cumulative stepwise excess cluster binding energy (over $\Delta H^\circ_{\text{condensation}}(H_2O)$) of the large ($n > 4$) solvated clusters.

However, present data suggests that the stepwise excess cluster binding energies may vanish after 4 H₂O molecules, where each stepwise binding energy may become equal to the macroscopic $\Delta H^\circ_{\text{condensation}}(H_2O)$. Born cycles then yield cluster-based truly single-ion solvation energies smaller by 70 ± 3 kcal/mol than the conventional values derived from electrolyte ion pairs. This would suggest that ion-pair interactions contribute this much even in dilute electrolyte solutions.

On the basis of cycle 38, the -70 ± 3 kcal/mol term is then either the further solvation energy from 4 H₂O molecules to bulk solvation or the difference between conventional and cluster-based, truly single-ion solvation energies, depending on the accurate binding energies of large clusters.

The observed relations between proton affinities, the binding enthalpies of clusters, and ion solvation can be combined. This yields a simple linear relation between gas-phase proton affinities PA(B) and bulk solvation enthalpies of BH⁺ ions, which in turn accounts for the compression of proton affinity scales by a factor of 5–6 in solution.

In summary, well-established thermochemical data yield *relative* ion solvation energies in clusters and in solution and allow for quantifying the energy contributions of physical factors in ion solvation. Born cycles yield information on the bonding energies of large clusters, or they yield truly single-ion solvation energies that differ significantly from the currently accepted values. The experimental observations and their interpretation is summarized as follows, with detailed analysis in subsequent sections.

9.1.2. Experimental Observations and Implications.

a. Experimental Observations.

- (1) The well-established thermochemistry of solvation of neutral bases and their protonation in the gas phase and solution yield the *relative* bulk solvation enthalpies of diverse ions (eq 37 and Table 11, column 6).
- (2) The energies of partial ion solvation by 1–4 H₂O molecules are known from gas-phase cluster thermochemistry.
- (3) The stepwise solvation enthalpies $\Delta H^\circ_{n-1,n}(BH^+\cdot nH_2O)$ approach the macroscopic condensation energy of water, -10.5 kcal/mol, already after 4–6 H₂O molecules.

b. Comparing Relative Cluster Binding and Bulk Solvation Energies.

- (4) Partial solvation by only 4 H₂O molecules reproduces the *relative* bulk solvation enthalpies of diverse alkali metal, oxonium, and ammonium ions from Na⁺ to CH₃OH₂⁺ and (C₂H₅)₃NH⁺ with an average difference of only 1 ± 3 kcal/mol over a range of 42 kcal/mol (Table 11,

Table 11. Relative Enthalpies of Protonation Bases B, Solvation and Clustering Energies of Bases B and Ions BH^+ , and Relative Solvation Enthalpies of the Clusters $\text{BH}^+\cdot 4\text{H}_2\text{O}$ ^a

	$-\Delta H^\circ_{\text{prot,g}}$ (B) ^b (PA(B))	$\delta\Delta H^\circ_{\text{prot,g}}$ (B) ^b	$\delta\Delta H^\circ_{\text{prot,aq}}$ (B) ^c	$\delta\Delta H^\circ_{\text{g}\rightarrow\text{aq}}$ (B) ^c	$\delta\Delta H^\circ_{\text{g}\rightarrow\text{aq}}$ (BH ⁺) ^d	$\delta\Delta H^\circ_{0,4}$ (BH ⁺ . n(H ₂ O) ^e)	$-\Delta H^\circ_{\text{g}\rightarrow\text{aq}}$ (BH ⁺) ^f	$-\Delta H^\circ_{\text{g}\rightarrow\text{aq}}$ correlation	$-\Delta H^\circ_{0,4}$ (BH ⁺ . nH ₂ O) ^e	$-\Delta H^\circ_{\text{g}\rightarrow\text{aq}}$ (BH ⁺ .4H ₂ O) ^h
protonated alcohols, ethers, and ketones										
H ₃ O ⁺	165.0	39.0	12.6	-2.0	-28.4	-21.2	117.0	113.4	83.7	75.3
MeOH ₂ ⁺	180.3	23.7	13.1	-2.1	-12.7	-10.3	101.3	100.5	72.8	70.5
EtOH ₂ ⁺	185.6	18.4	12.1	-4.1	-10.4	-7.4	99.0	96.1	69.9	71.1
Me ₂ OH ⁺	189.0	15.0	11.9	-0.9	-4.0	0.6	92.6	93.2	61.8	72.8
Et ₂ OH ⁺	198.0	6.0	11.8	-2.6	3.2	6.7	85.4	85.7	55.8 ⁱ	71.6
Me ₂ COH ⁺	194.0	10.0	11.8	-1.6	0.2	5.4	88.4	89.0	57.1	73.3
C ₆ H ₅ CHOH ⁺	199.3	4.7	14.4	-3.1	6.6	6.7	82.0	84.6	55.8 ⁱ	68.2
Me(c-C ₆ H ₁₁)COH ⁺	201.1	2.9	14.2	-4.4	6.9	8.5	81.7	83.1	54.0 ⁱ	69.7
Me(C ₆ H ₅)COH ⁺	205.8	-1.8	17.3	-4.6	14.5	9.1	74.1	79.1	53.4	62.9
Me(c-Pr)COH ⁺	204.3	-0.3	11.1	-3.5	7.9	12.3	80.7	80.4	50.2	72.4
(c-Pr) ₂ COH ⁺	210.4	-6.4	12.0	-6.2	12.2	16.8	76.4	75.3	45.7	72.7
amide										
Me(NMe ₂)COH ⁺	217.0	-13.0	14.9	-7.6	20.3	15.2	68.3	69.7	47.3	63.0
protonated amines										
NH ₄ ⁺	204.0	(0)	(0)	(0)	(0)	(0)	88.6	90.6	62.5	68.1
MeNH ₃ ⁺	214.9	-10.9	-0.7	-2.6	7.6	8.5	81.0	81.2	54.0	69.0
EtNH ₃ ⁺	218.0	-14.0	-1.2	-4.5	8.3	5.9	80.3	78.5	51.9	70.4
t-C ₄ H ₉ NH ₃ ⁺	223.3	-19.3	-1.9	-5.6	11.8	13.3	76.8	74.0	49.2 ⁱ	69.6
c-C ₆ H ₁₁ NH ₃ ⁺	223.3	-19.3	-1.9	-6.4	11.0	13.1	77.6	74.0	49.4 ⁱ	70.2
Me ₂ NH ₂ ⁺	222.2	-18.2	0.5	-4.7	14.0	13.1	74.6	74.9	49.4	67.2
Et ₂ NH ₂ ⁺	227.6	-23.6	-0.3	-6.8	16.5	16.7	72.1	71.0	45.8 ⁱ	68.3
Me ₃ NH ⁺	226.8	-22.8	3.7	-4.7	21.8	18.2	66.8	71.5	44.3	64.5
Et ₃ NH ⁺	234.7	-30.7	2.2	-8.2	24.7	25.4	63.4	64.2	37.3 ⁱ	68.6
pyridineH ⁺	222.2	-18.0	7.7	-3.4	22.3	21.4	66.3	74.9	41.1	67.2
C ₆ H ₅ NH ₃ ⁺	210.9	-6.9	5.1	-4.4	7.6	5.3	81.0	84.6	57.2 ⁱ	65.8
alkali metal ions										
Na ⁺					-17.8	-13.5	106.4 ^j		76	72.4
K ⁺					0.6	2.5	88.0 ^j		60	70.0
Rb ⁺					6.6	9.5	82.0 ^j		53	71.0
Cs ⁺					12.6	14.5	76.0 ^j		48	70.0

^aAll values in kcal/mol. Differential values for process X represent $\delta\Delta H^\circ(X) = \Delta H^\circ_x(\text{B}) - \Delta H^\circ_x(\text{NH}_3)$. Negative values for B or BH⁺ represent more exothermic processes than those for NH₃ or NH₄⁺, respectively. Absolute reference values were obtained as follows: $\Delta H^\circ_{\text{g}\rightarrow\text{aq}}(\text{NH}_3) = -8.0$ kcal/mol;^{44a} $\Delta H^\circ_{\text{prot,g}}(\text{NH}_3) = -204$ kcal/mol;²⁷ $\Delta H^\circ_{\text{prot,aq}}(\text{NH}_3) = -12.6$ kcal/mol; $\Delta H^\circ_{\text{g}\rightarrow\text{aq}}(\text{NH}_4^+) = -88.6$ kcal/mol, based on $\Delta H^\circ_{\text{g}\rightarrow\text{aq}}(\text{H}^+) = -272$ kcal/mol,^{42b} which using $\Delta H^\circ_{\text{g}\rightarrow\text{aq}}(\text{H}_2\text{O}) = -10.5$ kcal/mol and PA(H₂O) = 165 kcal/mol yields $\Delta H^\circ_{\text{g}\rightarrow\text{aq}}(\text{H}_3\text{O}^+) = -117.0$ kcal/mol; $\Delta H^\circ_{0,4}(\text{NH}_4^+) = -62.5$ kcal/mol³⁴ yields $\Delta H^\circ_{\text{g}\rightarrow\text{aq}}(\text{NH}_4^+\cdot 4\text{H}_2\text{O}) = -68.1$ kcal/mol. A recent value of $\Delta H^\circ_{\text{g}\rightarrow\text{aq}}(\text{H}^+) = -274.8$ kcal/mol^{430–432,433a} will make the numbers in column 8 for $-\Delta H^\circ_{\text{g}\rightarrow\text{aq}}(\text{BH}^+)$ and in column 11 for $-\Delta H^\circ_{\text{g}\rightarrow\text{aq}}(\text{BH}^+\cdot 4\text{H}_2\text{O})$ larger by 2.8 kcal/mol. ^bFrom data of ref 27. ^cReference 20. ^dFrom data of columns 2–4 and eq 37. ^eOn the basis of the experimental cluster energetics $\Delta H^\circ_{1,4}(\text{BH}^+\cdot n\text{H}_2\text{O})$ unless noted otherwise.³³ The cumulative experimental error of the four hydration steps is estimated as ± 3 kcal/mol. ^fCalculated from the relative solvation energies in column 6, using $\Delta H^\circ_{\text{g}\rightarrow\text{aq}}(\text{NH}_4^+) = -88.6$ kcal/mol as absolute reference value. ^gCalculated from the correlations $-\Delta H^\circ_{\text{g}\rightarrow\text{aq}}(\text{BH}^+) = 252 - 0.84(\text{PA(B)})$ for alkylxonium and $262 - 0.84(\text{PA(B)})$ for alkylammonium ions. ^hSolvation energies of the BH⁺.4H₂O clusters, calculated from eq 38, using conventional $\Delta H^\circ_{\text{g}\rightarrow\text{aq}}(\text{BH}^+)$ values from column 8 and cluster binding energies $\Delta H^\circ_{0,4}(\text{BH}^+\cdot n\text{H}_2\text{O})$ from column 10. These values are also equal to the sum of the excess cluster ion binding energies $\Delta H^\circ_{5,N(\text{exc})}$ from $n = 5$ to ∞ and to the difference between the conventional and cluster-based solvation energies. ⁱCalculated cluster binding energies from PA correlations in eqs 18 and 19. Note that PA(C₆H₅NH₂) is reduced by 9 kcal/mol due to resonance effects of the neutral, which does not affect the ion. Correcting for this effect, $\Delta H^\circ_{0,4}(\text{BH}^+\cdot n\text{H}_2\text{O})$ is estimated as -49 kcal/mol. ^jBased on Wagman et al. *J. Phys. Chem. Ref. Data* 1982, 11 (Suppl 2), and on $\Delta H^\circ_{\text{g}\rightarrow\text{aq}}(\text{H}^+) = -272$ kcal/mol.^{42b}

columns 6 and 7), although bulk solvation involves major factors that are absent in the clusters.

- (5) In other words, the total bulk solvation enthalpies beyond 4 H₂O molecules are equal for diverse ions, although it introduces continuum and hydrophobic solvation factors that vary up to 30 kcal/mol among these ions. These factors vary almost exactly compensatingly among the ions, although they arise from independent physical forces.

c. **Higher Solvation.** The above results on relative ion solvation energies derive from well-established thermochemis-

try, regardless of absolute single ion solvation energies. However, further analysis is possible by accepting conventional absolute single-ion solvation energies.

- (6) Assuming conventional single-ion solvation energies, the further solvation enthalpies $\Delta H^\circ_{\text{g}\rightarrow\text{aq}}(\text{BH}^+\cdot 4\text{H}_2\text{O})$ from 4 H₂O molecules to bulk solvation are a constant -70 ± 3 kcal/mol for diverse alkali metal, alkylxonium, and alkylammonium ions (Table 11, column 11), although it introduces very different solvation factors for these ions. This further solvation may be in one step, or stepwise through large clusters.

Table 12. Solvation Factors in the Hydration of Ions^a

	ionic radii ^b (Å)	−ΔH° _{g>aq} (BH ⁺) ^c	−ΔH° solvation factors				−ΔH° factors per hydrogen		
			dielectric ^d	cavity ^e	total continuum ^f	hydrophobic ^g	IHB ^h	hydrophobic/ <i>n</i> (CH) ⁱ	IHB/ <i>n</i> (XH ⁺) ^j
protonated alcohols, ethers, and ketones									
H ₃ O ⁺	1.74	117.0	72.8	−6.5	66.3	(4.9) ^k	45.8		15.2
MeOH ₂ ⁺	2.08	101.3	62.6	−9.2	53.4	9.9	38.0	3.3	19.0
EtOH ₂ ⁺	2.35	99.0	56.5	−11.8	44.7	14.3	40.0	2.9	20.0
Me ₂ OH ⁺	2.36	92.6	56.2	−11.9	44.3	21.6	26.8	3.6	26.8
Et ₂ OH ⁺	2.77	85.4	49.2	−16.4	32.8	27.1	25.6	2.7	25.6
Me ₂ COH ⁺	2.48	88.4	53.8	−13.2	40.6	24.0	23.9	4.0	23.9
C ₆ H ₅ CHOH ⁺	2.92	82.0	46.8	−18.3	28.5	26.4	27.2	4.4	27.2
Me(c-C ₆ H ₁₁)COH ⁺	3.20	81.7	43.4	−21.8	21.6	33.0	27.2	2.4	27.2
Me(C ₆ H ₅)COH ⁺	3.07	74.1	45.0	−20.1	24.9	23.6	25.7	2.9	25.7
Me(c-Pr)COH ⁺	2.75	80.7	49.4	−16.2	33.2	27.6	20.0	3.4	20.0
(c-Pr) ₂ COH ⁺	2.97	76.4	46.3	−18.8	27.5	31.4	17.6	3.1	17.6
amide									
Me(NMe ₂)-COH ⁺	2.81	68.3	48.4	−16.9	31.5	19.2	17.7	2.1	17.7
protonated amines									
NH ₄ ⁺	1.81	88.6	70.4	−7.0	63.4	0.0	25.2		6.3
MeNH ₃ ⁺	2.16	81.0	60.6	−10.0	50.6	4.9	25.6	1.6	8.5
EtNH ₃ ⁺	2.41	80.3	55.2	−12.4	42.8	10.0	27.6	2.0	9.2
t-C ₄ H ₉ NH ₃ ⁺	2.81	76.8	48.6	−16.8	31.8	15.7	29.4	1.7	9.8
c-C ₆ H ₁₁ NH ₃ ⁺	3.02	77.6	45.7	−19.4	26.3	20.1	31.3	1.8	10.4
Me ₂ NH ₂ ⁺	2.42	74.6	55.0	−12.6	42.4	12.0	20.2	2.0	10.1
Et ₂ NH ₂ ⁺	2.82	72.1	48.3	−17.1	31.2	19.8	21.1	2.0	10.6
Me ₃ NH ⁺	2.64	66.8	51.2	−14.8	36.4	17.9	12.6	2.0	12.6
Et ₃ NH ⁺	3.12	63.4	44.4	−20.8	23.6	30.6	9.8	2.0	9.8
pyridineH ⁺	2.72	66.3	49.9	−15.8	34.1	22.0	10.3	4.4	10.3
C ₆ H ₅ NH ₃ ⁺	2.87	81.0	47.7	−17.6	30.1	12.9	38.1	2.6	12.7
alkali metal ions									
K ⁺	1.33	88.0 ^l	91.0	−3.8	87.2		0.8 ^m		
Rb ⁺	1.47	82.0 ^l	83.9	−4.6	79.3		2.7 ^m		
Cs ⁺	1.67	76.0 ^l	75.4	−5.9	69.5		6.5 ^m		

^aAll values in kcal/mol. Data derived from cluster-based analysis of solvation factors; see ref 35 and text. ^bIonic radii from ref 35 based on ionic volumes from ref 445. ^cConventional single-ion solvation energies from Table 11. ^dDielectric charging of the solvent cavity, calculated in ref 35 using a double-shell model of ref 445. ^eSurface tension energy of the cavity created to accommodate a spherical ion.³⁵ ^fSum of dielectric and cavity terms in columns 4 and 5, respectively. ^gHydrophobic solvation of the alkyl substituents obtained from eq 43 using the solvation energy of the clusters, ΔH°_{g>aq}(BH⁺·4H₂O), in Table 11 and the parameters for ΔH°_{dielectric} and ΔH°_{cavity} for the BH⁺·4H₂O clusters used in refs 33 and 35. The values of ΔH°_{hydrophobic} are somewhat different from those in refs 33 and 35 because the new PA values of ref 27 and ΔH°_{residual hydrogen bonds} were used in the present calculations. Using the reference value ΔH°_{g>aq}(H⁺) = −274.8 kcal/mol,^{430–432,433a} the values of −ΔH°_{g>aq}(BH⁺) in column 3 and the values of −ΔH°_{g>aq}(hydrophobic) in column 7 will increase by 2.8 kcal/mol. For C₆H₅NH₂, resonance correction (Table 11, footnote i) would give −ΔH°_{hydrophobic} = 21 kcal/mol, −ΔH°_{IHB} = 30 kcal/mol, −ΔH°_{hydrophobic}/n(CH) = 4.2 kcal/mol, and −ΔH°_{IHB} = 10 kcal/mol, in line with other ammonium ions. ^hEnthalpy of ionic hydrogen bonding. ⁱHydrophobic solvation energy per alkyl hydrogen. ^jIonic hydrogen bond energy per protic hydrogen. ^kThe calculated “−ΔH°_{hydrophobic}” for H₃O⁺ reflects, rather, significant IHB interactions past the first shell for this ion. ^lSee footnote^j in Table 11. ^mAn analysis similar to that for the onium ions applied to metal ions gives small values for this term, consistent with the fact that ΔH°_{hydrophobic} is absent in the solvation of metal ions.

d. Binding Energies of Large Clusters. For stepwise solvation, it is convenient to define the excess stepwise binding energy over the bulk water condensation energy, (ΔH°_{n-1,n,excess}) = ΔH°_{n-1,n} − ΔH°_{cond}(H₂O)).

(7) Binding energies of large clusters. Assuming conventional single ion solvation energies, then Born cycles (eq 38) yield the total excess cluster binding energies Σ(ΔH°_{n-1,n,excess}) of large *n* > 4 clusters as −70 ± 3 kcal/mol for diverse ions.

e. Cluster-Based Single-Ion Solvation Energies. Stepwise solvation through large clusters forms truly single-ion solutions without counterions. Therefore truly single-ion solvation energies can be calculated from stepwise solvation through large clusters.

(8) Existing data (Figures 25 and 26 and Table 4) suggest that after 4 H₂O molecules the stepwise binding energies

become equal to the bulk ΔH°_{condensation}(H₂O). In that case, Born cycles then yield truly single-ion solvation enthalpies of diverse ions that are smaller (less negative) by 70 ± 3 kcal/mol than the conventional values based on solutions with ion pairs. This would imply that ion-pair interactions contribute this extra solvation energy even in dilute electrolyte solutions. The correct interpretation 7 or 8 can be decided by the accurate binding energies of large clusters.

f. Relations between Proton Affinities and Ion Solvation Energies, and the Compression of Basicity Scales in Solution.

(9) The experimental data show linear correlations between increasing proton affinities (PA(B)) and decreasing binding energies of the BH⁺ ions to 1 H₂O molecule,^{33,42,48} (Figure 8 and Table 2) and to 4 H₂O molecules (eqs 16 and 17), as well as a constant enthalpy

of cluster to bulk solvation $\Delta H^\circ_{g \rightarrow aq}(BH^+ \cdot 4H_2O)$ for diverse ions (Table 11, column 11). Combining these relations yields a simple linear relation for the weaker solvation of protonated stronger bases, as $\Delta H^\circ_{g \rightarrow aq}(BH^+) = a - 0.84PA(B)$ kcal/mol. This simple relation predicts the enthalpies of solvation of onium ions within experimental accuracy^{33,35} (Table 11, columns 8 and 9). These solvation effects in turn lead to the compression of relative enthalpies of protonation in solution, according to $\delta\Delta H^\circ_{prot,aq}(B) = 0.18\delta\Delta H^\circ_{prot,g}(B)$, by a factor of 5–6 due to relative ion solvation effects.

g. Cluster-Based Analysis of Solvation Factors. The factors responsible for the effects of ion solvation can be identified and quantified by a cluster-based analysis.

- (10) Clusters account for the strong inner-shell ion–solvent hydrogen bond interactions. The cavity and dielectric terms can be calculated from continuum models and the remaining solvation energy assigned to hydrophobic solvation. This cluster-based analysis yields physically reasonable solvation factors. For example, each CH hydrogen contributes −2.5 kcal/mol and each protic hydrogen contributes −10 kcal/mol to the solvation enthalpies of alkylammonium ions.

The experimental data show simple linear relations among the enthalpies of gas-phase protonation, partial solvation in clusters, bulk ion solvation, and protonation in solution. Qualitatively, these relations result from the increasing charge delocalization in BH^+ and weaker bonding to solvent molecules with increasing PA(B), and from the compensating variation of solvation factors of diverse ions. However, considering the complex forces involved in protonation and ion solvation, these simple relations are unexpected.

9.1.3. Historical Background of Partial Solvation in Clusters. Historically, Kearle first noted relationships between gas-phase acidities or basicities and cluster binding energies,^{38,39,51a,52} followed by similar studies and correlations by McMahon⁵⁰ and Meot-Ner,^{33,42,48} as summarized in Table 2. Going to larger clusters, linear relations between the binding energies of 1 and 4 H_2O molecules are given in eqs 16 and 17. The above workers and the Taft group also noted that 4 H_2O or 1 CH_3CN molecule reproduce relative full bulk solvation enthalpies,^{51b,c} and that further stepwise binding energies approach the bulk $\Delta H^\circ_{condensation}(H_2O)$. These relations were commented upon and used to calculate single-ion solvation energies by Kebal, Taft, Castleman, Klots, Hiraoka, Meot-Ner, Coe, Williams, and their co-workers.^{52,33,35,49,51a–c,153,163,164,174,219a,239,424–433a,b}

Kearle and co-workers also noted a linear relation between gas-phase and solution acidities of phenols, with a 7-fold attenuation in aqueous solution.^{51a} A relation between gas-phase proton affinities and ion solvation energies was noted also by Hiraoka.⁴²⁹ The Taft group also predicted that binding enthalpies of ions to 1 H_2O molecule will be linearly related to the bulk solvation enthalpies of oxonium ions, despite the complex factors of bulk solvation.^{51c} These relations were attributed to the effects of charge delocalization in the ions on the binding to solvent molecules.

These early observations, mostly on simple ions, were extended to more complex onium ions.⁴⁹ Meot-Ner found that 4 H_2O molecules reproduce relative bulk solvation energies also of these complex ions (Table 12),³⁵ although the 4 H_2O molecules interact only with protonated functional groups, and continuum and hydrophobic solvation effects are absent in the clusters.

9.1.4. Relative Ion Solvation Energies in Small Clusters and in Solution.

As noted above, *relative* ion solvation enthalpies can be calculated from well-established thermochemistry using the cycle of eq 37, regardless of absolute ion solvation energies that are derived indirectly.^{434a–c}

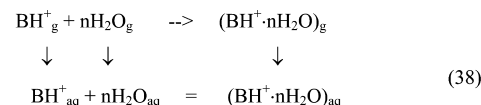
Here the ΔH°_{prot} values are protonation enthalpies, and the differential values $\delta\Delta H^\circ$ represent the differences between the solvation or protonation enthalpies of two ions or neutrals. The aqueous values refer to infinitely dilute solutions, and the gas-phase species are in equilibrium with these solutions. Importantly, the terms on the RHS of eq 37 do not include single-ion solvation energies. Therefore, the *relative* ion solvation energies $\delta\Delta H^\circ_{g \rightarrow aq}(BH^+)$ can be derived using only the well-established enthalpies of solvation of neutral bases and their relative enthalpies of protonation in the gas phase and solution. The relative values can be converted to absolute solvation energies using a reference ion (NH_4^+ in Table 11).

The relative bulk solvation energies calculated from eq 37 can be compared with relative cluster-binding energies for various core ions. The results show that the relative 4-fold solvation energies (referenced to NH_4^+) reproduce the relative bulk solvation energies with an average difference $\delta\Delta H^\circ_{g \rightarrow aq}(BH^+) - \delta\Delta H^\circ_{0,4}(BH^+ \cdot n(H_2O))$ of 1 ± 3 kcal/mol for 25 diverse onium ions and even alkali metal ions, whose solvation energies range over 42 kcal/mol, and within 0.5 ± 2.2 kcal/mol for 15 diverse alkylammonium and alkali metal ions (Table 11, columns 6 and 7). Solvation in larger, for example, 6-fold solvated, clusters gives similar results, because the cluster binding energies do not change much after 4 H_2O solvent molecules.

For example, the *relative* cluster binding energies, $\delta\Delta H^\circ_{0,4}(BH^+ \cdot nH_2O)$, reproduce, within experimental uncertainty, over a range of 42.5 kcal/mol, the *relative* bulk solvation enthalpies, $\delta\Delta H^\circ_{g \rightarrow aq}(BH^+)$, of ions as diverse as K^+ , Rb^+ , Cs^+ , NH_4^+ , $MeOH_2^+$, $C_6H_5CHOH^+$, $MeNH_3^+$, $c-C_6H_{11}NH_3^+$, Me_3NH^+ , and Et_3NH^+ (Table 11, columns 6 and 7).

These results have unexpected structural implications. In the clusters, the first water molecules solvate only the protonated functional groups. The alkyl substituents of varying sizes and structures are not solvated by 4 and even up to 20 H_2O molecules.³⁵⁸ The enthalpies of the cavity, dielectric, and hydrophobic terms in bulk solvation vary by up to 30 kcal/mol for the various among the ions in Table 12. These factors are absent in the clusters, but the *relative* cluster-binding energies nevertheless reproduce the *relative* bulk solvation enthalpies. This means that the factors that are added only in bulk solution vary in an almost exactly compensating manner for the diverse ions in Table 12. This is remarkable because these solvation terms result from independent physical forces.

9.1.5. Extrapolating from Clusters to Bulk Solvation and the Binding Energies of Large Clusters. The preceding sections compared small clusters and bulk solvation. They can be connected by further solvation of the small clusters by transfer into bulk solution in one step with enthalpy $\Delta H^\circ_{g \rightarrow aq}(BH^+ \cdot nH_2O)$ (eq 38) or, equivalently, stepwise through large clusters (see below).



$$\Delta H^\circ_{g \rightarrow aq}(BH^+) = [\Delta H^\circ_{0,n} - n\Delta H^\circ_{cond}(H_2O)] + \Delta H^\circ_{g \rightarrow aq}(BH^+ \cdot nH_2O)$$

Equation 38 can be used to derive the cumulative binding energies of large clusters or cluster-based single-ion solvation energies. For the first application, $\Delta H^\circ_{g\rightarrow aq}(BH^+)$ can be assigned the conventional single-ion solvation energies, referenced to $\Delta H^\circ_{g\rightarrow aq}(H^+)$, here -272 kcal/mol. As noted, 4 H₂O molecules reproduce the relative solvation enthalpies of the ions in Table 11, and therefore $n = 4$ is used. Equation 38 then yields the one-step cluster ion solvation enthalpies from 4H₂O molecules to bulk solution as a constant -70 ± 3 kcal/mol for most of these ions (Table 11, column 11).

This further solvation of the (BH⁺·4H₂O) cluster may be carried out also stepwise up to a “macroscopic” cluster size (BH⁺·NH₂O), after which every further stepwise binding enthalpy is equal to $\Delta H^\circ_{\text{condensation}}(H_2O)$. The total enthalpy of the further bulk solvation of the cluster, $\Delta H^\circ_{g\rightarrow aq}(BH^+·4H_2O)$, is then the sum of the steps from $n = 5$ to N H₂O molecules, leading to eq 39. By cycle 38, all the further steps from N to infinity are thermoneutral. Equivalently, the one-step transfer of the BH⁺·NH₂O cluster to bulk solution is then thermoneutral, and in this respect this cluster is equivalent to an infinitely dilute single-ion BH⁺ solution.

$$\Delta H^\circ_{g\rightarrow aq}(BH^+·4H_2O) = \Sigma(\Delta H^\circ_{n-1,n} - \Delta H^\circ_{\text{condensation}}(H_2O)) \text{ (sum from 5 to } N)$$

$$= \Sigma(\Delta H^\circ_{n-1,n, \text{excess}}) \text{ (summation from 5 to } N) \quad (39)$$

It is convenient to define the difference between the binding energy of the n th solvent molecule and the macroscopic condensation energy of water $\Delta H^\circ_{\text{condensation}}(H_2O)$ as the excess cluster ion binding energy $\Delta H^\circ_{n-1,n, \text{excess}}$, leading to the last term in eq 39.

In these terms, the solvation energy of an ion, $\Delta H^\circ_{g\rightarrow aq}(BH^+)$, is equal to the total cumulative excess binding energies from $n = 1$ to N (which may be infinity). The solvation energy of the clusters, $\Delta H^\circ_{g\rightarrow aq}(BH^+·4H_2O)$, is equal to the cumulative excess binding energies of the large clusters from 5 to N (or infinite) H₂O molecules, with the values in Table 11, column 11, i.e., -70 ± 3 kcal/mol for most of these diverse ions. This gives quantitative information on the binding energies of the large clusters.

In fact, various theories, for example, the liquid drop model, predict that the binding energies $\Delta H^\circ_{n-1,n}(BH^+·nH_2O)$ should exceed the bulk condensation energy, up to large cluster sizes.²³⁸ The resulting cumulative excess cluster ion binding energy of -70 kcal/mol may then build up in many steps, for example, as an excess binding energy of 0.1 kcal/mol in hundreds of steps.

9.1.6. Cluster-Based Single-Ion Solvation Energies. As an alternative to the preceding section, current data suggest that the stepwise binding energies become equal to, or slightly undershoot, the macroscopic $-\Delta H^\circ_{\text{condensation}}(H_2O) = 10.5$ kcal/mol already after 4 H₂O molecules (Table 4 and Figure 25). Then $\Sigma(\Delta H^\circ_{n-1,n, \text{excess}})$ (from 5 to N) and, equivalently, $\Delta H^\circ_{g\rightarrow aq}(BH^+·4H_2O)$ in eq 38 vanish. Treating $\Delta H^\circ_{g\rightarrow aq}(BH^+)$ as unknown, its value can be then calculated from eq 40.

$$\Delta H^\circ_{g\rightarrow aq}(BH^+)_{\text{cluster-based}} = \Delta H^\circ_{0,4} - 4\Delta H^\circ_{\text{condensation}}(H_2O) = \Delta H^\circ_{0,4, \text{excess}} \quad (40)$$

In comparison, eq 38 can be written as $\Delta H^\circ_{g\rightarrow aq}(BH^+)_{\text{conventional}} = \Delta H^\circ_{0,4, \text{excess}} + \Delta H^\circ_{g\rightarrow aq}(BH^+·4H_2O)$ (with the last term as calculated from this equation). Comparing this equation with eq 40 gives the difference between the conventional and cluster-based single-ion solvation enthalpies as $\Delta H^\circ_{\text{conventional}} - \Delta H^\circ_{\text{cluster-based}} = \Delta H^\circ_{g\rightarrow aq}(BH^+·4H_2O)$ with the values shown in Table 11, column 11. The cluster-based truly single-ion solvation energies are smaller (less negative)

than the conventional single-ion solvation energies, by 70 ± 3 kcal/mol for most of these diverse ions. The difference between the conventional and cluster-based solvation energies is illustrated also in Figure S6.

Note that the clusters are truly single-ion solutions, while the classical single-ion solvation energies are derived from solutions of ion pairs. The comparison would then imply that counterion interactions contribute -70 ± 3 kcal/mol to the solvation energies of ions, or -140 kcal/mol per ion pair, even in the dilute solutions from which the conventional ion solvation enthalpies values are derived.^{424,425,430–433a,b} The conventional and cluster-based values could come closer if cluster binding enthalpies $\Delta H^\circ_{n-1,n}$ remain more negative than $\Delta H^\circ_{\text{condensation}}(H_2O)$ for larger $n > 4$ clusters.

9.1.7. Alternative Thermochemical Cycle for Ion Solvation. Cycle 38 was used by the present author and others.^{33,35,194,225b} Other authors used an alternative cycle that starts with BH⁺ and n separate H₂O molecules.^{5,239,429} The water molecules are clustered stepwise to the ion or clustered to each other to give (H₂O) _{n} and BH⁺ is then transferred to the water cluster. Both paths give a BH⁺(H₂O) _{n} cluster that approaches a single-ion bulk solution with increasing n . The cycle gives eq 41.

$$\begin{aligned} \Delta H^\circ_{g\rightarrow aq}(BH^+)_{\text{cluster-based}} \\ = \Delta H^\circ_{0,n}(BH^+·nH_2O) - \Delta H^\circ_{0,n-1}(H_2O·nH_2O) \\ - 10.5 \text{ kcal/mol} \end{aligned} \quad (41)$$

Here the summation is carried to a size n where the ionic and neutral cluster-binding energies become equal. If $n = 4$ is used as above, and if the first three binding enthalpies of a neutral water cluster are 5, 6, and 7 kcal/mol, then this model gives cluster-based ion solvation energies larger (more negative) by 24 kcal/mol than eq 39. These values are still smaller by about 45 kcal/mol than the conventional single-ion solvation energies.

In summary, the cluster data quantifies the values of 70 ± 3 kcal/mol in Table 11, column 11, calculated from cycle 11 as the cluster solvation energy $\Delta H^\circ_{g\rightarrow aq}(BH^+·4H_2O)$, or equivalently as the cumulative excess cluster ion-binding energies for large clusters ($n > 4$); or alternatively, the cluster data yield single-ion solvation energies that are smaller (less negative) by 70 kcal/mol than the conventional values. The correct interpretation can be decided experimentally by accurate binding energies of large clusters. Either way, the results can be significant for ionic nucleation and for electrolyte theory.

9.1.8. Relations among Proton Affinities and Bulk Solvation Energies. Increasing proton affinities PA(B) reflect increasing charge delocalization in BH⁺ ions, which can weaken the bonds to solvent molecules. A relationship between PA(B) and ion solvation energies may be expected, and given the many factors in ion solvation, this may be a complex relation. However, as discussed in section 3.1.3 and eqs 12–20, a simple linear relation is found between PA(B) and $\Delta H^\circ_{g\rightarrow aq}(BH^+)$. This can be accounted for by the linear relationship between PA(B) and the binding energy to 4 H₂O molecules (e.g., for oxonium ions, $\Delta H^\circ_{0,4} = 0.84\text{PA(B)} - 224$ kcal/mol), combined with the constant bulk solvation enthalpy $\Delta H^\circ_{g\rightarrow aq}(BH^+·4H_2O)$ of -70 ± 3 kcal/mol for diverse ions.

As noted in section 3.1.3, despite the complex effects of ion solvation, these relations combine into a simple relation between the gas-phase PA(B) and the enthalpies of hydration

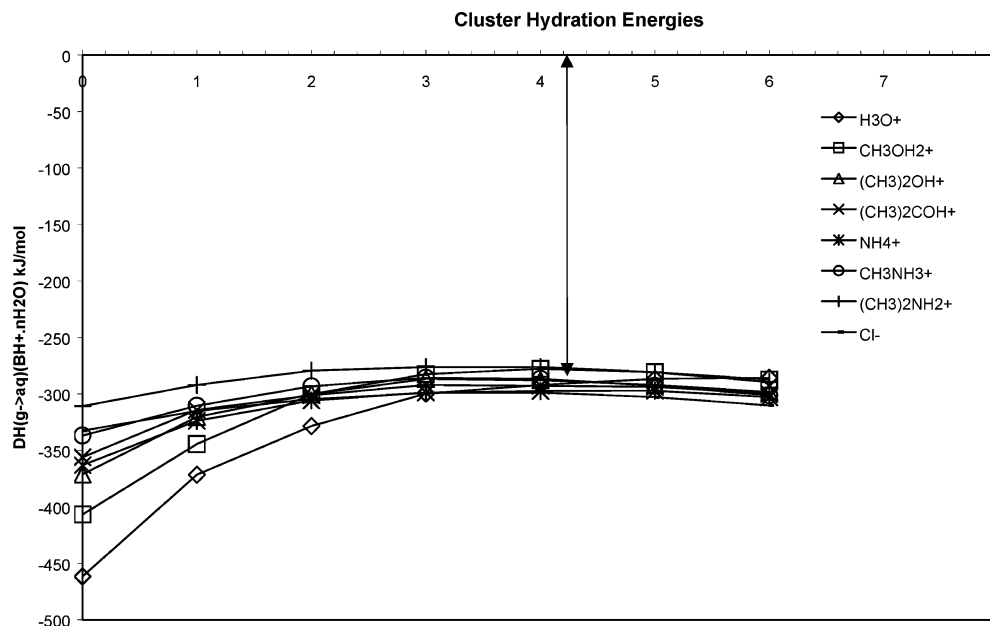


Figure 56. Difference between conventional and cluster-based ion solvation energies as a function of cluster size n . In eq 38, if $\Delta H^\circ_{\text{g-aq}}(\text{BH}^+)$ on the left-hand side (LHS) is assigned the conventional value, and if $\Delta H^\circ_{\text{g-aq}}(\text{BH}^+)_{\text{cluster-based}}$ is assigned as $(\Delta H^\circ_{0,n} - n\Delta H^\circ_{\text{condensation}}(\text{H}_2\text{O}))$, then the cluster solvation energy $\Delta H^\circ_{\text{g-aq}}(\text{BH}^+ \cdot n\text{H}_2\text{O})$ is equal to the difference $[\Delta H^\circ_{\text{g-aq}}(\text{BH}^+)_{\text{conventional}} - \Delta H^\circ_{\text{g-aq}}(\text{BH}^+)_{\text{cluster-based}}]$. If the cluster-based solvation energies approached the conventional values with increasing n , then $\Delta H^\circ_{\text{g-aq}}(\text{BH}^+ \cdot n\text{H}_2\text{O})$ should approach zero with increasing n . However, the plots approach -70 ± 3 kcal/mol (-292 ± 12 kJ/mol), reflecting the difference between conventional and cluster-based ion solvation energies.

of diverse ions given by the simple relation $\Delta H^\circ_{\text{g-aq}}(\text{BH}^+) = 0.84(\text{PA}(\text{B})) - a$ with $a = 252$ kcal/mol for alkyloxonium ions and 262.4 kcal/mol for alkylammonium ions (eq 20).³⁵ Columns 8 and 9 in Table 11 show that these simple relations reproduce the complex ion solvation enthalpies with a standard deviation of ± 2 kcal/mol, comparable to experimental uncertainty, for these diverse ions.

Deviations from these relations are reasonable structurally. These deviations occur for ions that contain aromatic groups, $\text{C}_6\text{H}_5\text{CHOH}^+$, $\text{Me}(\text{C}_6\text{H}_5)\text{COH}^+$, and pyridine H^+ . The hydration energies of these ions are smaller (less negative) by 2.6, 5.0, and 8.6 kcal/mol, respectively, than predicted from the PA correlations. This may be due to the fewer CH hydrogens, despite the larger hydrophobic solvation enthalpy/CH hydrogen in these ions (e.g., compare $\text{Me}(\text{c-C}_6\text{H}_{11})\text{COH}^+$, $\text{Me}(\text{C}_6\text{H}_5)\text{COH}^+$, and pyridine H^+ (Table 12, columns 7 and 9).

Qualitatively, stronger gas-phase basicities reflect increased charge delocalization in ions BH^+ , which makes less charge available for hydrogen bonds to solvent molecules. This accounts for the inverse relation between $\text{PA}(\text{B})$ and solvation exothermicity. However, the observed simple linear relations are unexpected.

In summary, the correlations among gas-phase proton affinities and solvation energies by 1 and 4 H_2O molecules, and the constant cluster solvation enthalpies $\Delta H^\circ_{\text{g-aq}}(\text{BH}^+ \cdot 4\text{H}_2\text{O})$ due to the canceling variation of solvation terms, account for the simple inverse linear relations between gas-phase proton affinities and hydration exothermicities.

9.1.9. Compression of Basicity Scales by Ion Solvation. It has long been noted that substituent effects on acidities and basicities in solution are irregular. For example, increasing methylation first increases and then decreases the basicities of methylamines (Table 11, column 4), leading to many speculations about molecular and solvent effects.

However, early gas-phase HPMS studies starting in the 1960s,^{435a,b} especially a pioneering study by Munson,^{435c} showed that the gas-phase proton affinities increase regularly with increasing methylation from ammonia to trimethylamine.^{435c} Similarly, the gas-phase acidities of alcohols increase regularly with increasingly large alkyl substituents.^{248–252,435d} In comparison, the range of basicities is compressed and sometimes reversed in solution (Table 11, columns 3 and 4), as noted in section 3.3.1 and Figure 37 above.

The compression of basicity scales by solvation is accounted for by the correlations in the preceding section. The relations in eq 20 between relative proton affinities and enthalpies of ion solvation give the relation $\delta\Delta H^\circ_{\text{g-aq}}(\text{BH}^+) = 0.84\delta\text{PA}(\text{B})$, and substituting in eq 37 gives $\delta\Delta H^\circ_{\text{prot,aq}}(\text{B}) = -0.16\delta\text{PA}(\text{B}) - \delta\Delta H^\circ_{\text{g-aq}}(\text{B})$. Neglecting the smaller effects of neutral solvation, these correlations reduce by about a factor of 6 the relative enthalpies of protonation of bases in solution versus in the gas phase, consistent with experimental trends.

For the ions in Table 11 (columns 3, 4, and 6), the relative gas-phase protonation enthalpies of the oxygen bases range over 45.4 kcal/mol, but the ion solvation enthalpies vary opposingly over 42.9 kcal/mol, and as a result, protonation enthalpies in solution range only over 6.2 kcal/mol. For nitrogen bases, the ranges of these values are 30.7, 24.7, and 9.6 kcal/mol, respectively. In these examples, the ranges of the solvation energies are compressed by factors of 7.3 and 3.2, respectively, and in some amines the orders of basicities are reversed, due mostly to differential ion solvation effects.

For example, the enthalpies of proton transfer from MeNH_3^+ to Me_2NH and Me_3N are -7.3 and -11.9 kcal/mol in the gas phase but $+1.2$ and $+4.4$ kcal/mol in solution. Table 12 shows the responsible solvation factors. Compared with MeNH_3^+ , for Me_2NH_2^+ and Me_3NH^+ the total continuum solvation factors (cavity + dielectric charging) are less exothermic by 8.2 and

14.2 kcal/mol for the larger ions; ionic hydrogen bonding is less exothermic by 5.4 and 13.0 kcal/mol due to the fewer protic hydrogens; while hydrophobic solvation is more exothermic by 5.1 and 13.0 kcal/mol with increasing number of $\text{CH}^+ \cdots \text{OH}_2$ bonds. Combined, ion solvation is less exothermic by 6.4 and 14.2 kcal/mol, respectively, for the larger ions.

The hydrogen-bond contributions result from weaker bonds of protonated stronger bases BH^+ to solvent molecules because of the delocalized charge in the ions. As noted, $4\text{H}_2\text{O}$ reproduces the relative solvation enthalpies, implying that the solvation effects result mostly from the first few solvent molecules. The other solvation factors vary compensatingly among the ions (Table 12) and therefore in sum for these compounds they have little effect on the relative solution basicities. These results illustrate the quantitative insights into solvation factors in acid–base thermochemistry that can be gained from a cluster-based analysis.

In summary, comparison of gas-phase and solution basicities identifies the solvation effects on acid/base chemistry, and a cluster-based analysis quantifies the responsible solvation factors. However, the simple linear relations observed above among the energies of protonation and ion solvation are notable.

9.2. Cluster-Based Analysis of Solvation Factors

9.2.1. Cluster-Based Procedure to Calculate Solvation Factors.

The solvation energies of onium ions, obtained from proton affinities and Born cycles,^{20,436a–d} can be used to assign physical factors in ion solvation. Pioneering studies by Aue, Webb, and Bowers found that electrostatic effects could account for the relative solvation energies of alkylammonium and pyridinium ions.^{436a–d} Many other theoretical and computational models also addressed ion solvation.^{437–443,444b,445}

The complex solvation terms include hydrogen bonding in the inner solvent shells, whose contributions are included mostly in the first 4 H_2O molecules. These cluster data can be combined with continuum models for bulk solvent factors to obtain the hydrophobic solvation energies and then all the solvation terms of onium ions.^{33,35}

This cluster-based analysis yields physically reasonable solvation terms (Table 12). In particular, each hydrogen bond of the protic and alkyl hydrogens contributes a constant term to ion solvation.

The cluster-based analysis of the solvation factors can be summarized as follows:

- (1) The solvation energies, $\Delta H^\circ_{\text{g-aq}}(\text{BH}^+\cdot 4\text{H}_2\text{O})$, of the clusters, obtained from eq 38, include the strong IHB interactions in the inner shell. The dielectric and solvent cavity terms for solvating the clusters are calculated from continuum models.^{33,35} The remaining solvation energy is assigned to $\Delta H^\circ_{\text{hydrophobic}}$, the solvation energies of the alkyl groups.
- (2) The solvation energies of the bare nonclustered ions themselves, $\Delta H^\circ_{\text{g-aq}}(\text{BH}^+)$, are then used to calculate the solvation factors of the ions. The dielectric and solvent cavity terms are calculated by continuum models and the hydrophobic terms are assigned from step 1. The remaining solvation energy yields $\Delta H^\circ_{\text{IHB}}$, the ionic hydrogen-bond energies between the protic hydrogens of the protonated functional groups and water molecules in the inner solvent shell.

The procedure and results are described in more detail in the next section. The solvation of ions involves the energy terms in eq 42.

$$\begin{aligned}\Delta H^\circ_{\text{g-aq}}(\text{BH}^+) = & \Delta H^\circ_{\text{cavity}} + \Delta H^\circ_{\text{dielectric}} + \Delta H^\circ_{\text{IHB}} \\ & + \Delta H^\circ_{\text{hydrophobic}} + \Delta H^\circ_{\text{RHB}}\end{aligned}\quad (42)$$

The energy to form a cavity for the ion is denoted ($\Delta H^\circ_{\text{cavity}}$), modeled by macroscopic surface tension or the scaled particle theory;^{444b} the dielectric charging of the solvent about the ion ($\Delta H^\circ_{\text{dielectric}}$), using a double-shell model;⁴⁴⁵ hydrogen bonds of the ions to the inner-shell water molecules ($\Delta H^\circ_{\text{IHB}}$) assigned from cluster data; the neutral-like residual hydrogen bonds of the inner-shell water molecules to the rest of the solvent ($\Delta H^\circ_{\text{RHB}}$); and hydrophobic solvation of the alkyl groups ($\Delta H^\circ_{\text{hydrophobic}}$).

9.2.2. Solvation Factors of the $(\text{BH}^+\cdot 4\text{H}_2\text{O})$ Clusters.

Equation 43 is used:

$$\begin{aligned}\Delta H^\circ_{\text{g-aq}}(\text{BH}^+\cdot 4\text{H}_2\text{O}) = & \Delta H^\circ_{\text{cavity}}(\text{BH}^+\cdot 4\text{H}_2\text{O}) + \Delta H^\circ_{\text{dielectric}}(\text{BH}^+\cdot 4\text{H}_2\text{O}) \\ & + \Delta H^\circ_{\text{hydrophobic}} + \Delta H^\circ_{\text{RHB}}\end{aligned}\quad (43)$$

The energies for creating and charging a cavity to accommodate the cluster $\text{BH}^+\cdot 4\text{H}_2\text{O}$ are calculated from continuum models. The term $\Delta H^\circ_{\text{RHB}}$ is the energy of the $n + 4$ (for an ion BH^+ with n protic hydrogens) residual neutral-like hydrogen bonds of the four inner-shell solvent molecules to the surrounding water molecules. These bonds should be neutral-like since the cluster-bonding energies become equal to the bulk condensation energy of neutral water after 4 H_2O molecules. The present analysis used $\Delta H^\circ_{\text{RHB}} = \Delta H^\circ_{\text{condensation}}(\text{H}_2\text{O})/2 = -5.25$ kcal/mol. With use of the cluster solvation energies from eq 38 and these calculated terms, the remaining energy is assigned to $\Delta H^\circ_{\text{hydrophobic}}$, the solvation of the alkyl groups.

9.2.3. Solvation Factors of Onium Ions. Equation 42 is used. The energies for creating and charging a cavity to accommodate the ion BH^+ are calculated from continuum models. It is assumed that $\Delta H^\circ_{\text{hydrophobic}}(\text{BH}^+)$ is equal to $\Delta H^\circ_{\text{hydrophobic}}(\text{BH}^+\cdot 4\text{H}_2\text{O})$ found in the preceding section, since the hydrophobic solvation is not affected significantly by the hydration of the protonated functional group in the clusters. The remaining solvation energy is assigned to $\Delta H^\circ_{\text{IHB}}$, the contribution of strong ionic hydrogen bonds to the solvation energy. The results of the analysis are presented in Table 12. The analysis yields solvation factors that vary reasonably with ion structure.

Continuum Terms. The total calculated continuum terms (cavity + dielectric charging, Table 12, column 6) change strongly with ion size, from -66.3 kcal/mol for H_3O^+ to -21.6 kcal/mol for $\text{Me}(\text{C}_6\text{H}_{11})\text{COH}^+$ and from -63.4 kcal/mol for NH_4^+ to -23.6 kcal/mol for Et_3NH^+ . Both the cavity and dielectric terms become less favorable for large ions, as the energy to create a cavity surface becomes more positive and the dielectric charging becomes less negative with increasing ionic size. These terms are the main factors that decrease the solvation energies of large ions.

Hydrophobic Solvation. The analysis yields hydrophobic solvation terms that vary reasonably with the number of alkyl hydrogens (Table 12, column 7). It is a small factor for the MeOH_2^+ and MeNH_3^+ ions that have small alkyl substituents (-9.9 and -4.8 kcal/mol, respectively). It becomes a major

term for ions such as $\text{Me}(\text{C}_6\text{H}_{11})\text{COH}^+$ (-33.0 kcal/mol) and Et_3NH^+ (-30.6 kcal/mol). For the ions in Table 12, the contribution of each alkyl hydrogen is $-3.5 \pm 1 \text{ kcal/mol}$ per hydrogen for most oxonium ions and $-1.8 \pm 0.2 \text{ kcal/mol}$ per alkyl hydrogen for most ammonium ions (Table 12, column 9). The hydrophobic solvation per CH hydrogen decreases somewhat in the larger ions as the charge is more dispersed and each CH hydrogens carries less positive charge. Aromatic CH hydrogens appear to be solvated more strongly, as the charge is more concentrated on each hydrogen on the hydrogen-deficient substituents. However, there are fewer CH donors on aromatic substituents, and this decreases somewhat the total hydrophobic solvation energies of ions with aromatic substituents.

$$\begin{aligned}\Delta H^\circ_{\text{hydrophobic}} &= -3.5 \pm 1 n_{\text{CH}} \text{ kcal/mol alkyloxonium ions} \\ &\quad -2.5 \pm 0.3 n_{\text{CH}} \text{ kcal/mol alkylammonium ions} \\ \Delta H^\circ_{\text{IHB}} = &-25 \pm 1 n_{\text{OH}^+} \text{ kcal/mol monoprotonic oxonium ions} \\ &-14 \pm 1 n_{\text{OH}^+} \text{ kcal/mol polyprotic oxonium ions} \\ &-9.8 \pm 1 n_{\text{NH}^+} \text{ kcal/mol alkylammonium ions}\end{aligned}\quad (44)$$

Ionic Hydrogen Bonds. The calculated IHB terms vary consistently with the number of protic hydrogens (Table 12, column 8), contributing -45.8 kcal/mol for H_3O^+ with three protic hydrogens, $-39 \pm 1 \text{ kcal/mol}$ for oxonium ions with two, and $-25 \pm 2 \text{ kcal/mol}$ for most oxonium ions with one protic hydrogen. Similarly, the IHB terms decrease regularly with the number of protic hydrogens in the ammonium ions, where it is a major term for NH_4^+ (-25.2 kcal/mol) but only a minor term for monoprotonic ions such as Et_3NH^+ (-9.8 kcal/mol). In general, the IHB term is larger for oxonium ions than for comparable alkylammonium ions as expected on the basis of $\Delta\text{PA}/\text{IHB}$ bond strength correlations. When the analysis is applied to non-hydrogen-bonding alkali metal ions, it indeed yields negligible terms for the IHB terms (Table 12, column 8).

The results show that each alkyl or protic hydrogen makes an approximately constant contribution to ion solvation (Table 12, column 10). The intermolecular forces in ion solvation are therefore decomposed to simple contributions per alkyl or protic hydrogen. The hydrogen-bonding energies are described by eq 44, where n_{CH} is the number of alkyl hydrogens and n_{OH^+} and n_{NH^+} are the numbers of protic hydrogens of alkyloxonium and alkylammonium ions, respectively. The weaker IHB bonds of the ammonium versus oxonium ions to the inner H_2O molecules are consistent with the ΔPA correlations discussed above.

Table 12 shows that in the hydration of ions with several protons, such as H_3O^+ , most polyprotic oxonium ions, and NH_4^+ and RNH_3^+ ions, IHB is the dominant intermolecular force, while in larger ions with less protic and more CH hydrogens, the hydrophobic terms are larger. These results are reasonable structurally.

The structurally reasonable result is encouraging, since no structural information was input. The analysis is based purely on the experimental binding energies of clusters and ion solvation energies and the continuum models for the cavity and dielectric terms based on ion radius alone. Nevertheless, the results correlate well with structure, and even deviations such as those observed for aromatics are structurally plausible.

Finally, note that the above solvation factors, as also covalent/electrostatic bond energies and inductive/resonance effects, cannot be measured separately. Nevertheless, they reduce solvation energies to physically reasonable predictive terms.

10. CONCLUSIONS AND OUTLOOK

Strong ionic hydrogen bonds are important in many natural and industrial processes. Mass spectrometric cluster studies have provided a quantitative understanding of these forces.

10.1. Correlations between Bond Strengths and the Relative Acidities and Basicities of the Components

The first basic findings were correlations between IHB bond energies and the relative basicities or acidities of the components. These correlations reflect the efficiency of sharing the bonding proton. The relations apply to dimers with various components and extend to larger clusters and even to bulk solvation. The correlations provide means to estimate IHB energies in more complex systems, such as in biomolecules.

10.2. Unconventional, Internal, and Polydentate Bonds

Special cases occur with carbon-based IHB donors and receptors. Also, polyatomic molecules exhibit internal and polydentate IHB complexes with energetics that correlate with structure in terms geometry, bond strain, and multiple IHB formation. Intramolecular and external solvation have mutually weakening effects, where the internal bond serves as the first solvent molecule. Solvent molecules insert into internal hydrogen bonds to form solvent bridges.

10.3. Hydrogen-Bond Networks

In larger clusters, unlimited hydrogen-bond networks may form, or limited networks surrounded by alkyl-blocked components. In the blocked clusters, the proton can be located in a strongly hydrogen-bonding core, even when it is surrounded by blocked components that are stronger bases. This has important consequences in biological membrane transport.

10.4. Effects on Acidities and Basicities

Gas-phase studies revealed the intrinsic molecular acidities and basicities of molecules. Comparison with solution showed that solvent effects can greatly compress or reverse the relative acidities and basicities. Cluster studies show the stepwise development of the solvent effects and demonstrate that up to 80% of the effects can be due to the inner-shell solvent molecules.

10.5. Biomolecules and the Condensed Phase

The principal trends observed in model organic ions— ΔPA correlations, internal and polydentate bonds, and solvent bridges—have been found more recently to be ubiquitous and crucial in biomolecules. Also, the contributions of IHBs to enzyme energetics, membrane transport, and molecular recognition can be assessed quantitatively from cluster models. More recently, spectroscopic and ion mobility studies have confirmed many structural conclusions from thermochemistry. Similar IHB effects are observed also in solution and in crystals.

10.6. Partial and Bulk Solvation

The comparison of ion solvation in small clusters and in bulk solution yields unexpected results. Partial solvation of the protonated functional groups by as few as 4–6 water molecules

reproduces the relative bulk solvation energies of diverse onium ions. In other words, the further bulk solvation energies of the $(BH^+ \cdot 4H_2O)$ clusters of diverse onium ions are equal, although bulk solvation introduces very different solvation factors for the various core ions. This result indicates an exactly canceling variation of cavity, dielectric, and hydrophobic solvation factors among diverse ions, although these factors should be physically independent. This effect allows prediction of bulk ion solvation energies based only on gas-phase proton affinities.

10.7. Large Clusters and Single-Ion Solvation Energies

The data on small clusters, combined with conventional bulk solvation energies, yield quantitative information on the cumulative binding energies of large clusters that bridge between clusters and solution. Alternatively, the cluster data can be used to calculate cluster-based truly single-ion solvation energies. These are much smaller (less negative) than the conventional values based on electrolyte solution, suggesting significant ion-pair interactions even in dilute electrolyte solutions. The correct interpretation requires accurate measurements of the binding energies of large clusters.

10.8. Compression of Basicity Scales by Ion Solvation

Protonated ions BH^+ of strong bases, with delocalized charge, form weak hydrogen bonds to solvent molecules. This leads to a surprisingly simple inverse linear relation between the gas-phase proton affinities and bulk solvation enthalpies. Ions of strong bases are less stabilized by solvation, which leads to a significant compression or reversal of basicity scales from the gas phase to solution. The underlying solvation factors are revealed by a cluster-based analysis of ion solvation factors.

10.9. Cluster-Based Analysis of Solvation Factors

The strong contributions of ionic hydrogen bonds of ions to the inner solvent shells are included in the energies of small clusters. The experiment-based solvation energies of the clusters allow an analysis that quantifies these IHB contributions, as well as the continuum and hydrophobic solvation energies. The analysis yields structurally reasonable terms, assigning the hydrogen-bonding contributions by each alkyl and protic hydrogen.

10.10. Outlook

Ionic hydrogen bonds are significant in many aspects of chemistry. The basic properties of these bonds have been established in the last four decades, and their study has developed into a mature quantitative science. Extensions of the thermochemical studies to biomolecules and large clusters and structural studies by spectroscopy and ion mobility, and applications to understand ion solvation, are active fields that pose challenges for the next decades.

AUTHOR INFORMATION

Corresponding Author

*E-mail: mmautner@vcu.edu.

Notes

The authors declare no competing financial interest.

Biography



Michael Mautner was born in 1942 in Budapest, Hungary, and was saved from the Holocaust with the help of a courageous woman, Irene Giger-Horvath. He obtained a B.Sc. from the Hebrew University (Meot-Ner, meaning "Hundreds of Lights", is a transliteration of Mautner), a M.Sc. from Georgetown University, and a Ph.D. from Rockefeller University, New York, using the historic mass spectrometer on which Prof. F. H. Field invented chemical ionization. Current research interests are fundamental ion kinetics and thermochemistry, gas-phase acidities and basicities, cluster ions, charge-transfer complexes, and ionic processes in astrochemistry and bioenergetics. The author served on the faculty of Rockefeller University and as Research Chemist at NIST, is currently Research Professor at Virginia Commonwealth University, and is also affiliated with The University of Canterbury in New Zealand. Other research interests concern space colonization, the biological fertilities asteroid and meteorite materials as future space resources, and the science and ethics of seeding other solar systems with microbial life (www.astro-ecology.com).

ACKNOWLEDGMENTS

The author thanks NASA, Grant NNG04GH45G, for partial funding of this work. I also thank Mrs. H. D. Mautner for help with organizing the manuscript, figures, and references.

REFERENCES

- (1) Moore, T. S.; Windmill, T. F. *J. Chem. Soc.* **1912**, 1011, 1635.
- (2) Pauling, L. *The Chemical Bond: A Brief Introduction to Modern Structural Chemistry*; Cornell University Press: Ithaca, NY, 1967.
- (3) Aakeroy, C. B.; Beatty, A. M. *Aust. J. Chem.* **2001**, 54, 409.
- (4) Field, F. H. *J. Am. Chem. Soc.* **1969**, 91, 2827.
- (5) Kebarle, P. *Annu. Rev. Phys. Chem.* **1977**, 28, 445.
- (6) Caldwell, G.; Rozeboom, M. D.; Kiplinger, J. P.; Bartmess, J. E. *J. Am. Chem. Soc.* **1984**, 106, 4660.
- (7) Larson, J. W.; McMahon, T. B. *J. Am. Chem. Soc.* **1984**, 106, 517.
- (8) Larson, J. W.; McMahon, T. B. *J. Am. Chem. Soc.* **1987**, 109, 6230.
- (9) Gorman, G. S.; Amster, J. I. *J. Am. Chem. Soc.* **1993**, 115, 5729.
- (10) Dearden, D. V.; Liang, Y.; Nicoli, J. B.; Kellersberg, A. J. *Mass Spectrom.* **2001**, 36, 989.
- (11) Mackay, G. I.; Bohme, D. K. *J. Am. Chem. Soc.* **1978**, 100, 327.
- (12) (a) von Helden, G.; Hsu, M.-T.; Kemper, P. R.; Bowers, M. T. *J. Chem. Phys.* **1991**, 95, 3835. (b) Bowers, M. T.; Kemper, P. R.; von Helden, G.; van Koppen, P. A. M. *Science* **1993**, 260, 1446. (c) Kemper, P. R.; Dupuis, N. F.; Bowers, M. T. *Int. J. Mass Spectrom.* **2009**, 287, 46. (d) Wyttenbach, T.; Bowers, M. T. *Chem. Phys. Lett.* **2009**, 480, 1. (e) Wyttenbach, T.; Bowers, M. T. *Annu. Rev. Phys. Chem.* **2007**, 58, 511.
- (13) Woenckhaus, J.; Hudgins, R. R.; Jarrold, M. F. *J. Am. Chem. Soc.* **1997**, 119, 9586.

- (14) Dalleska, N. F.; Honma, K.; Armentrout, P. B. *J. Am. Chem. Soc.* **1993**, *115*, 12125.
- (15) Dunbar, R. C.; McMahon, T. B.; Tholmann, D.; Tonner, D. S.; Salahub, D. R.; Wei, D. *J. Am. Chem. Soc.* **1995**, *117*, 12819.
- (16) Gross, D. S.; Williams, E. R. *J. Am. Chem. Soc.* **1995**, *117*, 883.
- (17) Gross, D. S.; Schnier, P. D.; Rodriguez-Cruz, S. E.; Fagerquist, C. K.; Williams, E. R. *Proc. Natl. Acad. Sci. U.S.A.* **1996**, *93*, 3143.
- (18) Price, W. D.; Schnier, P. D.; Williams, E. R. *J. Phys. Chem. B* **1997**, *101*, 664.
- (19) Yamdagni, R.; Kebarle, P. *J. Am. Chem. Soc.* **1976**, *98*, 1320.
- (20) Taft, R. W. *Prog. Phys. Org. Chem.* **1983**, *14*, 248.
- (21) Meot-Ner (Mautner), M.; Sieck, L. W. *J. Am. Chem. Soc.* **1991**, *113*, 4448.
- (22) Szulejko, J. E.; McMahon, T. B. *J. Am. Chem. Soc.* **1993**, *115*, 7839.
- (23) Smith, B. J.; Radom, L. *J. Am. Chem. Soc.* **1993**, *115*, 4885.
- (24) East, A. L. L.; Smith, B. J.; Radom, L. *J. Am. Chem. Soc.* **1997**, *119*, 9014.
- (25) Hunter, E. P. L.; Lias, S. G. *J. Phys. Chem. Ref. Data* **1998**, *27*, 413.
- (26) Meot-Ner (Mautner), M. *Int. J. Mass Spectrom.* **2003**, *227*, 525.
- (27) Hunter, E. P.; Lias, S. G. Proton Affinity Evaluation. In *NIST Chemistry WebBook*; Linstrom, P. J., Mallard, W. G., Eds.; NIST Standard Reference Database Number 69; National Institute of Standards and Technology: Gaithersburg, MD, March 2003 (<http://webbook.nist.gov>).
- (28) Keesee, R. G.; Castleman, A. W. *J. Phys. Chem. Ref. Data* **1986**, *15*, 1011.
- (29) Meot-Ner (Mautner), M.; Lias, S. G. Binding Energies Between Ions and Molecules, and The Thermochemistry of Cluster Ions. In *NIST Chemistry WebBook*; Linstrom, P. J., Mallard, W. G., Eds.; NIST Standard Reference Database Number 69; National Institute of Standards and Technology: Gaithersburg, MD, March 2003 (<http://webbook.nist.gov>).
- (30) Bartmess, J. E. Negative Ion Energetics Data. In *NIST Chemistry WebBook*; Linstrom, P. J., Mallard, W. G., Eds.; NIST Standard Reference Database Number 69; National Institute of Standards and Technology: Gaithersburg, MD, March 2003 (<http://webbook.nist.gov>).
- (31) Deakyne, C. A. In *Molecular Interactions*; Scheiner, S., Ed.; John Wiley: New York, 1997; p 217.
- (32) (a) Scheiner, S. In *Molecular Interactions*; Scheiner, S., Ed.; John Wiley: New York, 1997. (b) Perrin, C. L.; Nielson, J. B. *Annu. Rev. Phys. Chem.* **1997**, *48*, 511. (c) Perrin, C. L. *Acc. Chem. Res.* **2010**, *43*, 1550.
- (33) Meot-Ner (Mautner), M. In *Molecular Structure and Energetics*; Liebman, J. F., Greenberg, H., Eds.; VCH Publishers: New York, 1987; Vol. 4, p 71.
- (34) Meot-Ner (Mautner), M.; Lias, S. G. Binding Energies between Ions and Molecules and the Thermochemistry of Cluster Ions. In *NIST Chemistry Webbook*; Linstrom, P. J., Mallard, W. G., Eds.; NIST Standard Reference Database Number 69; National Institute of Standards and Technology: Gaithersburg, MD, July 2001 (<http://webbook.nist.gov>).
- (35) Meot-Ner (Mautner), M. *J. Phys. Chem.* **1987**, *91*, 417.
- (36) Deakyne, C. A. *J. Phys. Chem.* **1986**, *90*, 6625.
- (37) Desmeules, P. J.; Allen, L. C. *J. Chem. Phys.* **1980**, *72*, 4731.
- (38) Yamdagni, R.; Kebarle, P. *J. Am. Chem. Soc.* **1971**, *93*, 7139.
- (39) Yamdagni, R.; Kebarle, P. *J. Am. Chem. Soc.* **1973**, *95*, 3504.
- (40) (a) Davidson, W. R.; Sunner, J.; Kebarle, P. *J. Am. Chem. Soc.* **1979**, *101*, 1675. (b) Moore, D. T.; Oomens, J.; van der Meer, L.; von Helden, G.; Meijer, G.; Valle, J.; Marshall, A. G.; Eyler, J. R. *ChemPhysChem* **2004**, *5*, 740. (c) Fridgen, T. D.; MacAleese, L.; Maitre, P.; McMahon, T. B.; Boissel, P.; Lemaire, J. *Phys. Chem. Chem. Phys.* **2005**, *7*, 2747. (d) Diken, E. G.; Headrick, J. M.; Roscioli, J. R.; Bopp, J. C.; Johnson, M. A.; McCoy, A. B.; Huang, X.; Carter, S.; Bowman, J. M. *J. Phys. Chem. A* **2005**, *109*, 571. (e) Roscioli, J. R.; Diken, E. G.; Johnson, M. A.; Horvath, S.; McCoy, A. B. *J. Phys. Chem. A* **2006**, *110*, 4943. (f) Asmis, K. R.; Yang, Y.; Santambrogio, G.; Brummer, M.; Roscioli, J. R.; McCunn, L. R.; Johnson, M. A.; Kuhn, O. *Angew. Chem., Int. Ed.* **2007**, *46*, 8691. (g) Roscioli, J. R.; McCunn, L. R.; Johnson, M. A. *Science* **2007**, *316*, 249.
- (41) French, M. A.; Ikuta, S.; Kebarle, P. *Can. J. Chem.* **1982**, *60*, 1907.
- (42) Meot-Ner (Mautner), M.; Sieck, L. W.; Koretke, K. K.; Deakyne, C. A. *J. Am. Chem. Soc.* **1997**, *119*, 10430.
- (43) (a) Meot-Ner (Mautner), M.; Cybulski, S. M.; Scheiner, S.; Liebman, J. F. *J. Phys. Chem.* **1988**, *92*, 2738. (b) Wang, S. B.; Kowalski, K.; Wang, L. S.; Xantheas, S. S. *J. Chem. Phys.* **2010**, *132*, 124306.
- (44) Bieske, E. J.; Nizkorodov, S. A.; Bennett, F. R.; Maier, J. P. *Int. J. Mass Spectrom., Ion Processes* **1995**, *149*, 167.
- (45) Bieske, E. J.; Nizkorodov, S. A.; Bennett, F. R.; Maier, J. P. *J. Chem. Phys.* **1995**, *104*, 5152.
- (46) Hobza, P.; Zahradník, R. *Chem. Phys. Lett.* **1993**, *208*, 497.
- (47) Scheiner, S. *Acc. Chem. Res.* **1985**, *18*, 174.
- (48) Meot-Ner (Mautner), M. *J. Am. Chem. Soc.* **1984**, *106*, 1257.
- (49) Meot-Ner (Mautner), M. *J. Am. Chem. Soc.* **1984**, *106*, 1265.
- (50) Larson, J. W.; McMahon, T. B. *J. Am. Chem. Soc.* **1982**, *104*, 6255.
- (51) (a) Kebarle, P.; Davidson, W. R.; French, M.; Cumming, J. B.; McMahon, T. B. *Faraday Discuss.* **1977**, *64*, 220. (b) Taagepera, M.; DeFrees, D. J.; Hehre, W. J.; Taft, R. W. *J. Am. Chem. Soc.* **1980**, *102*, 424. (c) Bromilow, J.; Abboud, J. L. M.; Lebrilla, C. B.; Taft, R. W.; Scorrano, G.; Lucchini, V. *J. Am. Chem. Soc.* **1981**, *103*, 5448.
- (52) Arshadi, M.; Kebarle, P. *J. Phys. Chem.* **1970**, *74*, 1483.
- (53) Feng, W. Y.; Ling, Y.; Lifschitz, C. *J. Phys. Chem.* **1996**, *100*, 35.
- (54) Meot-Ner (Mautner), M.; Sieck, L. W. *J. Phys. Chem.* **1985**, *89*, 5222.
- (55) Meot-Ner (Mautner), M.; Sieck, L. W. *J. Am. Chem. Soc.* **1986**, *108*, 7525.
- (56) Sieck, L. W.; Meot-Ner (Mautner), M. *J. Phys. Chem.* **1989**, *93*, 1586.
- (57) Larson, J. W.; McMahon, T. B. *J. Am. Chem. Soc.* **1983**, *105*, 2945.
- (58) Meot-Ner (Mautner), M. *J. Am. Chem. Soc.* **1988**, *110*, 3858.
- (59) Meot-Ner (Mautner), M.; Field, F. H. *J. Chem. Phys.* **1977**, *66*, 4527.
- (60) Hiraoka, K.; Saluja, P. P. S.; Kebarle, P. *Can. J. Chem.* **1976**, *57*, 2159.
- (61) Meot-Ner (Mautner), M.; Field, F. H. *J. Am. Chem. Soc.* **1977**, *99*, 998.
- (62) (a) Hiraoka, K.; Takimoto, H.; Yamabe, S. *J. Phys. Chem.* **1986**, *90*, 5910. (b) Meot-Ner (Mautner), M.; Sieck, L. W. *J. Am. Chem. Soc.* **1983**, *105*, 2956. (c) Norrman, K.; McMahon, T. B. *Int. J. Mass Spectrom.* **1999**, *183*, 381.
- (63) (a) Witt, M.; Grutzmacher, H. F. *Int. J. Mass Spectrom.* **1997**, *165–166*, 49. (b) Witt, M.; Grutzmacher, H. F. *Eur. J. Mass Spectrom.* **2000**, *6*, 97. (c) Witt, M.; Kreft, D.; Grutzmacher, H. F. *Eur. J. Mass Spectrom.* **2003**, *9*, 81.
- (64) (a) Hiraoka, K.; Kebarle, P. *Can. J. Chem.* **1977**, *55*, 24. (b) Chan, B.; Del Bene, J. E.; Radom, L. *J. Am. Chem. Soc.* **2007**, *129*, 12197. (c) Chan, B.; Del Bene, J. E.; Radom, L. *Mol. Phys.* **2009**, *107*, 1095.
- (65) Long, J. W.; Franklin, J. L. *J. Am. Chem. Soc.* **1974**, *96*, 2320.
- (66) Meot-Ner (Mautner), M. *J. Am. Chem. Soc.* **1989**, *111*, 2830.
- (67) Allison, C. E.; Cramer, J. A.; Hop, C. E. C.; Szulejko, J. E.; McMahon, T. B. *J. Am. Chem. Soc.* **1991**, *113*, 4469.
- (68) Zeegers-Huyskens, Th. *J. Mol. Struct. (THEOCHEM)* **1986**, *135*, 93.
- (69) Zeegers-Huyskens, Th. *J. Mol. Struct. (THEOCHEM)* **1988**, *177*, 125.
- (70) Zeegers-Huyskens, Th.; Huyskens, P. L. In *Intermolecular forces. An Introduction to Modern Methods and Results*; Huyskens, P. L., Luck, W. A. P., Zeegers-Huyskens, Th., Eds.; Springer-Verlag: Berlin, Heidelberg, 1991; p 24.
- (71) Zeegers-Huyskens, Th. *J. Mol. Liq.* **1995**, *67*, 33.

- (72) Chandra, A. K.; Nguyen, M. T.; Uchimaru, T.; Zeegers-Huyskens, T. *J. Phys. Chem. A* **1999**, *103*, 8853.
- (73) Chandra, A. K.; Nguyen, M. T.; Zeegers-Huyskens, T. *J. Chem. Phys.* **2000**, *25S*, 149.
- (74) Payzant, J. D.; Yamdagni, R.; Kebarle, P. *Can. J. Chem.* **1971**, *49*, 3308.
- (75) Caldwell, G.; Kebarle, P. *Can. J. Chem.* **1985**, *63*, 1399.
- (76) Caldwell, G.; Kebarle, P. *J. Am. Chem. Soc.* **1984**, *106*, 967.
- (77) Evans, D. H.; Keesee, R. G.; Castleman, A. W. *J. Chem. Phys.* **1987**, *86*, 2927.
- (78) Larson, J. W.; Szulejko, J. E.; McMahon, T. B. *J. Am. Chem. Soc.* **1988**, *110*, 7604.
- (79) Meot-Ner (Mautner), M. *J. Am. Chem. Soc.* **1988**, *110*, 3854.
- (80) Gao, J.; Garner, D. S.; Jorgensen, W. L. *J. Am. Chem. Soc.* **1986**, *108*, 4784.
- (81) Cuming, J. B.; French, M. A.; Kebarle, P. *J. Am. Chem. Soc.* **1977**, *99*, 6999.
- (82) (a) Elmsley, J. E.; Hoyte, O. P. A.; Overill, R. E. *J. Chem. Soc., Perkin Trans. 2* **1977**, 2079. (b) Nieckarz, R. J.; Oldridge, N.; McMahon, T. B. *Int. J. Mass Spectrom.* **2007**, *267*, 338.
- (83) (a) Sieck, L. W. *J. Phys. Chem.* **1985**, *89*, 5552. (b) Bogdanov, B.; Lee, H. J. S.; McMahon, T. B. *Int. J. Mass Spectrom.* **2001**, *210–211*, 387. (c) Bogdanov, B.; McMahon, T. B. *Int. J. Mass Spectrom.* **2002**, *219*, 593.
- (84) Pudzianowski, A. T. *J. Chem. Phys.* **1995**, *102*, 8029.
- (85) Pudzianowski, A. D. *J. Phys. Chem.* **1996**, *100*, 4781.
- (86) Robertson, W. H.; Johnson, M. A. *Annu. Rev. Phys. Chem.* **2003**, *54*, 173.
- (87) Robertson, W. H.; Weddle, G. H.; Johnson, M. A. *J. Phys. Chem. A* **2003**, *107*, 9312.
- (88) (a) Corbett, C. A.; Martinez, T. J.; Lisy, J. M. *J. Phys. Chem. A* **2002**, *106*, 10015. (b) Nieckarz, R. J.; Oldridge, N.; Fridgen, T. D.; Guanping, P. L.; Hamilton, I. P.; McMahon, T. B. *J. Phys. Chem. A* **2009**, *113*, 644.
- (89) Liebman, J. F.; Romm, M. J.; Meot-Ner (Mautner), M.; Cybulski, S. M.; Scheiner, S. *J. Phys. Chem.* **1991**, *95*, 1112.
- (90) Meot-Ner (Mautner), M.; Sieck, L. W.; Liebman, J. F.; Scheiner, S. *J. Phys. Chem.* **1996**, *100*, 6445.
- (91) (a) Meot-Ner (Mautner), M.; Sieck, L. W. *J. Am. Chem. Soc.* **1983**, *105*, 2956. (b) Mo, O.; Yanez, M.; Elguero, J. *J. Org. Chem.* **1987**, *52*, 1713.
- (92) Glasstone, S. *Trans. Faraday Soc.* **1937**, *33*, 200.
- (93) (a) Meot-Ner (Mautner), M.; Deakyne, C. A. *J. Am. Chem. Soc.* **1985**, *107*, 468. (b) Prell, J. S.; Williams, E. R. *J. Am. Chem. Soc.* **2009**, *131*, 4110.
- (94) (a) Deakyne, C. A.; Meot-Ner (Mautner), M. *J. Am. Chem. Soc.* **1985**, *107*, 474. (b) Wu, R.; McMahon, T. B. *J. Am. Chem. Soc.* **2008**, *130*, 12554.
- (95) Blades, A. T.; Klassen, J. S.; Kebarle, P. *J. Am. Chem. Soc.* **1996**, *118*, 12437.
- (96) (a) Uggerud, E. *J. Am. Chem. Soc.* **1994**, *116*, 6873. (b) Audier, H. E.; Koyanagi, G. K.; McMahon, T. B.; Tholmann, D. *J. Phys. Chem.* **1996**, *100*, 8220. (c) Mabrouki, R.; Ibrahim, Y.; Enli, X.; Meot-Ner, M.; El-Shall, M. S. *J. Phys. Chem. A* **2006**, *110*, 7334.
- (97) Klassen, J. S.; Blades, A. T.; Kebarle, P. *J. Am. Chem. Soc.* **1994**, *116*, 12075.
- (98) Hiraoka, K.; Takao, K.; Nakagawa, F.; Iino, T.; Ishida, M.; Fujita, K.; Hiizumi, K.; Yamabe, S. *Int. J. Mass Spectrom.* **2003**, *227*, 391.
- (99) Hiraoka, K.; Shoda, T.; Kudaka, I.; Fujimaki, S.; Mizuse, S.; Yamabe, S.; Wasada, H.; Wasada-Tsutsui, Y. *J. Phys. Chem. A* **2003**, *107*, 775.
- (100) Meot-Ner (Mautner), M.; Ross, M. M.; Campana, J. E. *J. Am. Chem. Soc.* **1985**, *107*, 4839.
- (101) Hiraoka, K.; Takimoto, H.; Yamabe, S. *J. Am. Chem. Soc.* **1987**, *109*, 7346.
- (102) Meot-Ner (Mautner), M. *J. Am. Chem. Soc.* **1978**, *100*, 4694.
- (103) Grimsrud, E. P.; Kebarle, P. *J. Am. Chem. Soc.* **1973**, *95*, 7939.
- (104) Hahndorf, I.; Jiang, J. C.; Chang, H. C.; Wu, C. C.; Chang, H. C. *J. Phys. Chem. A* **1999**, *103*, 8753.
- (105) Dopfer, O.; Roth, D.; Maier, J. P. *J. Am. Chem. Soc.* **2002**, *124*, 494.
- (106) (a) Solca, N.; Dopfer, O. *Chem.—Eur. J.* **2003**, *9*, 3154. (b) Solca, N.; Dopfer, O. *J. Am. Chem. Soc.* **2004**, *126*, 9520. (c) Solca, N.; Dopfer, O. *J. Phys. Chem. A* **2005**, *109*, 6174.
- (107) Smith, R. D.; Futrell, J. H. *Chem. Phys. Lett.* **1976**, *41*, 64.
- (108) Audier, H. E.; Koyanagi, G. K.; McMahon, T. B.; Tholman, D. *J. Phys. Chem.* **1996**, *100*, 8220.
- (109) Bouchoux, G.; Hoppiliard, Y. *J. Am. Chem. Soc.* **1990**, *112*, 9110.
- (110) Swanton, D. J.; Marsden, D. C. D.; Radom, L. *Org. Mass Spectrom.* **1991**, *26*, 227.
- (111) Bouchoux, G.; Nguyen, M. T.; Longevaille, P. *J. Am. Chem. Soc.* **1992**, *114*, 10000.
- (112) Norrman, K.; McMahon, T. B. *J. Phys. Chem. A* **1999**, *103*, 7008.
- (113) Hiraoka, K.; Katsuragawa, J.; Sugiyama, T.; Kojima, T.; Yamabe, S. *J. Am. Soc. Mass Spectrom.* **2001**, *12*, 144.
- (114) Wincel, H. *Int. J. Mass Spectrom.* **2003**, *226*, 341.
- (115) Ma, J. C.; Dougherty, D. A. *Chem. Rev.* **1997**, *97*, 1303.
- (116) (a) Lee, J. Y.; Lee, S. J.; Choi, H. S.; Cho, S. J.; Kim, K. S.; Ha, T. K. *Chem. Phys. Lett.* **1995**, *232*, 67. (b) Soliman, A. R.; Hamid, A. M.; Abrash, S. A.; El-Shall, M. S. *Chem. Phys. Lett.* **2012**, *523*, 25.
- (117) (a) Meot-Ner (Mautner), M.; Hamlet, P.; Hunter, E. P.; Field, F. H. *J. Am. Chem. Soc.* **1978**, *100*, 5466. (b) Ibrahim, Y.; Alshraeh, E.; Rusyniak, M.; Watson, S.; Meot-Ner (Mautner), M.; El-Shall, M. S. *Chem. Phys. Lett.* **2003**, *380*, 21. (c) Miyazaki, M.; Fujii, A.; Mikami, N. *J. Phys. Chem. A* **2004**, *108*, 8269. (d) Ibrahim, Y.; Alsharaeh, E.; Dais, K.; Meot-Ner (Mautner), M.; El-Shall, M. S. *J. Am. Chem. Soc.* **2004**, *126*, 12766. (e) Ibrahim, Y.; Meot-Ner (Mautner), M.; Alsharaeh, E. H.; El-Shall, M. S.; Scheiner, S. *J. Am. Chem. Soc.* **2005**, *127*, 7053. (f) Ibrahim, Y.; Mabrouki, R.; Meot-Ner (Mautner), M.; El-Shall, M. S. *J. Phys. Chem. A* **2007**, *111*, 1006.
- (118) (a) Tzusuki, S.; Mikami, M.; Yamada, S. *J. Am. Chem. Soc.* **2007**, *129*, 8656. (b) El-Shall, M. S.; Ibrahim, Y. M.; Alshraeh, E. H.; Meot-Ner (Mautner), M.; Watson, S. P. *J. Am. Chem. Soc.* **2009**, *131*, 10066.
- (119) (a) Fujii, A.; Patwari, G. N.; Ebata, T.; Mikami, N. *Int. J. Mass Spectrom.* **2002**, *220*, 289. (b) Fujii, A.; Ebata, T.; Mikami, N. *J. Phys. Chem. A* **2002**, *106*, 8554.
- (120) Solca, N.; Dopfer, O. *J. Phys. Chem. A* **2003**, *107*, 4046.
- (121) Kosugi, K.; Inokuchi, Y.; Nishi, N. *J. Chem. Phys.* **2001**, *114*, 4805.
- (122) Fujimaki, E.; Fujii, A.; Ebata, T.; Mikami, N. *J. Chem. Phys.* **2000**, *112*, 137.
- (123) Norrman, K.; McMahon, T. B. *J. Am. Chem. Soc.* **1996**, *118*, 2449.
- (124) Deakyne, C. A.; Meot-Ner (Mautner), M. *J. Am. Chem. Soc.* **1999**, *121*, 1546.
- (125) Chabinyc, M. L.; Brauman, J. I. *J. Phys. Chem. A* **1999**, *103*, 9163.
- (126) Chabinyc, M. L.; Brauman, J. I. *J. Am. Chem. Soc.* **2000**, *122*, 8739.
- (127) Afeefy, H. Y.; Liebman, J. F.; Stein, S. E. Neutral Thermochemical Data. In *NIST Chemistry WebBook*; Linstrom, P. J., Mallard, W. G., Eds.; NIST Standard Reference Database Number 69; National Institute of Standards and Technology: Gaithersburg, MD, March 2003 (<http://webbook.nist.gov>).
- (128) Lias, S. G.; Bartmess, J. E.; Liebman, J. F.; Holmes, J. L.; Levin, R. D.; Mallard, W. G. Ion Energetics Data. In *NIST Chemistry WebBook*; Linstrom, P. J., Mallard, W. G., Eds.; NIST Standard Reference Database Number 69; National Institute of Standards and Technology: Gaithersburg, MD, March 2003 (<http://webbook.nist.gov>).
- (129) (a) Hiraoka, K.; Kebarle, P. *J. Am. Chem. Soc.* **1976**, *98*, 6119. (b) Aschi, M.; Cacace, F.; de Petris, G.; Pepi, F. *J. Phys. Chem.* **1996**,

- 100, 16522. (c) Mabrouki, R.; Ibrahim, Y.; Enli, X.; Meot-Ner (Mautner), M.; El-Shall, M. S. *Chem. Phys. Lett.* **2006**, *424*, 257.
- (130) Sirois, M.; George, M.; Holmes, J. L. *Org. Mass Spectrom.* **1994**, *29*, 11.
- (131) Zagorevskii, D. V.; Palii, S. P.; Holmes, J. L. *J. Am. Soc. Mass Spectrom.* **1994**, *5*, 814.
- (132) Hiraoka, K.; Kebarle, P. *J. Am. Chem. Soc.* **1977**, *99*, 360.
- (133) Walters, E. A.; Grover, J. R.; White, M. G.; Hui, E. T. *J. Phys. Chem.* **1985**, *89*, 3814.
- (134) McAdoo, D. J.; Morton, T. H. *Acc. Chem. Res.* **1993**, *26*, 295.
- (135) Terlouw, J. K.; deKoster, C. G.; Heerma, W.; Holmes, J. L.; Burgers, P. C. *Org. Mass Spectrom.* **1983**, *18*, 222.
- (136) Postma, R.; Ruttink, P. J. A.; van Duijneveldt, F. B.; Terlouw, J. K.; Holmes, J. L. *Can. J. Chem.* **1985**, *64*, 2798.
- (137) Postma, R.; Ruttink, P. J. A.; Terlouw, J. K.; Holmes, J. L. *J. Chem. Soc., Chem. Commun.* **1986**, 683.
- (138) Holmes, J. L.; Mommers, A. A.; Szulejko, J. E.; Terlouw, J. K. *J. Chem. Soc., Chem. Commun.* **1984**, 165.
- (139) Shao, J. D.; Baer, T.; Morrow, J. C.; Fraser-Monteiro, M. L. *J. Chem. Phys.* **1987**, *87*, 5242.
- (140) Hrusak, J.; McGibbon, G. A.; Schwartz, H.; Terlouw, J. K. *Int. J. Mass Spectrom. Ion Processes* **1997**, *160*, 117.
- (141) Miyazaki, M.; Fujii, A.; Ebata, T.; Mikami, N. *Phys. Chem. Chem. Phys.* **2003**, *5*, 1137.
- (142) Hiraoka, K.; Nakajima, G.; Shoda, S. *Chem. Phys. Lett.* **1988**, *146*, 535.
- (143) Hiraoka, K.; Nakajima, G. *J. Chem. Phys.* **1988**, *88*, 7709.
- (144) Hiraoka, K.; Mori, T. *Chem. Phys.* **1989**, *137*, 345.
- (145) Hiraoka, K.; Yamabe, S. *Chem. Phys. Lett.* **1989**, *154*, 139.
- (146) Hiraoka, K.; Mori, T.; Yamabe, S. *J. Chem. Phys.* **1991**, *94*, 2697.
- (147) Magnera, T. F.; David, D. E.; Michl, J. *Chem. Phys. Lett.* **1991**, *182*, 363.
- (148) Shi, Z.; Ford, J. V.; Wei, S.; Castleman, A. W. *J. Chem. Phys.* **1993**, *99*, 8009.
- (149) Payzant, J. D.; Cunningham, A. J.; Kebarle, P. *Can. J. Chem.* **1973**, *51*, 3242.
- (150) Meot-Ner (Mautner), M. *J. Am. Chem. Soc.* **1984**, *106*, 278.
- (151) Banic, C. M.; Iribarne, J. V. *J. Chem. Phys.* **1985**, *83*, 6432.
- (152) Hiraoka, K.; Grimsrud, E. P.; Kebarle, P. *J. Am. Chem. Soc.* **1974**, *96*, 3359.
- (153) Hiraoka, K.; Takimoto, H.; Morise, K. *J. Am. Chem. Soc.* **1986**, *108*, 5863.
- (154) Meot-Ner (Mautner), M.; Sieck, L. W.; Scheiner, S.; Duan, X. *F. J. Am. Chem. Soc.* **1994**, *116*, 7848.
- (155) Klassen, J. S.; Blades, A. T.; Kebarle, P. *J. Phys. Chem.* **1995**, *99*, 15509.
- (156) Fehsenfeld, F. C.; Ferguson, E. E. *J. Chem. Phys.* **1974**, *61*, 3181.
- (157) Meot-Ner (Mautner), M.; Speller, C. V. *J. Phys. Chem.* **1986**, *90*, 6616.
- (158) Kebarle, P.; Arshadi, M. *J. Chem. Phys.* **1968**, *49*, 817.
- (159) Arshadi, M.; Yamdagni, R.; Kebarle, P. *J. Phys. Chem.* **1970**, *74*, 1475.
- (160) Hiraoka, K.; Mizuse, S.; Yamabe, S. *J. Phys. Chem.* **1988**, *92*, 2943.
- (161) Keesee, R. G.; Lee, N.; Castleman, A. W. *J. Am. Chem. Soc.* **1979**, *101*, 2599.
- (162) Meot-Ner (Mautner), M.; Speller, C. V. *J. Phys. Chem.* **1989**, *93*, 3663.
- (163) Lee, N.; Keesee, R. G.; Castleman, A. W. *J. Colloid Interface Sci.* **1980**, *75*, 555.
- (164) Hiraoka, K.; Mizuse, S. *Chem. Phys.* **1987**, *118*, 457.
- (165) Keesee, R. G.; Castleman, A. W., Jr. *Chem. Phys. Lett.* **1980**, *74*, 139.
- (166) Markovich, G.; Pollack, S.; Giniger, R.; Cheshnovsky, O. *J. Chem. Phys.* **1994**, *101*, 9344.
- (167) Blades, A. T.; Klassen, J. S.; Kebarle, P. *J. Am. Chem. Soc.* **1995**, *117*, 10563.
- (168) Keesee, R. G.; Castleman, A. W. *J. Am. Chem. Soc.* **1989**, *111*, 9015.
- (169) Blades, A. T.; Ho, Y.; Kebarle, P. *J. Phys. Chem.* **1996**, *100*, 2443.
- (170) Blades, A. T.; Jayaweera, P.; Ikonomou, M. *J. Chem. Phys.* **1990**, *92*, 5900.
- (171) Dzidic, I.; Kebarle, P. *J. Phys. Chem.* **1970**, *74*, 1466.
- (172) Tang, I. N.; Castleman, A. W. *J. Chem. Phys.* **1972**, *57*, 3638.
- (173) Searles, S. K.; Kebarle, P. *Can. J. Chem.* **1969**, *47*, 2619.
- (174) Holland, P. M.; Castleman, A. W. *J. Chem. Phys.* **1982**, *76*, 4195.
- (175) Tang, I. N.; Castleman, A. W. *J. Chem. Phys.* **1974**, *60*, 3981.
- (176) Kochanski, E.; Constantin, E. *J. Chem. Phys.* **1987**, *87*, 1661.
- (177) Tang, I. N.; Lian, M. S.; Castleman, A. W. *J. Chem. Phys.* **1976**, *65*, 4022.
- (178) Meot-Ner (Mautner), M. *J. Am. Chem. Soc.* **1992**, *114*, 3312.
- (179) Guo, B. C.; Conklin, B. J.; Castleman, A. W. *J. Am. Chem. Soc.* **1989**, *111*, 6506.
- (180) (a) Kebarle, P.; Haynes, R. N.; Collins, J. G. *J. Am. Chem. Soc.* **1967**, *89*, 5753. (b) Meot-Ner (Mautner), M. *J. Am. Chem. Soc.* **1986**, *108*, 6189.
- (181) Hiraoka, K.; Morise, K.; Nishijima, T.; Nakamura, S.; Nakazato, M.; Ohkuma, K. *Int. J. Mass Spectrom. Ion Phys.* **1986**, *68*, 99.
- (182) Luczynski, Z.; Wlodek, S.; Winchel, H. *Int. J. Mass Spectrom. Ion Phys.* **1978**, *26*, 103.
- (183) Meot-Ner (Mautner), M.; Elmore, D. E.; Scheiner, S. *J. Am. Chem. Soc.* **1999**, *121*, 7625.
- (184) (a) Curtius, J.; Froyd, K. D.; Lovejoy, E. R. *J. Phys. Chem. A* **2001**, *105*, 10867. (b) Lovejoy, E. R.; Curtius, J. *J. Phys. Chem. A* **2001**, *105*, 10874. (c) Froyd, K. D.; Lovejoy, E. R. *J. Phys. Chem. A* **2003**, *107*, 9812. (d) Rosen, S.; Froyd, K. D.; Curtius, J.; Lovejoy, E. R. *Int. J. Mass Spectrom.* **2004**, *232*, 9.
- (185) (a) Lovejoy, E. R. *Int. J. Mass Spectrom.* **1999**, *190*–*191*, 231. (b) Froyd, K. D.; Lovejoy, E. R. *J. Phys. Chem. A* **2003**, *107*, 9800.
- (186) Deakyne, C. A.; Knuth, D.; Speller, C. V.; Meot-Ner (Mautner), M.; Sieck, L. W. *J. Mol. Struct. (THEOCHEM)* **1994**, *307*, 217.
- (187) Meot-Ner (Mautner), M. *J. Am. Chem. Soc.* **1988**, *110*, 3075.
- (188) Yamdagni, R.; Kebarle, P. *Can. J. Chem.* **1974**, *63*, 1399.
- (189) Mayer, P. M. *J. Phys. Chem. A* **1999**, *103*, 5905.
- (190) Davidson, W. R.; Kebarle, P. *J. Am. Chem. Soc.* **1976**, *98*, 6125.
- (191) Yamdagni, R.; Kebarle, P. *J. Am. Chem. Soc.* **1972**, *94*, 2940.
- (192) (a) Hiraoka, R.; Mizuse, S.; Yamabe, S. *J. Phys. Chem.* **1988**, *92*, 3943. (b) Winchel, H. *Chem. Phys. Lett.* **2010**, *488*, 219.
- (193) Schindler, T.; Berg, C.; Niedner-Shatteburg, G.; Bondybey, V. *J. Phys. Chem.* **1995**, *99*, 12434.
- (194) Tunon, I.; Rinaldi, D.; Ruiz-Lopez, M. F.; Rivail, J. L. *J. Phys. Chem.* **1995**, *99*, 3789.
- (195) Kebarle, P.; Searles, S. K.; Zolla, A.; Arshadi, M. *J. Am. Chem. Soc.* **1967**, *89*, 6393.
- (196) Cunningham, A. J.; Payzant, A. D.; Kebarle, P. *J. Am. Chem. Soc.* **1972**, *94*, 7627.
- (197) Lau, Y. K.; Ikuta, S.; Kebarle, P. *J. Am. Chem. Soc.* **1982**, *104*, 1462.
- (198) Kelterbaum, R.; Kochanski, E. *J. Phys. Chem.* **1995**, *99*, 12494.
- (199) Speller, C. V.; Meot-Ner (Mautner), M. *J. Phys. Chem.* **1985**, *89*, 5217.
- (200) Tholman, D. T.; Tonner, D. C.; McMahon, T. B. *J. Phys. Chem.* **1994**, *98*, 2002.
- (201) Lau, Y. K.; Kebarle, P. *Can. J. Chem.* **1981**, *59*, 151.
- (202) Lau, Y. K. Ph.D. Thesis, University of Alberta, Edmonton, Alberta, Canada, 1982.
- (203) (a) El-Shall, M. S.; Olafsdottir, S.; Meot-Ner (Mautner), M.; Sieck, L. W. *Chem. Phys. Lett.* **1991**, *185*, 193. (b) El-Shall, M. S.; Daly, G.; Gao, J.; Meot-Ner (Mautner), M.; Sieck, L. W. *J. Phys. Chem.* **1992**, *96*, 507.
- (204) Honma, K.; Sunderlin, L. S.; Armentrout, P. B. *J. Chem. Phys.* **1993**, *99*, 1623.

- (205) Bomse, D. S.; Beauchamp, J. L. *J. Am. Chem. Soc.* **1981**, *103*, 3292.
- (206) (a) Sieck, L. W.; Meot-Ner (Mautner), M. *J. Phys. Chem.* **1982**, *86*, 3646. (b) Meot-Ner (Mautner), M. *J. Phys. Chem.* **1991**, *95*, 6580.
- (207) Wei, S.; Tzeng, W. B.; Castleman, A. W. *J. Phys. Chem.* **1991**, *95*, 585.
- (208) Wenthold, P. G.; Squires, R. R. *J. Phys. Chem.* **1995**, *99*, 2002.
- (209) Masamura, M. *J. Mol. Struct. (THEOCHEM)* **1999**, *466*, 85.
- (210) Hirao, K.; Fujikawa, T.; Konishi, H.; Yamabe, S. *Chem. Phys. Lett.* **1984**, *104*, 184.
- (211) Lifshitz, C.; Luage, F. *J. Phys. Chem.* **1989**, *93*, 5633.
- (212) Wei, S.; Tzeng, W. B.; Castleman, A. W. *J. Chem. Phys.* **1990**, *92*, 332.
- (213) Price, J. M.; Crofton, M. W.; Lee, Y. T. *J. Phys. Chem.* **1991**, *95*, 2182.
- (214) Kim, N. J.; Kim, Y. S.; Jeong, G.; Ahn, T. K.; Kim, S. K. *Int. J. Mass Spectrom.* **2002**, *219*, 11.
- (215) Tzeng, W. B.; Wei, S.; Castleman, A. W. *J. Phys. Chem.* **1991**, *95*, 5757.
- (216) (a) Wei, S.; Tzeng, W. B.; Castleman, A. W. *Z. Phys. D* **1991**, *20*, 47. (b) Wei, S.; Tzeng, W. B.; Keesee, R. G.; Castleman, A. W. *J. Am. Chem. Soc.* **1991**, *113*, 1960.
- (217) (a) Searcy, J. Q.; Fenn, J. B. *J. Chem. Phys.* **1974**, *61*, 5282. (b) Miyazaki, M.; Fujii, A.; Ebata, T.; Mikami, N. *Science* **2004**, *304*, 1134. (c) Shin, J. W.; Hammer, N. I.; Diken, E. G.; Johnson, M. A.; Walters, R. S.; Jaeger, T. D.; Duncan, M. A.; Christie, R. A.; Jordan, K. D. *Science* **2004**, *304*, 1137. (d) Diken, E. G.; Hammer, N. I.; Johnson, M. A.; Christie, R. A.; Jordan, K. D. *J. Chem. Phys.* **2005**, *123*, 164309.
- (218) (a) Castleman, A. W.; Wei, S. *Annu. Rev. Phys. Chem.* **1994**, *45*, 685. (b) Castleman, A. W.; Bowen, K. H. *J. Phys. Chem.* **1996**, *100*, 12911.
- (219) (a) Christie, R. A.; Jordan, K. D. *J. Phys. Chem. B* **2002**, *106*, 8376. (b) Likholyot, A.; Hovey, J. K.; Seward, T. M. *Geochim. Cosmochim. Acta* **2005**, *69*, 2949. (c) Likholyot, A.; Lemke, K. H.; Hovey, J. K.; Seward, T. M. *Geochim. Cosmochim. Acta* **2007**, *71*, 2436. (d) Lemke, K. H.; Seward, T. M. *Geochim. Cosmochim. Acta* **2008**, *72*, 3293. (e) Chang, H. C.; Wang, Y. S.; Lee, Y. T.; Chang, H. C. *Int. J. Mass Spectrom.* **1998**, *180*, 91. (f) Jiang, J. C.; Chang, H. C.; Wang, Y. S.; Lee, Y. T.; Lin, S. H. *J. Phys. Chem. A* **1999**, *103*, 3123. (g) Bush, M. F.; Saykally, R. J.; Williams, E. R. *J. Am. Chem. Soc.* **2007**, *129*, 2220. (h) O'Brien, J. T.; Prell, J. S.; Bush, M. F.; Williams, E. R. *J. Am. Chem. Soc.* **2010**, *132*, 8428.
- (220) Feng, W. Y.; Iraqi, M.; Lifshitz, C. *J. Phys. Chem.* **1993**, *97*, 3510.
- (221) Feng, W. Y.; Lifshitz, C. *J. Phys. Chem.* **1994**, *98*, 3658.
- (222) Feng, W. Y.; Lifshitz, C. *J. Am. Chem. Soc.* **1995**, *117*, 11548.
- (223) Feng, W. Y.; Lifshitz, C. *J. Mass Spectrom.* **1995**, *30*, 1179.
- (224) Feng, W. Y.; Lifshitz, C. *Int. J. Mass Spectrom. Ion Processes* **1995**, *149/150*, 13.
- (225) (a) Stoyanov, E. S.; Stoyanova, I. V.; Tham, F. S.; Reed, C. A. *J. Am. Chem. Soc.* **2008**, *130*, 12128. (b) Tunon, I.; Silla, E.; Bertran, J. *J. Phys. Chem.* **1993**, *97*, 5547.
- (226) Newton, M. D.; Ehrenson, S. *J. Am. Chem. Soc.* **1971**, *93*, 4971.
- (227) Newton, M. D. *J. Chem. Phys.* **1977**, *67*, 5535.
- (228) Deakyne, C. A.; Meot-Ner (Mautner), M.; Campbell, C. L.; Hughes, M. G.; Murphy, S. P. *J. Chem. Phys.* **1986**, *84*, 4958.
- (229) Jiang, J. C.; Wang, Y. S.; Chang, H. C.; Lin, S. H.; Lee, Y. T.; Nieder-Schatteburg, G.; Chang, H. C. *J. Am. Chem. Soc.* **2000**, *122*, 1398.
- (230) Chang, H. C.; Jiang, J. C.; Hahndorf, I.; Lin, S. H.; Lee, Y. T.; Chang, H. C. *J. Am. Chem. Soc.* **1999**, *121*, 4443.
- (231) (a) Jiang, J. C.; Boo, D. W.; Lin, S. H.; Lee, Y. T.; Chang, H. C. *J. Chem. Phys.* **2000**, *112*, 176. (b) Chaudhuri, C.; Jiang, J. C.; Wang, X.; Lee, Y. T.; Chang, H.-C. *J. Chem. Phys.* **2000**, *112*, 7279. (c) Jiang, J. C.; Chaudhuri, C.; Lee, Y. T.; Chang, H. C. *J. Phys. Chem. A* **2002**, *106*, 10937.
- (232) Daly, G. M.; Gao, J.; El-Shall, M. S. *Chem. Phys. Lett.* **1993**, *206*, 500.
- (233) (a) Kim, K. Y.; Chang, H. C.; Lee, Y. T.; Cho, U. I.; Boo, D. W. *J. Phys. Chem. A* **2003**, *107*, 5007. (b) Akrou, A.; Chikh, Z.; Djazi, F.; Elbannay, M.; Berruyer, F.; Bouchoux, G. *Int. J. Mass Spectrom.* **2007**, *267*, 63. (c) Nieckarz, R. J.; Atkins, C. G.; McMahon, T. B. *Chem. Phys. Phys. Chem.* **2008**, *9*, 2816.
- (234) Wang, Y. S.; Chang, H. C.; Jiang, J. C.; Lin, S. H.; Lee, Y. T.; Chang, H. C. *J. Am. Chem. Soc.* **1998**, *120*, 8777.
- (235) Jiang, J. C.; Chang, H. C.; Lee, Y. T.; Lin, S. H. *J. Phys. Chem. A* **1999**, *103*, 3123.
- (236) Wu, C. C.; Chaudhuri, C.; Jiang, J. C.; Lee, Y. T.; Chang, H. C. *J. Phys. Chem. A* **2004**, *108*, 2859.
- (237) Lee, H. M.; Kim, K. S. *J. Chem. Phys.* **2001**, *114*, 4461.
- (238) Peslherbe, G. H.; Ladanyi, B. M.; Hynes, J. T. *J. Phys. Chem. A* **1999**, *103*, 2561.
- (239) Coe, J. V. *J. Phys. Chem. A* **1997**, *101*, 2055.
- (240) (a) Hiraoka, K.; Mori, T. *J. Chem. Phys.* **1989**, *90*, 7143. (b) Hiraoka, K. *J. Chem. Phys.* **1987**, *87*, 4048. (c) Hiraoka, K.; Mori, T.; Yamabe, S. *J. Chem. Phys.* **1991**, *94*, 2697. (d) Hiraoka, K.; Yamabe, S. *Chem. Phys. Lett.* **1989**, *154*, 139.
- (241) (a) Froyd, K. D.; Lovejoy, E. R. *J. Phys. Chem. A* **2003**, *107*, 9800. (b) Froyd, K. D.; Lovejoy, E. R. *J. Phys. Chem. A* **2003**, *107*, 9812.
- (242) Meot-Ner (Mautner), M.; Scheiner, S.; Yu, W. O. *J. Am. Chem. Soc.* **1998**, *120*, 6980.
- (243) El-Shall, M. S.; Olafsdottir, S. R.; Meot-Ner (Mautner), M.; Sieck, L. W. *Chem. Phys. Lett.* **1991**, *185*, 193.
- (244) (a) Herron, W. J.; Coolbaugh, M. T.; Vaidyanathan, G.; Peifer, W. R.; Garvey, J. F. *J. Am. Chem. Soc.* **1992**, *114*, 3684. (b) Feng, W. Y.; Goldenberg, M.; Lifshitz, C. *J. Am. Soc. Mass Spectrom.* **1994**, *5*, 695.
- (245) Martin, J. M. L.; Aviyente, V.; Lifshitz, C. *J. Phys. Chem.* **1997**, *101*, 2597.
- (246) Aviyente, V.; Zhang, R.; Varnali, T.; Lifshitz, C. *Int. J. Mass Spectrom. Ion Processes* **1997**, *161*, 123.
- (247) Chaudhuri, C.; Jiang, J. C.; Wu, C. C.; Wang, X.; Chang, H. C. *J. Phys. Chem. A* **2001**, *105*, 8906.
- (248) Brauman, J. I.; Blair, L. K. *J. Am. Chem. Soc.* **1968**, *90*, 6561.
- (249) Brauman, J. I.; Blair, L. K. *J. Am. Chem. Soc.* **1970**, *92*, 5986.
- (250) McIver, R. T.; Scott, J. A.; Riveros, J. M. *J. Am. Chem. Soc.* **1973**, *95*, 2706.
- (251) Bohme, D. K.; Rakshit, A. B.; Mackay, G. I. *J. Am. Chem. Soc.* **1982**, *104*, 1100.
- (252) Mackay, G. I.; Rashit, A. B.; Bohme, D. K. *Can. J. Chem.* **1982**, *62*, 2594.
- (253) Lias, S. L.; Liebman, J. F.; Levin, R. D. *J. Phys. Chem. Ref. Data* **1984**, *13*, 695.
- (254) Caskey, D. C.; Damrauer, R.; McGoff, D. *J. Org. Chem.* **2002**, *67*, 5098.
- (255) Snodgrass, J. T.; Coe, J. V.; McHugh, K. M.; Arnold, S. T.; Bowen, K. H. *J. Phys. Chem.* **1995**, *99*, 9675.
- (256) Yamabe, S.; Hirao, K.; Wasada, H. *J. Phys. Chem.* **1992**, *96*, 10261.
- (257) Szulejko, J. E.; McMahon, T. B.; Troude, V.; Bouchoux, G.; Audier, H. E. *J. Phys. Chem.* **1998**, *102*, 1879.
- (258) (a) Aue, D. H.; Webb, H. M.; Bowers, M. T. *J. Am. Chem. Soc.* **1973**, *95*, 2699. (b) Woźniak, K.; Raczyńska, E. D.; Korybut-Dasziewicz, B. *Isr. J. Chem.* **1999**, *39*, 245.
- (259) Meot-Ner (Mautner), M.; Hamlet, P.; Hunter, E. P.; Field, F. *H. J. Am. Chem. Soc.* **1980**, *102*, 6393.
- (260) Meot-Ner (Mautner), M. *J. Am. Chem. Soc.* **1983**, *105*, 4906.
- (261) Sharma, R. B.; Blades, A. T.; Kebarle, P. *J. Am. Chem. Soc.* **1984**, *106*, 510.
- (262) Bouchoux, G.; Hoppiliard, Y.; Houriet, R. *New J. Chem.* **1987**, *11*, 225.
- (263) Chen, Q. F.; Stone, J. A. *J. Phys. Chem.* **1995**, *99*, 1442.
- (264) Hu, C. H.; Shen, M.; Schaefer, H. F. *J. Am. Chem. Soc.* **1993**, *115*, 2923.
- (265) Engkvist, O.; Astrand, P. O.; Karlstrom, G. *J. Phys. Chem.* **1996**, *100*, 6950.

- (266) Aleman, C.; Navarro, E.; Puiggali, J. *J. Phys. Chem.* **1996**, *100*, 16131.
- (267) Aleman, C.; Puiggali, J. *J. Org. Chem.* **1997**, *62*, 307.
- (268) Price, D. J.; Roberts, J. D.; Jorgensen, W. L. *J. Am. Chem. Soc.* **1998**, *120*, 9672.
- (269) Rodriguez, C. F.; Cunie, A.; Shoeib, T.; Chu, I. K.; Hopkinson, A. C.; Siu, K. W. M. *J. Phys. Chem. A* **2000**, *104*, 5023.
- (270) Rodriguez, C. F.; Cunie, A.; Shoeib, T.; Chu, I. K.; Hopkinson, A. C.; Siu, K. W. M. *J. Am. Chem. Soc.* **2001**, *123*, 3006.
- (271) Boo, D. W. *Bull. Korean Chem. Soc.* **2001**, *22*, 693.
- (272) Furlani, T. R.; Garvey, J. F. *Mol. Phys.* **1997**, *92*, 449.
- (273) Wu, C. C.; Jiang, J. C.; Hahndorf, I.; Chaudhuri, C.; Lee, Y. T.; Chang, H. C. *J. Phys. Chem. A* **2000**, *104*, 9556.
- (274) Snoek, L. C.; Kroemer, R. T.; Hockridge, M. R. *J. Chem. Phys. Phys. Chem.* **2001**, *3*, 1819.
- (275) Wu, C. C.; Chaudhuri, C.; Jiang, J. C.; Lee, Y. T.; Chang, H. C. *Mol. Phys.* **2003**, *101*, 1285.
- (276) (a) Chang, H. C.; Jiang, J. C.; Chang, H. C.; Wang, L. R.; Lee, Y. T. *Isr. J. Chem.* **1999**, *39*, 231. (b) Bochoux, G. *Mass Spectrom. Rev.* **2007**, *26*, 775. (c) Bouchoux, G.; Salpin, J. Y. *Mass Spectrom. Rev.* **2012**, *31*, 353.
- (277) Morton, T. H. *Tetrahedron* **1982**, *38*, 3195.
- (278) Audier, H. E.; Milliet, A.; Leblanc, D.; Morton, T. H. *J. Am. Chem. Soc.* **1992**, *114*, 2020.
- (279) (a) Wyttenbach, T.; Kemper, P. R.; Bowers, M. T. *Int. J. Mass Spectrom.* **2001**, *212*, 13. (b) Liu, D. F.; Wyttenbach, T.; Barran, P. E.; Bowers, M. T. *J. Am. Chem. Soc.* **2003**, *125*, 8458. (c) Wyttenbach, T.; Paizs, B.; Barran, P.; Breci, L.; Liu, D. F.; Suhai, S.; Wysocki, V. H.; Bowers, M. T. *J. Am. Chem. Soc.* **2003**, *125*, 13768. (d) Liu, D. F.; Wyttenbach, T.; Bowers, M. T. *Int. J. Mass Spectrom.* **2004**, *236*, 81.
- (280) (a) Meot-Ner (Mautner), M. *J. Am. Chem. Soc.* **1979**, *101*, 2396. (b) Meot-Ner (Mautner), M. *J. Am. Chem. Soc.* **1983**, *105*, 4912.
- (281) Sharma, R. B.; Kebarle, P. *J. Am. Chem. Soc.* **1984**, *106*, 3913.
- (282) Ryzhov, V.; Dunbar, R. C. *J. Am. Soc. Mass Spectrom.* **1999**, *10*, 862.
- (283) Adoteldo, D.; Aviyente, V.; Martin, J. M. L.; Lifshitz, C. *J. Phys. Chem. A* **1998**, *102*, 6357.
- (284) Kim, S. G.; Kim, K. H.; Kim, Y. K.; Shin, S. K.; Ahn, K. H. *J. Am. Chem. Soc.* **2003**, *125* (45), 13819.
- (285) Schwartz, H. A. *J. Chem. Phys.* **1977**, *67*, 5525.
- (286) Yamabe, S.; Minato, T.; Hirao, K. *J. J. Chem. Phys.* **1984**, *80*, 1576.
- (287) Begeman, M. H.; Gudeman, C. S.; Pfaff, J.; Saykally, R. *J. Phys. Chem. Lett.* **1983**, *51*, 554.
- (288) Begemann, M. H.; Saykally, R. *J. J. Chem. Phys.* **1985**, *82*, 3570.
- (289) Liu, D. J.; Oka, T. *Phys. Rev. Lett.* **1985**, *54*, 1787.
- (290) Liu, D. J.; Oka, T.; Sears, T. *J. Chem. Phys.* **1986**, *108*, 335.
- (291) Davies, P. B.; Johnson, S. A.; Hamilton, P. A.; Sears, T. *J. Chem. Phys.* **1986**, *108*, 335.
- (292) (a) Yeh, L. I.; Myers, J. D.; Price, J. M.; Lee, Y. T. *J. Chem. Phys.* **1989**, *91*, 8319. (b) Okumura, M.; Yeh, L. I.; Myers, J. D.; Lee, Y. T. *J. Phys. Chem.* **1990**, *94*, 3416. (c) Yeh, L. I.; Lee, Y. T.; Hougen, J. *T. J. Mol. Spectrosc.* **1994**, *164*, 473. (d) Moore, D. T.; Oomens, J.; van der Meer, L.; von Helden, G.; Meijer, G.; Valle, J.; Marshall, A. G.; Eyler, J. R. *Chem. Phys. Phys. Chem.* **2004**, *5*, 740. (e) Asmis, K. R.; Pivonka, N. L.; Santambrogio, G.; Brummer, M.; Kaposta, C.; Neumark, D. M.; Woste, L. *Science* **2003**, *299*, 1375. (f) Fridgen, T. D.; McMahon, T. B.; MacAleece, L.; Lemaire, J.; Maitre, P. *J. Phys. Chem. A* **2004**, *108*, 9008. (g) Fridgen, T. D.; MacAleece, L.; McMahon, T. B.; Lemaire, J.; Maitre, P. *Phys. Chem. Chem. Phys.* **2006**, *8*, 955.
- (293) Bomse, D. S.; Beauchamp, J. L. *J. Am. Chem. Soc.* **1981**, *103*, 3292.
- (294) (a) Okumura, M.; Yeh, L. I.; Lee, Y. T. *J. Chem. Phys.* **1985**, *83*, 3705. (b) Okumura, M.; Yeh, L. I.; Myers, J. D.; Lee, Y. T. *J. Chem. Phys.* **1986**, *85*, 2328. (c) Okumura, M.; Yeh, L. I.; Lee, Y. T. *J. Chem. Phys.* **1988**, *88*, 79. (d) Duncan, M. A. *Int. J. Mass Spectrom.* **2000**, *200*, 545.
- (295) Liu, W. L.; Lisy, J. M. *J. Chem. Phys.* **1988**, *89*, 606.
- (296) Headrick, J. M.; Diken, E. G.; Walters, R. S.; Hammer, N. I.; Christie, R. A.; Cui, J.; Myshakin, E. M.; Duncan, M. A.; Johnson, M. A.; Jordan, K. D. *Science* **2005**, *308*, 1765.
- (297) Desfrancois, C.; Baillon, B.; Schermann, J. P.; Arnold, S. T.; Hendricks, J. H.; Bowen, K. H. *Phys. Rev. Lett.* **1994**, *72*, 48.
- (298) Michi, T.; Ohashi, K.; Inokuchi, Y.; Nishi, N.; Sekiya, H. *Chem. Phys. Lett.* **2003**, *371*, 111.
- (299) Kleinermanns, K.; Janzen, C.; Spangenberg, D.; Gerhards, M. J. *Phys. Chem. A* **1999**, *103*, 5232.
- (300) Roth, W.; Schmitt, M.; Sprangenberg, D.; Janzen, C.; Kleinermanns, K. *Chem. Phys.* **1998**, *239*, 1.
- (301) Jacoby, C.; Hering, P.; Schmitt, M.; Roth, W.; Kleinermanns, K. *Chem. Phys.* **1998**, *239*, 23.
- (302) Schmitt, M.; Jacoby, C.; Gerhards, M.; Unterberg, C.; Roth, W.; Kleinermanns, K. *J. Chem. Phys.* **2000**, *113*, 2995.
- (303) Macleod, N. A.; Simons, J. P. *Phys. Chem. Chem. Phys.* **2004**, *6*, 2821.
- (304) Price, E. A.; Robertson, W. H.; Diken, E. G.; Weddle, G. H.; Johnson, M. A. *Chem. Phys. Lett.* **2002**, *366*, 412.
- (305) Ayotte, P.; Weddle, G. H.; Kim, J.; Johnson, M. A. *J. Am. Chem. Soc.* **1998**, *120*, 12361.
- (306) Ayotte, P.; Bailey, C. G.; Weddle, G. H.; Johnson, M. A. *J. Phys. Chem. A* **1998**, *102*, 3067.
- (307) Wild, D. A.; Loh, Z. M.; Wolynec, P. P.; Weiser, P. S.; Bieske, E. *J. Chem. Phys. Lett.* **2000**, *332*, 531.
- (308) (a) Wild, D. A.; Bieske, E. J. *Int. Rev. Phys. Chem.* **2003**, *22*, 129. (b) Fridgen, T. D.; McMahon, T. B.; Maitre, P.; Lemaire, J. *Phys. Chem. Chem. Phys.* **2006**, *8*, 2483.
- (309) Radisic, D.; Xu, S. J.; Bowen, K. H. *Chem. Phys. Lett.* **2002**, *354*, 9.
- (310) Hendricks, J. H.; de Clercq, H. L.; Freidhoff, C. B.; Arnold, S. T.; Eaton, J. G.; Fancher, C.; Lyapustina, S. A.; Snodgrass, J. T.; Bowen, K. H. *J. Chem. Phys.* **2002**, *116*, 7926.
- (311) Gutowski, M.; Dabkowska, I.; Rak, J.; Xu, S.; Nilles, J. M.; Radisic, D.; Bowen, K. H. *Eur. Phys. J. D* **2002**, *20*, 431.
- (312) Meot-Ner (Mautner), M.; Field, F. H. *J. Chem. Phys.* **1974**, *61*, 3742.
- (313) Sieck, L. W.; Searles, S. K. *J. Chem. Phys.* **1970**, *53*, 2601.
- (314) Daly, G. M.; Meot-Ner (Mautner), M.; Pithawalla, Y. B.; El-Shall, M. S. *J. Chem. Phys.* **1996**, *104*, 7965.
- (315) Bernstein, E. R. *J. Phys. Chem.* **1992**, *96*, 10105.
- (316) (a) Brutschy, B. *Chem. Rev.* **1992**, *92*, 1567. (b) Castleman, A. W.; Wei, S. *Annu. Rev. Phys. Chem.* **1994**, *45*, 685.
- (317) (a) Audier, H. E.; Fossey, J.; Mourguès, P.; McMahon, T. B.; Hammerum, S. S. *J. Phys. Chem.* **1996**, *100*, 18380. (b) Audier, H. E.; McMahon, T. B. *J. Mass Spectrom.* **1997**, *32*, 201.
- (318) (a) Narcisi, R. S.; Bailey, A. D. *J. Geophys. Res.* **1965**, *70*, 3687. (b) Fehsenfeld, F. C.; Ferguson, E. E. *J. Geophys. Res. Space Phys.* **1969**, *74*, 2217. (c) Stace, A. J.; Winkel, J. F.; Lopez Martens, R. B.; Upham, J. E. *J. Phys. Chem.* **1994**, *98*, 2012. (d) Choi, J. H.; Kuwata, K. T.; Haas, B. M.; Cao, Y.; Johnson, M. S.; Okumura, M. *J. Chem. Phys.* **1994**, *100*, 7153. (e) Hammam, E.; Lee, E. P. F.; Dyke, J. M. *J. Phys. Chem. A* **2001**, *105*, 5528. (f) Relph, R. A.; Guasco, T. L.; Elliott, B. M.; Kamrath, M. Z.; McKoy, A. B.; Steele, R. P.; Schofield, D. P.; Jordan, K. D.; Viggiano, A. A.; Ferguson, E. E.; Johnson, M. A. *Science* **2010**, *327*, 308.
- (319) Raksit, A. B.; Bohme, D. K. *Can. J. Chem.* **1983**, *61*, 1683.
- (320) Meot-Ner (Mautner), M. *J. Am. Chem. Soc.* **1982**, *104*, 5.
- (321) (a) Ochran, R. A.; Mayer, P. M. *Eur. J. Mass Spectrom.* **2001**, *7*, 267. (b) Petrie, S.; Freeman, C. G.; Meot-Ner (Mautner), M.; McEwan, M. J.; Ferguson, E. E. *J. Am. Chem. Soc.* **1990**, *112*, 7121. (c) van der Rest, G.; Nedev, H.; Chamot-Rooke, J.; Mourguès, P.; McMahon, T. B.; Audier, H. E. *Int. J. Mass Spectrom.* **2000**, *202*, 161. (d) Marta, R. A.; Wu, R.; Eldridge, K. R.; Martens, J. K.; McMahon, T. B. *Phys. Chem. Chem. Phys.* **2010**, *12*, 3431.
- (322) (a) Shaffer, S. A.; Sadilek, M.; Turecek, F.; Hop., C. E. C. A. *Int. J. Mass Spectrom. Ion Processes* **1997**, *160*, 137. (b) Bohme, D. K.; Mackay, G. I. *J. Am. Chem. Soc.* **1981**, *103*, 978. (c) Henchman, M.; Paulson, J. F.; Hierl, P. M. *J. Am. Chem. Soc.* **1983**, *105*, 5509.

- (d) Henchman, M.; Hierl, P. M.; Paulson, J. F. *J. Am. Chem. Soc.* **1985**, *107*, 2812. (e) Bohme, D. K.; Rakshit, A. B. *J. Am. Chem. Soc.* **1984**, *106*, 3447. (f) Giles, K.; Grimsrud, E. P. *J. Phys. Chem.* **1993**, *97*, 1318. (g) O'Hair, R. A. J.; Davico, G. E.; Hacaloglu, J.; Dang, T. T.; DePuy, C. H.; Bierbaum, V. M. *J. Am. Chem. Soc.* **1994**, *116*, 3609. (h) Viggiano, A. A.; Arnold, S. T.; Morris, R. A.; Ahrens, A. F.; Hierl, P. M. *J. Phys. Chem.* **1996**, *100*, 14397. (i) Craig, S. L.; Brauman, J. I. *J. Am. Chem. Soc.* **1996**, *118*, 6786. (j) Seeley, J. V.; Morris, R. A.; Viggiano, A. A. *J. Phys. Chem. A* **1997**, *101*, 4598. (k) Seeley, J. V.; Morris, R. A.; Viggiano, A. A.; Wang, H.; Hase, W. L. *J. Am. Chem. Soc.* **1997**, *119*, 577. (l) Bogdanov, B.; McMahon, T. B. *Int. J. Mass Spectrom.* **2005**, *241*, 205. (m) Fridgen, T. D.; Burkell, J. L.; Wilsily, A. N.; Braun, V.; Wasylcica, A.; McMahon, T. B. *J. Phys. Chem. A* **2005**, *109*, 7519.
- (323) Warshel, A.; Russell, S. T. *J. Am. Chem. Soc.* **1986**, *108*, 6596. (324) Deligiannakis, Y.; Hanly, J.; Rutherford, A. W. *J. Am. Chem. Soc.* **1999**, *121*, 7653.
- (325) Wang, J.; El-Sayed, M. A. *J. Phys. Chem. A* **2000**, *104*, 4333. (326) Fenn, J. B.; Mann, M.; Meng, C. K.; Wong, S. F.; Whitehouse, C. M. *Science* **1989**, *246*, 64. (327) Cox, K. A.; Julian, R. K.; Cooks, R. G.; Kaiser, R. E. *J. Am. Soc. Mass Spectrom.* **1994**, *5*, 127. (328) Rodriguez-Cruz, S. E.; Klassen, J. S.; Williams, E. R. *J. Am. Soc. Mass Spectrom.* **1997**, *8*, 565. (329) Price, W. D.; Jockusch, R. A.; Williams, E. R. *J. Am. Chem. Soc.* **1997**, *119*, 11988. (330) Price, W. D.; Jockusch, R. A.; Williams, E. R. *J. Am. Chem. Soc.* **1998**, *120*, 3474. (331) Schnier, P. D.; Price, W. D.; Williams, E. R. *J. Am. Soc. Mass Spectrom.* **1996**, *9*, 972. (332) Gorman, G. S.; Speir, J. P.; Turner, C. A.; Amster, I. J. *J. Am. Chem. Soc.* **1992**, *114*, 3986. (333) Wu, Z.; Fenselau, C. *J. Am. Soc. Mass Spectrom.* **1992**, *3*, 863. (334) Cheng, X.; Wu, Z.; Fenselau, C. *J. Am. Chem. Soc.* **1993**, *115*, 4844. (335) Wu, Z.; Lebrilla, C. *J. Am. Chem. Soc.* **1993**, *115*, 3270. (336) Green, M. K.; Lebrilla, C. B. *Mass Spectrom. Rev.* **1997**, *16*, 53. (337) (a) Addario, V.; Guo, Y. Z.; Chu, I. K.; Ling, Y.; Ruggerio, G.; Rodriguez, C. F.; Hopkinson, A. C.; Siu, K. W. M. *Int. J. Mass Spectrom.* **2002**, *219*, 101. (b) Simon, A.; MacAleece, L.; Maitre, P.; Lemaire, J.; McMahon, T. B. *J. Am. Chem. Soc.* **2007**, *129*, 2829. (c) Forbes, M. W.; Bush, M. F.; Polfer, N. C.; Oomens, J.; Dunbar, R. C.; Williams, E. R.; Jockusch, R. A. *J. Phys. Chem. A* **2007**, *111*, 11759. (338) (a) Wu, J.; Gard, E.; Bregar, J.; Green, M. K.; Lebrilla, C. B. *J. Am. Chem. Soc.* **1995**, *117*, 9900. (b) Simon-Manso, Y. **2008**, personal communication. (339) Zhang, K.; Zimmerman, D. M.; Chung-Phillips, A.; Cassady, C. *J. Am. Chem. Soc.* **1993**, *115*, 10812. (340) Campbell, S.; Rodgers, M. T.; Marzluff, E. M.; Beauchamp, J. L. *J. Am. Chem. Soc.* **1995**, *117*, 12840. (341) (a) Wu, R.; McMahon, T. B. *J. Am. Chem. Soc.* **2007**, *129*, 11312. (b) Wu, R.; McMahon, T. B. *J. Phys. Chem. B* **2009**, *113*, 8767. (342) Counterman, A. E.; Clemmer, D. E. *J. Phys. Chem. B* **2004**, *108*, 4885. (343) Counterman, A. E.; Clemmer, D. E. *J. Phys. Chem. B* **2002**, *106*, 12045. (344) Counterman, A. E.; Clemmer, D. E. *J. Am. Chem. Soc.* **2001**, *123*, 1490. (345) Counterman, A. E.; Clemmer, D. E. *J. Phys. Chem. B* **2003**, *107*, 2111. (346) Gross, D. S.; Rodriguez-Cruz, S. E.; Bock, S.; Williams, E. R. *J. Phys. Chem.* **1995**, *99*, 4034. (347) (a) Gao, B.; Wyttenbach, T.; Bowers, M. T. *J. Am. Chem. Soc.* **2009**, *131*, 4695. (b) Gao, B.; Wyttenbach, T.; Bowers, M. T. *J. Phys. Chem. B* **2009**, *113*, 9995. (348) (a) Wincel, H. *Int. J. Mass Spectrom.* **2006**, *251*, 23. (b) Wincel, H. *Chem. Phys. Lett.* **2007**, *439*, 157. (c) Wincel, H. *J. Phys. Chem. A* **2007**, *111*, 5784. (d) Wincel, H. *J. Am. Soc. Mass Spectrom.* **2007**, *18*, 2083. (e) Wincel, H. *J. Am. Soc. Mass Spectrom.* **2008**, *19*, 1091. (f) Prell, J. S.; Correra, T. C.; Chang, T. M.; Biles, J. A.; Williams, E. R. *J. Am. Chem. Soc.* **2010**, *132*, 14733. (349) Liu, D. F.; Wyttenbach, T.; Carpenter, C. J.; Bowers, M. T. *J. Am. Chem. Soc.* **2004**, *126*, 3261. (350) Wyttenbach, T.; Liu, D.; Bowers, M. T. *Int. J. Mass Spectrom.* **2005**, *240*, 221. (351) (a) Jensen, J. H.; Gordon, M. S. *J. Am. Chem. Soc.* **1995**, *117*, 8159. (b) Kassab, E.; Langlet, J.; Evleth, E.; Akadem, Y. *J. Mol. Struct. (THEOCHEM)* **2000**, *531*, 267. (c) Jockusch, R. A.; Lemoff, A. S.; Williams, E. R. *J. Phys. Chem. A* **2001**, *105*, 10929. (d) Lemoff, A. F.; Williams, E. R. *J. Am. Soc. Mass Spectrom.* **2004**, *15*, 1014. (e) Lemoff, A. F.; Bush, M. F.; Wu, C. C.; Williams, E. R. *J. Am. Chem. Soc.* **2005**, *127*, 10276. (f) Kamariotis, A.; Boyarkin, O. V.; Mercier, S. R.; Beck, R. D.; Bush, M. F.; Williams, E. R.; Rizzo, T. R. *J. Am. Chem. Soc.* **2006**, *128*, 905. (g) Lemoff, A. F.; Bush, M. F.; O'Brien, J. T.; Williams, E. R. *J. Phys. Chem. B* **2006**, *110*, 8433. (352) (a) Schnier, P. D.; Price, W. D.; Jockusch, R. A.; Williams, E. R. *J. Am. Chem. Soc.* **1996**, *118*, 7178. (b) Strittmatter, E. F.; Williams, E. R. *J. Phys. Chem. A* **2000**, *104*, 6069. (c) Prell, J. S.; O'Brien, J. T.; Steill, J. D.; Oomens, J.; Williams, E. R. *J. Am. Chem. Soc.* **2009**, *131*, 11442. (353) Strittmatter, E. F.; Williams, E. R. *Int. J. Mass Spectrom.* **1999**, *185*, 186, 187, 935. (354) (a) Counterman, D. E.; Clemmer, D. E. *J. Phys. Chem. B* **2001**, *105*, 8092. (b) Locke, M. J.; McIver, R. T. *J. Am. Chem. Soc.* **1983**, *105*, 4226. (c) Wu, R.; McMahon, T. B. *Can. J. Chem.* **2005**, *83*, 1978. (d) Wu, R.; McMahon, T. B. *J. Mass Spectrom.* **2008**, *43*, 1641. (e) Wu, R.; McMahon, T. B. *J. Am. Chem. Soc.* **2008**, *130*, 3065. (f) Wu, R.; McMahon, T. B. *Angew. Chem., Int. Ed.* **2007**, *46*, 3668. (g) Wu, R.; McMahon, T. B. *J. Am. Chem. Soc.* **2007**, *129*, 4864. (h) O'Brien, J. T.; Prell, J. S.; Steill, J. D.; Oomens, J.; Williams, E. R. *J. Am. Chem. Soc.* **2009**, *131*, 3905. (355) Kohtani, M.; Breaux, G. A.; Jarrold, M. F. *J. Am. Chem. Soc.* **2004**, *126*, 1206. (356) Kohtani, M.; Jarrold, M. F. *J. Am. Chem. Soc.* **2004**, *126*, 8454. (357) Kohtani, M.; Jarrold, M. F. *J. Am. Chem. Soc.* **2002**, *124*, 11148. (358) Lee, S. W.; Freivogel, P.; Schindler, T.; Beauchamp, J. L. *J. Am. Chem. Soc.* **1998**, *120*, 11758. (359) Woenckhaus, J.; Mao, Y.; Jarrold, M. F. *J. Phys. Chem. B* **1997**, *101*, 847. (360) Fye, J. L.; Woenckhaus, J.; Jarrold, M. F. *J. Am. Chem. Soc.* **1998**, *120*, 1327. (361) (a) Wyttenbach, T.; von Helden, G.; Bowers, M. T. *J. Am. Chem. Soc.* **1996**, *118*, 8355. (b) Jarrold, M. F. *Annu. Rev. Phys. Chem.* **2000**, *51*, 179. (c) Niekarz, R. J.; Atkins, C. G.; McMahon, T. B. *ChemPhysChem* **2008**, *9*, 2826. (362) (a) Raspopov, S. A.; McMahon, T. B. *J. Mass Spectrom.* **2005**, *40*, 1536. (b) Luke Mac Aleese, L.; Simon, A.; McMahon, T. B.; Ortega, J. M.; Scuderi, D.; Lemaire, J.; Maitre, P. *Int. J. Mass Spectrom.* **2005**, *249*–*250*, 14. (c) Simon, A.; McMahon, T. B. *Int. J. Mass Spectrom.* **2006**, *255*–*256*, 301. (d) Price, W. D.; Schnier, P. D.; Williams, E. R. *J. Phys. Chem. B* **1997**, *101*, 664. (363) Jockusch, R. A.; Williams, E. R. *J. Phys. Chem. A* **1998**, *102*, 4543. (364) Meot-Ner (Mautner), M.; Dongre, A. R.; Somogyi, A.; Wysocki, V. H. *Rapid Commun. Mass Spectrom.* **1995**, *9*, 829. (365) Schnier, P. D.; Price, W. D.; Strittmatter, E. F.; Williams, E. R. *J. Am. Soc. Mass Spectrom.* **1997**, *8*, 771. (366) (a) Kaleta, D. T.; Jarrold, M. F. *J. Phys. Chem. B* **2003**, *107*, 14529. (b) Kaleta, D. T.; Jarrold, M. F. *J. Phys. Chem. A* **2002**, *106*, 9655. (367) (a) Kitova, E. N.; Bundle, D. R.; Klassen, J. S. *J. Am. Chem. Soc.* **2002**, *124*, 9340. (b) Kitova, E. N.; Wang, W.; Bundle, D. R.; Klassen, J. S. *J. Am. Chem. Soc.* **2002**, *124*, 13980. (c) Kitova, E. N.; Seo, M.; Roy, P. N.; Klassen, J. S. *J. Am. Chem. Soc.* **2008**, *130*, 1214. (d) Liu, L.; Bagal, D.; Kitova, E. N.; Shnier, P. D.; Klassen, J. S. *J. Am. Chem. Soc.* **2009**, *131*, 15980. (e) Grabenauer, M.; Wu, C.; Soto, P.; Shea, J. E.; Bowers, M. T. *J. Am. Chem. Soc.* **2010**, *132*, 532. (f) Grabenauer, M.; Wyttenbach, T.; Sanghera, N.; Sanghera, N.;

- Slade, S. E.; Pinheiro, T. J. T.; Scrivens, J. H.; Bowers, M. T. *J. Am. Chem. Soc.* **2010**, *132*, 8816.
- (368) (a) Meot-Ner (Mautner), M. *J. Am. Chem. Soc.* **1988**, *110*, 3071. (b) Wu, R.; McMahon, T. B. *J. Am. Chem. Soc.* **2007**, *129*, 569. (c) Wincel, H. *J. Am. Soc. Mass Spectrom.* **2009**, *20*, 1900.
- (369) (a) Gidden, J.; Bushnell, J. E.; Bowers, M. T. *J. Am. Chem. Soc.* **2001**, *123*, 5610. (b) Gidden, J.; Bowers, M. T. *J. Phys. Chem. B* **2003**, *107*, 12829. (c) Gidden, J.; Bowers, M. T. *J. Am. Soc. Mass Spectrom.* **2003**, *14*, 161.
- (370) Schnier, P. D.; Klassen, J. S.; Strittmatter, E. E.; Williams, E. R. *J. Am. Chem. Soc.* **1998**, *120*, 9605.
- (371) (a) Strittmatter, E. E.; Schnier, P. D.; Klassen, J. S.; Williams, E. R. *J. Am. Soc. Mass Spectrom.* **1999**, *10*, 1095. (b) Liu, D.; Wyttenbach, T.; Bowers, M. T. *J. Am. Chem. Soc.* **2006**, *128*, 15155. (c) Wincel, H. *J. Am. Soc. Mass Spectrom.* **2009**, *20*, 1900.
- (372) Meot-Ner (Mautner), M.; Hunter, E. P.; Field, F. H. *J. Am. Chem. Soc.* **1979**, *101*, 686.
- (373) Locke, M. J.; McIver, R. T. *J. Am. Chem. Soc.* **1983**, *105*, 4226.
- (374) Meot-Ner (Mautner), M.; Field, F. H. *J. Am. Chem. Soc.* **1974**, *96*, 3168.
- (375) Jonsson, B.; Karlstrom, G.; Wennerstrom, H. *J. Am. Chem. Soc.* **1978**, *100*, 1658.
- (376) Yang, X.; Castleman, A. W. *J. Am. Chem. Soc.* **1991**, *113*, 6766.
- (377) Apel, C. L.; Deamer, D. W.; Mautner, M. N. *Biochim. Biophys. Acta Biomembr.* **2002**, *1559*, 1.
- (378) Zundel, G. In *Advances in Chemical Physics*. Prigogine, I., Rice, S., Eds.; John Wiley and Sons: New York, 2000; Vol. 3, pp 1–217.
- (379) Zundel, G.; Noller, H.; Schwab, G. M. Z. *Elektrochem. Ber. Bunsen-Ges. Phys. Chem.* **1962**, *66*, 129.
- (380) Schiøberg, D.; Zundel, G. *Z. Phys. Chem.* **1963**, *67*, 771.
- (381) Rabold, A.; Bauer, R.; Zundel, G. *J. Phys. Chem.* **1995**, *99*, 1889.
- (382) Zundel, G.; Schwab, G. M. *J. Phys. Chem.* **1963**, *67*, 771.
- (383) Danninger, W.; Zundel, G. *J. Chem. Phys.* **1987**, *74*, 2769.
- (384) Huyskens, P.; Zeegers-Huyskens, Th. *J. Chem. Phys.* **1964**, *61*, 1964.
- (385) Huyskens, P.; Fernandez, G. *Ind. Chem. Belg.* **1973**, *38*, 1237.
- (386) (a) Lindemann, R.; Zundel, G. *J. Chem. Soc., Faraday Trans. 2* **1977**, *73*, 788. (b) Park, S.; Moilanen, D. E.; Fayer, M. D. *J. Phys. Chem. B* **2008**, *112*, 5279.
- (387) Brzezinski, B.; Zundel, G. *Chem. Phys. Lett.* **1982**, *87*, 400.
- (388) Brzezinski, B.; Zundel, G. *J. Chem. Soc., Faraday Trans. 2* **1983**, *79*, 1249.
- (389) Brzezinski, B.; Zundel, G. *Can. J. Chem.* **1981**, *59*, 786.
- (390) Brzezinski, B.; Zundel, G. *J. Chem. Soc., Faraday Trans. 2* **1980**, *76*, 0611.
- (391) Brzezinski, B.; Rabold, A.; Zundel, G. *J. Phys. Chem.* **1995**, *99*, 8519.
- (392) Brezinski, B.; Zundel, G. *J. Chem. Phys.* **1984**, *81*, 1600.
- (393) Brzezinski, B.; Zundel, G.; Kramer, R. *J. Phys. Chem.* **1988**, *92*, 7012.
- (394) Brzezinski, B.; Zundel, G.; Kramer, R. *Chem. Phys. Lett.* **1988**, *146*, 138.
- (395) Brezinski, B.; Kramer, R.; Zundel, G. *Chem. Phys. Lett.* **1989**, *157*, 512.
- (396) Brzezinski, B.; Olejnik, J.; Zundel, G.; Kramer, R. *Chem. Phys. Lett.* **1989**, *156*, 213.
- (397) Eckert, M.; Zundel, G. *J. Phys. Chem.* **1988**, *92*, 7016.
- (398) Eckert, M.; Zundel, G. *THEOCHEM* **1988**, *50*, 141.
- (399) Eckert, M.; Zundel, G. *J. Phys. Chem.* **1989**, *93*, 5327.
- (400) Zundel, G.; Muhlinghaus, J. Z. *Naturforsch.* **1971**, *26*, 546.
- (401) Rastogi, P. P.; Kristof, W.; Zundel, G. *Biochem. Biophys. Res. Commun.* **1980**, *95*, 902.
- (402) Kristof, W.; Zundel, G. *Biophys. Struct. Mech.* **1980**, *6*, 209.
- (403) Kristof, W.; Zundel, G. *Biopolymers* **1980**, *19*, 1753.
- (404) Hargreaves, W. R.; Deamer, D. W. *Biochemistry* **1978**, *17*, 3759.
- (405) Lindemann, R.; Zundel, G. *Biopolymers* **1977**, *16*, 2407.
- (406) Lindemann, R.; Zundel, G. *Biopolymers* **1978**, *17*, 1285.
- (407) Olejnik, J.; Brzezinski, B.; Zundel, G. *J. Mol. Struct.* **1992**, *271*, 157.
- (408) Zundel, G. *J. Mol. Struct.* **1994**, *322*, 33.
- (409) Gogol, E. P.; Lucken, U.; Capaldi, R. A. *FEBS Lett.* **1987**, *219*, 274.
- (410) Wellner, N.; Zundel, G. *J. Mol. Struct.* **1994**, *317*, 249.
- (411) Iliadis, G.; Zundel, G.; Brzezinski, B. *Biospectroscopy*, **1997**, *3*, 291.
- (412) Bartl, F.; Brzezinski, B.; Rozalski, B.; Zundel, G. *J. Phys. Chem. B* **1998**, *102*, 5234.
- (413) Baran, J.; Malarski, Z.; Sobczyk, L.; Grech, E. *Spectrochim. Acta* **1988**, *44A*, 933.
- (414) Videnova-Adrabinska, V.; Baran, J.; Ratajczak, H.; Orville-Thomas, W. J. *Can. J. Chem.* **1985**, *63*, 3597.
- (415) Sobczyk, L. *Phys. Chem. Chem. Phys.* **1998**, *102*, 371.
- (416) Braga, D.; Angeloni, A.; Maini, L.; Gotz, A. W.; Grepioni, F. *New J. Chem.* **1999**, *1*, 17.
- (417) Dominiak, P. M.; Grech, E.; Barr, G.; Teat, S.; Mallinson, P.; Wozniak, K. *Chem.—Eur. J.* **2003**, *9*, 963.
- (418) Steiner, T. *Angew. Chem.* **2002**, *41*, 48.
- (419) Steiner, T. *Crystallogr. Rev.* **2003**, *9*, 177.
- (420) Epstein, L. M.; Shubina, E. S. *Coord. Chem. Rev.* **2002**, *231*, 165.
- (421) Brammer, L. *Dalton Trans.* **2003**, *16*, 3145.
- (422) Braga, D.; Grepioni, F.; Desiraju, G. R. *Chem. Rev.* **1998**, *98*, 1375.
- (423) Desiraju, G. R. *Acc. Chem. Res.* **2002**, *35*, 565.
- (424) Taft, R. W.; Wolf, J. F.; Beauchamp, J. L.; Scorrano, G.; Arnett, E. M. *J. Am. Chem. Soc.* **1978**, *100*, 1240.
- (425) Klots, C. E. *J. Phys. Chem.* **1981**, *85*, 3585.
- (426) Castleman, A. W.; Holland, P. M.; Keesee, R. G. *Radiat. Phys. Chem.* **1982**, *20*, 57.
- (427) Holland, P. M.; Castleman, A. W., Jr. *J. Phys. Chem.* **1982**, *86*, 4181.
- (428) Hiraoka, K. *Bull. Chem. Soc. Jpn.* **1987**, *60*, 2555.
- (429) Hiraoka, K. *Can. J. Chem.* **1987**, *65*, 1258.
- (430) Coe, J. V. *Chem. Phys. Lett.* **1994**, *229*, 161.
- (431) Tissandier, M. D.; Cowen, K. A.; Feng, W. Y.; Gundlach, E.; Cohen, M. H.; Earhart, A. D.; Coe, J. V.; Tuttle, T. R. *J. Phys. Chem. A* **1998**, *102*, 7787.
- (432) Coe, J. V. *Int. Rev. Phys. Chem.* **2001**, *20*, 33.
- (433) (a) Tuttle, T. R.; Malaxos, S.; Coe, J. V. *J. Phys. Chem. A* **2002**, *106*, 925. (b) Donald, W. A.; Williams, E. R. *J. Phys. Chem. B* **2010**, *114*, 13189.
- (434) (a) Rosseinsky, D. R. *Chem. Rev.* **1965**, *65*, 467. (b) Rosano, H. L.; Christodolou, A. P.; Feinstein, M. E. *J. Colloid Interface Sci.* **1969**, *29*, 335. (c) Hunenberger, P.; Reif, M. *Single-Ion Solvation: Experimental and Theoretical Approaches to Elusive Thermodynamic Quantities*; RSC Publishing: Cambridge, 2011.
- (435) (a) Field, F. H. *J. Am. Chem. Soc.* **1961**, *83*, 1523. (b) Field, F. H.; Franklin, J. L.; Munson, M. S. B. *J. Am. Chem. Soc.* **1963**, *85*, 3575. (c) Munson, M. S. B. *J. Am. Chem. Soc.* **1965**, *87*, 2332. (d) Bartmess, J. E.; Scott, J. A.; McIver, R. T. *J. Am. Chem. Soc.* **1979**, *101*, 6047.
- (436) (a) Aue, D. H.; Bowers, M. T.; Webb, H. M. *J. Am. Chem. Soc.* **1972**, *94*, 4726. (b) Aue, D. H.; Webb, H. M.; Bowers, M. T. *J. Am. Chem. Soc.* **1976**, *98*, 311. (c) Aue, D. H.; Webb, H. M.; Bowers, M. T. *J. Am. Chem. Soc.* **1976**, *98*, 318. (d) Aue, D. H.; Webb, H. M.; Bowers, M. T. *J. Am. Chem. Soc.* **1976**, *98*, 854.
- (437) Born, M. Z. *Phys.* **1920**, *1*, 45.
- (438) Bernal, J. D.; Fowler, R. H. *J. Chem. Phys.* **1933**, *1*, 515.
- (439) Bockris, J. O.; Reddy, A. K. N. *Modern Electrochemistry*; Plenum Press: New York, 1970; Vol. 1, p 61.
- (440) Abraham, M. H.; Liszi, J. *J. Chem. Soc., Faraday Trans. 1* **1978**, *74*, 1604.
- (441) Jorgensen, W. L.; Gao, J. *J. Phys. Chem.* **1986**, *90*, 2174.
- (442) (a) Singh, U. C.; Brown, F. K.; Bash, P. A.; Kollman, P. A. *J. Am. Chem. Soc.* **1987**, *109*, 1607. (b) Rao, B. J.; Singh, U. C. *J. Am. Chem. Soc.* **1989**, *111*, 3125.

- (443) Boudon, S.; Wip, G. *J. Comput. Chem.* **1991**, *12*, 42.
- (444) (a) Wagman, D. D.; Evans, W. H.; Parker, V. B.; Schumm, R. H.; Halow, I.; Bailey, S. M.; Churney, K. L.; Nuttall, R. L. *J. Phys. Chem. Ref. Data* **1982**, *11* (Suppl. 2). (b) Pierotti, R. A. *J. Phys. Chem.* **1965**, *69*, 281.
- (445) Ford, G. P.; Scribner, J. D. *J. Org. Chem.* **1983**, *48*, 2226.